Ultimate Limit State Analysis of Externally Post-tensioned Structures

by
Johnny Wong Liang Heng

A thesis submitted to the University of Sheffield for the Degree of Doctor of Philosophy.

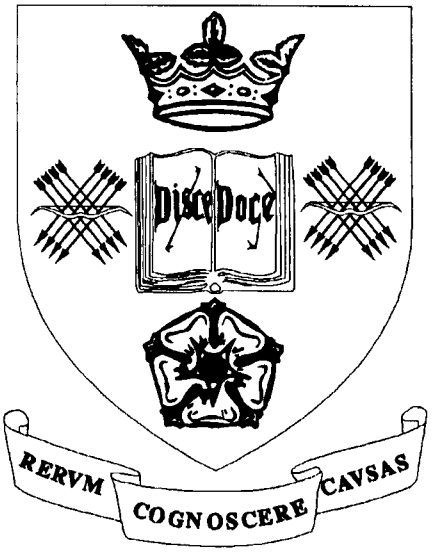

Civil and Structural Engineering Department
University of Sheffield

July 1997

Abstract

The UK Department of Transport (DoT) has recently encouraged the use of externally post-tensioned structures for bridge construction. This is due to the durability problems encountered with the conventional internally bonded post-tensioned structures. However, due to the lack of bond between the concrete and the external tendons, the ultimate strength of these structures cannot be determined by just performing a sectional analysis at the section of maximum moment. Although several recommendations have been made for the ultimate analysis of these structures, none were considered satisfactory here. Hence the purpose of this investigation is to study the flexural behaviour of these structures of all stages up to collapse, and to propose a practical methodology for estimating their ultimate strength.

The study introduces eight non-linear analytical models developed for the prediction of the moment vs. deflection response of simply supported externally post-tensioned beams (with and without deviators located along their spans) up to ultimate. The models employ an iterative procedure that involves the application of loads to the structure in increments up to the collapse condition, where the curvature distribution predicted at each loading sequence is used to estimate the stress increase and variation in eccentricity in the external tendons. Second-order effects due to variation in eccentricity of external tendons and frictional behaviour of tendons at the deviators are both taken into account in these models. The eight models were then verified by comparing the results derived from them with reported experimental data, whereby good correlation was obtained. An extensive parametric study was subsequently conducted using the proposed models applied to the various parameters that influence the ultimate behaviour of externally prestressed structures Finally, the recommendations in the codes of practice for the ultimate design of these structures were also investigated here.

Acknowledgements

I am most grateful to my supervisor, Professor Peter Waldron, for giving me the opportunity to conduct the research presented and his interest, patience, guidance and friendship.

I would also like to thank Dr R.S. Crouch, Dr. K. Pilakoutas, Dr. I.W. Burgess for their technical help and suggestions on computer programming. My gratitude also to L.Y. Yeo and P. Hayes for helping to proof read my thesis.

Finally, I wish to thank my parents and girlfriend, Farn Ling, for their unfailing support and encouragement.

Declaration

This thesis is a report of research work carried out in the Department of Civil and Structural Engineering, The University of Sheffield, between September 1993 and July 1997. Except where references are made to other work, the content of this thesis is original and have not been submitted for any other qualifications.

Wong Liang Heng Johnny
Civil and Structural Engineering Department
The University of Sheffield.

Contents

List of Figures

List of Tables

Notation

a	shear span
A_c	area of concrete section
A_{ps}	area of prestressed reinforcement
$A_{ps.e}$	area of prestressed reinforcement (referring specifically to external tendons)
A_s	area of non-prestressed longitudinal reinforcement
$A_s\%$	reinforcement ratio
A_{sv}	area of web reinforcement
b	breadth of the beam
c	depth to neutral axis
c_u	depth of neutral axis at ultimate limit state
C	resulting compressive force in the concrete section (or C_{conc})
df	frictional resistance generated at the deviator
d	overall depth of the section
d_{conc}	distance from neutral axis to the concrete's tensile force
d'_{conc}	distance from neutral axis to the concrete's compressive force
d_e	effective depth to centroid of tensile force in the internal reinforcement
d_{pres}	distance from neutral axis to the prestress steel's tensile force
d_{ps}	effective depth to prestressing steel
$d_{ps.e}$	effective depth to prestressing steel (referring specifically to external tendons)
d_{reinf}	distance from neutral axis to the reinforcement steel's tensile force
e	eccentricity of tendon from centroid of the section
$e_{initial}$	initial eccentricity of the structure before application of load
e_{max}	maximum eccentricity of the structure
E_c	modulus of elasticity of concrete
E_{ps}	modulus of elasticity of prestressing steel

$E_{ps\,e}$	modulus of elasticity of prestressing steel (referring specifically to external tendons)
f_{bot}	stress on bottom fiber of concrete section
f'_c	specified cylinder strength of concrete
f_{ct}	stress in the extreme concrete fiber in compression
f_{cu}	specified cube strength of concrete
f_{pe}	effective prestress in tendons after losses
f_{ps}	stress in prestress tendons
$f_{ps(ult)}$	stress in prestress tendons at the ultimate conditions
f_{pu}	specified tensile strength of prestressing steel
f_{py}	specified yield strength of prestressing steel
$f_{py,e}$	yield strength of external prestress steel (referring specifically to external tendons)
f_r	modulus of rupture of concrete
f_{top}	stress on top fiber of concrete section
f_y	specified yield strength of non-prestressed reinforcement
f_{yv}	specified yield strength of web reinforcement
F	prestress force
F'	redistributed prestress force
F_1, F_2	prestress force in tendons on both sides of the deviators
F_{pe}	effective prestress force
$F_{transfer}$	force transferred on either sides of the deviator to maintain equilibrium
g	tendon slip
h	overall depth of the section
I_g	moment of inertia
I_g	moment of inertia of gross concrete section
I_{cr}	moment of inertia of cracked section
L	overall span of beam
L'	overall span of beam after deformation
ℓ	span of the beam
$\ell_{(i)}$	length of deviator segment *i*
ℓ_{12}	length of the prestress steel from point 1 to point 2 (figure 2.7)

l_{free}	free-length of the prestress steel left unsupported
$l_{plastic}$	length of the plastic hinge
l_{ps}	length of the prestress steel
m	gradient of curves
M	moments applied on section
M_{add}	additional moments to be added for each loading stage at the pre-crack state
$M_{difference}$	difference between $M_{cr(bot)}$ and M_{ext}
M_{cr}	cracking moment
$M_{cr(bot)}$	moment that causes cracking at the bottom concrete fibre
$M_{cr(top)}$	moment that causes cracking at the top concrete fibre
M_d	moments applied on structure due to dead loads
M_{ext}	moment at section due to external loading
M_{int}	section's moment of resistance
M_{exp}	maximum bending moment capacity of the beam derived from experiments
M_{max}	maximum bending moment of the structure
$M_{(limit)}$	material limit moment derived from sectional analysis
M_{pred}	maximum bending moment capacity of beam predicted from analyses
N'	Concentrated point force acting on the deviator
P	external point load
s	spacing of web reinforcement
T	total tensile force
T_{conc}	tensile force in concrete section
T_{ps}	tensile force in prestressing steel (or T_{pres})
T_{reinf}	tensile force in reinforcement steel
u	horizontal deformation
v	vertical deformation
V_c	shear strength of concrete
V_{ci}	shear resistance to flexure shear crack
V_s	vertical component of force taken up by stirrup
V_x	applied shear forces

w	angular deformation
x_{point}	minimum number of pre-crack points defined in the load-deflection curve
y_t	distance from the centroid to the extreme tension fiber
z_p	distance between the resultant compressive force and the centre of the tendon
z_s	distance between the resultant compressive force and the centre of the passive reinforcement
Z_{bot}	section modulus with respect to extreme bottom fiber
Z_{top}	section modulus with respect to extreme top fiber
α	deviation angle at deviators or coefficient
α_{free}	free length-depth ratio
β	deviation angle at deviators or coefficient
ε_{bot}	strain in concrete extreme bottom fiber
ε_{ce}	strain in concrete at the level of the external tendons due to effective prestress
ε_{cu}	limiting strain at which the concrete in beam crushes
ε_{pe}	strain in prestress steel under effective prestress
ε_{ps}	strain in prestress steel at section considered
$\varepsilon_{ps(ult)}$	strain in prestress steel at section considered at the ultimate conditions
ε_s	strain of passive reinforcement
ε_{top}	strain in concrete extreme top fiber
ϕ	curvature at a section
ϕ_m	mean curvature at a section
ρ_p	ratio of prestress reinforcement ($\rho_p = \frac{A_{ps}}{bd_{ps}}$)
Ω	strain reduction coefficient introduced by Naaman (1990)
Δ	vertical deflection at a specific point along the span of the beam
Δ_{eccen}	eccentricity variation of tendons
$\Delta_{eccen(ult)}$	eccentricity variation of tendons at ultimate condition
$\Delta_{eccen(limit)}$	eccentricity variation of tendons at material limit condition
$\Delta\varepsilon$	pre-set strain increment for post-crack state analysis
$\Delta\varepsilon_{slip}$	change in strain due to slippage at deviators

Δf	out of balance force at the deviators
Δf_{ps}	change in prestress due to external loads
$\Delta f_{ps(max)}$	change in prestress due to external loads at the maximum moment conditions
$\Delta f_{ps(ult)}$	change in prestress due to external loads at the ultimate condition
$\Delta f_{ps(limit)}$	change in prestress due to external loads at material limit condition
$\Delta \ell_{ps}$	change in length of unbonded tendons due to external loading
$\Delta \ell_{12}$	change in length of the prestress steel from point 1 to point 2 (Figure 2.7)
$\Delta \ell_{plastic}$	change in length of the plastic hinge
ΔM_{shear}	fictitious additional moment on a section due to shear cracking
$\Delta \varepsilon_{cs}$	strain change in prestress steel due to external loading
$\Delta \varepsilon_{ps}$	strain change in concrete at the level of prestress steel due to external loading
μ	coefficient of friction

In addition to these symbols, a number of other symbols are defined and used locally.

Chapter 1

Introduction

1.1 General

Conventionally, the post-tensioning of bridges involves the practice of embedding tendon ducts to straight or draped profiles within the webs and flanges of girder sections. After the concrete is placed and cured, or, after the precast segments are assembled, the tendons are pulled through the embedded ducts and stressed. These ducts are then normally filled with cement grout after the stressing process. This method of prestressing is known as internal bonded post-tensioning.

Cement grout helps to establish a bond between the concrete and the tendon, hence full bond is usually assumed for the analysis of these structures. The cement grout also helps protect the tendons from possible attacks by aggressive agents which may lead to the corrosion of the tendons. However, it has been found from bridge inspections that the grouting procedures were often not properly carried out and, in many cases, voids have been found to exist in the grout, thereby permitting the ingress of water, chlorides and other aggressive agents to attack the tendons. This occurrence rarely shows any visual evidence of corrosion, such as spalling, discoloration or local cracking. As a result it is very difficult to detect or quantify the deterioration of these structures.

In December 1985, a segmental post-tensioned bridge in Wales, *Ynys-y-Gwas*, collapsed without warning due to localised corrosion problems caused by poor grouting procedures (Woodward and Williams (1988)). This event led the Department of Transport in the United Kingdom to commission several checks on existing bridges for corrosion problems. These checks were found to be both difficult and expensive (Winkler and Zenobi (1993)). Furthermore, even if the bridges inspected had been found to be suffering from corrosion problems, the impossibility

of replacing grouted tendons would have required the structure to be either demolished or repaired at some considerable cost. In light of these problems, the Department of Transport (DoT) in the United Kingdom imposed a temporary ban on the use of internal post-tensioning for the construction of new bridges and encouraged instead the use of external post-tensioning. Externally post-tensioned bridges are preferred to internally post-tensioned bridges because they allow easy maintenance and monitoring of tendons (Raiss (1995)). If defective tendons are found, the possibility of replacement and re-stressing allows repairs to be made on the structure with relative ease.

1.2 External Post-tensioning

With externally post-tensioned bridges, the tendons are located within the voids of box-girders or between webs of non-box girder sections (see Figure 1.1). The tendons may be straight or draped, where the required profile is maintained by passing tendons through devices called deviators. The only positive contact between the concrete and the tendons for these structures occurs at the anchorages and deviators. Because of this, external tendons are considered to be unbonded and the tendon strains to be independent of the strains in the adjacent concrete section.

The free lengths of the tendons are usually protected from corrosion by one of the following methods:

- grouting along the tendon length with cement
- coating the tendons with protective paints
- encasing the tendons with concrete encasement
- enclosing the tendons with HDPE (high-density Polyethylene) sheathings
- galvanising the tendons.

In the United Kingdom, the Department of Transport BA 58/94 (1995) states that the galvanisation of the tendons in accordance to BS5493 and BS183 is sufficient for corrosion protection. Furthermore, the tendons are not to be placed in either empty ducts or in ducts which are subsequently grouted, greased or filled with wax, in order to allow ease of inspection and replacement of tendons.

Externally post-tensioning of bridges has been greatly influenced by the technological developments in the United States and France. However, the reasons for using this form of prestressing in bridge construction differs between the two countries (Virlogeux (1993)). In the United States, the principal objectives for using external post-tensioning are to reduce the cost and increase the speed of bridge construction. In France, however, the direction of the technology is centred on improvements in construction quality. The replacement possibility of tendons is thus of major concern in France, and as a result higher costs are usually incurred. In the case of the United Kingdom, the use of external tendons was not encouraged as an alternative for bridge construction until recently. This may primarily be attributed to the lack of understanding of the behaviour of these structures at the ultimate limit state. Although, recent corrosion problems encountered in existing bridges have forced this technique to be preferred over conventional methods of post-tensioning, there is still a great need for more research to be conducted to improve the understanding of the behaviour of these structures at ultimate conditions.

1.3 Components of External Post-tensioning

1.3.1 External Tendons

External tendons are placed outside the concrete section and are usually deviated along the span so as to resist the flexural bending moments caused by loading the structure. These external tendons must generally meet the following requirements (Jungwirth *et al* (1993)):

- provide reliable transfer for static and dynamic loads
- durability provided by the resistance to chemical and mechanical influence
- damping of the tendon vibration caused by wind and live loads (if necessary)
- possibility for adjustment of tendon forces during the whole life of the structure
- economy with regards to the cost of manufacture as well as maintenance of the structure.

Steel tendons are commonly used for external post-tensioning and may either be in the form of high strength bars, wires or strands. Though glass, aramid or carbon fibers are some of the alternative materials suggested to replace steel, the cost of these

materials is currently too high for them to be considered for general use. The advantage of high strength steel bars is that they are easy to handle. However, they are only suitable for short length requirements and, if high forces are involved, the bars must be bundled together and anchored at one anchor plate. Tendon wires and strands normally consist of three components: the tensile member, filling material and sheathing, and may be installed either in the form replaceable or non-replaceable tendons.

Non-replaceable external tendons are more commonly used in the United States, where the provisions for tendon inspection and replacement are not essential. For this non-replaceable system, steel pipes are first placed at the deviators. The tendons, which are normally enclosed in ducts made up of HDPE sheathings, are then installed along the beam by passing them through these deviators. The sheaths are subsequently grouted with concrete and this makes replacement of the external tendons very difficult.

There are several methods suggested for the installation of replaceable tendons in external post-tensioned structures. One method of design for replaceable external system is to use galvanised external tendon strands in bunches without enclosing them in ducts. Galvanised tendons will give adequate protection against corrosion and, since no ducts are used, easy inspection and replacement of the tendons are also possible. However, for safety reasons, galvanised tendons have to be attached at close intervals, and the use of long free strands is generally not allowed.

The injection of grease or wax into ducts with tendons is another method of providing for the replacement of tendons in external systems. Grease and wax give the required protection against corrosion for the tendons and also allows them to be replaced easily. This method is applicable to both external and internal unbonded tendons, and ducts used must be designed to withstand the relatively high temperatures during installation; typically 80-90 degree Celsius.

The *double tubing method* was developed and patented by the French to allow easy replacement of external tendons. This method involves the injection of cement grout into HDPE ducts, but with a duplicate tubing system fixed at the deviators to allow for future replacement of tendons.

Finally, Freyssinet International developed a replaceable system for external post-tensioning known as the *individually protected system*, which involves the use of individually protected strands. For the purposes of corrosion protection and easy replacement, grease or wax are applied on the strands used in this method before extruding them through HDPE ducts. The ducts are then injected with cement grout along their full length except at the anchorages. After the cement grout injection, the strands are stressed and the anchorages injected with wax. The advantage of this installation method lies in the fact that; if one element in the system suffers from corrosion problem, it will not lead to the complete breakdown of the corrosion protection of the other tendons.

1.3.2 Deviation Devices

Deviation devices or deviators are required in an external post-tensioning system so as to deviate the external tendons in order to give the required tendon profile. The deviator is a critical design detail (Powell *et al* (1988)) since, other than the anchorages, it is the only positive contact between unbonded tendons and the concrete. Deviators vary in shape and size, though the most commonly used forms are the saddle block (see Figure 1.2) and intermediate cross beam (see Figure 1.3).

The saddle blocks or small deviation blisters usually deviate tendons one at a time at each deviator. As every tendon can only be deviated near the web, it is necessary to get the tendons away from the web after deviation, resulting in a complex layout plan for tendons (Virlogeux (1993)).

The intermediate cross beams are similar to the cross beams located at the supports but are much lighter in weight. They permit a simplified tendon layout compared to using deviation blisters and provide a means for tendons to be anchored along the span should the need arise (Section 1.3.3).

1.3.3 Anchorages

Anchorages for external tendons are usually placed in the diaphragms situated at the piers. Special attention must be given to the anchorage of external tendons, since these are responsible for the transmission of prestressing force to the structure

(Winkler and Zenobi (1993)). Also, as no bond exists between the tendons and the concrete for externally post-tensioned structures, it is essential that the end anchorages remain fully effective at all times.

As proposed by the UK Department of Transport, the design of anchorages in the external system should allow them to be open and inspectable (BA 58/94 (1995)). The anchorages should also be designed to accommodate detensioning and re-stressing of the tendons. This may be made possible by including galleries in the abutments to allow prestressing jacks to be installed at anchorages for the detensioning and re-stressing process.

For continuous externally post-tensioned beams, tendons typically overlap at the support cross beams for continuity. Overlapping the tendon anchorages in these beams by extending tendons over two bays will generally lead to (Virlogeux (1993)):

- reduction in the number of anchorages at the support cross beams
- prevention of geometric congestion due to large numbers of anchorages
- economy.

Since there is a high risk of bimetallic corrosion occurring at the anchorages where the tendons are gripped at high forces, it has been suggested that anchorages should be of the same steel as the external tendons to prevent this problem.

1.3.4 Intermediate Blocking Device

The intermediate blocking device, first developed by Freyssinet International (Lacroix and Jartoux (1994)), was used in the construction of the Second Severn Crossing. A sketch of the device is reproduced in Figure 1.5. Proposed for continuous externally post-tensioned structures, the device serves two main purposes. The first is to allow a more controlled variation of tensile force in tendons between deviators and anchorages; the second is to help limit slippage of the tendons at supports and deviators due to adverse loading. Thus improvements in both safety and performance of externally prestressed structures, especially at the ultimate limit state, are gained from the use of this device.

The intermediate blocking device is added to the structure by first placing the device alongside the tendon at contact points along the span and then accurately clamping it

in position using the clamp incorporated. This clamp is placed perpendicular to the tendon's direction and facilitates the adjustment of the tensile force in the tendon, F, according to design requirements. Variation of tensile force, δF, is thus transmitted to the structure as shown in Figure 1.4 using the proposed device.

1.4 Design Considerations

1.4.1 Service Limit State

For service limit state design, there is no major difference between structures with internal and those with external post-tensioning (Virlogeux (1993)). In both cases, the same specifications may be applied, especially with regards to the limitation of concrete tensile stresses. However, in the design notes for externally post-tensioned bridges prepared by the UK Department of Transport BA 58/94 (1995), some relaxation in the service limit state is permitted. This line of reasoning is based on the fact that external tendons do not rely on the concrete for corrosion protection, and the fact that the problem of high stress fluctuations in tendons associated with cracks are not relevant to external unbonded tendons

The same notes also pointed out that the design rules for shear in beams specified in BS 5400 Part 4 is not considered appropriate for externally post-tensioned structures. This is because these rules have been derived empirically from test results obtained from beams with bonded tendons. The preferred approach for the design of shear resistance is therefore to treat the unbonded prestressing structure as a reinforced section with an externally applied load.

1.4.2 Ultimate Limit State

In the case of the ultimate limit state design, there is a great difference between internal and external tendons (Virlogeux (1993) and Jackson (1994)). For internally bonded structures, factored loads will produce cracks and plastifications in the cross section at supports and midspan. Due to the bond with the concrete, the internal tendons increase in tension in these cracked zones, thus enabling the yielding of the prestressing steel. This behaviour however does not occur in external tendons, because no bond exists between the tendons and the concrete. Therefore, for such

beams, the tension generated in the external tendons during the application of load will be uniform along their free length and dependent on the deformation of the whole structure. Stress variations are thus more limited in these tendons and yield does not occur except when the beam deflections become very high. The strength of the prestressing steel is thus not usually fully utilised when calculating the ultimate bending resistance of externally prestressed structures.

It is often advantageous to produce *mixed beams* by providing some untensioned bonded reinforcement in the design of externally unbonded post-tensioned structures (Jungwirth *et al* (1993)). This is because the passive reinforcement not only helps to increase the ultimate capacity, but also helps to limit shrinkage and thermal cracking of the beam. Especially for segmental structures where external tendons are used, ductility can be provided by convenient placement of untensioned reinforcement across the joints prone to opening under excessive loading, in a subsequent concreting operation. Provision of ductility in externally prestressed beams helps to prevent them from failing in a brittle manner at the ultimate limit state.

For externally post-tensioned structures, failure of one tendon at any point along the beam will render that tendon ineffective over its entire length, thus causing the structure to be vulnerable to disproportionate collapse. This is particularly true for continuous beams where localised failure of one span could result in a progressive failure of adjacent spans. Such progressive failure of continuous externally prestressed structures can be prevented by staggering the anchorages in continuous structures.

1.4.3 Other Design Considerations

In practice, when bonded post-tensioned tendons are cut or broken, they re-anchor and hence the energy stored in them is not fully released. However, cutting unbonded tendons will release a large amount of energy, causing problems in the demolition of such structures. If externally prestressed structures are designed in such a way as to facilitate re-stressing, the tendons can be easily removed by simply destressing them. In recognition of this problem, the UK Department of Transport BA 58/94 (1995)

specified that the designs of all externally post-tensioned bridges must provide allowance for the detensioning of tendons.

Poor ventilation in enclosed box-girders prestressed with external tendons is known to cause serious corrosion problems in tendons. Hence, another important design consideration is that of ensuring proper ventilation in these structures. In addition, the concrete boxes housing external tendons should ideally have a reasonable working headroom to allow easy access for the inspection and maintenance of tendons.

1.5 Material Quantities and Cost Comparison

Jungwirth *et al* (1993) made a comparison between the use of internally bonded and externally unbonded tendons for post-tensioned bridges in terms of cost and materials used in construction. Their results revealed that, despite the higher prestressing level used (i.e. f_{pe}/f_{pu} specified for internally bonded structure was 0.55 while those for externally prestressed structures was 0.7 in Germany) and the lower weight of the externally post-tensioned structure, the quantity of prestressing steel used only differed slightly between the two methods (see Figure: 1.7). This may be due to the fact that the preferred parabolic profiles corresponding to the required bending moments can only be approximately achieved for external tendons with the use of deviators. On the other hand, with internal tendons, these profiles can be easily acquired. Also, since external tendons usually lie within the void of box-girder sections near the upper surface of the soffit, the maximum possible eccentricity attainable is thus reduced.

The cost of external tendons are reported to be about 50% - 100% higher than that of internal tendons with the same prestressing force (Figure 1.6). This higher cost is due to the additional system-related cost for the provision of deviators and the use of special corrosion protection materials (e.g. sheathings, galvanising, etc.). On the other hand, there is a notable saving with externally post-tensioned structures, due to the lower maintenance costs involved. This is one of the primary reasons why external post-tensioning is often preferred to the conventional method of post-tensioning (Winkler and Zenobi (1993)).

1.6 Advantages and Disadvantages

The following section will briefly outline the advantages and disadvantages of using external post-tensioning as discussed by Winkler and Zenobi (1993), Lacroix and Jartoux (1994), Powell *et al* (1988) and Hindi *et al* (1995).

1.6.1 Advantages

- **Section free from ducts**

  For externally post-tensioned structures, since the steel tendons are placed outside the concrete section, concrete webs and flanges are free from ducts used to contain these tendons. The absence of ducts in the concrete section allows a possible reduction in the thickness of the web with a resulting saving in the cost of construction. Another advantage of having the webs free of ducts is the increased efficiency of the web area for shear resistance.

- **No interference with passive reinforcement**

  With the ducts outside the section, construction speed of post-tensioned structures is improved due to the omission of the task of placing, positioning and securing ducts inside the reinforcement cage.

- **Reduced congestion**

  The absence of ducts within the reinforcing cage relieves congestion, resulting in better conditions for placement and consolidation of concrete. Incidents of poorly consolidated concrete occur frequently when ducts are grouped together in closely spaced bundles, which is often the case for conventional internal post-tensioning.

- **Accessibility of tendons**

  Exposed external tendons allow easy checks and maintenance to be made on them. Rectification works may then be carried out more easily if ruptured tendons are detected from these checks. The ease of accessibility also facilitates installation of the tendons and sheathing during the construction phase.

- **Replaceability of tendons**

  The replaceabilty of external tendons may not be a major issue in the United States, but it is the main reason why the method is so attractive in Europe. Externally post-tensioned structures can be designed to allow defective tendons to be easily and cheaply replaced. This is an important advantage as it will mean that bridges found with defective tendons can be repaired without much effort or disruption to the use of the bridge itself.

- **Reduced friction losses**

  The use of external tendons reduces the overall loss of prestressing during installation due to friction. Since the tendon is straight between attachment points and the duct (if used) is unrestrained, the effect of wobble of tendon is effectively nullified.

- **Relaxation of serviceability requirements**

  Relaxation of service limit state stress criteria are possible because the opening and the closing of the cracks do not cause high fluctuations of stresses in external tendons as compared to internally bonded ones. In addition, the tendons do not depend on the concrete for corrosion protection hence crack width limitations are relaxed.

- **Signs of failure are detectable before collapse**

  Flexural failures of these structures will always be preceded by extensive cracking and excessive deflections, thus giving early warning signs before collapse.

1.6.2 Disadvantages

- **Vibration of unrestrained tendons**

  Attachment of external tendons to the concrete section are often spaced far apart, and problems relating to the vibration of external tendons have been experienced. Special precautions are thus required to avoid this problem. Most code specifications give a limiting value for the length of external tendons spanning between deviators and anchorages, in order to control this vibration problem.

- **Reduced eccentricity**

  For a box-girder section, the external tendon typically lies inside the void. This reduces the eccentricity allowed for external tendons as internal tendons normally extend into the soffit region. This therefore decreases the flexural efficiency of externally prestressed structures.

- **Reduced ductility**

  A major concern in developing the design criteria for externally prestressed structures is the possibility of reduced ductility. Tests have shown that the loss of tendon strength development may result in an explosive (brittle) failure. This explosive failure occurs due to the crushing of the concrete before the yielding of the tendons.

- **Reduced efficiency at ultimate conditions**

  Due to the lack of bond between the concrete and unbonded tendons, tendon strains are averaged out over their free length. This results in a reduction in efficiency for unbonded tendons at the ultimate limit state, as the stress in the tendons at this state will only be slightly above the initial stressing level. If the number of tendons required is based on the ultimate strength considerations, this loss of potential tension force capacity could be a serious economic problem. A short study was conducted by the author (Section 2.4) to check if bridges designed using the present specifications stated by the UK DoT for externally prestressed structures, is controlled by the service or ultimate limit state design. The conclusions of the study strongly suggest that the design of externally post-tensioned structures, following these specifications, is controlled by the ultimate limit state conditions.

- **Concentrated forces acting at the attachments**

  As deviators and anchorages are the only physical attachment between the external tendon and the concrete structure, high concentrated forces are experienced at these points. These elements must thus be carefully designed, as distress or failure of such elements could be catastrophic.

- **Prone to attacks**

  As cables are not protected by concrete, they are more susceptible to vandalism, terrorist attacks and fire.

- **Inability to rebond**

  In the event of tendon failure, the unbonded tendon would not have the capability to rebond as in the case of internal prestressing and would be ineffective over its whole length.

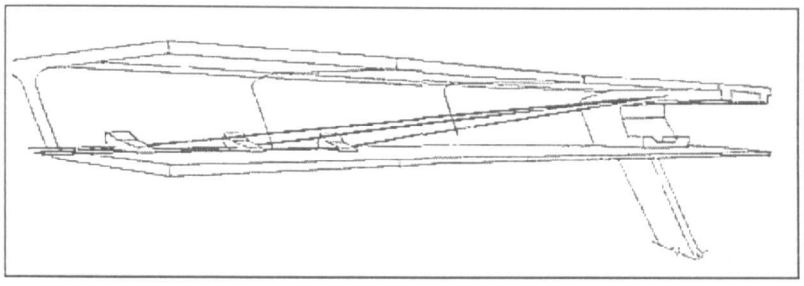

Figure 1.1: External Post-Tensioning in Long Key Bridge
(taken from Powell *et al* (1988))

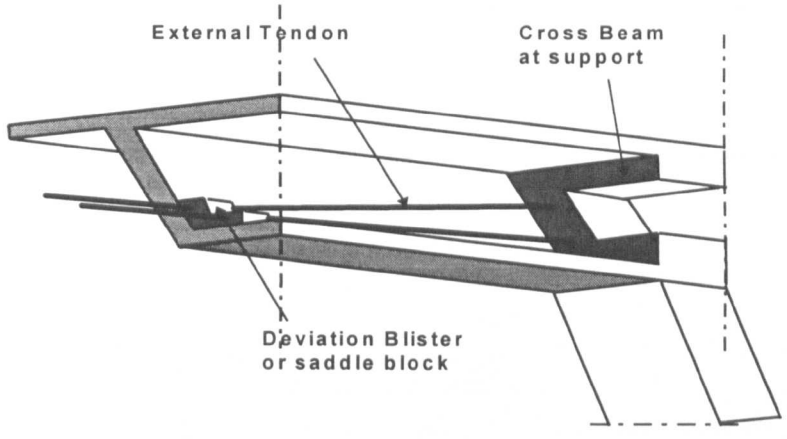

Figure 1.2: Deviation blister or saddle block

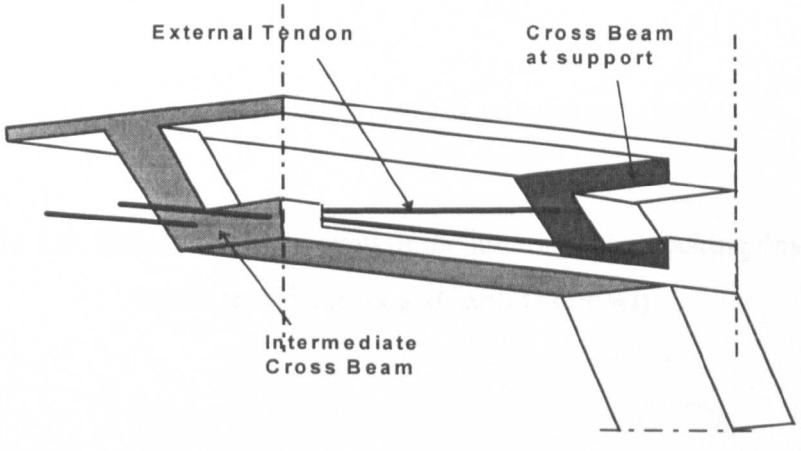

Figure 1.3: Intermediate Cross Beam

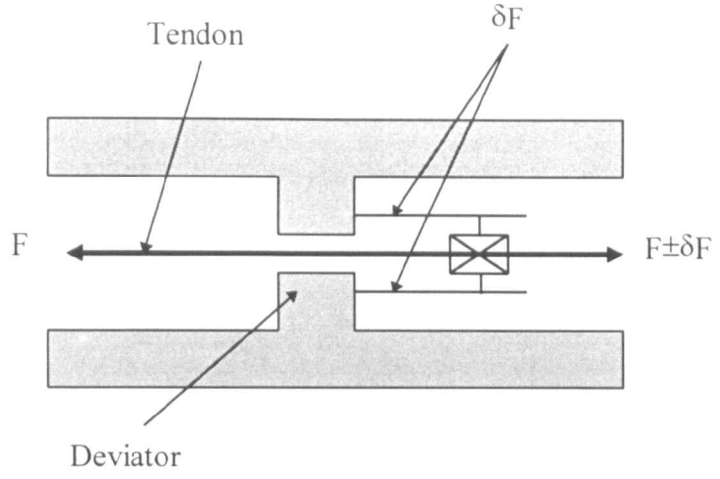

Figure 1.4: The principle of intermediate blocking device
(taken from Lacroix and Jartoux (1994))

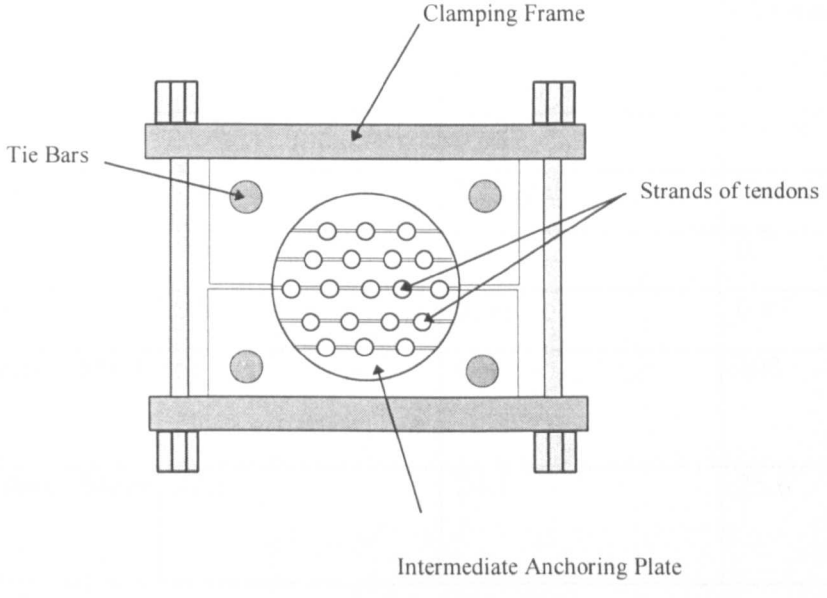

Figure 1.5: Sketch of arrangement of the intermediate blocking device
(taken from Lacroix and Jartoux (1994))

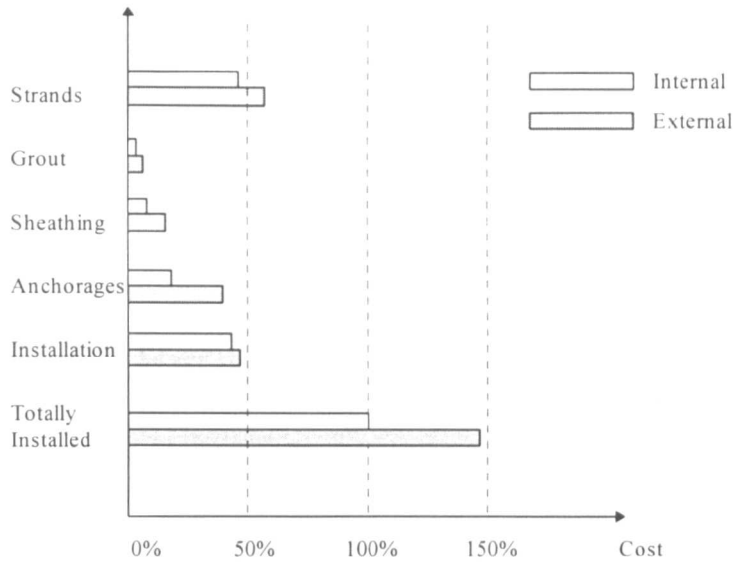

Figure 1.6: Cost comparison between internal and external post-tensioning (adopted from Jungwirth *et al* (1993))

	Wannebach	**Berbke**	**Wintrop**
Span-depth	42.00/3.02	45.00/3.30	43.00/3.30
Width (m)	14.85	14.25	15.28
Prestressing	Internal	External	External
f_{pe}/f_{pu}	0.55	0.7	0.7
Concrete	0.81	0.66	0.67
Reinforced Steel (Kg/m^2)	69	127	103
Prestressing Steel (Kg/m^2)	27.1	24.1	25.6

Figure 1.7: Material comparison between internal and external post-tensioning (adopted from Jungwirth *et al* (1993))

Chapter 2

A Review on the Ultimate Limit State Behaviour and Problem Definition

2.1 General

This chapter presents the literature review conducted on the ultimate flexural behaviour of externally post-tensioned structures.

Post-tensioning of structures can generally be classified into three major forms:

- **Internally Bonded Post-Tensioning**

  This is the conventional method of post-tensioning where the tendon ducts are placed within the concrete section. The ducts are grouted after the stressing process and full bond is usually assumed between the concrete and the tendons.

- **Internally Unbonded Post-Tensioning**

  The tendon ducts are placed within the concrete section as in the internal bonded case, but the tendons are not grouted after the stressing process.

- **Externally Unbonded Post-Tensioning**

  The tendons are located outside the concrete section. The required profile for tendons is maintained by providing deviators along the span of the structure.

The ultimate limit state analysis is performed differently for these three types of post-tensioned structures because of the different bonding conditions between the concrete and the prestressing tendons in these structures. For internally bonded structures, the conventional method adopted to evaluate the ultimate response of these structures is to conduct a sectional analysis at the section of maximum moments. This method is not appropriate for prestressed structures with unbonded tendons (i.e. internally and externally unbonded tendons) because of the absence of bond between the concrete

and the prestressing steel. The analytical procedures commonly adopted for estimating the ultimate strengths of these post-tensioned structures are presented in Section 2.2.

For internally unbonded post-tensioned structures, the ultimate flexural strengths can be computed if the increase in stress in the tendons $\Delta f_{ps(ult)}$ is known. However, because of the absence of bond between the concrete and the prestress tendons, $\Delta f_{ps(ult)}$ is not easily predicted for these structures. Several empirical expressions and methods were thus suggested by various codes of practice and researchers, for the estimation of $\Delta f_{ps(ult)}$ at the ultimate conditions, and these are presented in Section 2.3.1.

Similar to internally unbonded tendons, the stress increase in external tendons is not easily predicted due to the lack of bond between concrete and prestress tendons. Furthermore, since the concrete and prestressed tendons are connected only at the anchorages and deviators; the eccentric distance of the tendons varies as the beams deform under different loading conditions. Section 2.3.2 describes the various methods suggested by several researchers to predict the ultimate behaviour of these structures.

The designs of internally bonded post-tensioned structures are found to be usually controlled by the service limit state conditions. This however may not be the case for externally post-tensioned structures because of the small increase in stress and eccentricity variations in tendons at the ultimate conditions. Section 2.4 presents the study conducted by the author to find out if the design of externally prestressed structures are controlled by their ultimate or service limit state behaviour. If these structures are controlled by their ultimate behaviour, then an accurate method for performing the ultimate analysis becomes vital. This is to ensure that these structures are designed both safely and economically.

Finally, after conducting an extensive state-of-the-art review on the ultimate limit state behaviour of externally post-tensioned concrete structures, several research objectives were defined for the research investigation. These research objectives are listed in Section 2.5.

2.2 Ultimate Limit State Analysis

2.2.1 Internally Bonded Prestressed Structures

The ultimate limit state analysis for internally bonded post-tensioned structures is well established in many texts and papers (Mosley and Bungey (1990), Lin and Burns (1982), Naaman (1982)). Since full bond is usually assumed for these structures, strain compatibility between the concrete and the tendons is maintained at the critical section. This implies that the strain change in the tendons is equal to the strain change in the concrete at the section of interest, enabling the ultimate limit state behaviour to be estimated by performing a sectional analysis at the critical section of the structure.

The assumptions normally made for the analysis are:

1) Plane sections remain plane under loading. Consequently, it is assumed that strains in the concrete and the reinforcing steel are directly proportional with the distance from the neutral axis at which the strain is zero, up to the ultimate load.
2) The ultimate limit state of collapse is reached when the concrete strain at the extreme fibre (compression) reaches a specific value (BS8110 states ε_{cu} to be 0.0035).
4) The tensile strength of concrete is often neglected; i.e. $f_r = 0$.
5) The stress-strain relationships of the materials are known.

A typical step-by-step description of the sectional analysis for the ultimate moments of internally bonded structures is shown in Figure 2.1.

2.2.2 Internally Unbonded Prestressed Structures

Due to the lack of bond between concrete and prestress tendons for internally unbonded post-tensioned structures, the ultimate moments cannot be easily estimated by just performing a simple sectional analysis at the section of maximum moment. This is because an increase in prestressing force is not localised at the critical section, but is instead averaged along the free length of the tendons. Stress in an unbonded tendon at any load level during the load response history is thus dependent on the total change in length of the concrete at the level of prestressing steel between the

anchorages (Harajli (1990)). This makes the deformation of these structures important for estimating the increase in stress in the prestress tendons.

The moment curvature method (see Figure 2.2) can be used satisfactorily to calculate the ultimate moment of unbonded structures, provided the stress increase in the tendons at the ultimate limit state can be predicted with reasonable accuracy (Tao and Du (1985)). The stress increase in the tendons, $\Delta f_{ps(ult)}$, is required to predict the prestress in tendons at the ultimate conditions using Equation (2.1).

$$f_{ps(ult)} = f_{pe} + \Delta f_{ps(ult)} \quad \text{.....(2.1)}$$

$\Delta f_{ps(ult)}$ at the ultimate limit state is assumed to be uniform along the length of the unbonded tendon and can either be estimated by iterative procedures (Naaman and Alkhairi (1993) and Harajli and Kanji(1992)) or by empirical formulations suggested by various researchers (Baker (1949), Warwaruk *et al* (1962), Mattock *et al* (1971), Tao and Du (1985), Tam and Pannell (1976), Harajli (1990), I'vanyi *et al* (1985) and Balaguru (1981)).

The usual assumptions used for the ultimate analysis of internally unbonded post-tensioned structures are:

1) Plane sections remain plane after loading.
2) Constitutive relationships for the steel and concrete are known.
3) The beam is assumed to be at a cracked state whenever the applied tensile stress exceeds the modulus of rupture, f_r.
4) Frictional behaviour between the steel and the concrete is assumed to be negligible.

Note that for internally unbonded structures, the deflected shape of the tendons follow the deformation of the beam throughout the entire span, and hence there is no change in eccentricity at any loading level (see Figure 2.3).

2.2.3 Externally Unbonded Prestressed Structures

The stress increase in an external tendon is generally small and depends on the overall deformation of the whole structure. At the ultimate limit state, the increase in stress in the tendons for these structures is not localised at the critical section, but is averaged along the free length of the tendons between the contact points. Also, if no passive

reinforcement is provided in these structures, failure is characterised by the formation of a single wide crack at the section of maximum moment. For these reasons, the flexural behaviour of externally post-tensioned structures is very similar to that for internally unbonded post-tensioned structures.

However, unlike internally unbonded tendons which deflect or deform with the adjacent concrete, external tendons move together with the concrete structure only at the contact points (i.e. anchorages or deviators). This causes the eccentricity between the tendons and the centroid of the section to change along the span (Figure 2.4) under different external loads. This phenomenon is referred to as *second-order effect* by Virlogeux (1988).

Furthermore, high frictional forces are produced at the points along the span where tendons come in contact with the concrete at the deviators. These frictional forces cause stress variations to occur in the free length of the external tendons between deviators, whereas, in the case of internally unbonded tendons, the stress in the tendons is fairly constant between anchorages.

The moment curvature method can also be used to analyse for the ultimate moment of externally unbonded post-tensioned structures using the following assumptions:

1) Plane sections remain plane after loading.
2) Constitutive relationships for the steel and concrete are known.
3) The beam is assumed to be at a cracked state whenever the applied tensile stress exceeds the modulus of rupture, f_r.

The stress increase in tendons, $\Delta f_{ps(ult)}$, at ultimate is also required to be predicted for the ultimate moment analysis of externally post-tensioned structures. It has been suggested that the formulations used for stress increase at ultimate for internally unbonded prestressed structures can also be used for externally prestressed structures (ACI 318-83 (1983), Naaman (1994)). This might be considered to be inappropriate because these formulations were derived without considering second-order effect and frictional behaviour at deviators which are the two crucial factors that distinguish internally and externally unbonded structures. Hence, new formulations should be derived exclusively for external tendons.

2.3 State-of-the-art Review on the Ultimate Limit State Analysis of Unbonded Post-tensioned Structures

2.3.1 $\Delta f_{ps(ult)}$ for Internally Unbonded Prestressed Structures

Although this research is primarily concerned with the study of the ultimate limit state response of structures prestressed with external tendons, it is considered beneficial also to conduct a review on the research developments of internally unbonded prestressed structures. This is due to the fact that the two types of structure behave quite similarly to each other at ultimate conditions and that more research effort in the past has been focused on internally unbonded structures. The aim is to uncover important information about the ultimate behaviour of internally unbonded structures and to relate it to externally prestressed structures where relevant.

As described in Section 2.2.2, the prediction of the ultimate moment capacity of unbonded structures requires the stress increase in the tendons, $\Delta f_{ps(ult)}$, to be estimated. Numerous methods have been suggested by various codes of practice and researchers for the prediction of this stress increment.

2.3.1.1 Code Specifications

This section presents a summary of the methods, recommended by different design codes to predict $\Delta f_{ps(ult)}$ at ultimate for internally unbonded tendons.

- **AASHTO (1983)**

The stress increment $\Delta f_{ps(ult)}$ is given a fixed value of 103 N/mm^2, and hence the value is independent of the span-depth ratio, amount of passive reinforcement, etc.

This fixed value serves as a safe recommendation for the design of bridges with long spans. However, some researchers regard the method as being extremely conservative for structures with small span-depth ratios (Sowlat and Rabbat (1987) and Ramos and Aparicio (1996)).

- **ACI 318-83 (1983)**

  For beams with span/depth ratio ≤ 35

$$f_{ps(ult)} = f_{pe} + 10000 + \frac{f'_c}{100\rho_p} \quad psi \quad \langle f_{pe} + 60000\,psi \quad and\ f_{py} \quad \ldots\ldots (2.2)$$

  For beams with span/depth ratio >35

$$f_{ps(ult)} = f_{pe} + 10000 + \frac{f'_c}{300\rho_p} \quad psi \quad \langle f_{pe} + 30000\,psi \quad and\ f_{py} \quad \ldots\ldots (2.3)$$

  where $\rho_p = \frac{A_{ps}}{bd_{ps}}$

The equations are based on results reported by Mattock *et al* (1971) and provide a lower bound solution to the estimation of the increase in stress at the ultimate limit state for unbonded tendons.

- **BS8110 (1985)**

BS8110 (1985) states that for unbonded tendons, the stress in tendons $f_{ps(ult)}$ and distance to neutral axis c at the ultimate conditions, may be determined using Equations (2.4) and (2.5) respectively based on the studies of Tam and Pannell (1976). Note that the values of $f_{ps(ult)}$ should not be greater than $0.7 f_{pu}$.

$$f_{ps(ult)} = f_{pe} + \frac{7000}{\ell / d_{ps}}\left(1 - 1.7\frac{f_{pu}A_{ps}}{f_{cu}bd_{ps}}\right) N/mm^2 \quad \ldots\ldots (2.4)$$

$$c = 2.47\left(\frac{f_{pu}A_{ps}}{f_{cu}bd_{ps}}\right)\left(\frac{f_{ps}}{f_{pu}}\right)d_{ps} \quad \ldots\ldots (2.5)$$

Equation (2.4) is derived by taking the length of the zone of inelasticity (i.e. plastic hinge length) within the concrete as $10c$, and length ℓ is the length of tendons between anchorages.

- **Canadian Standard Association (1984)**

$$f_{ps(ult)} = f_{pe} + \frac{5000}{l_e}\left(d_{ps} - c_y\right) N/mm^2 \quad \ldots\ldots (2.6)$$

  where

  c_y = neutral axis depth assuming the tendons have yielded

l_e = length of tendons between anchors divided by the number of plastic hinges required to develop a failure mechanism in the span considered.

In order to derive Equation (2.6), the Canadian Standard Association (1984) replaced the unknown neutral axis depth at ultimate, c_u, in the formulation suggested by Tam and Pannell (1976), with the neutral axis depth when the tendons yield, c_y. Since the unbonded tendons generally remain within the elastic range, the values of c_y will always be conservatively larger than the true neutral axis depth, c_u.

However, Campbell and Chouinard (1991) found that Equation (2.6) under-estimates the value of $\Delta f_{ps(ult)}$ by approximately 50%. MacGregor and Breen (1989) also reported that there seemed to be a small conceptual error in Equation (2.6) when used for continuous structures. In the Canadian Standard Association (1984) the value of l_e is defined as the length of tendons between anchorages divided by the number of plastic hinges required to develop a failure mechanism. This definition would imply that for an interior span, where three hinges are formed in a mechanism, the effective length would be divided by three. This is considered by MacGregor and Breen (1989) to be incorrect because support hinges rotate only half the value of mid-span hinges, and hence the effective length should be divided by two instead.

- **Dutch Code (1984)**

The Dutch Code (1984) recommends that $f_{ps(ult)}$ at ultimate be five percent larger than f_{pe}.

$$f_{ps(ult)} = 1.05 f_{pe} \quad \text{.....(2.7)}$$

- **German Code (1980)**

Equation (2.8) is recommended in the German Code (1980) for the stress increase in unbonded tendons at ultimate conditions.

$$\Delta f_{ps(ult)} = E_{ps}\left(\frac{\Delta \ell_{ps}}{\ell_{ps}}\right) \quad \text{.....(2.8)}$$

where $\Delta \ell_{ps} = d_{ps}/17$

- **Swiss Code (1979)**

Swiss Code (1979) recommends Equations (2.9) and (2.10) for the ultimate limit state analysis of slabs with unbonded tendons.

End span:

$$f_{ps(ult)} = f_{pe} + 0.075E_{ps}\left(\frac{d_{ps}}{\ell_{ps}}\right) \quad \text{.....(2.9)}$$

Interior span:

$$f_{ps(ult)} = f_{pe} + E_{ps}\left(\frac{0.00125\ell_{ps} + 0.10h}{\ell_{ps}}\right) \quad \text{.....(2.10)}$$

2.3.1.2 Investigations Related to Ultimate Limit State Analysis

Baker (1949) recommended the following expression for evaluating the strain in unbonded tendons:

$$\varepsilon_{ps(ult)} = \varepsilon_{pe} + \lambda\Delta\varepsilon_{bps} \quad \text{.....(2.11)}$$

where

ε_{pe} = the effective strain.

$\Delta\varepsilon_{bps}$ = maximum strain increase in concrete at the level of prestress beyond effective prestress, assuming the tendon is bonded.

λ = coefficient defined as the ratio of change in the unbonded tendon strain to the change in the concrete strain adjacent to the tendon at the failure section assuming the tendon is bonded.

The stress in the tendons, $f_{ps(ult)}$, can then be evaluated from the calculated strain, $\varepsilon_{ps(ult)}$, using the stress-strain model of the prestress steel. Baker (1951) proposed that the safe limiting value for λ should be equal to 0.1 when used in the ultimate limit state analysis. Expressions for calculating λ were also suggested by Gifford (1954) and Janney *et al* (1956), but they were found to be too tedious to be used for practical design purposes (Mattock *et al* (1971)).

Warwaruk *et al* (1962) conducted an investigation on eighty-two simply supported partially prestressed beams and suggested that the increase in stress in the tendons is

related to the parameter ρ_p/f'_c. They proposed the following equation for the prediction of stress in unbonded tendons at the ultimate limit state:

$$f_{ps(ult)} = f_{pe} + \left(2110 - 49.4 \times 10^6 \rho_p / f'_c\right) \quad kgf/cm^2 \quad \text{.....(2.12)}$$

Mattock *et al* (1971) conducted tests on seven simply-supported and three continuous beams. They reported that the failure of an unbonded post-tensioned beam with no passive reinforcement is characterised by the development of a single wide crack at the section of maximum moment, instead of several well distributed cracks along the span. Thus, after cracking, the beam behaves as a *shallow tied arch* rather than as a flexural member, and failure is very sudden and explosive. It was observed that the cracking behaviour and the ultimate strength of these unbonded structures can be greatly improved by providing a moderate amount of bonded passive reinforcement in the prestressed beam. This behaviour was also reported to be true by Warwaruk *et al* (1962), Harajli and Kanji (1992), Tao and Du (1985) and Cooke *et al* (1981). In view of the advantage to be gained, Mattock *et al* (1971) suggested that a minimum area of reinforcement, equal to 0.4 percent of the area of that part of the beam section between the flexural tension face and the neutral axis of the gross area, should be provided in the design of unbonded structures.

Mattock *et al* (1971) also showed that the equation recommended by Warwaruk *et al* (1962) was too conservative and proposed Equation (2.13) to replace it:

$$f_{ps(ult)} = f_{pe} + \frac{1.4 f'_c}{100\rho_p} + 700 \quad kgf/cm^2 \quad \text{.....(2.13)}$$

Equation (2.13) was adopted with slight modifications by the 1971 and 1977 ACI Building Codes:

$$f_{ps(ult)} = f_{pe} + \frac{f'_c}{100\rho_p} + 10{,}000 \quad psi \quad \text{.....(2.14)}$$

where

$$f_{ps(ult)} \le f_{pe} + 60{,}000 \quad psi$$

Mojtahedi and Gamble (1978) reported that the span-depth ratio has a significant influence on the estimation of stress increase in the unbonded prestressing steel at the

ultimate limit state. Although they did not recommend any method for estimating the ultimate resistance of unbonded structures, a simple truss model was introduced (Figure 2.5) to demonstrate the influence of span-depth ratio on the stress increase in unbonded tendons.

In the truss model, it was assumed that the tie remained straight and that the strain in the tie was found by imposing a deflection, Δ, at the hinge. Figure 2.6 shows the graph ε_{ps} vs ℓ/d for a deflection of span/200. From Figure 2.6 it can be observed that, as the span-depth ratio increases, the strain in the tie decreases for the same deflection at the hinge. Although this work refers only to internally unbonded post-tensioned structures, it should be noted that other researchers reported that span-depth ratio also influences the behaviour of externally post-tensioned structures (Yaginuma and Kitada (1987,1988,1989) and Ramos and Aparicio (1996)). Based on the findings by Mojtahedi and Gamble (1978), Equation (2.14) was modified for ACI 318-83 to reflect the effect of span-depth ratio (see Equations (2.2) and (2.3)).

Tam and Pannell (1976) performed an extensive experimental and analytical investigation on the behaviour of beams prestressed with internal unbonded tendons. They tested a total of eight simply supported beams and proposed the following equation for estimating the stress in the prestress tendon at the ultimate limit state:

$$f_{ps(ult)} = f_{pe} + \left(\psi \varepsilon_{cu} E_{ps} \left(\frac{d_{ps} - c_u}{\ell_{ps}} \right) \right) \quad \text{.....(2.15)}$$

where

ψ was suggested to be 10.5 by Tam and Pannell (1976) from experimental results.

Equation (2.15) was found to give reasonable estimations for the prestress in unbonded tendons at the ultimate limit state and was adopted with slight alterations in BS8110 (1985) (see Equations (2.4) and (2.5)). However it should be noted that ψ = 10.5 was suggested based only on tests conducted on simply supported beams that were loaded with a concentrated point load at mid-span. This value may not be appropriate for beams with different configurations and loading conditions.

From their experimental tests on nine unbonded and three bonded one-way prestressed concrete slabs, Cooke *et al* (1981) proposed that Equation (2.14), used in ACI 318-77, is not applicable for prestressed structures with high span-depth ratios.

They also commented that although the equation suggested by Tam and Pannell (1976) takes span-depth ratio into consideration (Equation (2.15)), the use of the equation gives a large scatter of results when compared to the experimental data.

Tao and Du (1985) tested twenty-two partially prestressed beams with unbonded tendons that were loaded under third-point loading. Their main interests in the investigation were on the effects of the amount of unbonded prestressed steel, and bonded non-prestressed reinforcement on the stress increase in the unbonded tendons at ultimate. They concluded that $\Delta f_{ps(ult)}$ at ultimate conditions does depend on the amount of prestressed and non-prestressed steel, and it may be predicted using the following equation:

$$\Delta f_{ps(ult)} = 786 - 1920\, q_o \text{ N/mm}^2 \quad \text{..... (2.16)}$$

where

$q_o = q_e + q_s$

$q_e = (A_{ps}/bd_{ps}) \times (f_{pe}/f'_c)$

$q_s = (A_s/bd_{ps}) \times (f_y/f'_c)$

Campbell and Chouinard (1991) confirmed that the combined reinforcement ratio q_o introduced by Tao and Du (1985) is a rational parameter for the prediction of the ultimate stress level in unbonded prestress steel. They conducted tests on six unbonded beams and found that the stress in the prestressing steel at ultimate decreases with increasing amounts of bonded non-prestressed reinforcement. The authors also reported that Equation (2.16), recommended by Tao and Du (1985), gives reasonably good estimates for the stress increase in tendons at the ultimate limit state for the beams tested by them.

I'vanyi *et al* (1985) conducted experimental tests on twenty-eight prestressed slabs to study the collapse mechanism and the increase in strain in unbonded tendons. They observed that the cracks achieved at ultimate were nearly horizontal in the compression zone. These cracks initiate a very high concentration of compressive strain in the concrete which will eventually lead to crushing at failure condition. From their experimental results, the authors developed an analytical model for calculating the increase in strain in unbonded tendons for different loading stages. The method proposed is described by them as the *single cracked method.*

Harajli and Kanji (1990) conducted an experimental and analytical investigation on unbonded prestressed structures. They concluded that understanding the development of the plastic hinge length at ultimate is crucial for the estimation of stress in the prestressing steel, and that the parameter ρ_p/f'_c used in Equations (2.2) and (2.3) is not a rational design parameter. Harajli (1990) conducted an analytical study on the ultimate behaviour of internally unbonded structures, and proposed Equation (2.17) to replace Equations (2.2) and (2.3) in the 1983 ACI Building Codes. It is observed that the parameter span-depth ratio is actually incorporated into Equation (2.17):

$$f_{ps(ult)} = f_{pe} + \left(10000 + \frac{f'_c}{100\rho_p}\right)\left(0.4 + \frac{8}{l/d_{ps}}\right) \quad psi \quad \text{.....(2.17)}$$

where $f_{ps(ult)}$ shall not be taken greater than f_{py} nor f_{pe}+60000 psi.

Harajli and Hijazi (1991) developed a *non-linear analytical model* and a *span-depth ratio* model to estimate the stress increase in unbonded tendons up to the ultimate limit state. Both models were used to conduct parametric studies on the parameters that were believed to influence the strength of these beams. They concluded that span-depth ratio, loading arrangement , length of plastic hinge at ultimate and amount of passive reinforcement are the main parameters that influence the ultimate strength of unbonded beams. They also recommended the following equation for computing $f_{ps(ult)}$ in bonded and unbonded tendons:

$$\frac{f_{ps(ult)} - f_{pe}}{f_{pu}} = \gamma\left(\alpha - \beta\frac{c}{d_{ps}}\right) \quad \text{.....(2.18)}$$

where

$$\gamma = \frac{\ell_{plastic}}{\ell} = 1.0 + \left(\frac{1.0}{\frac{\ell}{d_{ps}}\left(0.95/f + 0.05\right)}\right)\left(\frac{n_o}{n}\right)$$

$\frac{n_o}{n}$ = ratio of number of loaded spans to total number of spans in the member

$\alpha = 0.4$; $\beta=0.7$ for two equal 1/3 point loads ($f = 3$)

$\alpha = 0.25$; $\beta=0.44$ for uniform distributed load ($f = 6$)

$\alpha = 0.1$; $\beta=0.18$ for a single concentrated load ($f = \infty$)

Sun (1991) introduced an analytical model for the ultimate analysis of unbonded structures. The assumptions used for the model were quite similar to those adopted by Harajli and Hijazi (1991). Harajli and Hijazi however emphasised that the single crack assumption used by Sun (1991) is only applicable to prestressed structures with no bonded passive reinforcement. They explained that if some passive reinforcement is included in the beam, the beam will behave as a flexural member and hence the assumption of single crack does not apply.

Friction between cable and duct has been listed as one of the parameters that influences the ultimate behaviour of unbonded tendons (Tam and Pannell (1976), Balaguru (1981)). However, little information is known about the extent of the effect in which friction has on the stress increase in unbonded tendons. As Burns *et al* (1991) stated, ' *When unbonded tendons are used in post-tensioned structures, the question is often raised, 'Does the prestress loss due to friction tend to balance out or redistribute with repetitious application of service loads?'*'. In an attempt to understand the frictional effects between ducts and tendons in unbonded structures, Burns *et al* (1991) tested two continuous unbonded beams with rectangular sections. From their tests, they observed that application of repeated service level loadings did not have a significant effect on the redistribution of tendon stress in unbonded tendons. However at ultimate conditions, when one of the continuous spans was overloaded whilst leaving the other unloaded, the tendon slipped towards the loaded span. Subsequently when the overload was removed, the slip caused the tendon stress to decrease on the loaded span and to increase on the unloaded span.

Alkhairi and Naaman (1991) conducted an extensive analysis on a large number of reported experimental results and introduced a coefficient, Ω_u, called the strain reduction coefficient at ultimate, for the prediction of ultimate stress in unbonded tendons. The strain reduction coefficient, Ω, was first introduced by Naaman (1990) for estimating the stress of external or unbonded tendons at the elastic or uncracked range of the beam behaviour. It represents the ratio of average strain increase in the unbonded tendon to the strain increase in the equivalent bonded tendon at the section of maximum moment (Equation (2.19)).

$$\Omega_u = \frac{\Delta\varepsilon_{ps\ \ unbonded}}{\Delta\varepsilon_{ps\ \ bonded}} \quad \text{.....(2.19)}$$

The new AASHTO LRFD Specification for Bridge Design has used the above methodology and recommended the following equation for the prediction of stress in unbonded tendons at the ultimate limit state (Naaman (1994)):

$$f_{ps} = f_{pe} + \Omega_u E_{ps}\varepsilon_{cu}\left(\frac{d_{ps}}{c} - 1\right)\ell_1/\ell_2 \leq 0.94 f_{py} \quad \text{.....(2.20)}$$

where

ℓ_1= length of loaded span or spans affected by the same tendon

ℓ_2 = total length of tendon between anchorages

ℓ' = length of span for which computation is carried out

$$\Omega_u = \frac{3}{\left(\ell'/d_{ps}\right)} \quad \text{for uniform or third point loading}$$

$$\Omega_u = \frac{1.5}{\left(\ell'/d_{ps}\right)} \quad \text{for uniform or third point loading}$$

Note that Equation (2.20) was derived from a rational analysis that takes into account the effects of the span-depth ratio and the loading condition of the beam.

2.3.2 Ultimate Analysis of Externally Prestressed Structures

2.3.2.1 Code Specifications

To the best of the author's knowledge, no proper formulation strictly for the estimation of stress increase in external tendons at the ultimate limit state has been provided in any code or specification to date. It has often been suggested that the formulae used for the prediction of stress increase in internally unbonded tendons be used as a guide for externally prestressed structures. However, as discussed earlier, external tendons behave differently from internal unbonded tendons due to second-order effects and frictional forces at the deviators.

Adopting a conservative approach, the UK Department of Transport BD 58/94 (1995) and Eurocode 2 (draft 1994) have recommended that zero increase in stress at the

ultimate limit state be used by engineers in the design of externally post-tensioned structures. This crude estimation has been found here to be too conservative and does not reflect the true behaviour of these structures.

2.3.2.2 Investigations Related to Ultimate Limit State Analysis

Sowlat and Rabbat (1987) conducted tests on three simply supported segmental beams to failure. Although all three specimens were dry jointed and prestressed with steel tendons, the method of prestressing was different for each beam. The tendons of the first beam were embedded within the beam's cross section and grouted after the prestressing process. The second and third beams were both prestressed with external tendons, but for the third beam, portions of the external ducts were embedded in a second stage concrete casting. They reported that the first beam with bonded tendons failed in a flexural mode, that is with the crushing of concrete in the compression zone and the yielding of tendons in the tensile zone. On the other hand, for the second and third beams, failures were observed to be due to shear compression at the top flange. This mode of failure for external tendons with no bonded reinforcement was also reported to be the case by MacGregor *et al* (1989).

Sowlat and Rabbat (1987) also analysed the ultimate flexural strength of the unbonded test beams, using equations recommended in the ASSHTO (1983) and ACI 318-83 Codes (1983). They concluded that while the ACI code equation gave a reasonably good estimate for the flexural strength, ASSHTO provisions underestimated it significantly. However it should be noted that the equations recommended in both codes are intended for beams with internally unbonded tendons. It is believed that the ACI code equation was only found to be reasonable because the externally prestressed test beam had several deviators placed along its span. The presence of closely spaced deviators reduce the free length-depth ratios, which consequently reduce the second-order effects; a phenomenon that differentiates the analysis of internal from external unbonded structures.

Virlogeux (1988) discussed the technical aspects related to the service and ultimate behaviour of externally prestressed structures. He identified two important characteristics that cause the flexural behaviour of externally and internally unbonded

post-tensioned structures to differ. They are the second-order effects and the frictional behaviour at the deviators. The second-order effect is defined by Virlogeux (1988) as '*the change in eccentric distance of the tendon for each loading sequence, caused by the fact that the tendon remains rectilinear between points of contact with concrete while the structure deforms non-linearly under load*'.

Frictional forces are developed at the deviators where tendons come into contact with the concrete. If the difference in prestress force in the tendon on either side of the deviator exceeds the generated frictional resistance, then the tendon will slip. These slippages, which are non-linear and not always reversible on removal of loads, are responsible for the variation in tendon force along the span between deviators.

Virlogeux (1988) introduced a non-linear analytical model for the evaluation of the flexural behaviour of external beams up to the ultimate limit state. The model was described to take into consideration, the second-order effect and frictional slippage at the deviators. The model uses an iterative procedure for the estimation of the stress increase in the tendons under a specified loading condition. The procedure first assumes a value for the stress increase in the prestress tendon, from which the curvatures and precompression strains of a number of sections defined along the span are calculated. With the evaluated curvatures and precompression strains, the change in length of the external tendon is estimated using Equations (2.21) or (2.22):

$$\Delta \ell_{12} = \ell_{12} - \sqrt{\ell^2 - (e_1 - e_2)^2} \quad \text{.....(2.21)}$$

where

$$\ell_{12} = \sqrt{(\ell - u_1 + u_2 + e_1 \sin w_1 - e_2 \sin w_2)^2 + (v_2 - v_1 + e_2 \cos w_2 - e_1 \cos w_1)^2}$$

If ℓ_{12} is much greater than e_1 & e_2, Equation (2.21) is simplified to:

$$\Delta \ell_{12} = u_2 - u_1 - e_2 w_2 + e_1 w_1 \quad \text{.....(2.22)}$$

Note: see Figure 2.7 for an explanation of the notation.

The increase in stress in the tendon is then evaluated and compared to the previously assumed value. If the two stresses do not come within a defined error of tolerance, the procedure is repeated. Virlogeux (1988) also described the technique of introducing frictional behaviour at deviators into the model. It involved the use of a complex

formulation for estimating the amount of tendon slip required to satisfy the force equilibrium conditions at the deviators.

Hindi *et al* (1995) and MacGregor *et al* (1990) performed studies on the behaviour of externally prestressed structures by testing a three-span continuous beam. The principal objectives were to determine if the action of bonding external tendons at the deviators and the provision of supplementary internal tendons will help increase the strength and ductility performance of such structures. From the tests results, they showed that the strength and ductility are greatly improved when tendons are anchored at closely spaced deviators. The reason for this is because for a given change in tendon length $\Delta\ell_{ps}$ at the ultimate condition, the reduced effective unbonded free length ℓ_{free} will yield a higher change in strain $\Delta\varepsilon_{ps(ult)}$ in the tendon (i.e. $\Delta\varepsilon_{ps(ult)} = \Delta\ell_{ps}/\ell_{free}$). This will consequently give a higher stress increase $\Delta f_{ps(ult)}$ in the tendon at the critical sections, thereby resulting in an increase in the ultimate strength. On the other hand, when the tendons were not anchored at the deviators it was observed that slippage of all tendons occurred during the ultimate load cycles, and a lower strength capacity was achieved. They also confirmed that providing supplementary bonded internal tendons in the structures improves ultimate behaviour.

MacGregor *et al* (1989) described a simple *rigid body* model for the analysis of externally post-tensioned bridges. He explained that after cracking or joint opening, the behaviour of externally prestressed structures may be characterised by the formation of hinges at critical sections. Hence, a simply supported structure can be modelled by two rigid members connected by a hinge, as shown in Figure 2.8. A similar model was introduced by Virlogeux (1988).

Assumptions used for the model:

1) When cracking occurs, only a single crack appears at the critical section.

2) The two lengths between the cracked section remains as rigid bodies.

Using the model, MacGregor *et al* derived Equation (2.23), which provides an expression for relating applied moments to mid-span deflections for external structures (see Figure 2.9):

$$\Delta \ell_{ps} = \frac{(\Delta T_j)\ell_{free}}{A_{ps} E_{ps}}$$

From mechanism and joint geometry:

$$\Delta = \frac{\ell_{free}\,\ell}{4 A_{ps} E_{ps} z_p^2}(M - M_d) \quad \text{..... (2.23)}$$

where

$\Delta \ell_{ps}$ = (shaded area above T_e) / $A_{ps}E_{ps}$

$\Delta T_j = (M\text{-}M_d)/z_p$

$T_e = A_{ps} f_{pe}$

See Figure 2.9 for the explanation of the notation.

The model can be used to simulate the ultimate behaviour of externally prestressed structures by introducing the plastic behaviour into Equation (2.23). This was done by assuming that concentrated rotations occur in the concrete adjacent to the critical section over a finite length. This length is defined as the *plastic hinge length,* and maximum curvatures over this length are limited by the current capacity of the concrete structure. Virlogeux (1988) suggested that the concentrated rotations may be assumed to be distributed over a plastic hinge length of $2z_s$, where z_s is equal to the distance from the compressive force to the passive reinforcement. This effectively gives a force diffusion angle of 45°. He also suggested that concrete compressive strains at the ultimate limit state be limited to ε_{cu} = 0.002 and the tensile strains be limited in the passive reinforcement to ε_s=0.01. MacGregor *et al* (1989) however commented that these limitations suggested by Virlogeux (1988) were too conservative and needed to be revised for more realistic results. Using Virlogeux's (1988) assumptions, the tendon elongation occurring in the concrete hinge region is given by Equation (2.24):

$$\Delta \ell_{plastic} = \phi_m \times z_p \times z_s \quad \text{..... (2.24)}$$

where ϕ_m is the allowable curvature

A drawback to the simple rigid models suggested by MacGregor (1989) and Virlogeux (1988) is that the second-order effect is not taken into consideration in the analysis. This means that changes in tendon eccentricity are ignored, which might not be a realistic assumption for beams with high span-depth ratio.

As described in Section 2.3.1.2, Naaman (1990) had introduced a technique for the stress evaluation of externally and internally unbonded tendons within the elastic uncracked and elastic cracked ranges. In the proposed method, the strains ε_{ps} in the unbonded tendons are analysed by first assuming that the tendons are bonded. The evaluated 'bonded' strains are then reduced to the unbonded condition by means of *strain reduction coefficients* (i.e. Ω or Ω_c). Naaman (1990) stated that the coefficients Ω and Ω_c depend on only two parameters: (1) the tendon profile, and (2) the loading condition. Hence the strain reduction coefficients need only to be determined once for the same loading and tendon configuration.

The general terms for evaluating the strain reduction coefficient at the uncracked state Ω is given in Equation (2.25). At the elastic cracked state, Naaman (1990) used an idealised elastic cracked beam (see Figure 2.11) to derive Equation (2.26), which is used to evaluate the strain reduction coefficient Ω_c.

$$\Omega = \frac{2}{M_{\max} e_{\max}} \int_0^{\ell/2} M(x)e(x)dx \quad \text{.....(2.25)}$$

$$\Omega_c = \Omega \frac{I_{cr}}{I_g} + \frac{2}{\ell}\left(1 - \frac{I_{cr}}{I_g}\right) \int_0^{\ell/2} \frac{M(x)e(x)}{M_{\max} e_{\max}} dx \quad \text{.....(2.26)}$$

Solutions for Ω and Ω_c were derived by Naaman (1990) for various combinations of loadings and tendon profiles (see Figure 2.10), and are reproduced in Tables 2.1 and 2.2 respectively. The representations of elastic uncracked, elastic cracked and idealised elastic cracked beam used by Naaman for the derivation of Ω and Ω_c are also presented in Figure 2.11.

Although Naaman's methodology is for the service state conditions, he suggested that the concept of a strain reduction coefficients can also be extended to cover the ultimate limit state. However, this method assumes that the second-order effect is negligible. This again might not be a valid assumption for external tendons, because several researchers (Virlogeux (1988) and Zhang *et al* (1993)) had reported that the second-order effects do significantly influence the behaviour of externally prestressed structures when the free tendon length-depth ratio is relatively high.

Naaman and Alkhairi (1993) introduced a non-linear analytical model for the prediction of the complete moment versus deflection response of a concrete beam prestressed with bonded, unbonded or external tendons. Alkhairi (1991) stated that the model is able to consider the effects of span-depth ratio, the shear effects on flexural deformation and second-order effects. The model uses an iterative procedure for estimating the stress increase in the prestress tendons, Δf_{ps}, by performing a non-linear analysis at various locations along the beam.

The assumptions used in the model are:

1) Plane sections remain plane after bending.
2) The constitutive relationships of materials are known.
3) Tension stiffening effects after cracking are neglected.
4) The beam is assumed to be cracked whenever the flexural tensile stress exceeds the modulus of rupture.
5) The cracked beam is composed of an elastic and/or inelastic cracked region, and an elastic uncracked region (see Figure 2.12).
6) Concrete within the cracked region is considered effective in resisting diagonal tensile stresses as long as the applied shear force is less than the cracking strength.
7) The beam is assumed to be reinforced with a minimum amount of vertical stirrups necessary to resist shear stresses at all the cracked sections along the beam.

The first step of the analysis proposed by Alkhairi (1991) is to assume that the stress in the unbonded tendon is equal to that calculated from the previous loading stage. The uncracked and cracked regions of the beam are then located (see Figure 2.12). The cracked region defines the portion of the beam where the external moment exceeds the cracking moment, M_{cr}, and the uncracked region marks the portion where no tensile cracking of the concrete has occurred. The elastic and inelastic cracked region is then subdivided into a number of *integration points*.

The second step involves the analysis of the section at the mid-span of the beam. A strain increment is introduced to the top concrete fiber strain at this section, and a force equilibrium analysis is then conducted to determine the various forces acting on

the section. This will lead to an estimation of the nominal internal moment at mid-span and consequently the external loading which is to be imposed on the structure for the next loading stage.

In the third step, force and moment equilibrium analyses are conducted at all other integration points away from the mid-span for the top and bottom concrete stresses and strains at these points. The process involves nested iteration procedures, conducted to determine the top concrete fiber strain and neutral axis depth at all integration points. Note that Equation (2.27) is used in the moment equilibrium analysis, where ΔM_{shear} is a fictitious moment introduced to take shear cracking effects into consideration. The variable ΔM_{shear} is derived from the truss mechanism introduced by Park and Paulay (1975).

$$M_{ext} = M_{int} + \Delta M_{shear} \quad (2.27)$$

The fourth step involves the estimation of the average strain increase in the concrete at the level of the unbonded tendon between end anchorages and/or deviators. After the stresses and strains are evaluated from the third step, the strains of the concrete at the initial eccentricity of the prestress are calculated at all the integration points along the span. These strains are integrated to provide an estimation of the increase in tendon length due to the deformation of the structure, from which the average stress and strain increments in the tendon are subsequently evaluated.

As an additional feature, Alkhairi (1991) incorporated an algorithm that takes into consideration the variation of eccentricity in the external tendons. The eccentricity variation is introduced to all the integration points, where force and moment equilibrium analyses are conducted again for a new estimation of the stress increase in the tendons. This newly evaluated stress increment in the tendons is then compared to the previously calculated value and the whole process is repeated until a stable value for Δf_{ps} is obtained.

The model suggested by Alkhairi (1991) appears to have three flaws when used to analyse externally prestressed structures. Firstly, in the proposed model, the tendon elongation due to external loading is estimated by integrating the strains in the concrete at the initial eccentricity of the prestress tendon. The evaluated tendon elongation is then used to predict the average stress increment in the tendon. This is

not considered strictly correct for external prestressing because the tendons do not move together with the concrete when the structure deforms. Hence integrating the concrete strain at the initial tendon eccentricity of the prestress tendon will not yield the correct elongation of the tendon length. As such, it may be more practical to evaluate the stress increase in external tendons by studying the change in position of the points of contact, as suggested by Virlogeux (1988). Secondly, the method used to introduce second-order effects appears to be very tedious and, new equations need to be derived for different tendon profiles used in the beam. Finally, Alkhairi did not consider the effects of tendon slippage at the deviators placed along the span of the externally prestressed structures.

Tan and Naaman (1993) presented a model, based on the *strut-and-tie method*, used to predict the strength of simply supported, externally prestressed concrete beams subjected to a mid-span concentrated load. The model involved the derivation of four inequality equations that define the four anticipated failure modes for external structures. The four failure modes and their corresponding equations are:

- failure of diagonal compressive strut

$$\lambda_p - 2\lambda_f \sin\alpha \le 0.8\frac{w_p}{h}\left(1 - 0.5\tan 15^o\right) + 0.72\frac{d_e}{h}\tan 15^o \quad \text{.....(2.28)}$$

- yielding of web reinforcement

$$\lambda_p - 2\lambda_f \sin\alpha \le \omega_v\left(1.8\frac{d_e}{h} + 1\right) + 2\lambda_{ci} \quad \text{.....(2.29)}$$

- yielding of internal longitudinal reinforcement

$$\lambda_p \frac{a}{h} - 2\lambda_f \frac{0.9d_{ps,e} + a\sin\alpha - a\tan\alpha}{h} \le 1.8\omega_f \frac{d_e}{h} \quad \text{.....(2.30)}$$

- yielding of external tendons

$$\lambda_f \le \omega_e \quad \text{.....(2.31)}$$

where

$$\lambda_p = \frac{P}{bhf'_c}$$

$$\lambda_f = \frac{F}{bhf'_c}$$

$$\lambda_{ct} = \frac{V_{ct}}{bhf'_c}$$

$$\omega_v = \frac{A_{sv} f_{yv}}{bsf'_c}$$

$$\omega_l = \frac{\left(A_s f_y + A_{ps} f_{py}\right)}{bhf'_c}$$

$$\omega_e = \frac{A_{ps,e} f_{py,e}}{bhf'_c}$$

α = angle of inclination of external tendons on each side of deviator, and

w_p = loading platen width.

The four failure inequality equations are linear and create a safe domain which defines the load and prestress force that can be safely applied on the structure (see Figures 2.13 and 2.14). The actual mode of failure of the beam is obtained by plotting a loading path defined by $\lambda_f = g(\lambda_p)$ where $g(\lambda_p)$ is a function based on load. Using the strain reduction concept introduced by Naaman (1990) and Naaman and Alkhairi (1991), the authors suggested the following equations for the definition of the loading function:

- linear elastic uncracked range of behaviour

$$\lambda_f = \lambda_{pe} \quad \text{.....(2.32)}$$

where

$$\lambda_{pe} = \frac{F_{pe}}{bhf'_c}$$

- linear elastic cracked range of behaviour

$$\lambda_f = \left[E_{ps,e}\left(\varepsilon_{pe} + \Omega_c \varepsilon_{cc}\right) + \Omega_c \frac{E_{ps}}{E_c} f_{ct}\left(\frac{d_{ps}}{c} - 1\right)\right]\frac{A_{ps,e}}{bhf'_c} \quad \text{.....(2.33)}$$

- ultimate flexural strength limit state

$$\lambda_f = \left[f_{pe} + \Omega_u E_{ps} \varepsilon_{cu}\left(d_{pe}/c - 1\right)\right]\frac{A_{ps,e}}{bhf'_c} \quad \text{.....(2.34)}$$

where for one point loading

$$\Omega_u = \frac{2.6}{\left(\ell / d_{ps,e}\right)}$$

Failure of the beam is deemed to occur when the loading path crosses one of the lines given by the failure equations (see Figure 2.13). However, it was considered that the method has very limited use in solving practical design problems, and too many assumptions were used for the derivation of the failure and loading path equations. It should be further noted that the method is dependent on the authenticity of the equations introduced by Naaman (1990) and Naaman and Alkhairi (1991).

Ten simply supported externally post-tensioned beams were tested by Zhang *et al* (1993), and the parameters that were studied in their investigation included the amount of reinforcing steel, loading pattern and tendon configuration. From the test results, they noted that the provision of more reinforcement steel in externally post-tensioned structures will generally improve the strength performance of these structures. It was also pointed out that the stress increment of tendons was higher when the beam was under a two point equidistant loading as compared to a one point loading system. This indicates that loading patterns do influence the ultimate behaviour of external structures. As for the tendon configuration, test results showed that beams with draped profiles can produce higher ultimate moments of resistance than for those with straight undeviated tendons. According to Zhang *et al* (1993) the increased strength is due to the reduced second-order effect experienced by beams with draped tendon profiles. In fact, the provision of deviators along the span of an externally prestressed beam will generally not only reduce second-order effect but also increases the stress in the tendons due to the frictional effects at the deviators (MacGregor (1989) and Yaginuma (1993)). Both these factors help to increase the strength of the structure at ultimate conditions. It was further observed from the tests that straight tendons did not reach their yield strength while draped tendons yielded at ultimate. From this, they concluded that the more rigorous design of such beams could lead to more efficient use of external tendons.

Zhang *et al* (1993) also introduced an analytical model for the prediction of ultimate moment of resistance of externally prestressed structures. The assumptions used for their model are:

1) Perfect bond exists between concrete and passive reinforcement.
2) Plane sections remain plane after bending.
3) Concrete in the tension zone is neglected.
4) Stress-strain laws of materials are known.
5) Frictional behaviour between tendons and deviators is conservatively neglected.
6) Changes in tendon length between two deviators or anchorages is estimated using the equation recommended by Virlogeux (1988) (Equation 2.22).

Curvature distribution along the span is first evaluated for an assumed ultimate load using the diagram introduced by Zhang *et al* (1993) (see Figure 2.15), based on experimental observations. The angular and vertical deformations for the assumed load are then calculated using Equations (2.35) and (2.36).

$$w_i = \int_{x_i}^{\frac{\ell}{2}} \phi(x)dx \quad \text{.....(2.35)}$$

$$v_i = \int_0^{x_i} x\phi(x)dx + x_i \int_{x_i}^{\ell/2} \phi(x)dx \quad \text{.....(2.36)}$$

The elongation of the tendon is estimated using Equation (2.22) and the moment of resistance at ultimate is determined by performing a force and moment equilibrium analysis at the critical section. The calculated ultimate load is checked with the assumed load, and the procedure is repeated if the two loads are not in reasonable agreement. Zhang *et al* (1993) compared the results derived from the analytical model with the experimental results and reported good correlation. However, two disadvantages were noted in the analytical model proposed by Zhang *et al* (1993). Firstly, frictional effects at the deviators are neglected, which may not be a reasonable assumption for beams with tendons that have large drape angles (Takebayashi *et al* (1994)). Secondly, only the curvature distributions for one point and two point loading systems were presented by the authors, which means that the curvature

distributions for other loading patterns would need to be investigated before the analytical model can be extended to more realistic situations.

Yaginuma and Kitada (1987, 1988, 1989) tested a total of twenty-two beams to study the flexural behaviour of externally prestressed structures at ultimate limit state conditions. From the experimental tests, they concluded that providing more passive reinforcement will increase the strength of externally prestressed beams, and that the ultimate moment of resistance decreases as the span-depth ratio of the structure increases. However, they found that the ultimate moment of beams with high span-depth ratios can be increased by providing deviators along the beam spans.

Yaginuma (1993) presented a finite element model for the analysis of these unbonded structures (shown in Figure 2.16), which he validated by comparing analytical results with test results.. The assumptions used in his model are:

1) Plane sections remain plane after bending.
2) Axial and flexural rigidity are constant within each element.
3) Forces acting on the centroid of a section do not change their direction after deformation.
4) Section forces in the element vary linearly in the element.
5) Shear deformations are negligible.

In order to help understand the behaviour of externally post-tensioned structures beyond the range of design loads, Muller and Gauthier (1990) developed a computer program (DEFLECT) to analyse the flexural behaviour up to the ultimate limit state. The program utilises finite-element principles to give the relationship between rotations and applied loads for each node defined along the span, from which the ultimate capacity of the beam can be estimated. The computer program was validated by comparing the results derived from it with those obtained experimentally. Although the moment-deflection curves obtained from the computer analyses and experimental tests were consistent at loads within the service range, inconsistencies were observed at ultimate load. This is because the analyses were conducted assuming the materials remained in the elastic range up to failure. Another drawback of the program is its inability to consider slippage of tendons at the deviators.

Muller and Gauthier (1990) conducted two computer runs on a similar beam with DEFLECT, one assuming tendons to be external and the second assuming the tendons to be bonded internally along its full length. It is surprising to note that the moment-deflection curves obtained from both runs were quite similar to each other.

The construction of the Bangkok Second Stage Expressway in Thailand involved one of the largest ever applications of external tendons for a viaduct project. The design and construction of it are described by Takebayashi (1993) and Hewson (1992, 1993). The bridge decks of this viaduct were formed from match-cast, precast segments with dry joints and external tendons. Due to the poor ground conditions, the decks were designed to be simply supported in order to overcome high differential settlements expected at the piers.

Dry jointing refers to the technique of constructing segmental bridge decks without applying epoxy resin to the joints between the segments. For this bridge, multiple unreinforced shear keys were used to help transfer the shear forces across the dry joints at all loading stages. Furthermore, sufficient longitudinal prestressing force was provided to ensure that the dry joints did not open under normal loading conditions.

Under ultimate loading conditions, the decks were checked for the ultimate moment of resistance using the same method as that for internally post-tensioned structures, but with a smaller value for the increase in stress in the external tendons. Whereas a stress increase of 103 N/mm^2 is permitted in the external tendon at ultimate by AASHTO (1983) specifications, Takebayashi *et al* (1993) reported that a value of 250 N/mm^2 was used in the design. They did not explain in detail how this higher value was derived, but stated that it was found to be reasonable based on *'a study on the failure mechanism of the simply supported structure which included a full length 3-D Finite Element Model'*.

Wieland (1990) conducted a computer study of the externally prestressed structure used for the bridge deck in the Bangkok Second Stage Expressway Project. He designed a two-dimensional finite-element model using the computer program ANSYS to predict the load versus deformation history and reported that the model is capable of considering geometric non-linearities. The model is also able to simulate the opening of the dry joints between the segments. This is done by placing a gap

element that allows only the transfer of compressive forces but not tensile forces, between the bottom nodal points at each joint. However, one major drawback about the model is that it cannot be used to check if the beam has failed due to the crushing of concrete at the joints. This is important because experimental tests have shown that the expected mode of failure for external beams is mostly due to the crushing of concrete and not the yielding of the prestress tendons. Hence if the proposed model is used, a separate analysis would be required to define the ultimate load which causes the failure of the beam due to crushing of the concrete.

A full scale loading test was also conducted on a typical segmental beam structure used in the Bangkok Second Stage Expressway Project (Takebayashi *et al* (1993)). The beam tested was made up of fourteen segments with a total span of about 45m. Figure 2.17 shows the arrangement of the test. The test beam was designed in accordance to the specifications stated in AASHTO Standard Specifications (AASHTO (1983)) and the Guide Specifications for Segmental Bridges (AASHTO (1989)). The main objectives in performing the test were to

- ensure that the diaphragms and deviators were adequately designed to resist the high post-tensioning forces
- study the behaviour of the span at service load conditions
- verify the safety of the beam at the ultimate load conditions.

The test was divided into two phases: the *design load phase* (Takebayashi *et al* (1993)) and the *destructive load phase* (Takebayashi *et al* (1994)). The design load phase involved loading the test span progressively to the service, decompression, design ultimate and design ultimate + 7% loads. This is achieved using kentledge of precast concrete segments and steel rebars. The destructive load phase was conducted two years later and involved loading the beam to collapse. Note that steel billets were used as imposed loading in the destructive test phase.

From the full scale test, Takebayashi *et al* reported that the actual flexural failure of the beam was 1.8 times higher than the designed ultimate moment. Hence the full scale test confirmed the adequacy of the design. They also noted that the stress increases in the external tendons were not uniform over their full length for tendons with large deviation angles at the deviators. They explained that this was due to the

large frictional forces generated at the deviators which prevented slippage of the tendons consequently producing force variations in the tendons between the deviators. They did not recommend any formulation for the prediction of the increase in stress at the ultimate limit state.

Ramos and Aparicio (1995,1996) developed a finite element model for the ultimate limit state analysis of externally prestressed concrete bridges. They introduced three kinds of elements for their finite element model:

- linear reinforced concrete elements with six degrees of freedom at each node
- prestressing elements (bonded internally and unbonded externally)
- joint elements for segmental bridges.

The following assumptions were made in the proposed model:

1) Shear deformations are neglected.
2) The sections remain plane after deformation.
3) Saint-Venant torsion is assumed, where free warping of the cross section is permitted

It was recognised that the external tendons may slip at the deviators and cause a reduction in the ultimate carrying capacity of the beam. This slippage of tendons at the deviators is dependent on the static frictional coefficient which is influenced by a large number of variables; for example kind of deviator, duct type, etc. Hence, they considered that it would be very difficult to obtain a reliable single value for the static frictional coefficient. Moreover, when friction at deviators is taken into consideration, the analysis becomes very complicated due to the non-linear and non-reversible nature of the problem, as described by Virlogeux (1988). For these reasons, they argued that it would be more practical to consider two extreme behaviours: (1) tendons slipping freely, and (2) tendons fixed at deviators; producing the lower and upper bounds to the ultimate load respectively. If the results obtained from the analysis of a beam using the two extreme assumptions did not vary much, as in the case of short beams, it would indicate that these beams are not sensitive to the slippage conditions at the deviators.

The proposed model has the following features

- considers material and geometric nonlinearity

- able to analyse simply supported or continuous beams
- able to assume that the contact points between tendons and concrete at the deviators are either fixed or frictionless
- able to model structures with both internal bonded and external unbonded tendons
- able to perform analysis on either monolithic or segmental structures.

Ramos and Aparicio (1996) used the proposed model to perform a parametric study on the ultimate behaviour of externally post-tensioned structures. The study involved 104 analyses on 74 different bridges and the assumptions used were:

1) Live load centred on the bridge axis.
2) Free slippage of tendons at deviators.
3) Joints of the segmental bridges analysed assumed frictionless.

Based on their parametric studies, they found that the formulations recommended in AASHTO LRFD Specifications for Bridge Design (Naaman (1994)) and ACI Committee 318-83 (1983) were too unconservative for normal bridge configurations. As a result of this, the authors recommended the following guidelines be included in the Spanish Design Codes, for the estimation of stress increase in external tendons:

- for simply supported box girder bridges, both monolithic and segmental, the $\Delta f_{ps(ult)}$ recommended for design is:

$$\Delta f_{ps(ult)} = 108 \text{ N/mm}^2 \quad (2.37)$$

- for simply supported double T-section monolithic bridges

$$\Delta f_{ps(ult)} = 122.5 \text{ N/mm}^2 \quad (2.38)$$

- for continuous monolithic box girder bridges, the increment of tendon stress $\Delta f_{ps(ult)}$ depends on the span-to-depth ratio and the prestressing layout; and graphs showing their relationship are presented in Ramos and Aparicio (1996).
- for continuous segmental box girder bridges:

$$\Delta f_{ps(ult)} = 39 \text{ N/ mm}^2 \quad (2.39)$$

However, Ramos and Aparicio (1996) stated that the increase in stress in the tendons, $\Delta f_{ps(ult)}$, is not affected by the variation in span-depth ratio or the amount of reinforcing

steel. This is contradictory to the experimental observations made by Zhang *et al* (1993) and Yaginuma and Kitada (1987, 1988 and 1989).

2.4 Ultimate Limit State vs. Service Limit State

The usual practice adopted for designing internally bonded prestressed structures is first to perform the design based on the service limit state, and then to check for the ultimate strength. The ultimate limit state checks for these structures are usually found to be satisfactory, if not, additional unstressed reinforcements can easily be provided to cover the shortfall without affecting the serviceability design. If the serviceability limit state is also critical for externally post-tensioned structures, then it may be sufficient to just introduce a simple and conservative method for estimating their ultimate strength (e.g. assuming that the stress increase in the prestress tendons is equal to zero at the ultimate conditions as suggested by UK DoT BD 58/94 (1995)). However, due to the eccentricity variations and small stress increments in the external tendons at the ultimate limit state condition, it is possible that serviceability checks alone might not be enough to yield a safe structure under overload conditions. Hence for externally post-tensioned structures, the level of accuracy of the ultimate checks may be important for the purpose of producing safe and reasonably economical designs.

A study was conducted by the author (Wong, (1994(e))), to check if the designs of externally post-tensioned structures using the specifications given in the British and American bridge codes, are controlled by either their service or ultimate limit state behaviour. The study was divided into three parts:

1) The first part of the study involved comparing two beams (denoted Design 1 and 2 respectively) designed using the British Codes (BS5400 (1985), BD 58/94 and BA 58/94). Design 1 utilised internally bonded tendons while Design 2 utilised external tendons. In the study, the resulting design cross sectional areas, tendon eccentricities and required prestressing forces were compared.

2) The second part of the study compared the two similar beams, denoted Design 3 and 4 respectively, designed using the American codes AASHTO (1985) and AASHTO (1989).

3) Finally, the third part of the study examined the analytical approach used to determine the ultimate strength of the externally prestressed structure used for the Bangkok Second Stage Expressway (Takebayashi (1993), Hewson (1993) and Hewson (1992)).

In order to allow easy comparison of the designs derived from the study, the design specification for the Bangkok Second Stage Expressway was adopted for all the bridge structures: a single box girder 10.7 m wide and 2.4 m deep, simply supported with a span of 45 m, of segmental construction incorporating dry joints. Only flexural behaviour was considered in the study.

Tables 2.3 and 2.4 show a summary of the structural properties of the beams derived from Part 1 and 2 of the study respectively. It may be observed that the structures obtained from Designs 1 and 2 (using the BS 5400 (1985), BA 58/94 (1995) and BD 58/94 (1995)) had higher service and ultimate loadings imposed on them when compared to those obtained from Designs 3 and 4 (using the AASHTO (1985) and AASHTO (1989)). This is because the HS loading system of the American Code is much smaller than the HA and HB loadings of the British Code. As a result of this, larger sections were derived for the structures designed using the British Code.

When Designs 1 and 2 were compared, based on serviceability limit states, the cross sectional area of Design 2 was smaller and required fewer strands as compared to Design 1. However, Design 2 failed to satisfy the ultimate strength requirements given in the specified code and had to be re-designed. The re-designed structure (denoted. Design 2*) showed an increase in the cross sectional area of approximately ten percent and an increase in the prestressing force of approximately forty percent. After this re-design to satisfy the ultimate limit state requirements, Design 2* was compared to Design 1. The following observations were made:

- the concrete cross sectional area of Design 2* was found to be twenty-three percent less than Design 1
- the eccentricities of the tendons in Design 2* were reduced
- the amount of prestressing force required for Design 2* was four percent higher than for Design 1.

Comparing Designs 3 and 4 based on service limit states alone indicated that the cross sectional area of Design 4 was twenty-four percent smaller than that of Design 3. Design 4 however did not satisfy the ultimate limit state checks and was therefore re-designed (Design 4*). The re-design caused the cross sectional area of Design 4 to increase by seven percent and the prestressing force of the system to increase by thirty-three percent. The final Design 4* as compared to Design 3 yielded the following information:

- the concrete cross sectional area given by Design 4* was about two percent less than Design 3
- the eccentricities of the tendons for Design 4* were reduced
- the amount of prestressing force required for Design 4* was eleven percent lower than Design 3.

The re-designed structure using the British Code (Design 2*) showed larger increases in the concrete section and initial prestressing force when compared to the re-designed structure using the American Code (Design 4*). This was to be expected, since the British Code specified a zero increase in stress in the tendons above initial prestress level at ultimate conditions, whereas the American specification permitted Equations (2.2) and (2.3) to be used for estimating the stress increase in external tendons at the ultimate conditions.

Part 1 and 2 of the study showed that designing externally prestressed structures based on their serviceability limit states (using both British and American bridge codes) may not always imply a safe structure at the ultimate conditions. In fact, both externally prestressed beams designed in the study based on service conditions had to be re-designed to satisfy their ultimate conditions. The degree of change required by the re-design, depends on the stress increment permitted in the tendons when estimating the ultimate strength of these structures. Generally, a smaller stress increment in the tendons permitted at the ultimate conditions will cause a greater change in the cross-sectional and prestressing force used for the structures.

The third part of the study was performed to evaluate the approach used for the design of the externally prestressed structure used in the Bangkok Second Stage Expressway. The structure was first checked for serviceability requirements using AASHTO (1983)

code and then subsequently for the ultimate limit state conditions using three different approaches for estimating the stress increase in the tendons at ultimate:

1) the recommendations given by the UK Department of Transport in (BD 58/94, 1995), where the stress increase in the tendons is recommended to be zero.
2) the recommendations given in ACI (1983) where the equations given by Equations (2.2) and (2.3) are recommended for the stress increment in prestressing tendons at the ultimate conditions.
3) a stress increase in tendons at the ultimate limit state of 250 N/mm^2, as recommended by the designers of the Bangkok Second Stage Expressway.

From the study, it was found that the structure failed to satisfy the ultimate requirements when the stress increase in the tendons was estimated using approaches (1) and (2). On the other hand, when approach (3) was adopted in the ultimate checks, the structure was found to be satisfactory. However, as mentioned in Section 2.3.2.2, it was not clear how the value 250 N/mm^2 was derived by the designers. Hence, the third part of the study shows that the stress increment assumed at the ultimate limit state is very important in the design of these structures. Structures may need to be re-designed if the assumed increase in tendon stress at ultimate is very small and conservative, resulting in a relatively uneconomical structure. On the other hand, the structure may be found to be satisfactory at ultimate conditions when a very high stress increase in the tendons is assumed, however such an increment will need to be justified unless the safety of the structure is to be compromised..

The study showed that the design of externally post-tensioned structures may well be controlled by their performance at the ultimate limit state. Hence an accurate estimation of the ultimate strength is essential for the design of these structures.

2.5 Research Objectives

A detailed review of the available literature on the ultimate limit state analysis of post-tensioned structures has been presented in this chapter. The review reveals that most studies that have been conducted on the behaviour of unbonded post-tensioned structures were directed towards structures with internally unbonded tendons. As such, when externally post-tensioned structures became more commonly used for

bridge construction, most design codes suggested that the guidelines recommended for internally unbonded prestressed structures may also be used for externally prestressed structures. This is erroneous because the flexural behaviour of internally unbonded structures has been shown to be very different from that of externally prestressed structures.

From the literature review, it is also evident the behaviour of externally prestressed structures at the ultimate conditions is influenced by several factors. These factors include second-order effects, span-depth ratio, and the amounts of prestress and passive reinforcement. However, not all of these factors have been considered in a single method to date for estimating the ultimate capacity of these structures.

Although service conditions usually control the design of internally bonded prestressed structures, this may be quite different for externally prestressed structures. Since the design of such structures may be controlled by the ultimate limit state, an accurate estimation of the ultimate strength becomes important for the design of safe and reasonably economical externally post-tensioned structures.

From the above arguments, the following is a list of objectives that has been defined for the research programme:

1) There is a need to build a rational analytical model exclusively for externally post-tensioned structures that is able to predict their flexural response at various loading stages accurately up to ultimate conditions.
2) The proposed model must be validated by comparing results derived from the model with those obtained experimentally.
3) It is considered crucial to identify the various factors that influence the behaviour of externally post-tensioned structures and to use the proposed model to study the extent of their influence on the flexural behaviour of these structures.
4) There is also a need to check if the existing recommendations given in the codes of practice can be used accurately to predict the ultimate strength of externally prestressed structures for the practical analysis and design of these structures.

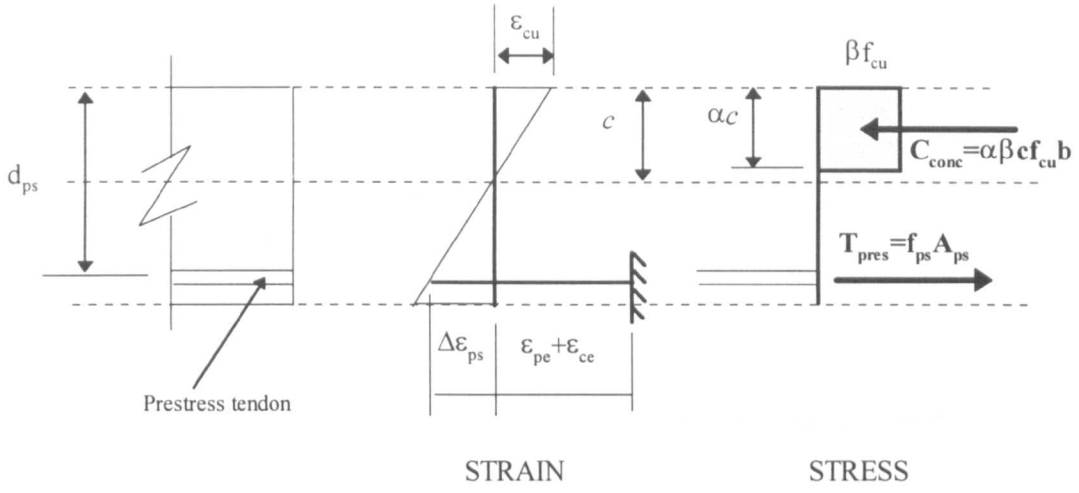

1) Assume an ultimate strain at top fiber (eg. $\varepsilon_{cu} = 0.0035$)
2) Assume depth of neutral axis c and compute internal compressive force C_{conc}
3) Compute total strain in prestressing steel ($\varepsilon_{ps}=\Delta\varepsilon_{ps}+\varepsilon_{pe}$)
4) Check to see if assumed c gives $C_{conc}=T_{pres}$; if not go to step 1
5) With evaluated c find ϕ and moment of resistance

Figure 2.1: The ultimate limit state for internally bonded post-tensioned structures (taken from Lin and Burns (1982))

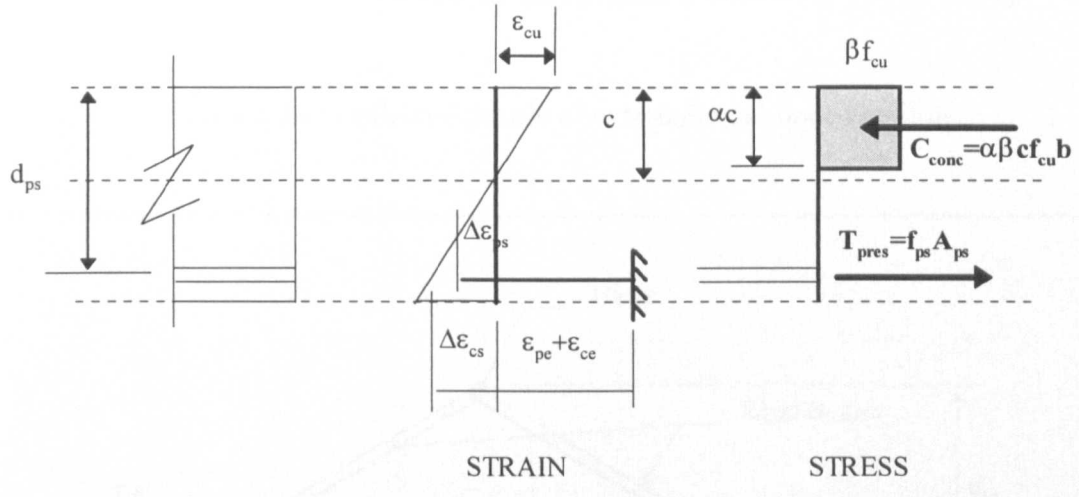

Figure 2.2: Stress and strain distribution at the ultimate limit state for unbonded post-tensioned structures

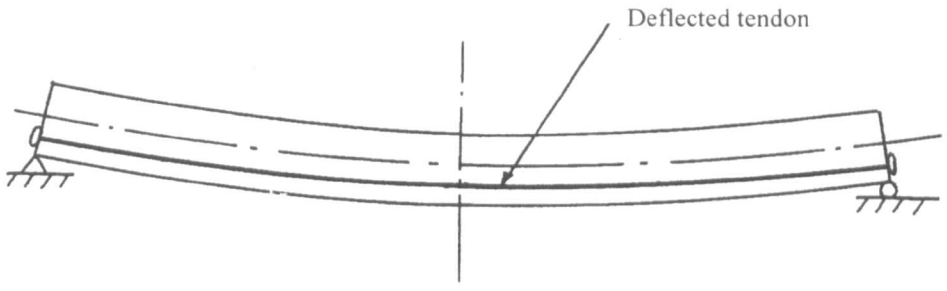

Figure 2.3: Deflected profile of internally unbonded tendon

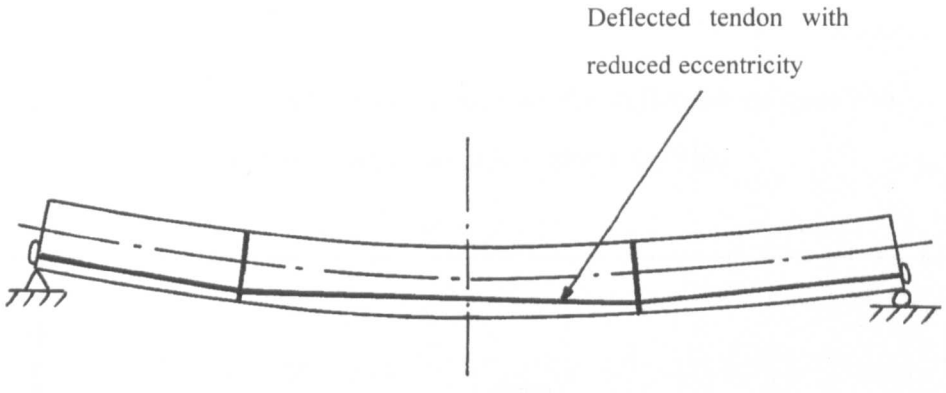

Figure 2.4: Deflected profile of externally unbonded tendon

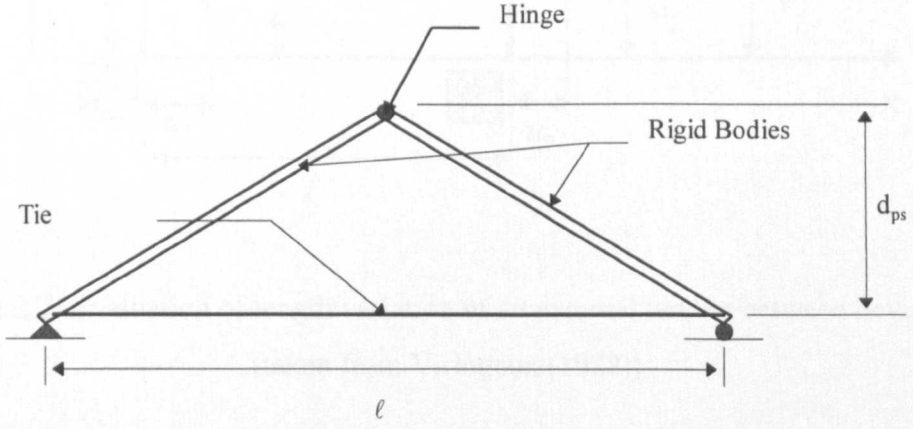

Figure 2.5: Truss model taken from Mojtahedi and Gamble (1978))

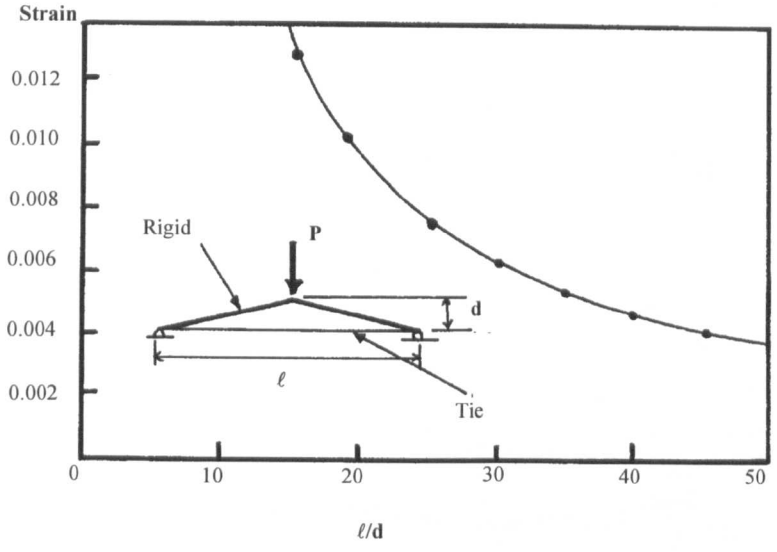

Figure 2.6: Steel strain vs Span-depth ratio for deflection of span/200
(taken from Mojtahedi and Gamble (1978))

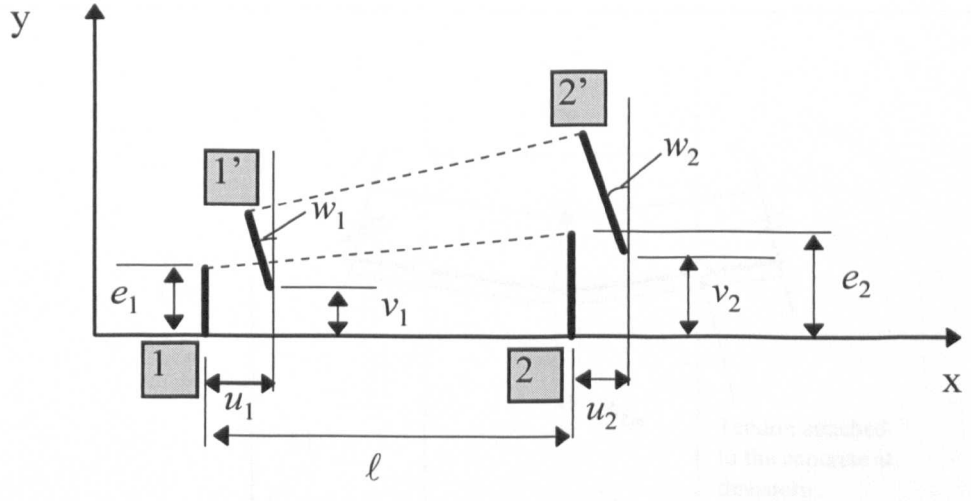

Figure 2.7: Evaluation of length variation of an external tendon between deviators
(taken from Virlogeux (1988))

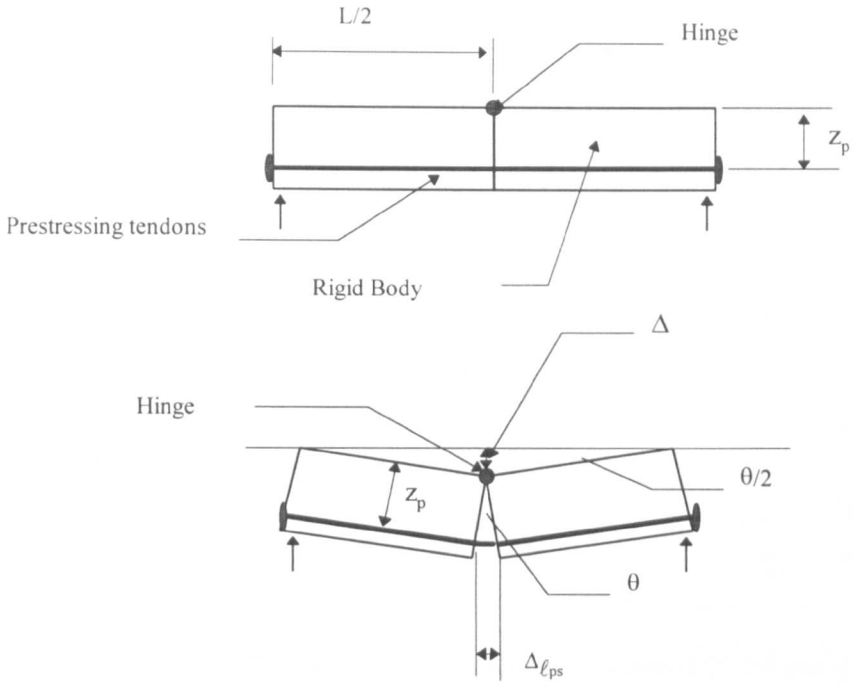

Figure 2.8: Rigid body model for externally post-tensioned structures suggested by MacGregor *et al* (1989)

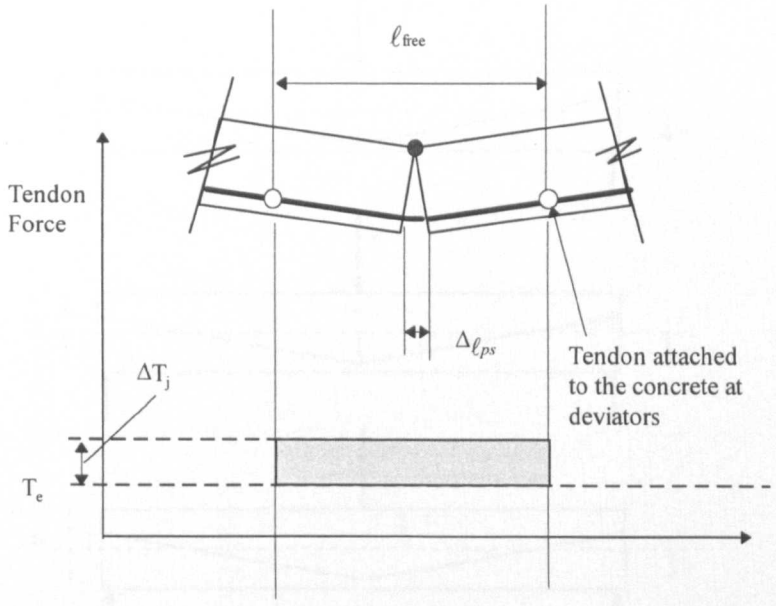

Figure 2.9: Tendon force variation near the cracked section for unbonded tendons (adopted from MacGregor *et al* (1989))

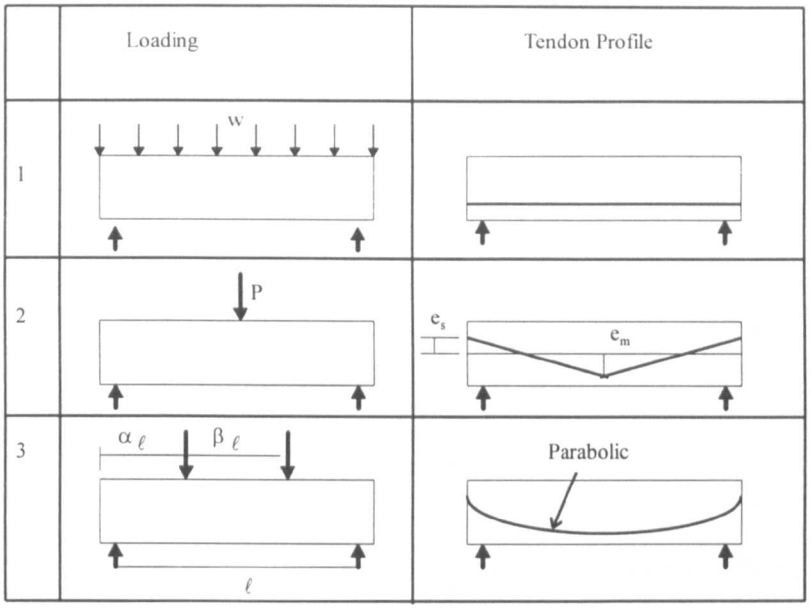

Figure 2.10: Typical loadings and tendon profiles considered in the computation of the strain reduction coefficients Ω and Ω_c
(taken from Naaman (1990))

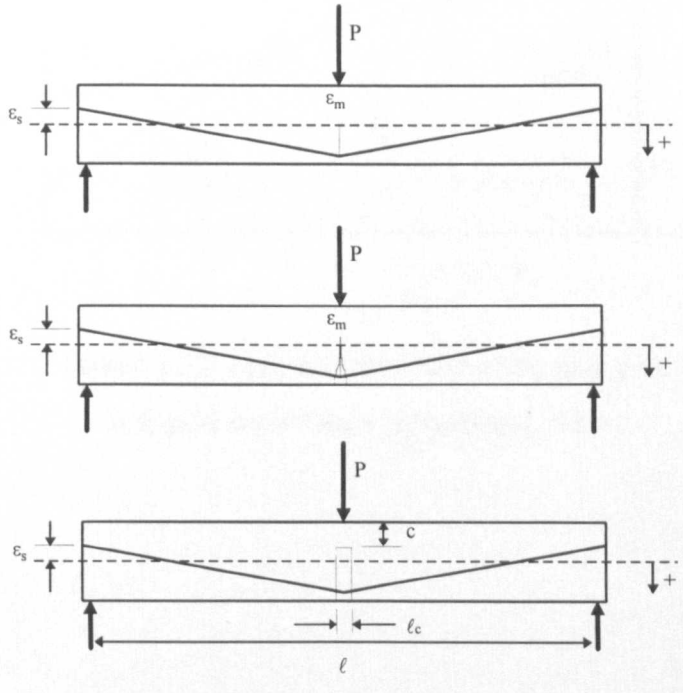

Figure 2.11: Typical representation of elastic uncracked, elastic cracked and idealised elastic cracked beam
(taken from Naaman (1990))

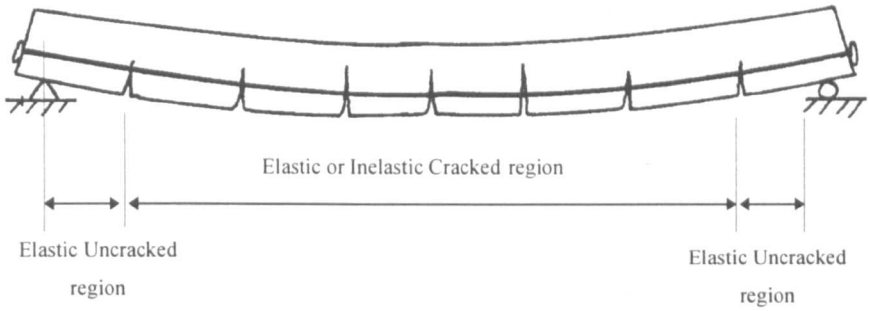

Figure 2.12: Idealization of beam deformation after cracking by Naaman and Alkhairi (1993)

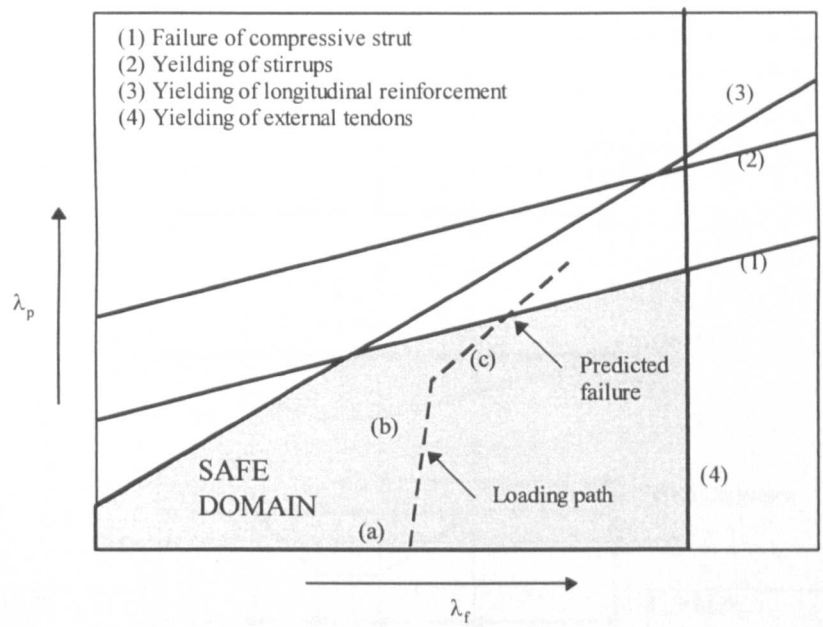

Figure 2.13: Safe domain and loading path plot (adopted from Tan and Naaman (1993))

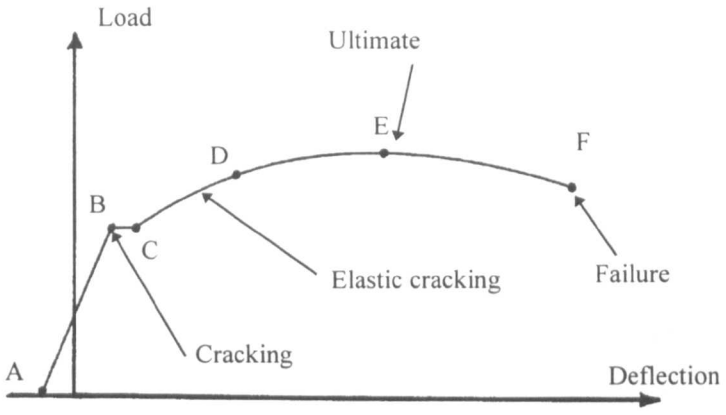

Figure 2.14: Modes of failure for externally prestressed beams

(adopted from Tan and Naaman (1993))

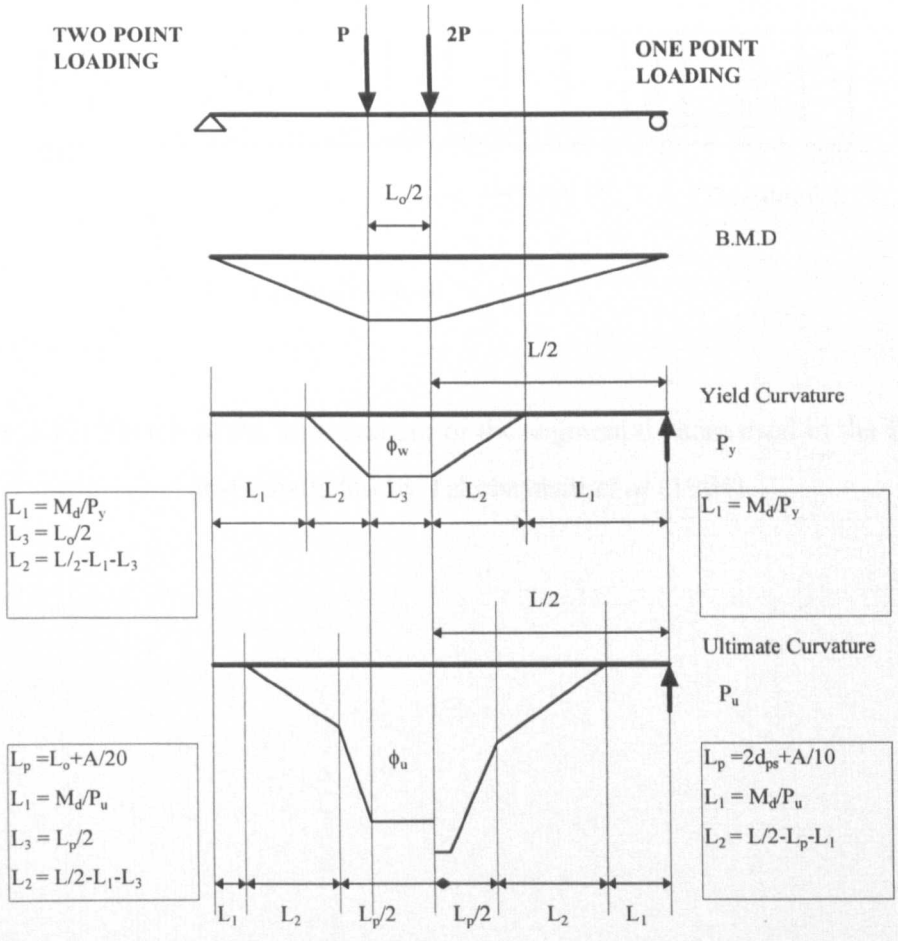

Figure 2.15: Idealised curvature distribution for one and two point loading systems

(adopted from Zhang *et al* (1993))

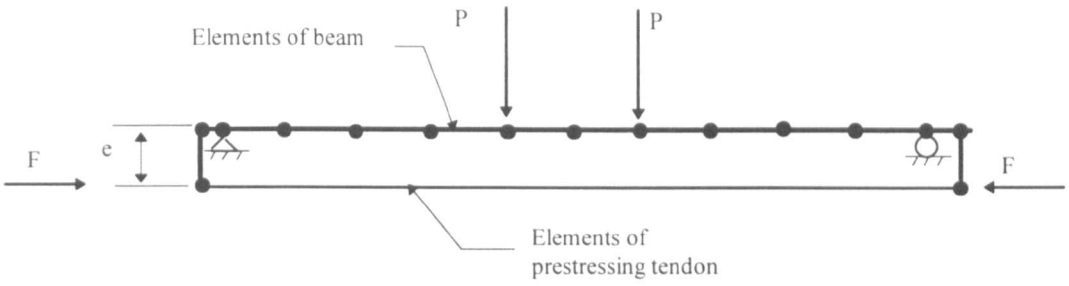

Figure 2.16: Model of external prestressed beam by Yaginuma (1993)

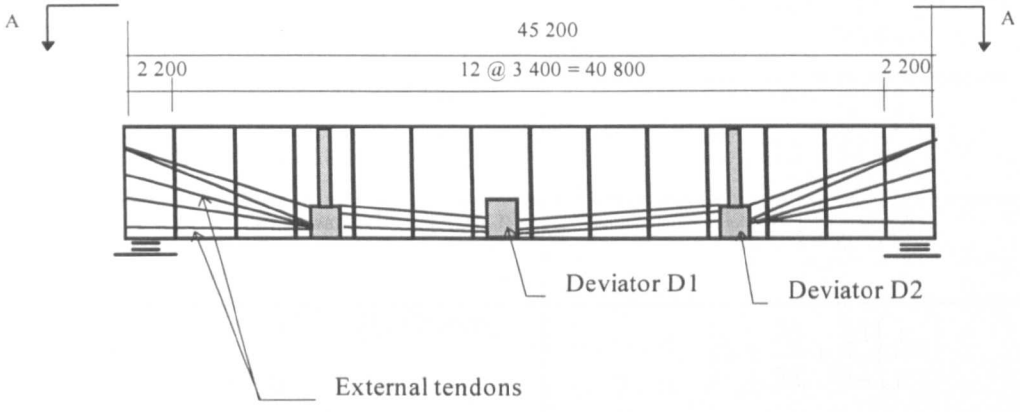

Figure 2.17: Sketch of the arrangement of the segmental beam used in the full-scale test conducted by Takebayashi *et al* (1994)

Loading Type and Tendon Profile	**Strain Reduction Coefficient: Uncracked State**
Uniform Load and Straight Tendons	$\Omega = \frac{2}{3}$
Uniform Load and Single Draping Point	$\Omega = \frac{5}{12} + \frac{1}{4}\left(\frac{e_s}{e_m}\right)$
Uniform Load and Parabolic Tendon	$\Omega = \frac{8}{15} + \frac{2}{15}\left(\frac{e_s}{e_m}\right)$
Concentrated Midspan Load and Straight Tendons	$\Omega = \frac{1}{2}$
Concentrated Midspan Load and Single Draping Point	$\Omega = \frac{1}{3} + \frac{1}{6}\left(\frac{e_s}{e_m}\right)$
Concentrated Midspan Load and Parabolic Tendon	$\Omega = \frac{5}{12} + \frac{1}{12}\left(\frac{e_s}{e_m}\right)$
Third Point Loads and Straight Tendons	$\Omega = 1 - \alpha = \frac{2}{3}$
Third Point Loads and Single Draping Point	$\Omega = \frac{23}{54} + \frac{13}{54}\left(\frac{e_s}{e_m}\right)$
Third Point Loads and Parabolic Tendons	$\Omega = \frac{44}{81} + \frac{10}{81}\left(\frac{e_s}{e_m}\right)$

* Refer to figures 2.10 and 2.11 for notation

Table 2.1: Expressions for the Strain Reduction Coefficient Ω for the Uncracked State.

(taken from Naaman (1990))

Loading Type and Tendon Profile	**Strain Reduction Coefficient: Cracked State**
Uniform Loads and Straight Tendons	$\Omega_c = \Omega\frac{I_{cr}}{I_g} + \left(1 - \frac{I_{cr}}{I_g}\right)\left(\frac{\ell_c}{\ell} - \frac{1}{3}\left(\frac{\ell_c^3}{\ell^3}\right)\right)$
Uniform Load and Single Draping Point OR Concentrated Midspan Load and Parabolic Tendon	$\Omega_c = \Omega\frac{I_{cr}}{I_g} + \left(1 - \frac{I_{cr}}{I_g}\right)\left[\frac{1}{2}\left(\frac{e_s}{e_m}\right)\frac{\ell_c^2}{\ell} - \frac{1}{4}\left(\frac{e_s}{e_m}\right)\frac{\ell_c^4}{\ell} + \frac{\ell_c}{\ell} - \frac{1}{2}\left(\frac{\ell_c^2}{\ell^2}\right) - \frac{1}{3}\left(\frac{\ell_c^3}{\ell^3}\right) + \frac{1}{4}\left(\frac{\ell_c^4}{\ell^4}\right)\right]$
Uniform Load and Parabolic Tendon	$\Omega_c = \Omega\frac{I_{cr}}{I_g} + \left(1 - \frac{I_{cr}}{I_g}\right)\left[\frac{e_s}{e_m}\left(\frac{1}{3}\left(\frac{\ell_c^3}{\ell^3}\right) - \frac{1}{5}\left(\frac{\ell_c^5}{\ell^5}\right)\right) + \frac{\ell_c}{\ell} - \frac{2}{3}\left(\frac{\ell_c^3}{\ell^3}\right) + \frac{1}{5}\left(\frac{\ell_c^5}{\ell^5}\right)\right]$
Concentrated Midspan Load and Straight Tendons	$\Omega_c = \Omega\frac{I_{cr}}{I_g} + \left(1 - \frac{I_{cr}}{I_g}\right)\left[\frac{\ell_c}{\ell} - \frac{1}{2}\left(\frac{\ell_c^2}{\ell}\right)\right]$
Concentrated Midspan Load and Single Draping Point	$\Omega_c = \Omega\frac{I_{cr}}{I} + \left(1 - \frac{I_{cr}}{I_g}\right)\left[\left(\frac{\ell_c}{\ell}\right)\left(1 - \frac{1}{2}\left(\frac{\ell_c}{\ell}\right)\right) + \left(\frac{1}{2} - \frac{1}{3}\left(\frac{\ell_c}{\ell}\right)\right)\left(\frac{e_s}{e_m} - 1\right)\frac{\ell_c^2}{\ell^2}\right]$

* Refer to figures 2.10 and 2.11 for notation

Table 2.2: Expressions for the Strain Reduction Coefficient Ω_c for the Cracked State. (taken from Naaman (1990))

CRITERIA	Beam no.		
	1	2	2*
Post-tensioning system	Internal	External	External
Loading			
M_{min} (KNm)	43,538	30,193	33,564
M_{max} (KNm)	87,899	74,554	77,926
M_{ult} (KNm)	113,873	98,533	102,416
Properties of derived structure			
Area of concrete (mm^2)	$7.14x10^6$	$4.97x10^6$	$5.525x10^6$
Weight (KN/m)	172	119	132.6
Z_t (mm^3)	$4.78x10^9$	$4.3x10^9$	$4.37x10^9$
Z_b (mm^3)	$3.93x10^9$	$3.29x10^9$	$3.74x10^9$
eccentricity (mm)	973.5	765	595
No. of strands	456	342	475
A_{ps} (mm^2)	63,840	47,880	66,500
P_i (KN)	84,600	63,450	88,125
M_r at ultimate (KNm)	161,263	82,107	103,048
Ultimate Checks	Pass	Fail	Pass

Table 2.3: Summary of structures designed with the British bridge code.

(taken from Wong (1994(b)))

CRITERIA	Beam no.		
	3	4	4*
Post-tensioning system	Internal	External	External
Loading			
M_{min} (KNm)	37,463	25,758	27,581
M_{max} (KNm)	56.814	45,151	46,974
M_{ult} (KNm)	82,575	67,610	69,980
Properties of derived structure			
Area of concrete (mm^2)	$5.58x10^6$	$4.24x10^6$	$4.54x10^6$
Weight (KN/m)	134	102	109
Z_t (mm^3)	$2.99x10^9$	$2.82x10^9$	$2.91x10^9$
Z_b (mm^3)	$2.47x10^9$	$2.06x10^9$	$2.48x10^9$
eccentricity (mm)	973	1038.5	848
No. of strands	342	228	304
A_{ps} (mm^2)	47,880	31,920	42,460
P_i (KN)	63,450	42,300	56,400
M_r at ultimate (KNm)	143,830	60,262.5	56,400
Ultimate Checks	Pass	Fail	Pass

Note : * Effective property

Table 2.4: Summary of structures designed with the American bridge codes.

(taken from Wong (1994(b)))

Chapter 3

Parameters Affecting the Ultimate Behaviour of Externally Post-Tensioned Structures

3.1 General

An extensive literature review on the ultimate limit state behaviour of externally post-tensioned structures has been conducted by the author and presented in Chapter Two. From the literature review, it is evident that externally post-tensioned structures are slowly gaining world wide acceptance as a solution for many bridge design projects. The principle reasons for this are that the tendons can be easily inspected for corrosion problems, re-stressed for any loss in prestressing and replaced if they become faulty. However, in spite of all these advantages, engineers still use this technique of bridge construction with reservation. In part this is due to a lack of understanding of the behaviour of these structures under ultimate limit state conditions.

As explained in Chapter Two, the ultimate behaviour of these structures is very different from internally bonded post-tensioned structures because of the lack of bond between concrete and steel, and the loss of eccentricity of the tendons at the ultimate conditions due to second-order effects. Hence the conventional analytical method used to predict the ultimate moment capacity of internally bonded prestressed structures cannot be used directly for externally prestressed structures.

Some researchers however have suggested that the conventional analytical method can still be used for externally prestressed structures, provided the stress increase in the tendons at the ultimate conditions can be predicted. This, however, is not an easy task because the stress increase in the tendons at the ultimate conditions is dependent on many parameters. As a result, several empirical methods for predicting the stress increase have been proposed by several codes of practice and researchers with the common purpose of providing an easy design method.

However, this analytical method is not considered satisfactory for two main reasons. Firstly, the loss of eccentricity due to second-order effects is not taken into consideration, possibly resulting in an over-estimation of the ultimate flexural strength. Secondly, the empirical methods for stress increase are either in the form of a single value (making them appropriate for only a small group of externally post-tensioned structures) or were originally proposed for internally unbonded post-tensioned structures. Hence, there is a need to propose a more reliable analytical solution for predicting the ultimate strength of these structures. Before such a method can be proposed, it is crucial that a preliminary investigation of the parameters that may influence ultimate behaviour is first carried out.

From the literature review and analytical studies conducted by the author, the following is a list of parameters that are believed to have an influence on ultimate behaviour:

1) span-depth ratio,
2) amount of non-prestressed reinforcement,
3) initial prestress force and amount of prestressed reinforcement,
4) loading pattern,
5) frictional effects at deviators,
6) free-length to depth ratio.

Note that parameters (1) - (4) are applicable to all externally post-tensioned structures while parameters (5) and (6) only apply to those with deviators located along their span.

This chapter presents an introductory discussion on the influence of each parameter. Subsequently a detailed parametric study has been conducted on these parameters using the non-linear models proposed in Chapter Four, the results from which are presented in Chapter Six.

3.2 Externally Prestressed Beams with and without any Deviators

3.2.1 Span-Depth Ratio

Span-depth ratio is defined here as the ratio of the effective depth to the centroid of the prestressing tendon group to the overall span of the structure between simple supports. From the literature review, it was found that the span-depth ratio is indirectly related to two important variables which are used for the ultimate analysis of externally prestressed structures. These are:

1) the stress increment in the external tendons $\Delta f_{ps(ult)}$, and

2) the variation in tendon eccentricity $\Delta_{eccen(ult)}$, at ultimate limit state.

Mojtahedi and Gamble (1978) were the first to propose that there may be a relationship between the stress increase in internally unbonded prestress tendons at the ultimate limit state and the span-depth ratio. As discussed in Chapter Two, they introduced a simple rigid-body model (Figure 2.5) to represent the behaviour of unbonded prestressed structures. The model was used to show the relationship between the increase in strain in the tie member (which represented the prestressing tendon) $\Delta\varepsilon_{ps}$ and the span-depth ratio L/d_{ps} for a fixed deflection value Δ at the hinge (see Figure 2.6). They found that the strain induced in the tie member decreases as the span-depth ratio of the structure increases.

Furthermore, Harajli (1990) and Tam and Pannell (1976) reported that the total elongation of the internal unbonded tendons between anchorage ends was due mainly to the lengthening of the tendons occurring at the plastic regions of the beam. Using Equation (3.1), Harajli (1990) showed that the lengthening of the tendons at the plastic region, and consequently the stress increase in the tendons, depended on both the span-depth ratio and the loading geometry of the beam.

$$\ell_{plastic} = L\left(\frac{0.95}{f} + 0.05 + \frac{1}{L/d_{ps}}\right) \quad \text{.....(3.1)}$$

where f is a load geometry factor defined by Harajli (1990)

From his studies, Harajli also found that increasing the span-depth ratio of unbonded structures will generally lead to a significant decrease in the stress increment in the tendons at ultimate. This is similar to the conclusion made by Mojtahedi and Gamble (1978).

However, in the case of external tendons, the tendons do not move together with the adjacent concrete as the structure deforms. Hence, there is no concentration of tendon elongation at plastic regions in the structure. In fact, the change in length of the external tendons under any loading sequence, depends primarily on the overall deformation of the structure. As a result, the effect which the span-depth ratio has on the stress increase in internally unbonded tendons, described earlier, cannot be expected to be the same for external tendons. It is interesting to note that Ramos and Aparicio (1996) confirmed this by reporting that, from their studies, they found that the increase of stress in external tendons does not change significantly with a variation of the span-depth ratio.

Virlogeux (1988) and Zhang *et al* (1993) considered that the span-depth ratio may have an influence on the variation in eccentricity occurring in externally prestressed structures. They explained that when loads are applied to such a structure, only at the contact points (i.e. deviators or anchorages) will the tendons move together with the structure. As such, a reduction in the eccentricity will occur at sections away from the deviators, since the deformation of the tendons are rectilinear between the contact points and do not conform with those elsewhere along the structure. This reduction in eccentricity will result in a direct loss of strength at ultimate conditions for such beams. The phenomenon is referred to as the *second-order effect* by Virlogeux (1988), and is described to be one of the primary characteristic that distinguish the flexural behaviour of externally post-tensioned structures from internally unbonded post-tensioned structures.

Yaginuma and Kitada (1988) found that structures with low span-depth ratio (less than or equal to 11) are not significantly affected by the second-order effect. They also reported that the flexural performance at ultimate for externally prestressed structures decreases as the span-depth ratio increases.

As part of a preliminary exercise carried out to study the relationship between the span-depth ratio and the ultimate behaviour of externally prestressed structures, two rigid-body models were developed by the author to represent the ultimate mechanism of internally and externally unbonded post-tensioned structures. Note that both models were extensions to the original rigid-body model suggested by Mojtahedi and Gamble (1978). These models assumed that when an unbonded beam reaches its ultimate capacity, failure is characterised by the formation of a hinge and single wide crack at the critical section (mid-section for simply supported structures). The proposed rigid-body models for the internally and externally unbonded post-tensioned structures are shown in Figures 3.1 and 3.2 respectively.

For the internally unbonded model (Figure 3.1), the following equations were derived to obtain a relationship between the strain increments in the tendons $\Delta\varepsilon_{ps}$ and the deflection Δ at mid-span:

$$\delta h = \theta \times d_{ps}$$

$$\delta h = \frac{4\Delta d_{ps}}{L}$$

$$\Delta\varepsilon_{ps} = \frac{\delta h}{L}$$

$$\Delta\varepsilon_{ps} = \frac{4\Delta d_{ps}}{L^2} \qquad \text{.....(3.2)}$$

The deflection Δ was fixed at $L/200$, and Equation (3.2) was rewritten as:

$$\Delta\varepsilon_{ps} = \frac{1}{50} \times \frac{1}{L/d_{ps}} \qquad \text{.....(3.3)}$$

Figure 3.3 shows the relationship between $\Delta\varepsilon_{ps}$ and L/d_{ps}, plotted using Equation (3.3). Note that $\Delta\varepsilon_{ps}$ was observed to be inversely proportional to L/d_{ps}.

Equation (3.2) cannot be simply used to represent the relationship between $\Delta\varepsilon_{ps}$ and L/d_{ps} for externally post-tensioned structures since the depth to the centroid of the external tendons d_{ps} is not constant. Studying the model shown in Figure 3.2, the following equations were derived to express a relationship between the strain increment in the tendons and the span-depth ratio for externally prestressed structures:

$$L' = 2\left[\frac{L}{2\cos(\frac{2d_{ps}}{L})}\cos\left(\alpha - \frac{\theta}{2}\right)\right]$$

$$L' = \left[\frac{L}{\cos\alpha} \times \cos\left(\alpha - \frac{\theta}{2}\right)\right]$$

$\Delta\ell = L' - L$

$$\Delta\ell = \frac{L}{\cos\alpha} \times \cos\left(\alpha - \frac{\theta}{2}\right) - L$$

$$\Delta\ell = L\left[\frac{\cos(\alpha - \theta/2)}{\cos\alpha} - 1\right]$$

$$\frac{\Delta\ell}{L} = \Delta\varepsilon_{ps} = \left[\frac{\cos(\alpha - \theta/2)}{\cos\alpha} - 1\right] \quad \text{.....(3.4)}$$

where

$\alpha = (2d_{ps}/L)$

$\theta = (4\Delta/L)$

see Figure 3.2 for explanation of notation.

Again the deflection was fixed at $L/200$, and Equation (3.4) was used to plot a series of points to define the relationship between $\Delta\varepsilon_{ps}$ and L/d_{ps} (see Figure 3.3).

It was observed that the trend of the curve representing the behaviour of the externally prestressed beam (obtained from Equation (3.4)) was very similar to that obtained for internally unbonded beams (plotted using Equation (3.3)). Figure 3.3 also shows that the increase in strain for external tendons decreases more rapidly than that for internally unbonded tendons as the span-depth ratio increases. This was attributed to the second-order effect.

From the above discussion, it is evident that an investigation needs to be conducted to find out what effect span-depth ratio has on the increase in stress $\Delta f_{ps(ult)}$ and variation in eccentricity $\Delta_{eccen(ult)}$ of external tendons at the ultimate conditions. Once the relationships between span-depth ratio and these variables are established, the variation of the ultimate moment with the span-depth ratio parameter for these structures may then be understood more clearly.

3.2.2 Amount of Non-prestressed Reinforcement

Mattock *et al* (1971) and Tao and Gu (1985) found that the amount of passive reinforcement used in the design of internally unbonded post-tensioned structures influences the strength of these structures at the ultimate limit state conditions. They performed tests on several completely unbonded post-tensioned beams (i.e. internally unbonded structures where the unbonded tendons were the only component of flexural reinforcement), and noted that the failures of these beams were characterised by the formation of a single crack at the section of maximum moment. They also noted that after cracking these beams were observed to behave as shallow tied arches rather than flexural members. The failure of these unbonded beams were described by them to be brittle and sudden. They found that providing a moderate amount of non-prestressed reinforcement to these unbonded beams, not only improved their ductility but also the distribution of cracking at the ultimate conditions.

Sowlat and Rabbat (1987) tested three prestressed beams and reported that the influences of non-prestressed reinforcement described above for internally unbonded prestressed structures, were also found to be true for externally prestressed structures. In fact, Yaginuma and Kitada (1987) performed tests on six unbonded prestressed beams with varying amounts of passive reinforcement and concluded that the ultimate flexural behaviour of internally and externally unbonded structures having the same reinforcement ratios were almost the same, provided the span-depth ratios of these beams were small (i.e. L/d_{ps} less than 11). They further stated that when the span-depth ratios of these beams were high, greater variations in the flexural behaviour were observed. They attributed this to the second-order effect (discussed in Section 3.2.1), which causes the tendon eccentricity in external beams to change as the beam deforms.

Yaginuma and Kitada (1987) and Zhang *et al* (1993) found that increasing the reinforcement ratios generally improves the flexural performance of externally prestressed structures (see Figure 3.4). However, if too much passive reinforcement was used, failure was found to be brittle. This loss of ductility was considered undesirable. Yaginuma and Kitada also observed from their tests that the stress increase in the tendons $\Delta f_{ps(ult)}$ at the ultimate limit state decreases as the

reinforcement ratio of the externally prestressed beams increases. This, however, was contradictory to the observations made by Ramos and Aparicio (1996), who stated that the increase in stress $\Delta f_{ps(ult)}$ at the ultimate limit state for external tendons does not vary much with different reinforcement ratios. These reported inconsistencies in the results regarding the influence of reinforcement ratio on externally prestressed structures are investigated and discussed further in Chapter Six.

3.2.3 Initial Prestress Force and Amount of Prestress Reinforcement

According to MacGregor and Kreger (1989), the initial effective prestress force after allowance for all the prestress losses, is one of the most important parameters affecting the ultimate behaviour of externally post-tensioned structures. This, they explained, is because the stress increase in the external tendons $\Delta f_{ps(ult)}$ at ultimate is usually very small as compared to the effective initial prestress f_{pe} ,and its value at the ultimate limit state was found to be dependent on f_{pe}. Hence, the amount of initial prestress force applied on the structure usually predominates the ultimate strength and deflection response of these unbonded structures.

Yaginuma and Kitada (1989) found that increasing the initial prestress force will generally increase the ultimate strength but reduce the deflection capacity of externally prestressed structures at the ultimate limit state conditions. The reverse is true for structures with a low initial prestress force. According to Yaginuma (1993), span-depth ratio plays a vital role on the influence which the initial effective prestress force has on the ultimate flexural behaviour of externally prestressed structures. He stated that for beams with low span-depth ratios, the maximum moment increases as the initial prestress force increases. On the other hand, for beams with high span-depth ratios, the maximum moment is almost constant as the initial prestress force increases.

As for the influence of the amount of prestressed reinforcement on ultimate behaviour, Yaginuma and Kitada (1989) found that the stress increase in tendons decreases as the reinforcement ratio (q_p+q_s) increases (see Figure 3.5). However, the ultimate strength of these beams increases as the prestress reinforcement ratio increases.

3.2.4 Loading Pattern

Unbonded post-tensioned structures exhibit linear behaviour until they begin to crack or the joints opens (for segmental beams). After cracking or joint opening, the structures behave as a mechanism, forming plastic hinges over a finite length (referred to as the *plastic hinge length*) at the critical sections. Hence a flexural member may be divided into two distinct regions: the elastic and plastic region (see Figure 3.6). According to MacGregor *et al* (1989), the flexural strength of the beam occurs when the rotational capacity at the cracks or segmental joints is reached.

Tam and Pannell (1976), Harajli (1990) and Virlogeux (1988) reported that the lengthening of the concrete at the level of the prestressing steel for unbonded prestressed structures in the elastic zone is negligible as compared with the lengthening of the concrete in the plastic region. In fact, test evidence has shown that strain readings remained fairly constant outside the plastic zone after the first appearance of cracks. Hence the deformation of an unbonded structure depends critically on the plastic hinge length development at ultimate load conditions.

Since the loading geometry affects the development of the plastic hinge length (Harajli (1990)) for unbonded structures, it should therefore also have some influence on the behaviour of these structures at the ultimate limit state. Zhang *et al* (1993) performed tests on several externally post-tensioned beams and observed that the plastic hinge length for the beams under two point equi-distant loading were greater than those under one-point loading at the mid-span. However, they found that the maximum curvature achieved at the critical section of the beam under the two-point loading was much lower than that for the case of one-point loading.

Zhang *et al* (1993) reported that prior to yielding of the non-prestressed reinforcement, the deflection and stress increment of the tendons under the two-point loading system were about the same as those for the one-point loading system. However, after yielding, the deflections for the two-point loading system were found to be greater than those under the one-point loading system. The higher deflection caused a decrease in the eccentricity of the tendons which resulted in a higher stress increment induced in the tendons for the same external moments. Generally, slightly higher ultimate strength was observed for beams under the two point loading system.

Hence, the type of external loading applied to an externally prestressed structure was shown by Zhang *et al* (1993) to have a slight influence on the ultimate flexural behaviour.

3.3 External Beams with Deviators

3.3.1 Frictional Effects at Deviators

Takebayashi *et al* (1993, 1994) conducted a full scale destructive test on a segmental externally post-tensioned bridge beam, and found that the stress increase in the external tendons were not fully transmitted beyond the deviators for tendons with large deviation angles. They considered that this was due to the large deviation angles which caused high frictional forces to develop at the deviators preventing the tendons from slipping at these contact points. Since the tendons were prevented from slipping, no redistribution of stresses in the tendons between deviators was therefore possible. This consequently caused the experimental externally prestressed beam to exhibit a higher ultimate moment capacity. They also found that while slippage at the deviators for relatively straight tendons were observed to occur at all loading stages, slippage of draped tendons with large deviation angles occurred only when approaching the true collapse load.

The redistribution of stresses due to slippage of the tendons is a phenomenon unique to externally post-tensioned structures and is presently a subject of much interest to many bridge engineers and researchers (Virlogeux (1988), MacGregor *et al* (1989) Ramos and Aparicio (1996) and Takebayashi *et al* (1993, 1994)). Note that at the start of this research programme, very little information was available to the author about the frictional behaviour of external tendons at the deviators. As such the author had to conduct an extensive study on the phenomenon (Wong (1994(b), 1994(c))) in order to understand it better. The study included building a numerical model to simulate the frictional behaviour at the deviators and consideration of the experimental data obtained from the full scale test conducted by Takebayashi *et al* (1993, 1994). This section briefly presents the important information obtained from the study conducted by the author; about how and why external tendons slip at deviators and what are the main factors that influence these slippages.

Deviators are sometimes placed along the span of an externally post-tensioned structure for the purpose of either deviating the tendons to the required profile along the beam or limiting the free length of the tendons between the deviators (Figure 3.7). The slippage of tendons at these deviators is determined by the frictional behaviour between the two contact materials present at these points. Note that, other than at the anchorages, these deviators are the only positive contact points which the tendons have with the concrete structure. Hence, a high concentration of forces acts at these points (see Figure 3.8) which in turn causes high frictional forces *df* to be generated at the deviators to resist the tendons from slipping. Using the basic laws of friction given in Chirgwin and Plumpton (1978), the author derived Equations (3.5)and (3.6) which may be used to estimate the amount of frictional resistance *df* generated at the deviators.

$$N' = F_2 cos\alpha + F_1 cos\beta \quad (3.5)$$

$$df = N'\mu \quad (3.6)$$

$$\Delta f = |F_2 - F_1| \quad (3.7)$$

where

α and β: deviation angles at deviators

F_1 and F_2: amount of prestress force in the tendons on both sides of the deviator

N': the component of concentrated force acting on the deviator

μ: the coefficient of friction at the contact points

df: the frictional resistance generated at the deviator

Δf: the force difference between the deviators

As the structure deforms due to external loading, the stress increments in the tendons change between the deviators. Since the tendon stresses are initially prevented from redistributing between deviators due to the frictional forces, the force difference between deviators increases steadily. Slippage of tendons will only occur when the unbalanced force on both sides of the deviator Δf (see Equation (3.7)), becomes greater than the frictional resistance *df* generated there. Slippages of tendons result in a redistribution of stresses in the tendons between the deviators; and this redistribution continues until a stable condition is achieved at all the deviators (i.e. $\Delta f \leq df$). Figure

3.9 shows a sketch of the variation in prestress force in the external tendons due to the frictional phenomenon.

The redistribution of stresses in the tendons between the deviators, subsequently causes the ultimate capacities of externally prestressed structures to be reduced. As a matter of fact, Ramos and Aparicio (1996) found that, at the ultimate limit state, the slippage of tendons at the deviators may produce a reduction in the ultimate carrying capacity sufficient to cause collapse.

From Equations (3.5) and (3.6), it is evident that the amount of frictional resistance generated at the deviator is dependent on the following parameters:

- the coefficient of friction μ at the contact surfaces
- the angles of deviation on both sides of the deviators (i.e. α and β)
- the prestress forces in the tendons F_1 and F_2.

The coefficient of friction μ at the contact surfaces was found to be dependent on a large number of variables (Ramos and Aparicio (1996)), and hence cannot be easily represented by a single reliable value. These variables include the deviation angle, the kind of deviator, duct type and grout type (if used). As for the influence of deviation angle on the frictional forces generated, it has already been reported that Takebayashi *et al* (1993, 1994) found that larger deviation angles on either side of the deviators will cause higher frictional forces to be generated at these points. The prestress force in the tendons directly contributes to the amount of the concentrated direct force acting on the concrete structure. This concentrated force is in turn directly related to the amount of frictional force generated at the deviators. Hence the higher the prestress force in the tendons, the higher the frictional resistance will be at the deviators.

As explained above, the estimation of a reliable value for the coefficient of friction at the contact points is a difficult task because of the large number of variables involved. Also, the analysis of externally prestressed structures with deviators becomes very complicated when the frictional behaviour at the deviators are included This complication is due to the fact that the friction-induced behaviour is both non-linear and non-reversible (Virlogeux, (1988)), which makes the analysis dependent on the load history of the structure. For these reasons, Ramos and Aparicio (1996) and

Virlogeux (1988) both suggested that it may be easier just to make two extreme assumptions about the slippage behaviour of external tendons at the deviators at the ultimate limit state, either fully fixed (Figure 3.10) or zero friction (Figure 3.11).

For the first assumption, where the tendons are assumed to be fixed at the deviators, the prestress force in the external tendons varies greatly due to the restriction of stress redistribution in the tendons between deviators. As such, analyses conducted using this assumption will always give an upper bound solution for the behaviour of the externally prestressed structure at the ultimate limit state. The second assumption will on the other hand produce a constant prestress force in the tendons throughout the whole span since the contact points are assumed to be frictionless. Hence analyses conducted using the second assumption will always give the lower bound solution for the ultimate limit state. The true behaviour of the structure lies between the results derived from the analyses conducted using these two extreme boundary conditions.

It is clear that very little is presently known about the frictional phenomenon of external tendons at the deviators. These unknowns include:

- the extent which the frictional response at the deviators has on the ultimate limit state behaviour
- the influence which the coefficient of friction, the deviation angles of the tendons at the deviators and the prestress force in the tendons have on the amount of frictional resistance generated at the deviators
- whether considering the two extreme conditions for slippage of the tendons at the deviators are sufficient for estimating the actual ultimate behaviour of such structures.

3.3.2 Free-length to Depth Ratio

The influence of the span-depth ratio on the ultimate limit state behaviour of externally post-tensioned structures has already been discussed in Section 3.2.1 principally for beams without deviators where the tendons extend freely between the anchorages. Hence the free length of these tendons ℓ_{free} is approximately equal to the span of the beam. When deviators are placed within the span, the free length of the

tendons becomes reduced. This may cause the ultimate flexural behaviour of these structures to change, as observed by Yaginuma and Kitada (1988).

Yaginuma and Kitada (1988) tested several beams to investigate the influence of the span-depth ratio on the behaviour of partially prestressed concrete beams with external tendons. The beams were categorised into three main series. The first, denoted series N beams, were prestressed with internal unbonded tendons; the second (series O beams) consisted of beams which were prestressed with external tendons but without provision of any deviators; the third were also prestressed with external tendons, but with several deviators placed along the span of these structures, denoted series S beams.

Figure 3.12 shows the relationship M_{max}/bd^2f_{cu} vs. L/d_{ps} for the three series of beams (O, S and N) tested by Yaginuma and Kitada (1988). From Figure 3.12, it was observed that the maximum moment capacity for all the beams tested decreased as the span-depth ratio increased (as described in Section 3.2.1). It was also observed that the maximum moment capacities for the external beams with deviators (Series N), seemed to be higher than those without any deviators (Series O) for the same span-depth ratio. This confirms that the ultimate flexural performance of externally prestressed structures can be increased, by providing a proper arrangement of deviators along their span.

The increased flexural strength observed above may be due to several reasons, one of them being that the deviators help to minimise the loss of tendon eccentricity due to second-order effects (see Section 3.2.1). When deviators are placed along the span of these structures, the free lengths of the tendons at the critical sections are reduced. Since the loss of eccentricity due to second-order effects is dependent on the length of the tendons left unsupported, the change in eccentricity at ultimate for these beams will consequently be smaller resulting in a higher ultimate flexural strength.

Another reason for the increased strength applies to beams with high frictional forces developed at their deviators which prevent the tendons from slipping. The strain increase in the tendons is thus evaluated using the following equation $\Delta\varepsilon_{ps} = \Delta\ell/\ell_{free}$ instead of $\Delta\varepsilon_{ps} = \Delta\ell/\ell_{ps}$. Since ℓ_{free} is less than ℓ_{ps}, the change in strain in tendons $\Delta\varepsilon_{ps}$

will always be greater for those beams with deviators for the same elongation in tendon length, thereby resulting in a higher flexural strength.

For the above reasons, Zhang *et al* (1993) recommended that a parameter termed *the free-length to depth ratio* α_{free} be used to describe the second-order effect and ultimate behaviour of these beams instead of the conventional span-depth ratio. They defined the free-length to depth ratio as the ratio of the effective depth of the tendon group d_{ps} to the free length of the tendons ℓ_{free}. Chapter Six presents the results of the parametric study conducted on this ratio.

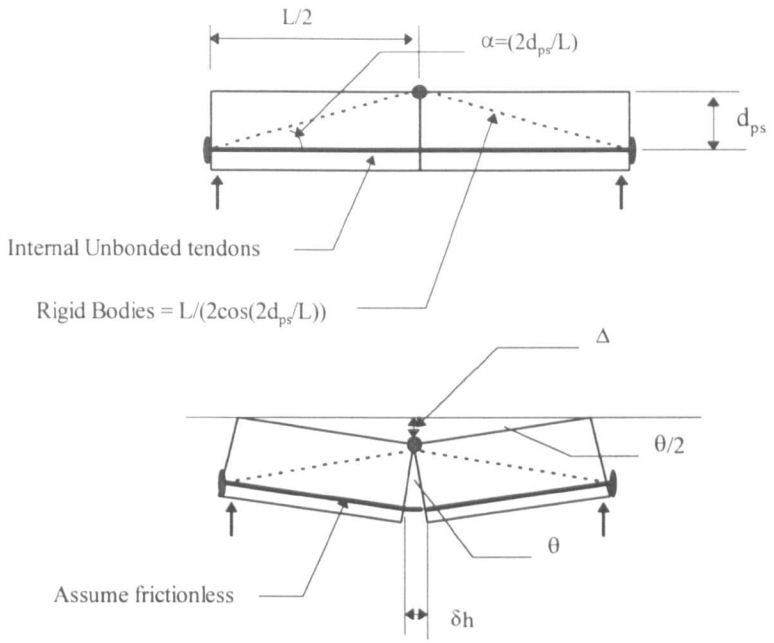

Figure 3.1: Rigid-body model for an internally unbonded post-tensioned structure

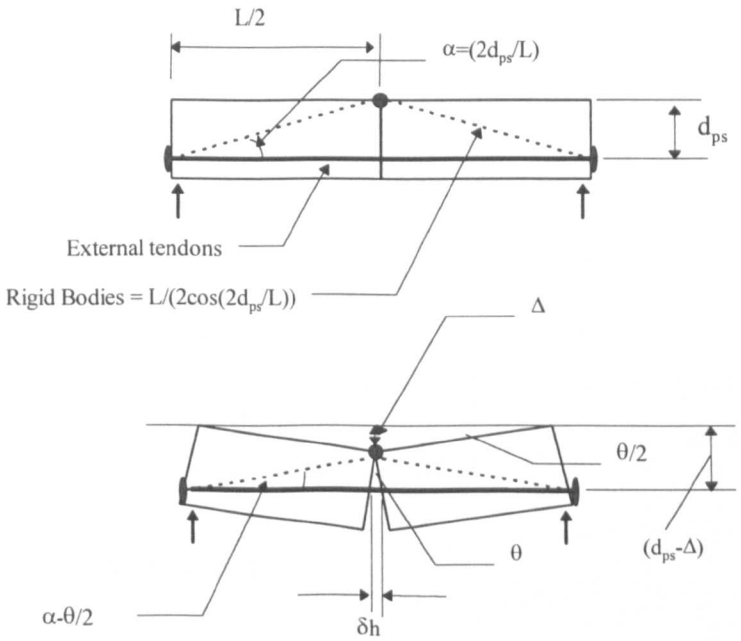

Figure 3.2: Rigid-body model for an externally post-tensioned structure

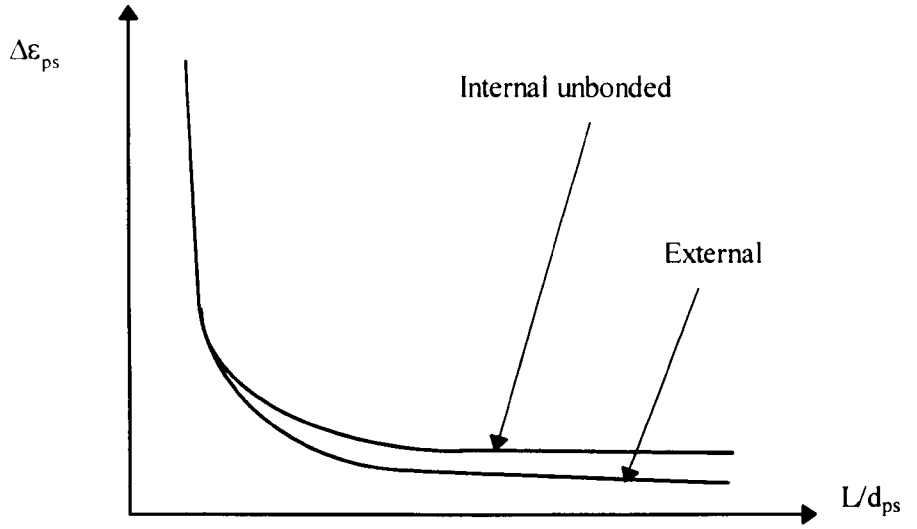

Figure 3.3: The relationship between $\Delta\varepsilon_{ps}$ and L/d_{ps} for internally and externally unbonded tendons

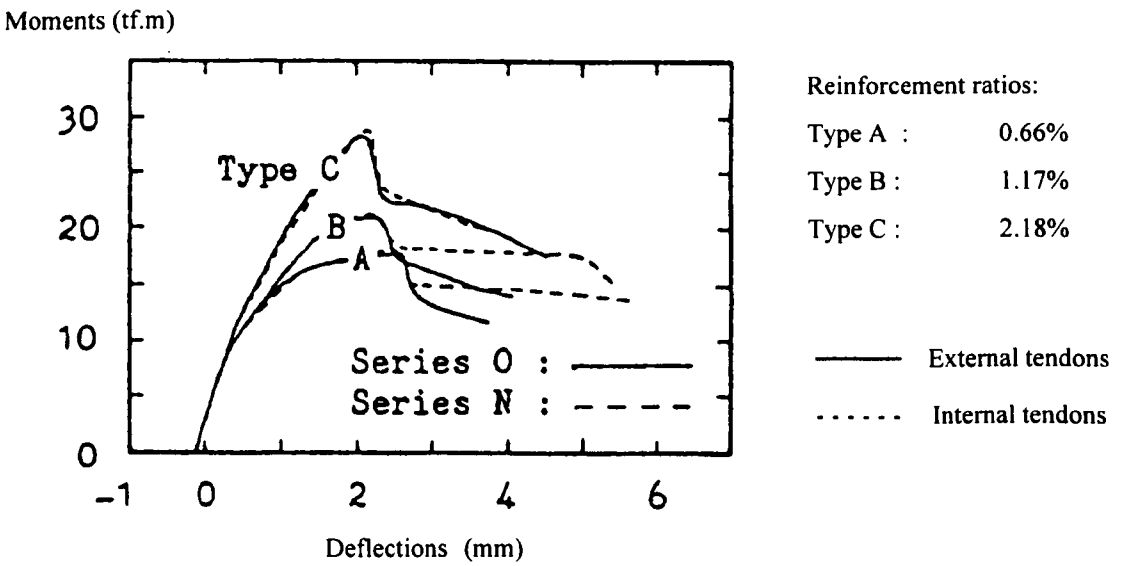

Figure 3.4: Moment-deflection curves for externally post-tensioned structures with different reinforcement ratios
(reproduced from Yaginuma and Kitada (1987))

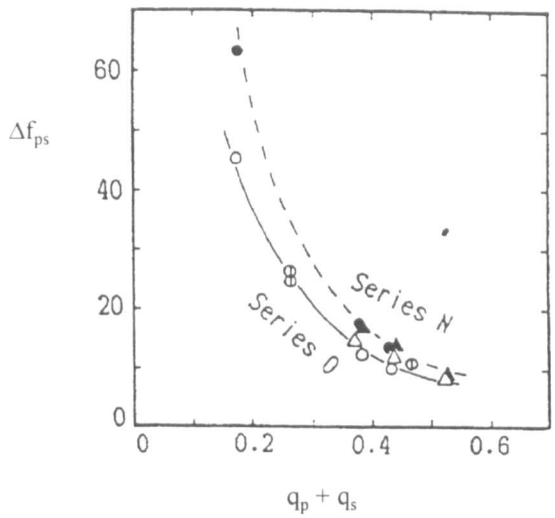

Series N : Internally unbonded prestressed structures

Series O : Externally prestressed structures

Figure 3.5: Relationship between Δf_{ps} and (q_p+q_s)
(sketched from Yaginuma and Kitada (1989))

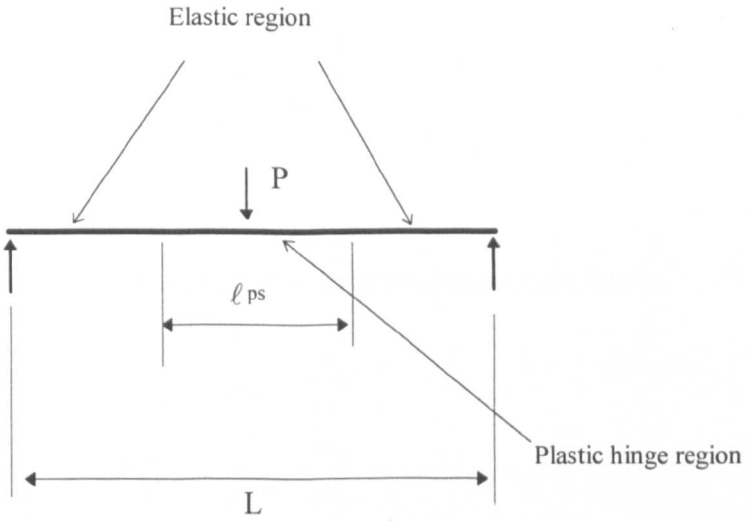

ℓ_{ps} = Plastic hinge length

Figure 3.6: Plastic hinge length

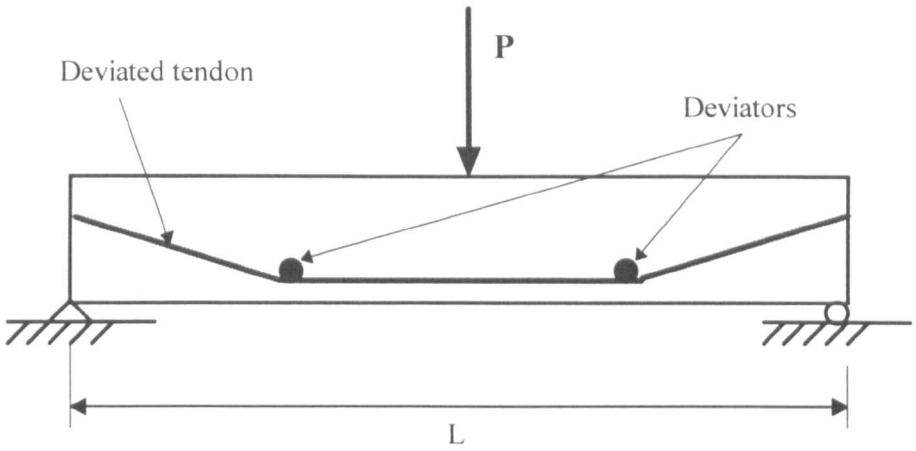

Figure 3.7: External tendons deflected along the span by deviators

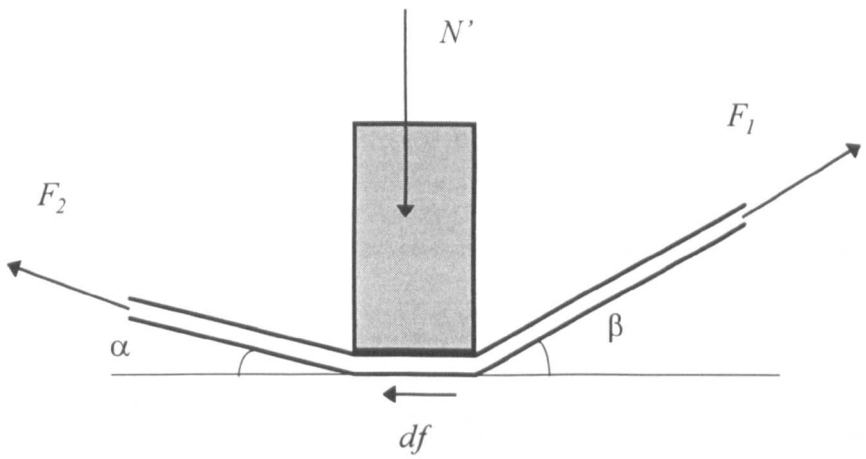

Figure 3.8: Frictional resistance *df* generated at deviators

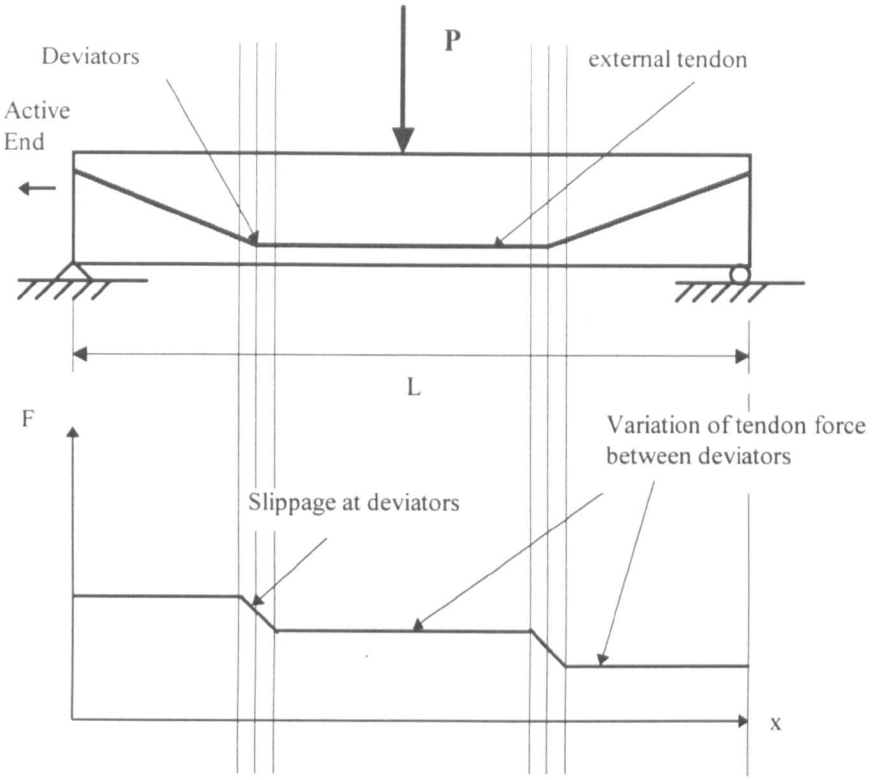

Figure 3.9: Tendon force variation along the span of an externally post-tensioned structure

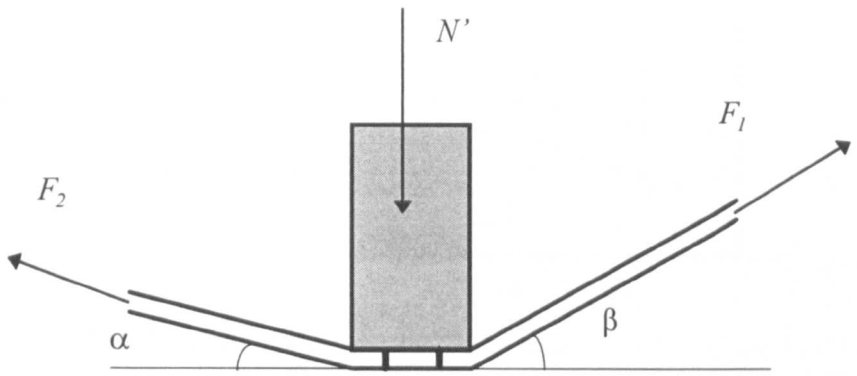

$F_1 \neq F_2$

Figure 3.10: Sketch of forces acting at a deviator assuming the tendons are fixed

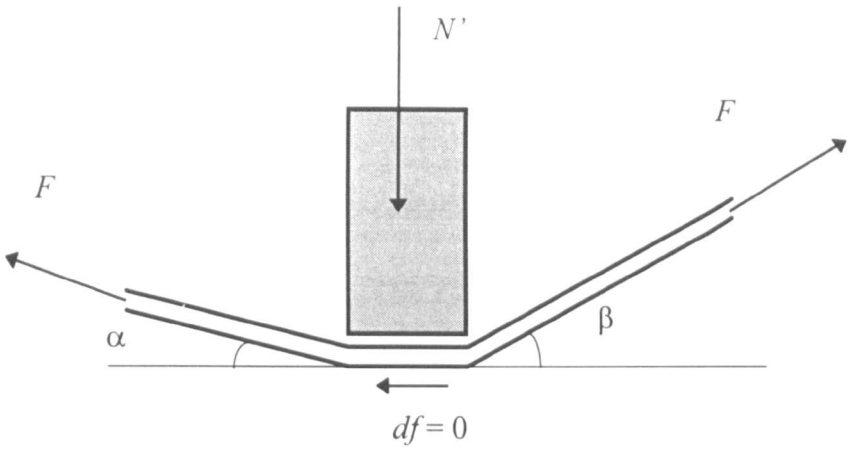

Slip occurs to reestablsih equilibrium since μ is assumed to be zero.

Figure 3.11: Sketch of forces acting at a deviator assuming the contact surface is frictionless

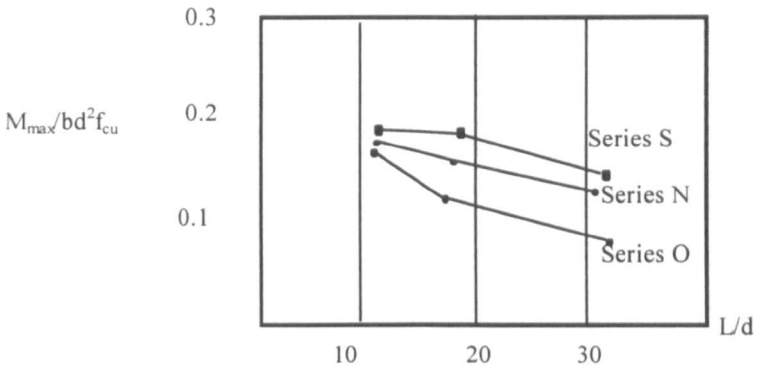

Reinforcement Ratio = 0.66%

Series O - External tendons without deviators
Series S - External tendons with deviators
Series N - Internal tendons

Figure 3.12 : Relationship between M_{max}/bd^2f_{cu} and L/d_{ps} for beams tested by Yaginuam and Kitada (1988)

Chapter 4

Non-linear Analytical Models

4.1 General

The literature review on the ultimate limit state analysis of externally post-tensioned structures was presented in Chapter Two. From this, it was evident that the analysis of these structures cannot be performed in the same manner as that for internally bonded post-tensioned structures. Due to the lack of bond between the concrete and the prestressing tendon, the stress increases in the external tendons are not localised at the cracked concrete sections but 'averaged' along the free-length of the tendons. Also, the eccentricity of external tendons vary as the beam deforms under different loading conditions. The stress increase in the tendons Δf_{ps} and the variation in tendon eccentricity Δ_{eccen} for any loading stage can only be determined by studying the deformation response of the structure. Hence, the ultimate strength of an externally prestressed structure must be predicted by performing a non-linear analysis to determine its deflected profile at ultimate conditions. One such approach would be to use a finite element model which has the potential for including both material and geometric non-linearities.

The finite element method is essentially a numerical method for the approximate solution of practical problems arising in engineering and scientific analysis. There are presently many commercial finite element packages available (i.e. ANSYS, ABACUS, etc.), which are commonly used by engineers to analyse the behaviour of irregular structures, i.e. structures having unique geometry or external loading conditions that cannot be easily analysed by conventional methods. Section 4.2 describes a short study conducted here to check the applicability of using finite element methods to predict the flexural response of such structures.

An alternative approach has been proposed by Naaman and Alkhairi (1991) who introduced a non-linear analytical model that uses the concept of strain compatibility to simulate the flexural behaviour of internally unbonded beams up to ultimate. They also stated that their analytical model could be used for externally prestressed structures. However, as discussed in Chapters Two and Three, the behaviour of internally unbonded and externally unbonded prestressed structures are very different and their model may not be entirely appropriate.

Adopting the strain compatibility concept introduced by Naaman and Alkhairi (1991), eight non-linear analytical models were designed exclusively for investigating the flexural response of externally post-tensioned structures, denoted EXT3 to EXT10 respectively. In these non-linear models, loads are placed on the external beams in increments up to ultimate. The behaviour of these structures are then modelled for each loading stage, by performing an extensive non-linear analysis on them to determine their curvature distributions, from which the changes in tendon stress and eccentricity are then predicted. The basic assumptions used in these models are:

1) Plane sections remain plane after bending.
2) Constitutive relations for the reinforcement, prestressing steel and the concrete are known.
3) The beam is simply supported.
4) The beam is assumed to be at the cracked state whenever the applied tensile stress exceeds the modulus of rupture of the concrete.
5) Minimum flexural passive reinforcement is provided and is bonded perfectly with the concrete.
6) The variation in length of the tendons between two successive anchorages or deviators may be determined by using Virlogeux's (1988) equation.
7) The beam is assumed to be reinforced with the minimum amount of vertical stirrups necessary to resist the shear stresses at all cracked sections along the span.

Although the eight analytical models were programmed into eight separate computer programmes, the same global algorithm was used in all of them. This is presented in Section 4.3. The global algorithm is divided into two parts; (1) the analysis of the structure before cracking (presented in Section 4.4.1); and (2) the analysis of the

structure after cracking (presented in Section 4.4.2). The effect of diagonal tensile cracking on the flexural behaviour of these structures was also considered, and is discussed in Section 4.5.1.

The global algorithm for the eight models had a common structure but was amended in detail to enable it to perform the unique analysis for each case. The following is a brief description of the eight non-linear models proposed:

1) EXT3 model

   designed to analyse externally post-tensioned structures where the external tendons span between the anchorages and no deviators are placed along the span of the structure (see Figure 4.1).

2) EXT4 model

   similar to the EXT3 model except that the effect of tension stiffening is included. The effect of tension stiffening is discussed further in Section 4.5.2.

3) EXT5 model

   designed to analyse externally post-tensioned structures with deviators within their spans, where the external tendons are assumed to be fixed at the deviators (see Figure 4.2). The methodology used for building this analytical model is discussed in Section 4.7.1.

4) EXT6 model

   similar to the EXT5 model, except that the effects of tension stiffening were included.

5) EXT7 model

   designed to analyse externally post-tensioned structures with deviators where the frictional effects at the deviators are taken into account in the analysis (see Figure 4.3). The analytical methodology used to evaluate the frictional behaviour at deviators is presented in Section 4.7.3.

6) EXT8 model

   similar to the EXT7 model, except that the tension stiffening effect is incorporated.

7) EXT9 model

designed to analyse externally post-tensioned structures with frictionless deviators included in their spans (see Figure 4.4). The frictionless behaviour at the deviators is discussed further in Section 4.7.2.

8) EXT10 model

similar to the EXT9 model but includes the effects of tension stiffening.

4.2 Finite Element Modelling

4.2.1 Test Beam

The viaducts for the Bangkok Second Stage Expressway were constructed using external tendons and dry joints. Since the number of precast segments amounted to about 14,500 for the first phase of the project alone, the designers considered it worthwhile to conduct a full scale loading test on a span of the proposed structure prior to finalising the design (Takebayashi *et al* (1993)). The test beam was constructed in a casting yard using piled foundations and short piers. The distance between the piers for the test beam was approximately forty-four metres and comprised of 14 segments. Figure 2.17 shows the set-up of the test beam.

The experimental test was conducted in two phases: the *Design Load Phase* (Takebayashi *et al* (1993)) and the *Destructive Load Phase* (Takebayashi *et al* (1994)) and both phases were briefly described in Section 2.3.2.2. However, only the technical report for the Design Load Phase was available to the author[1]. As a result, the finite element analyses performed here were only conducted up to the stage where maximum load was placed on the structure at the Design Load Phase.

4.2.2 Finite Element Modelling with ANSYS

A short study was conducted to check the applicability and convenience of using finite element methods to predict the flexural response of externally post-tensioned structures. Two finite element models were designed using ANSYS to simulate the

[1] Report No. SR479, Unpublished report.

flexural behaviour of the beam tested by Takebayashi *et al* (1993), denoted *VER2* and *VER5* respectively (detailed information of these models are presented elsewhere, Wong (1994(d))). In both models, the concrete and tendon elements were fixed at the deviators because the frictional behaviour of the tendons at these points cannot be easily modelled. Although it is possible to simulate the frictional slippage of tendons by using gap elements available in ANSYS, the redistribution of stresses as a consequent of this slippage was however not easily modelled because this would require the finite element model to be re-structured before the next load sequence can be analysed.

The *VER2* model was a one-dimensional finite element model where linear line elements were used to represent the beam, tendon and deviator elements (see Figure 4.5). For the deviator elements, line elements with very high levels of rigidity were used. Although this model was only a simplified representation of the test beam, it possessed the advantage of being simple thereby reducing the amount of computational time required for the analysis. However, as the test beam was a segmental bridge structure, the main disadvantage of the *VER2* model was its inability to simulate the opening of joints when decompression of the structure occurred. Also, the tendons were assumed to be fixed at the deviators throughout the loading history of the beam.

Figure 4.6 shows the two-dimensional model *VER5* at the design ultimate loading condition. This model was an improvement on the one-dimensional model since it consisted of two-dimensional elastic plate elements and contact elements were incorporated to permit possible gap opening at the segmental joints. However, the tendons were also assumed to be fixed at the deviators due to reasons given earlier.

4.2.3 Comparison of Results

Figure 4.7 shows the moment-deflection relationships for the test beam derived from the one-dimensional (*VER2*) and two-dimensional (*VER5*) finite element models. From Figure 4.7, it can be seen that the curve derived from the *VER2* model was linear up to the design ultimate load. Before the joint opening at the critical section, the *VER2* curve was noted to be very closely related with the experimental curve.

However, after joint opening, the *VER2* curve maintained the same stiffness and over-estimated the gradient of the experimental curve by approximately forty-five percent. The total computing time taken for analysing this model with ANSYS was only about two hours on a personal computer of moderate capacity.

The *VER5* curve was also found to be in close agreement with the experimental curve before the occurrence of joint opening but over-estimated the joint opening moment by about eighteen percent. After the opening of joint at the critical section, the *VER5* curve indicated a loss in stiffness, but the reduced stiffness was still higher than the experimental value and hence the model over-estimated the experimental moments by about ten percent. The reason for this over-estimation was due to the tendons being fixed at the deviators in the finite element model and may be avoided by either considering the frictional slippage at the deviators or assuming that the tendons slipped freely at the deviators. Another major disadvantage of this model was the large amount of computing time required since it took approximately twenty-three hours to evaluate the flexural response of the experimental beam to the design ultimate load.

The study therefore shows that finite element analysis may be employed to predict the flexural response of externally prestressed beams reasonably accurately before the occurrence of cracking or joint opening. However, after cracking or joint opening, the finite element model must be able to simulate the following factors in order to produce accurate estimation of the beam behaviour:

- cracking and opening of joint
- slippage of the external tendons at the deviators and consequently re-distribution of tendon stresses.

Failing to consider either or both of these factors has been shown here to cause an over-estimation of the beam flexural behaviour.

The computing time required to conduct an analysis on such structures with finite element analysis was also observed to be dependent on the complexity of the model used. For simple models, e.g. *VER2* model, less time was required but at the expense of less accurate results. For a more sophisticated model, while more accurate results were possible, the computing time required was on the other hand very much longer.

Furthermore, if such an approach is to be extended to predict the flexural behaviour up to collapse, it will be necessary to use large deflection theory and non-linear material models. This is likely to extend the time taken for the solution to such an extent as to make it unattractive as either a research or a design tool. Hence the approach taken in this investigation was to develop a non-linear analytical model utilising the strain compatibility method introduced by Naaman and Alkhairi (1991) to estimate the flexural behaviour of these structures instead.

4.3 Global Algorithm for Models

For externally post-tensioned structures, due to the absence of bond between the concrete and the external tendons, the force transfer-mechanisms from the tendons to the beam are limited at the anchorages and the deviators. As such, the flexural behaviour of these beams is dependent on the deformation of the whole structure and can therefore be evaluated up to collapse, by modelling the deflections and curvatures along the span at all stages of loading.

The methodology adopted here in the proposed analytical models involves defining several nodes along the span of the structure (see Figure 4.9) and determining the curvature of these nodes separately at each loading sequence. The curvature distributions are then used to predict the end rotations and deflection profiles along the beam. Consequently, the deformations are used to estimate the stress increase and eccentricity variations of the external tendons at each loading sequence. The global algorithm used for building the non-linear computer programmes is summarised in the flowchart shown Figure 4.8. This section briefly describes the various steps used in the global algorithm.

The geometry of the beam to be analysed is first defined in the form of an input file. The input information required by the programmes includes: the number of equally spaced nodes to be defined along the beam, the shape of the cross-section, the properties of the various materials used in the beam, the strain increments to be used for defining each loading sequence, etc. Details on how the input file should be prepared for a computer run is discussed in Wong (1997). The sectional properties of

the structure are then analysed with the information provided in the input file. Note that transformed properties of the section are used in these models.

For each loading stage, the stress increase in the tendons Δf_{ps} and the variation in eccentricity Δ_{eccen} for each node are initially assumed to be zero. Using these assumptions, the eccentricity of the tendons at each node and the prestressing force over the free length of the tendons are calculated from Equations (4.1) and (4.2) respectively:

$$e(k,i) = e_{initial}(i) + \Delta_{eccen}(k,i) \quad \text{.....(4.1)}$$

$$F(k) = A_{ps}(f_{pe} + \Delta f_{ps}(k,i)) \quad \text{.....(4.2)}$$

where

k = load sequence

i = the node number

The cracking moment M_{cr} at each of the nodes defined along the span are next evaluated. The cracking moment M_{cr} is defined as the moment at which the tensile stress at the extreme fiber of the concrete section reaches a value equal to the modulus of rupture, f_r. In the proposed models, the cracking moments are evaluated using Equations (4.3) and (4.4):

$$M_{cr(top)} = \left[Fe - \frac{FZ_{top}}{A_c} - f_r Z_{top} \right] \quad \text{.....(4.3)}$$

$$M_{cr(bot)} = \left[\frac{FZ_{bot}}{A_c} + Fe + f_r Z_{bot} \right] \quad \text{.....(4.4)}$$

Note that for externally prestressed structures, the cracking moment varies along the span at different loading stages. The variation is due to the continuous change in prestress force (F) and eccentricity (e) of the externally unbonded tendons throughout the loading history of the beams.

Each node along the beam is then analysed separately for its curvature. The computational method used for estimating the curvature at a node depends on the condition of cracking at that section; that is whether the node is in the *pre-crack state* or the *post-crack state*. Theoretically, a section is described to be at the pre-crack state when the external moment M_{ext} is lower than the cracking moment M_{cr}. If the

external moment exceeds the cracking moment, then the section is said to be at the post-crack state. Hence, the external moments and cracking moments for all the nodes along the span are first analysed and compared to determine the type of analysis to be performed at each node for the curvature. The different computational approaches for calculating the curvature of a section at the pre-crack and post-crack state are described in Sections 4.4.1 and 4.4.2 respectively.

Once the curvatures along the span have been analysed, the deflection and rotation at each node are then predicted by integrating the curvatures along the member. The total rotation occurring at the anchorages or deviators are computed using the *first moment area theorem* (or *rotation theorem*). The first moment area theorem is given by Naaman (1982) as: '*The change in angle between points i and j on the deflected elastic curve of a flexural member, or the slope at point j relative to the slope at point i, is equal to the area under the curvature diagram between points i and j*' (see Figure 4.10), that is;

$$\theta_{ji} = \int_{x_i}^{x_j} \phi(x)dx \quad \text{..... (4.5)}$$

The deflection of the beam is given by the *second moment area theorem* (or *deflection theorem*) expressed by Naaman (1982) as: '*the deflection of point j of a flexural member measured with respect to the tangent at another point i of the member is equal to the static moment taken about point j of the area under the curvature diagrams along the member between points i and j*' (see Figure 4.10); that is;

$$\Delta x_{ji} = \int_{x_i}^{x_j} x\phi(x)dx \quad \text{..... (4.6)}$$

See Figure 4.10 for explanation of the notation used in Equations (4.5) and (4.6).

Equations (4.5) and (4.6) are generalisations of the moment area theorems and they are applicable whether elastic or plastic curvatures are involved (Park and Paulay (1975)). However, using these two equations ignores the effect of the additional deformations caused by diagonal tension cracking due to shear and any increase in stiffness due to tension stiffening. The effects of diagonal tension cracking and tension stiffening are discussed in Sections 4.5.1 and 4.5.2.

The stress increase in the tendons Δf_{ps} is next predicted by first estimating the total elongation of the tendons $\Delta \ell_{12}$ between the anchorages or deviators using Equation (2.22) given by Virlogeux (1988).

The change of strain in the prestressing tendon is thus given by:

$$\Delta \varepsilon_{ps} = \frac{\Delta \ell_{12}}{\ell_{12}} \quad \text{.....(4.7)}$$

The change in stress in the tendons Δf_{ps} is subsequently estimated from the stress-strain constitutive model of the prestressing steel. The newly calculated Δf_{ps} (denoted $\Delta f_{ps(calculated)}$) is compared with the Δf_{ps} assumed earlier (denoted $\Delta f_{ps(assumed)}$). If the two Δf_{ps} values are within the required tolerance, then the $\Delta f_{ps(calculated)}$ value will be accepted as the stress increase in the tendons for the particular load sequence. However, if the difference between the two values does not meet the required tolerance, the $\Delta f_{ps(calculated)}$ value will be taken as the newly assumed Δf_{ps}, and the analytical procedure described above is repeated from the point where the prestress force in the tendons is evaluated (see Figure 4.8). This procedure is repeated until a satisfactory solution is derived for Δf_{ps}.

The next step is to check the variation in eccentricity occurring at each node along the beam. The eccentricities between the centre of the tendon group and the centroid of the section e_x' are calculated for all the nodes from the deformed shape of the beam (Figure 4.11) , using Equation (4.8):

$$e_x'(i) = e_x(i) - \Delta(i) \quad \text{.....(4.8)}$$

where

$e_x(i)$ = the eccentricity of the tendons at node i due to the rotations at the anchorages only

$\Delta(i)$ = vertical deflection of the beam centroid at node i.

Thus, the change in eccentricity Δ_{eccen} is evaluated using Equation (4.9):

$$\Delta_{eccen}(i) = e_{initial}(i) - e_x'(i) \quad \text{.....(4.9)}$$

where

$\Delta_{eccen}(i)$ = the change in eccentricity at node i

$e_{initial}(i)$ = the initial eccentricity of the tendons at node i.

The calculated Δ_{eccen} values (denoted $\Delta_{eccen(calculated)}$) at all the nodes are compared with the earlier assumed values (denoted $\Delta_{eccen(assumed)}$) and are accepted when the required tolerance is achieved. If the tolerance is exceeded at any node, then the described procedure is repeated from the point where the eccentricities are calculated for the beam structure (see Figure 4.8); using the assumption $\Delta_{eccen(assumed)} = \Delta_{eccen(calculated)}$. Again the procedure described for determining the variation in eccentricity along the span of the beam is repeated until satisfactory values of Δ_{eccen} are achieved for all the nodes.

After the values of Δ_{eccen} and Δf_{ps} have been calculated within tolerance for loading sequence k, the whole procedure is repeated for the next loading sequence (k+1). This is done repeatedly until one of the termination conditions listed in Section 4.8 has been met. Note that the increment of load to be applied to the structure for the next loading sequence (k+1), depends on the state of cracking at the present loading stage (k).

If the whole beam is uncracked then a calculated increment of load will be added to the structure for the next loading stage. This calculated additional load is initially based on a proportion of the loading predicted to cause cracking at the critical section of the beam. When the critical section approaches the cracked condition, a bisection algorithm is used to add external loads to the beam until it just cracks at the critical section.

After cracking, the procedure for adding loads to the structure for the next loading stage is different from that described earlier. Instead of adding a calculated external load directly, a pre-set strain increment is added to the extreme compressive fiber of the concrete at the critical section. A force equilibrium analysis is then conducted with the new compressive strain at the critical section. The internal moment at the critical section is subsequently estimated with the forces evaluated from the force equilibrium analysis. Using the internal moments evaluated and the loading pattern, the external loads to be applied to the structure for the next loading sequence are thus estimated. More details regarding the evaluation of load increments to be applied on the structure at the pre-crack and post-crack states are presented in Sections 4.4.1 and 4.4.2 respectively.

4.4 Curvature Analysis

4.4.1 Pre-crack Analysis

Prior to cracking, linear elastic laws are used to solve for the stresses and strains over the depth of the section. During this stage, both the stress and strain distributions over the section depth under combined bending and axial force are assumed to be linear (see Figure 4.12).

When a section is found to be at the pre-crack state, i.e. $M_{cr} < M_{ext}$, the stresses at the extreme top and bottom fibers of the concrete are computed using the following equations:

$$f_{top} = \frac{F}{A_c} - \frac{Fe}{Z_{top}} + \frac{M_{ext}}{Z_{top}} \quad \text{.....(4.10)}$$

$$f_{bot} = \frac{F}{A_c} + \frac{Fe}{Z_{bot}} - \frac{M_{ext}}{Z_{bot}} \quad \text{.....(4.11)}$$

The evaluated extreme top and bottom concrete stresses (f_{top}, f_{bot}) are then converted to strain values (ε_{top}, ε_{bot}) using the Young's modulus for the concrete (see Section 4.6).

Since the curvature of a section ϕ is defined as the gradient of the strain profile, and the strain profile along the depth of the section is assumed to be linear (Figure 4.12), the curvature of a section is thus given by:

$$\phi = \frac{\varepsilon_{top} - \varepsilon_{bot}}{d} \quad \text{.....(4.12)}$$

After the curvature for each of the nodes along the beam has been evaluated, the analysis proceeds as described in Section 4.3.

As mentioned in Section 4.3, the increment of load to be placed on the structure at every loading sequence is determined differently for the pre-crack and post-crack states. After analysing the initial loading sequence (i.e. $k = 1$ for dead load only), the difference between M_{ext} and the calculated $M_{cr(bot)}$ at the critical section for the initial load stage is determined:

$$M_{difference} = M_{cr(bot)} - M_{ext} \quad \text{.....(4.13)}$$

This difference, $M_{difference}$, is then divided by the minimum number of points required before cracking in the load deflection curve (x_{point}). This gives the additional moments M_{add} to be added on the structure at the critical section for each successive loading stage (see Figure 4.13):

$$M_{add} = M_{difference}/x_{points} \quad (4.14)$$

The external moment to be applied at the critical section for the next loading sequence $M_{ext}(k+1)$ is computed, by adding the existing moment $M_{ext}(k)$ to the calculated additional moment M_{add} :

$$M_{ext}(k+1) = M_{ext}(k) + M_{add} \quad (4.15)$$

With $M_{ext}(k+1)$ calculated and the loading geometry defined, the amount of external loading to be placed on the structure for the next loading sequence can then be determined.

The cracking moment is defined as the applied moment at which cracking occurs at the critical section of the structure (see Figure 4.13); that is when $M_{cr} = M_{ext}$ at the critical section. It marks the end of the pre-crack state and the beginning of the post-crack state. The method described above defines a series of points on the load-deflection curve, before defining the cracking moment. However, because of the variation in the eccentricities of the external tendons, the cracking moment M_{cr} calculated at the critical section differs at different loading stages. As a result, the cracking moment is not usually easily defined. An algorithm that uses the bisection method was therefore designed to enable the cracking moment to be determined. The algorithm uses Equation (4.16) to determine the successive external moments to be applied on the critical section of the structure until the external moment M_{ext} is very close to the cracking moment M_{cr} evaluated. When this occurs, the cracking moment is defined.

$$M_{ext}(k+1) = M_{ext}(k) + (M_{cr}(k)-M_{ext}(k))/2 \quad (4.16)$$

4.4.2 Post-crack Analysis

When the externally applied moment M_{ext} exceeds the cracking moment M_{cr} at the critical section, cracking occurs and the post-crack analysis is employed. The computation of the curvature distribution along the span of the structure becomes

more complicated when this occurs. Firstly, the new load level is found by adding the concrete strain at the extreme compression fiber at the critical section of the beam $\varepsilon_{top}(k)$ with a pre-set strain increment $\Delta\varepsilon$.

$$\varepsilon_{top}(k+1) = \varepsilon_{top}(k) + \Delta\varepsilon \quad (4.17)$$

For the new value of $\varepsilon_{top}(k+1)$, the neutral axis depth c is found by conducting a force equilibrium analysis at the critical section (see Figure 4.14). This is performed by using a bisection routine, that varies the position of the neutral axis until the internal forces calculated satisfies Equation (4.18). Note that the bisection routine used in the algorithm for the force equilibrium analysis, is based on *Brent's Method* introduced by Press *et al* (1986).

$$C_{conc} - T_{reinf} - T_{conc} - T_{pres} = 0 \quad (4.18)$$

The internal forces and neutral axis so found are then used to determine the internal moment of resistance M_{int} and curvature ϕ at the critical section using Equations (4.19) and (4.20) respectively, corresponding to the new strain value $\varepsilon_{top}(k+1)$.

$$M_{int} = C_{conc}d'_{conc} + T_{conc}d_{conc} + T_{reinf}d_{reinf} + T_{pres}d_{pres} \quad (4.19)$$

$$\phi = \frac{\varepsilon_{top}}{c} \quad (4.20)$$

The notation used in Equations (4.19) and (4.20) is defined in Figure 4.14.

The external loads to be applied to the structure for the next loading sequence are then determined by equating the calculated internal moment of resistance M_{int} to the external moment M_{ext}, at the critical section. After determining the external loads for the next loading stage, the external moments M_{ext} to be applied to all the other nodes are evaluated.

The external moments M_{ext} are next compared to the cracking moments M_{cr} at all the nodes defined along the span (except at the critical section). If M_{ext} is found to be lower than M_{cr} at any node, Equations (4.10) to (4.12) for the pre-crack state are used to calculate the curvature at the node. However, if M_{ext} is found to be greater than M_{cr}, both a force equilibrium and moment equilibrium analysis are conducted at the node to establish its curvature. This is done by first assuming a value for the concrete strain at the extreme compression fiber ε_{top} at the section. The force equilibrium

analysis described earlier is next conducted at the section for the position of the neutral axis c (iterative level one). When the neutral axis has been determined, Equation (4.19) is used to calculate the internal moment of resistance M_{int}.

The moment equilibrium analysis is then performed by comparing the internal moment of resistance M_{int} with the external moment applied at the section M_{ext}. If the two values are not within the required tolerance, the earlier assumed concrete strain at the compression fiber is changed and the procedure repeated until Equation (4.21) is satisfied (iterative level two).

$$| M_{int} - M_{ext} | < tolerance \quad (4.21)$$

Note that if the shear deformations described in Section 4.5.1 are to be taken into account, the moment equilibrium equation is given by:

$$| M_{int} - M_{ext} - \Delta M_{shear} | < tolerance \quad (4.22)$$

where ΔM_{shear} is the apparent increase in moments used to express the additional stresses acting in the concrete at the level of the flexural steel due to diagonal tensile cracking (Section 4.5.1)

When force and moment equilibrium have been ensured at all the cracked nodes, the curvatures for these nodes are then estimated using Equation (4.20). A flowchart illustrating the procedure adopted for the force and moment equilibrium analyses are shown in Figures 4.15 and 4.16 respectively.

4.5 Additional Effects on the Deformation of Members

4.5.1 Effects due to Shear Deformation

Principal tensile stresses are developed in a concrete section when the section is subjected to both flexural and shear stresses. These principal tensile stresses are usually inclined at an angle to the axis of the beam, the angle of inclination being dependent on the combination of flexural and shear stresses acting on the section. When the principle tensile stresses exceed the tensile strength of the concrete, inclined or diagonal cracks will form which will cause additional deformations to the structure. These are referred to as shear deformations by Park and Paulay (1975). In the proposed analytical models, the effect of shear deformation on the flexural behaviour

of externally prestressed structures is considered by using the *truss mechanism* described by Park and Paulay (1975) and Alkhairi (1991).

The concept of the displaced bending moment diagram was first introduced by Park and Paulay (1975) to take account of the effect of shear deformation on flexural members. They showed that after the formation of diagonal tensile cracks, the tension force in the flexural steel becomes greater than that required to resist the external moment of the section. The increase in the tension forces in the flexural steel can be expressed as an additional moment ΔM_{shear}, which is added to the moments due to the externally applied load M_{ext}. For the proposed models, ΔM_{shear} is derived using the truss mechanism theorem and added to the external moments M_{ext}, at the sections where diagonal tensile cracking occurs.

The truss mechanism adopted here uses the analogy of a truss representing a beam; with diagonal concrete struts acting as compression members and the stirrups as tension members.

The following assumptions are used for the truss mechanism model:

- the angle of inclination of all the diagonal struts specified in the truss model were conservatively assumed to be 45°
- diagonal tensile cracking occurs whenever the applied shear force, V_x, exceeds the theoretical shear strength provided by the concrete, V_c.

The calculation of the theoretical shear strength of concrete V_c in the proposed models, are based either on the expressions given by the ACI 318-83 (1983) or the BS8110 (1985) codes even though they are only empirical and are more applicable for internally bonded post-tensioned structures. This is because of the lack of other rational expressions or procedures available in the technical literature. An unpublished report by Rubakantha and Daly (1994) states that they are presently studying the applicability of these equations for externally post-tensioned structures. However, in the absence of any results by them, it is considered sufficiently conservative to use the expressions from the two codes mentioned above in the proposed models.

According to the ACI 318-83 (1983) code, V_c for prestressed concrete members is defined as the lesser of V_{ci} and V_{cw} given in Equations (4.23) and (4.24) respectively:

$$V_{ci} = 0.0498\sqrt{f'_c}bd + V_d + \frac{V_i M_{cr}}{M_{\max}} \quad \text{.....(4.23)}$$

$$V_{cw} = \left[\left(0.29\sqrt{f'_c} + 0.3f_{pc}\right)bd\right] + V_p \quad \text{.....(4.24)}$$

where

$$M_{cr} = \frac{I}{y_t}\left(0.498\sqrt{f'_c} + f_{ppe} - f_d\right) \quad \text{.....(4.25)}$$

b = width of rectangular section or web width of flanged section

d = effective depth of the section ($< 0.8d_p$)

V_d = shear force due to self-weight of member at section considered

V_i = factored shear force due to superimposed dead load plus live load at section considered under same load as M_{max}

f_{ppe} = stress due to the prestress force at tension level

f_d = stress due to self weight at the tension level

f_{pc} = compressive stress in the concrete at the centroid of the cross section or at the junction of web and flange if the centroid is in the flange, due to effective prestress

V_p = vertical component of prestressing force at section considered

According to BS8110 (1985) codes, V_c for prestressed concrete members is defined by the lesser of V_{co} and V_{cr} given in Equations (4.26) and (4.27) respectively:

$$V_{co} = 0.037bd\sqrt{f_{cu}} + 0.37\sqrt{f_{cu}}\frac{IV_x}{y_t M} + \frac{M_o V_x}{M} \quad \text{.....(4.26)}$$

$$V_{cr} = \left(\frac{Ib}{A\tilde{y}}\right)\left(f'_{prt} + 0.8f_{prt}f_{cp}\right)^{1/2} + V_p \quad \text{.....(4.27)}$$

where

$$M_o = 0.8f_{pt}\frac{I}{y_t} \quad \text{.....(4.28)}$$

f_{pt} = stress due to the prestress force at the level of the prestress tendon

$A\tilde{y}$ = the first moment of area about the centroid of the portion above the point in the section being considered

f_{prt} = allowable principal tensile stress ($0.24\sqrt{f_{cu}}$)

f_{cp} = compressive stress at the centroid

Park and Paulay (1975) used the truss mechanism theorem to derive equations for calculating the apparent increase in moments in a cracked section due to shear deformations; i.e. ΔM_{shear}. For the truss models introduced by them, the stirrup reinforcement was assumed to resist only tensile forces while the concrete struts were assumed to resist only compressive forces. In deriving expressions for ΔM_{shear}, two types of beam actions were considered; those with web reinforcements and those without. The force equilibrium diagrams for the truss models with and without web reinforcements are shown in Figures 4.18 and 4.17 respectively.

Considering the model with web reinforcement shown in Figure 4.18, the vertical component of the force taken by the stirrups V_s and the spacing of the web reinforcement s may be expressed as:

$$V_s = C_d \sin\alpha = T_s \sin\beta \quad \text{.....(4.29)}$$

$$s = z_p (\cot\alpha + \cot\beta) \quad \text{.....(4.30)}$$

See Figure 4.18 for explanation of the notation.

Taking moments about the centroid of the compressive force C':

$$M'_1 = M'_2 + V_s z_p \cot\alpha = T' z_p + \frac{s}{2} T_s \sin\beta \quad \text{.....(4.31)}$$

where

M'_1 = moments at section (1) shown in Figure 4.18

M'_2 = moments at section (2) shown in Figure 4.18

Substituting Equations (4.29) and (4.30) into Equation (4.31), and rearranging the resulting equation; the force in the tensile reinforcement T' may be expressed as:

$$T' = \frac{M'_2}{z_p} + \frac{V_s}{2}(\cot\alpha - \cot\beta) \quad \text{.....(4.32)}$$

Studying the model without web reinforcement shown in Figure 4.17, similar derivations may be performed on the model and the increase in the tensile force in the tensile reinforcement contributed by the concrete T'' is given by:

$$T'' = \frac{M''_2}{z_d} + V_c \cot\alpha \quad \text{.....(4.33)}$$

where

M''_2 = moments at section (2) shown in Figure 4.17

Combining the two mechanisms shown in Figures 4.17 and 4.18:

$$V_x = V_c + V_s \quad (4.34)$$

$$M_x = M'_2 + M''_2 \quad (4.35)$$

$$T_x = T' + T'' \quad (4.36)$$

Hence the total tension force in the flexural reinforcement in section (2) may be expressed as:

$$T_x = \frac{M_x}{z_p} + V_c \cot\alpha + \frac{V_s}{2}(\cot\alpha - \cot\beta) \quad (4.37)$$

If the term $\eta = \frac{V_s}{V_x} = \frac{V_x - V_c}{V_x}$ is introduced, the equation may be simplified to:

$$T_x = \frac{M_x}{z_p} + \frac{e_v}{d} V_x \quad (4.38)$$

where $e_v = d\left(\cot\alpha - \frac{\eta}{2}(\cot\alpha + \cot\beta)\right) \geq 0$

From Equation (4.38), it is evident that after the formation of the diagonal tensile cracks, the tension force T_x in the flexural steel is increased and can be expressed as an apparent additional moment, which is added to the external moment acting on the section:

$$M_{int} = M_{ext} + \Delta M_{shear} \quad (4.39)$$

$$\Delta M_{shear} = e_v V_x \quad (4.40)$$

Note that V_x, M_x and T_x are the total shear force, moment and flexural tension force at the section considered respectively.

4.5.2 Tension Stiffening

When a concrete flexural member is loaded, cracking will occur at sections where the tensile strength of the concrete has been exceeded. At these cracked sections, all the tension is usually assumed to be carried by the reinforcement. However, between the

cracks, some of the tension is transferred from the reinforcement to the concrete through the action of bond stresses. Billig (1960) reported that, before cracking, the distributions of stress in the steel and concrete along the line of the reinforcement in the tensile zone were observed to be uniform; but after cracking both distributions changed to wave-shaped profiles. For the concrete tensile stress this is characterised by zero concrete stress at the cracked sections and maximum concrete stress at the sections lying midway between the cracks. As a consequence of the greater flexural rigidity in the uncracked concrete between cracks, overall stiffness of the beam will be enhanced, an effect known as *tension stiffening*.

The deformation of a structure is usually predicted by integrating the curvatures evaluated along the span using Equations (4.5) and (4.6). It is common practice to determine the curvature at cracked sections by assuming that the sections are fully cracked, and ignoring the tension in the concrete. However since the effects of tension stiffening are ignored, this will over-estimate the deflection. In order to incorporate the effects of tension stiffening in the proposed analytical models, the *mean curvature method* discussed by Ghali (1993) was adopted.

The mean curvature method uses a smeared crack methodology for considering the effects of tension stiffening in cracked concrete structures. In the method, two extreme states of behaviour are assumed for a cracked section termed State I and State II. State I assumes that the section is uncracked and the curvature ϕ_I of the section is calculated using Equations (4.10) to (4.12), given in the pre-cracked analysis (Section 4.4.1). In State II, the section is assumed to be fully cracked and the curvature ϕ_{II} of the section is calculated by using the procedure described in Section 4.4.2 for the post-cracked analysis. Note that integrating the curvatures in State I will always under-estimate the deformation response of the cracked structure while using curvatures in State II will always over-estimate it. In order to consider the tension stiffening effect in cracked structures, the mean curvature method uses a variable known as mean curvature ϕ_m. The mean curvature ϕ_m lies between the values of the two extreme curvatures ϕ_I and ϕ_{II} (Equation (4.41)), and may be estimated by using the equation given in the CEB-FIP model code (1978) shown in Equation (4.42).

$$\phi_I < \phi_m < \phi_{II} \quad \text{.....(4.41)}$$

$$\phi_m = (1-\zeta)\phi_I + \zeta\phi_{II} \quad \text{(4.42)}$$

where

$$\zeta = 1 - \beta\left(\frac{M_{cr}}{M_{ext}}\right)^2 \quad (\text{with } M_{ext} \geq M_{cr}; \text{ and } \zeta \geq 0.4)$$

$\beta =$ $\beta_1\beta_2$

$\beta_1 =$ 1 for high bond bars

$\beta_2 =$ 1 and 0.5 for first loading and for loads applied in a sustained manner or for a large number of cycles respectively

Ghali (1993) showed that the deflection of a flexural concrete member can be determined quite accurately using the concept of mean curvature ϕ_m described above.

4.6 Material Constitutive Models

One of the assumptions used for building the non-linear analytical models is that the material constitutive models are known. Hence, sets of material stress-strain relationships have been taken from various sources (i.e. BS8110 (1985), Naaman and Harajli (1985) and Saenz (1964)) and incorporated into the algorithms of the computer programmes developed here for the analysis of externally post-tensioned structures. This section describes the various concrete and steel constitutive relationships used in the investigation, although the facility exists to incorporate other material models in due course.

4.6.1 Concrete

The stress-strain curves for concrete may be divided into three distinct parts:

- the first part is depicted by a near linear curve, which extends up to about 30% of maximum compressive strength
- between 30% - 90% of the maximum compressive strength, the gradient of the stress-strain curve decreases gradually to zero at the peak point
- beyond the peak point, the slope of the stress-strain curve descends until crushing failure occurs at ultimate strain ε_{cu}.

The profiles of the stress-strain curve for concrete are similar for low, normal and high strength concrete, although, for higher strength concrete, the initial slope is higher as a

result of the higher modulus of elasticity for such materials. Also, since higher strength concrete tends to behave in a more brittle manner; the stress drops off more sharply after peak than it does for concrete of low strength.

The strength of concrete may either be defined by conducting a cylinder test f'_c (used in the United States) or a cube test f_{cu} (used in the UK). According to Lin and Burns (1982), the strength of concrete obtained from a cylinder test is within 70%-90% of the strength obtained from a cube test; that is:

$$1.25 f'_c \cong f_{cu} \quad \text{.....(4.43)}$$

The tensile strength of the concrete may be evaluated by means of bending tests conducted on plain concrete beams. The tensile strength in flexure, known as the modulus of rupture, f_r, is then computed from the flexural formula M/Z, where M is the bending moment at the failure of the specimen and Z is the section modulus of the cross section. Approximate relationships for the modulus of rupture are also given by the following authors:

- **Park and Paulay(1975):**

$$f_r = k\sqrt{f_c'}psi \quad \text{.....(4.44)}$$

where

k = 7 - 13 (7 often used)

- **Naaman (1982):**

Normal weight concrete : $f_r = 7.5\sqrt{f_c'}psi$ to $12\sqrt{f_c'}psi$ .....(4.45)

Light weight concrete : $f_r = 5\sqrt{f_c'}psi$ to $9\sqrt{f_c'}psi$ .....(4.46)

- **Chen (1982):**

$$f_r = 7.5\sqrt{f_c'}psi \quad \text{.....(4.47)}$$

Due to the low tensile strength of concrete, concrete in tension is usually ignored in strength calculations of concrete members. However, as it was intended to take the tensile strength of concrete into account in the proposed models, the stress-strain curve in tension was idealised by a straight line up to the tensile strength. Within this range the modulus of elasticity in tension was assumed to be the same as that in compression.

The three concrete constitutive models incorporated into the computer programmes are:

- **BS8110 (1985) model**

  Figure 4.19 shows the stress-strain curve for concrete, taken from BS8110 (1985). Note that the factor 0.67 used in the model takes into account the relationship between the measured characteristic cube strength f_{cu} (in N/mm^2) and the bending strength of the flexural member. It is a coefficient and not a safety factor. The material safety factor, γ_m, for flexure and axial force is recommended in BS8110 (1985) to be 1.5.

- **Saenz (1964) model**

  Chen (1982) introduced the concrete constitutive model suggested by Saenz (1964). In this model, the stress-strain curve for the concrete is divided into two distinct portions, i.e. the ascending and descending portion (Figure 4.20). The ascending branch of the stress strain curve is given by

$$f_c = \frac{E_o \varepsilon}{1 + \left[\left(E_o / E_s\right) - 2\right]\left(\frac{\varepsilon}{\varepsilon_c}\right) + \left(\frac{\varepsilon}{\varepsilon_c}\right)^2} \qquad (4.48)$$

  where

  E_o = tangent modulus of elasticity at zero stresses

  f'_c = maximum compressive strength (cylinder test)

  ε_c = corresponding strain at f'_c

  ε_u = crushing strain

  E_s = f'_c / ε_c

  And the falling branch is assumed to be a straight line passing through two points (f'_c, ε_c) and ($0.2f'_c$, $4\varepsilon_u$).

- **Naaman and Harajli (1985) model**

  The concrete constitutive model suggested by Naaman and Harajli (1985) was taken from the works of Wang (1977) and Ahmad (1981). The proposed model takes the form of a single empirical relationship between stress and strain:

$$f_c = \left[\frac{\left(A\left(\frac{\varepsilon_c}{\varepsilon_{cm}}\right) + B\left(\frac{\varepsilon_c}{\varepsilon_{cm}}\right)^2 \right)}{\left(1 + C\left(\frac{\varepsilon_c}{\varepsilon_{cm}}\right) + D\left(\frac{\varepsilon_c}{\varepsilon_{cm}}\right)^2 \right)} \right] \times f'_c \quad ksi \quad \text{.....(4.49)}$$

where

ε_{cm} = $0.001648 + 0.000114 f'_c$ (ksi)

A, B, C, D = coefficients used and values are given in Table 4.1.

While simple to incorporate within computer models, one of the limitation is that the coefficients A, B, C and D were only given for a few values of f'_c.

4.6.2 Reinforcing Steel

Typical stress-strain curves for steel reinforcement are usually characterised by an initial linear elastic portion, a yielding plateau, a strain hardening range in which stress again increases with strain and finally a range where the stress drops off until fracture occurs. Two steel constitutive models were incorporated into the non-linear analytical models:

- **BS8110 (1985) model**

  BS8110 (1985) recommends a simple elastic perfect plastic curve to represent the stress-strain relationship of reinforcing steel (Figure 4.21). Though only an approximation, it has the advantage of being simple and conservative.

- **Naaman and Harajli (1985) model**

  Naaman and Harajli (1985) proposed the following expressions for plotting the stress-strain curve of steel reinforcement:

  For $0 \leq \varepsilon_s \leq \varepsilon_y$

  $$f_s = \varepsilon_s E_s \text{.....(4.50)}$$

  For $\varepsilon_y \leq \varepsilon_s \leq \varepsilon_{sh}$

  $$f_s = f_y \text{.....(4.51)}$$

  For $\varepsilon_s \geq \varepsilon_{sh}$ then;

  $$f_s = f_y + E_{sh}(\varepsilon_s - \varepsilon_{sh})\left[\frac{1 - E_{sh}(\varepsilon_s - \varepsilon_{sh})}{4(f_{su} - f_y)}\right] \text{.....(4.52)}$$

where

E_s = modulus of rupture

E_{sh} = modulus of elasticity of the strain hardening portion

ε_{sh} = hardening strain

ε_{su} = ultimate strain

f_{su} = ultimate strength

ε_y = yielding strain

f_y = yielding strength.

Note that the recommended values for the variables used in Equation (4.52) for Grade 60 ($f_y = 413.7\ N/mm^2$) steel are listed in Table 4.2.

Using the model suggested by Naaman and Harajli (1985) will take strain hardening into account which is neglected in the model proposed by BS8110 (1985).

4.6.3 Prestressing Steel

The stress-strain curve of prestressing steel may be represented by three successive portions; namely, an initial elastic portion up to the proportional limit, a non-linear portion with gradually decreasing slope and a final almost linear strain-hardening portion with a small positive slope leading to failure. Because the yielding of prestressing steel is usually not well defined, the yield strength is determined according to a strain criterion. Two prestressing steel constitutive models were included in the non-linear computer programme:

- **BS8110 (1985) model**

  BS8110 (1985) gives the stress-strain relationships for various types of prestressing steel materials. These relationships are illustrated in Figure 4.22.

- **Naaman and Harajli (1985) model**

  The stress-strain relationship proposed by Naaman and Harajli (1985) is given by:

$$f_{ps} = E_{ps}\varepsilon_{ps}\left[Q + \frac{(1-Q)}{\left(1+\left(\frac{E_{ps}\varepsilon_{ps}}{Kf_{py}}\right)^{N}\right)^{1/N}}\right] \quad \text{.....(4.53)}$$

where:

E_{ps} = modulus of elasticity of the prestressing steel

f_{py} = prestressing steel yield stress

Q,K,N = coefficients (values given in Table 4.3)

4.7 External Beams with Deviators

The global algorithm presented in Section 4.3 was used for all the eight analytical models proposed in the investigation. However, for the non-linear models, EXT5 to EXT10, which were developed for analysing externally prestressed structures with deviators placed along their spans, additional routines were included into the global algorithm to reflect the influence of frictional effects at the deviators.

Sections 4.7.1 and 4.7.2 describe the additional analytical procedures used to predict the flexural behaviour of externally prestressed structures assuming that (1) the tendons are fixed at deviators, and (2) the contact points are frictionless at deviators, respectively.

In order to consider the deviator friction in the analysis, the conditions for slippage to occur must first be defined in the algorithm. In general, slippage will occur whenever the out of balance force Δf at a deviator is greater than the frictional resistance df generated. Hence, procedures must be included to enable the frictional resistance df and out of balance force Δf to be determined at each loading stage. Once slippage is detected at a deviator, the stresses in the tendon on either side of the deviator will be redistributed. Section 4.7.3 presents the additional routines included into the global algorithm to take account of these effects.

4.7.1 Tendons Fixed at the Deviators

EXT5 and EXT6 are analytical models developed to analyse externally post-tensioned structures with deviators, with the assumption that the tendons are fully fixed at the deviators. The input files for running these analytical models must include information regarding the number of deviators and their locations. The initial residual prestress force in the tendons at each spacing between deviators need to be defined

separately in the input files. Note that the spacing between a pair of deviators is referred to as the *deviator spacing* in this text (see Figure 4.25).

For EXT5 and EXT6, the elongations of the tendons at each deviator spacing are analysed individually using Equation (2.22). Equation (4.7) is then used to determine the corresponding strain increases, the stress increases being determined subsequently from the prestressing steel constitutive model. Since the tendons are assumed to be fixed at the deviators, no redistribution of stress between the deviators is conducted in the analysis and any stress increase is dependent only on the movement of the contact points.

4.7.2 Contact Points Assumed to be Frictionless

The contact surfaces at the deviators are assumed to be frictionless for the analytical models EXT9 and EXT10. Similar to the case where tendons are assumed to be fixed at the deviators (Section 4.7.1), the number of deviators and their locations must be defined in the input files. However, the initial residual prestress force is now assumed to be the same throughout the whole span.

The initial total length of the tendons $\ell_{ps(initial)}$, spanning between the anchorages, is first determined. When the beam is loaded, the new total length of the tendons $\ell_{ps(new)}$ between the anchorages is evaluated from the deflected profile of the whole beam. The elongation of the tendons is then calculated using Equation (4.54)

$$\Delta\ell_{ps} = \ell_{ps(new)} - \ell_{ps(initial)} \quad (4.54)$$

The strain increase in tendons throughout the entire span is next calculated using Equation (4.7), followed by the stress increase determined from the material stress-strain relationship.

4.7.3 Frictional Effects at Deviators Considered

EXT7 and EXT8 are analytical models designed to analyse the flexural behaviour of externally post-tensioned structures with deviators in which the possibility of tendon slippage at the deviators and the redistribution of stress due to this slippages are taken into consideration. This is done by incorporating a *frictional slippage model*, developed by the author, into the global algorithms of EXT7 and EXT8.

Due to the extensive procedures involved with the proposed model, it is divided into three analytical stages:

1) *slippage check analysis*
2) *force equilibrium redistribution analysis*
3) *tendon slip redistribution analysis.*

This section describes briefly, with the help of an example, how each stage of the frictional slippage model is introduced into the analytical models EXT7 and EXT8.

In the first stage of the frictional slippage model (i.e. *slippage check analysis*), the slippage conditions at all the deviators placed along the span of the structure are determined. This is performed by first assuming that the tendons are fixed at the deviators (see Section 4.7.1) and no movement is allowed. Using this assumption, the deflected shape of the beam due to external loading is estimated. A localised force equilibrium analysis is then conducted at all the deviators using the prestress force in the tendons evaluated from the deformation of the structure. Figure 4.23 shows the various forces acting on a typical deviator. The normal force N', frictional resistance df and out of balance force Δf, shown in Figure 4.23, are determined with Equations (4.55), (4.56) and (4.57) respectively.

$$N' = F''_{(i)} sin\alpha + F''_{(i+1)} sin\beta \quad (4.55)$$

$$df = N'\mu \quad (4.56)$$

$$\Delta f = | F_{(i)} - F_{(i+1)} | \quad (4.57)$$

where

F = horizontal component of prestress forces acting at deviator

i = subscript to indicate the deviator spacing number

After evaluating df and Δf at all the deviators, the slippage conditions are defined using Equations (4.58) and (4.59).

No slippage occurs at the deviator when:

$$\Delta f \leq df \quad (4.58)$$

Slippage occurs at the deviator when:

$$\Delta f > df \quad (4.59)$$

After the slippage conditions for all the deviators have been determined, stage two of the frictional slippage model involves performing a *force equilibrium redistribution analysis* on the structure. The purpose of conducting such an analysis is to obtain a preliminary estimation of the amount of stress to transfer on either side of the deviators where slippage has occurred, to satisfy the force equilibrium conditions.

In this analysis, when slippage is detected to occur at a deviator, stresses are transferred on either sides of the deviator to maintain force equilibrium. However, redistributing the stresses to maintain force equilibrium at a particular deviator will often affect the global force equilibrium conditions at other deviator locations. For this reason, stresses may need to be redistributed again to ensure that the global equilibrium of forces in the tendons between deviators are satisfied. Conversely, conducting such a global force redistribution analysis alone to maintain global equilibrium of forces, may upset the localised equilibrium conditions achieved earlier. As a result, the localised and the global force equilibrium analyses should both be conducted simultaneously, since the two analyses are dependent on each other. The proposed force equilibrium redistribution analysis has been designed to achieve this.

The procedure for the force equilibrium redistribution analysis performed on structures with only one deviator is different than for those with more than one deviator. For structures with only one deviator placed along their span, the force equilibrium redistribution analysis is performed as follows (see Figure 4.23 for notations used):

If $F_{(i)} > F_{(i+1)}$, a force $F_{transfer}$ is transferred from deviator spacing i to deviator spacing $i+1$ to maintain force equilibrium at the deviator ; i.e.

$$\Delta f = df$$

$$(F_{(i)} - F_{transfer}) - (F_{(i+1)} + F_{transfer}) = df \quad \text{.....(4.60)}$$

Rearranging Equation (4.60):

$$F_{transfer} = \frac{1}{2}\left(\left(F_{(i)} + F_{(i+1)}\right) + df\right) \quad \text{.....(4.61)}$$

If $F_{(i)} < F_{(i)+1}$, a similar derivation can be made to derive an equation for $F_{transfer}$ in this condition:

$$F_{transfer} = -\frac{1}{2}\left(\left(F_{(i)} - F_{(i+1)}\right) + df\right) \quad \text{.....(4.62)}$$

Hence Equation (4.61) or (4.62) may be used to estimate the amount of force to be transferred when only one deviator is present in the external system depending on the direction of the slip.

If more than one deviator is included in an external structure, the redistribution of forces must be conducted in such a manner as to ensure that the localised and global equilibrium of forces at all the deviators are maintained. The methodology adopted in the model to conduct such a redistribution, can best be explained with an example. Figure 4.24 shows an externally prestressed structure with four deviators. From the figure, a set of equations can be derived by studying the localised force equilibrium conditions at the deviators.

At deviator d_1:

$$(F_{(2)} - F_{transfer(1)} + F_{transfer(2)}) - (F_{transfer(1)} + F_{(1)}) = df_{(1)}$$

$$-2F_{transfer(1)} + F_{transfer(2)} = (F_{(1)} - F_{(2)}) + df_{(1)} \quad \text{.....(4.63)}$$

At deviator d_2:

$$(F_{(3)} - F_{transfer(2)} - F_{transfer(3)}) - (F_{(2)} + F_{transfer(2)} - F_{transfer(1)}) = df_{(2)}$$

$$F_{transfer(1)} - 2F_{transfer(2)} - F_{transfer(3)} = (F_{(2)} - F_{(3)}) + df_{(2)} \quad \text{.....(4.64)}$$

At deviator d_3:

$$(F_{(3)} - F_{transfer(2)} - F_{transfer(3)}) - (F_{(4)} + F_{transfer(3)} - F_{transfer(4)}) = df_{(3)}$$

$$F_{transfer(2)} + 2F_{transfer(3)} - F_{transfer(4)} = (F_{(3)} - F_{(4)}) - df_{(3)} \quad \text{.....(4.65)}$$

At deviator d_4:

$$(F_{(4)} + F_{transfer(3)} - F_{transfer(4)}) - (F_{(5)} + F_{transfer(4)}) = df_{(4)}$$

$$-F_{transfer(3)} + 2F_{transfer(4)} = (F_{(4)} - F_{(5)}) - df_{(4)} \quad \text{.....(4.66)}$$

Equations (4.63) to (4.66) are then grouped into matrices and solved by using *the Gauss-Jordan Elimination Method* (Press (1986)) for the values of $F_{transfer(j)}$. Where the subscript j denotes the deviator number. After $F_{transfer(j)}$ for all the deviators are evaluated, the redistributed horizontal prestress force components $F'_{(i)}$ are determined using the following equations:

$$F'_{(1)} = F_{(1)} + F_{transfer(1)} \quad (4.67)$$

$$F'_{(2)} = F_{(2)} - F_{transfer(1)} + F_{transfer(2)} \quad (4.68)$$

$$F'_{(3)} = F_{(3)} - F_{transfer(2)} + F_{transfer(3)} \quad (4.69)$$

$$F'_{(4)} = F_{(4)} - F_{transfer(3)} + F_{transfer(4)} \quad (4.70)$$

$$F'_{(5)} = F_{(5)} - F_{transfer(4)} \quad (4.71)$$

The new horizontal prestress forces $F'_{(i)}$ are subsequently converted to stresses $f'_{(i)}$. The new effective prestress $f'_{pe(i)}$ of the tendons in each deviator spacing after redistribution are then computed using Equation (4.72):

$$f'_{pe(i)} = f'_{(i)} - \Delta f_{ps(i)} \quad (4.72)$$

where:

$f'_{pe(i)}$ = new effective prestress in deviator spacing i due to redistribution.

$f'_{(i)}$ = new stress in deviator spacing i after redistribution of stresses.

$\Delta f_{ps(i)}$ = change in prestress in deviator spacing i due to deformation of the structure.

The redistributed effective prestress f'_{pe} in the tendons for each deviator spacing is next changed to an equivalent strain value ε'_{pe}, using the stress-strain model of the prestressing steel. The slippage strains $\Delta\varepsilon_{slip(j)}$ for the deviator spacings shown in Figure 4.25 are consequently computed by solving Equations (4.73) to (4.77).

$$\varepsilon'_{pe(1)} = \varepsilon_{pe(1)} + \Delta\varepsilon_{slip(1)} \quad (4.73)$$

$$\varepsilon'_{pe(2)} = \varepsilon_{pe(2)} - \Delta\varepsilon_{slip(1)} + \Delta\varepsilon_{slip(2)} \quad (4.74)$$

$$\varepsilon'_{pe(3)} = \varepsilon_{pe(3)} - \Delta\varepsilon_{slip(2)} + \Delta\varepsilon_{slip(3)} \quad (4.75)$$

$$\varepsilon'_{pe(4)} = \varepsilon_{pe(4)} - \Delta\varepsilon_{slip(3)} + \Delta\varepsilon_{slip(4)} \quad (4.76)$$

$$\varepsilon'_{pe(5)} = \varepsilon_{pe(5)} - \Delta\varepsilon_{slip(4)} \quad (4.77)$$

However, Equations (4.73) to (4.77) are derived based only on satisfying the force equilibrium conditions at the deviators. When tendons slip at the deviators, the slippage actually result in a change of tendon length from one deviator spacing to another, and not just a variation in the stress and strain values. As such, it is necessary to check the redistribution again, this time considering the change of tendon length, i.e. tendon slip $g_{(j)}$, from one deviator spacing to another. This redistribution analysis

is referred to as the *tendon slip redistribution analysis*, and is conducted at the third stage of the frictional slippage model.

Figure 4.25 shows a simplified sketch of how the tendon slip redistribution analysis is conducted and the various variables used in the analysis. Note that two new variables are used in this analysis, $k_{(j)}$ and $g_{(j)}$. The variable $k_{(j)}$, which is either +1 or -1, gives the direction of the slippage movement, i.e.;

If $F_{(i)} \leq F_{(i+1)}$ then

$$k_{(j)} = +1 \quad \text{(4.78)}$$

If $F_{(i)} > F_{(i+1)}$ then

$$k_{(j)} = -1 \quad \text{(4.79)}$$

The variable $g_{(j)}$ is the tendon slip occurring at the deviators, that is, the amount of tendon movement from one deviator segment to another. The tendon slippages $g_{(j)}$ at deviators d_1 to d_4 of the externally prestressed system shown in Figure 4.25, are calculated using Equations (4.80) to (4.83) respectively. Note that the derivations of Equations (4.80) to (4.83) are also shown in Figure 4.25.

$$g_{(1)} = \ell_{(1)} \Delta\varepsilon_{slip(1)} \quad \text{(4.80)}$$

$$g_{(2)} = \left[\Delta\varepsilon_{slip(2)} + \frac{k_{(1)} g_{(1)}}{\ell_{(2)}} \right] \frac{\ell_{(2)}}{k_{(2)}} \quad \text{(4.81)}$$

$$g_{(3)} = \left[\Delta\varepsilon_{slip(4)} + \frac{k_{(4)} g_{(4)}}{\ell_{(4)}} \right] \frac{\ell_{(4)}}{k_{(3)}} \quad \text{(4.82)}$$

$$g_{(4)} = \ell_{(4)} \Delta\varepsilon_{slip(4)} \quad \text{(4.83)}$$

where

$\ell_{(i)}$ = length of the deviator spacing i

After evaluating the tendon slippage occurring at all the deviators, a new estimation of the changes in strain at the deviators $\Delta\varepsilon'_{slip(i)}$ are given by Equations (4.84) to (4.88):

$$\Delta\varepsilon'_{slip(1)} = \frac{k_{(1)} g_{(1)}}{\ell_{(1)}} \quad \text{(4.84)}$$

$$\Delta\varepsilon'_{slip(2)} = \frac{-k_{(1)}g_{(1)} + k_{(2)}g_{(2)}}{\ell_{(2)}} \quad \text{.....(4.85)}$$

$$\Delta\varepsilon'_{slip(3)} = \frac{-k_{(2)}g_{(2)} + k_{(3)}g_{(3)}}{\ell_{(3)}} \quad \text{.....(4.86)}$$

$$\Delta\varepsilon'_{slip(4)} = \frac{-k_{(3)}g_{(3)} + k_{(4)}g_{(4)}}{\ell_{(2)}} \quad \text{.....(4.87)}$$

$$\Delta\varepsilon'_{slip(5)} = \frac{k_{(5)}g_{(5)}}{\ell_{(5)}} \quad \text{.....(4.88)}$$

The new changes in strain in the tendons $\Delta\varepsilon'_{slip(i)}$ are then converted to equivalent stress changes $\Delta f'_{slip(i)}$, and added to the initial effective prestress $f_{pe(i)}$ of the tendons, to provide the redistributed effective prestress $f'_{pe(i)}$ (see Equation (4.89)). The deformation of the structure is re-analysed with the new effective prestress forces, and the non-linear procedure continued until a stable solution for the structure is obtained for the particular load stage being analysed.

$$f'_{pe(i)} = f_{pe(i)} - \Delta f_{slip(i)} \quad \text{.....(4.89)}$$

The external system given in Figure 4.25 shows a typical even arrangement beam with four deviators. The term *even arrangement* refers to an even number of deviators placed in the structure; while an *odd arrangement* refers to an odd number of deviators used. The procedure for the tendon slip redistribution analysis, described above, can be adopted for any beam with an even number of deviators. However, when an odd arrangement of deviators is specified, the tendon slip redistribution analysis is conducted slightly differently.

Figure 4.26 shows an odd arrangement externally prestressed beam with three deviators. The procedure for the tendon slip redistribution is conducted as explained for the even arrangement beam (shown in Figure 4.25), except that at the middle deviator of the structure, two equations are derived for the tendon slip, $g_{(middle\ deviator)}$. Equations (4.90) and (4.91) gives the two equations obtained for deviator d_2 shown in Figure 4.26:

$$g_2 = \left[\Delta\varepsilon_{slip(2)} + \frac{k_1 g_1}{\ell_2} \right] \frac{\ell_2}{k_2} \quad \text{.....(4.90)}$$

$$g_2 = \left[-\Delta\varepsilon_{slip(3)} + \frac{k_3 g_3}{\ell_3} \right] \frac{\ell_3}{k_2} \quad \text{.....(4.91)}$$

The average of the two values evaluated for the middle deviator is used in the proposed redistribution analysis.

An algorithm has been designed to incorporate the frictional slippage model presented in this section into EXT7 and EXT8.

4.8 Termination Conditions

The analytical models proposed in this investigation have been designed to simulate the flexural responses of simply supported externally prestressed beams up to the ultimate conditions. In these models, loads are applied on the externally prestressed structure in increments, until the structure reaches ultimate limit state. For each incremental load stage, the stress increase in the tendons and the change in eccentricity of the tendons are estimated based on the deformed profile of the structure.

The loading methods used in the proposed algorithm are different for the pre-crack and the post-crack analyses. Before cracking, load increments are added directly on the structure until cracking occurs. After cracking, the strains at the extreme compression fiber of the concrete at the critical section are increased incrementally, and the amount of load to be placed on structure at each stage are subsequently determined. Hence, unless some pre-set conditions are specified in the algorithms to terminate the analysis, the algorithm will continue increasing the external loads and analysing the structure with the increased loads endlessly.

These pre-set conditions programmed into the proposed models are referred to as the termination conditions of the models, and they determine whether or not the execution of the computer analysis should be stopped. The termination conditions include:

1) Termination condition 1: The external moment at the critical section for each loading stage is analysed by increasing the strain of the concrete at the extreme

compression fiber. When this moment increase is less than 0.05% from that of the previous load stage, for a total of five load stages continuously, the analysis will be terminated.

2) Termination condition 2: The analysis is terminated when the tensile reinforcement strain exceeds the specified ultimate steel strain.

3) Termination condition 3: The analysis is terminated when the concrete compressive strain at any node exceeds the specified ultimate concrete strain.

4) Termination condition 4: In the post-crack state, a force equilibrium analysis is conducted to estimate the position of the neutral axis. When no solution is derived from this analysis after performing 50 iterative cycles, the programme will be stopped.

5) Termination condition 5: When no solution is obtained for the stress increase in the tendons Δf_{ps} in the analysis for the uncracked state after 20 iterative cycles, the programme will be terminated.

6) Termination condition 6: When no solutions are obtained for the variations in tendon eccentricity Δ_{eccen} before cracking, after 20 iterative cycles, the programme will be terminated.

7) Termination condition 7: The analysis is terminated when no solutions are derived from the bisection method conducted to locate the cracking point in the load-deflection curve.

8) Termination condition 8: When no solution is obtained for the stress increase in tendons Δf_{ps} at the post-crack state after 20 iterative cycles, the programme will be terminated.

9) Termination condition 9: When no solutions are obtained for the variations in tendon eccentricity Δ_{eccen} after cracking, after 20 iterative cycles, the programme will be terminated.

10) Termination condition 10: When no solutions are obtained for the change in tendon stress due to slippage at the deviators Δf_{slip} before cracking, after 20 iterative cycles, the programme will be terminated.

11) Termination condition 11: When no solutions are obtained for the change in tendon stress due to slippage at the deviators Δf_{slip} after cracking, after 20 iterative cycles, the programme will be terminated.

12) Termination condition 12: When convergence problems are encountered due to the occurrence of large deflections (see Section 5.4) the analysis will be stopped.

Not all the termination conditions listed above are applicable for all the proposed analytical models because the requirements for each individual model are different. In fact, the algorithms for all the models were designed in such a manner that termination conditions could easily be removed, added or changed.

4.9 Concluding remarks

A short study was conducted here to determine if the finite element method was the most appropriate non-linear analytical tool to be used in this research investigation to simulate the behaviour of externally post-tensioned structures. However, because of the problems encountered (see Section 4.2) and the large amount of computing time required for solution, it was therefore not considered an appropriate approach to be used for this investigation.

As a result, eight non-linear analytical models were developed, denoted EXT3 to EXT10 respectively, which may be used to analyse the flexural response of simply supported externally prestressed structures up to the ultimate conditions. These proposed analytical models take into consideration the second-order effects, shear deformations, tension stiffening and tendons slippage at the deviators.

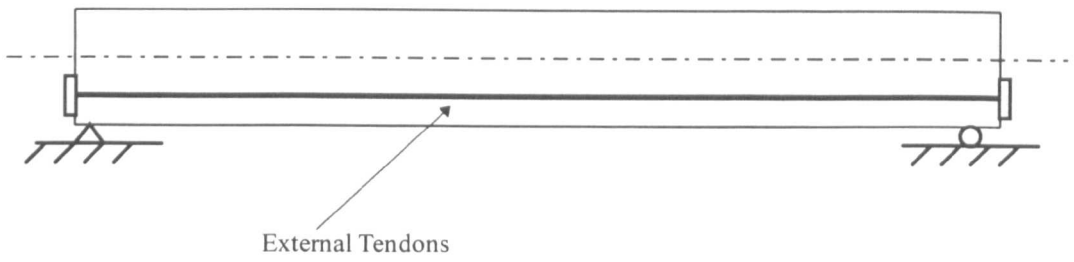

Figure 4.1 : Externally prestressed beam with straight tendons fixed at the anchorages

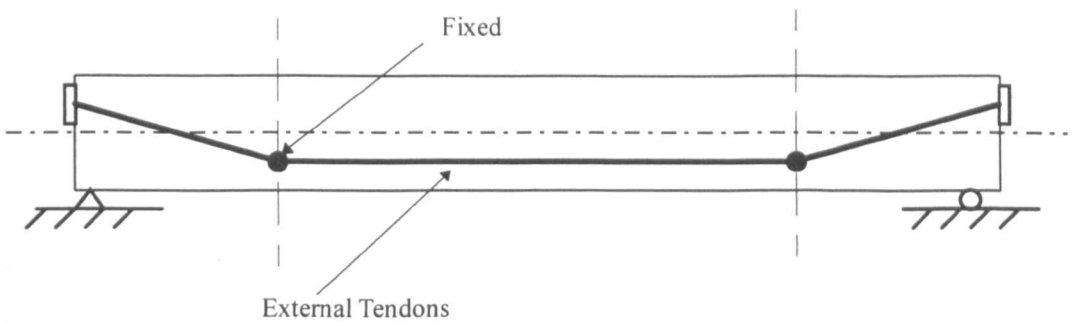

Figure 4.2 : Externally prestressed beam with deviated tendons where tendons are also fixed at the deviators

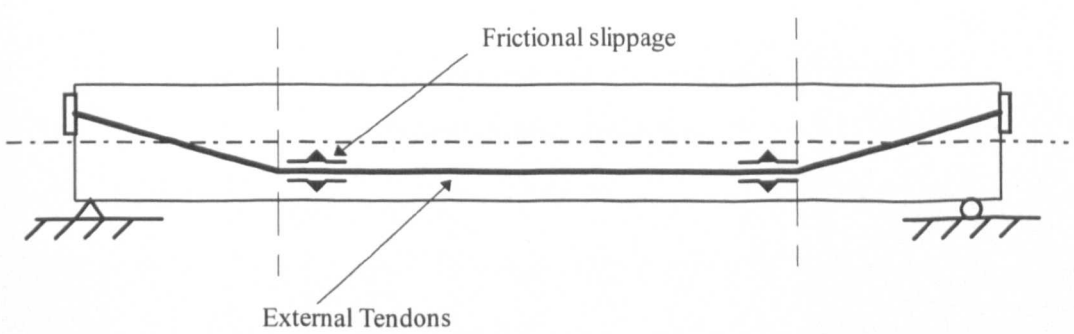

Figure 4.3 : Externally prestressed beam with deviated tendons where frictional slip is permitted

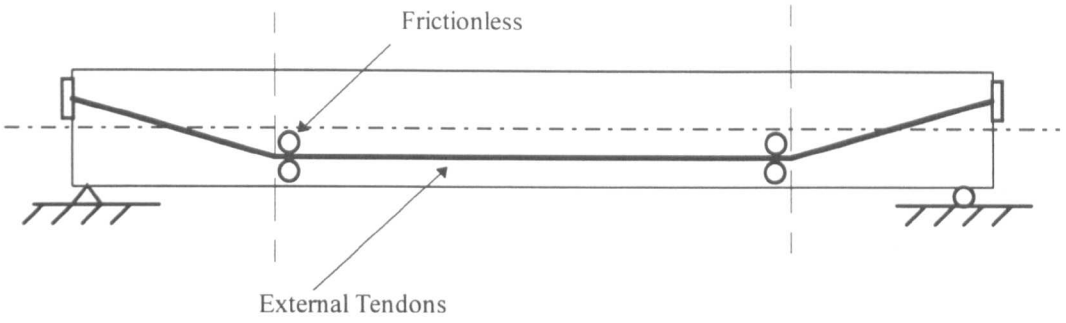

Figure 4.4 : Externally prestressed beam with deviated tendons where contact points are assumed frictionless

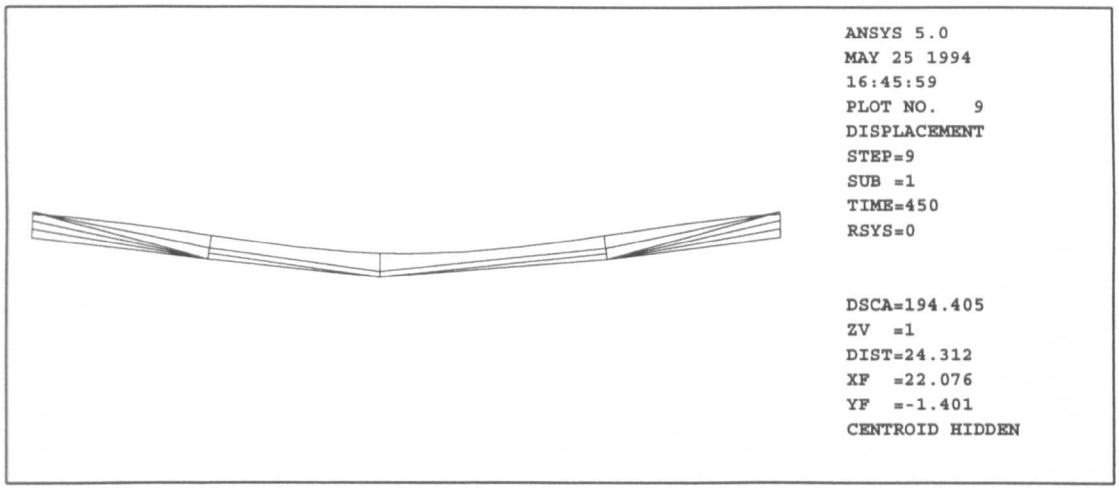

Figure 4.5 : One-dimensional line element model (*VER2*) at design ultimate condition.

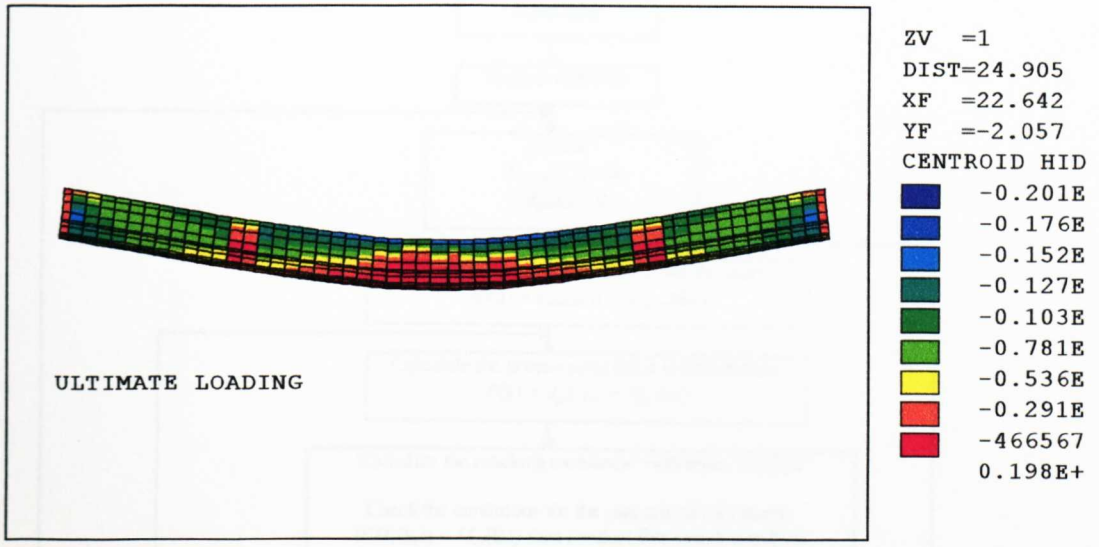

Figure 4.6 : Two-dimensional plane element model (*VER5*) at design ultimate condition.

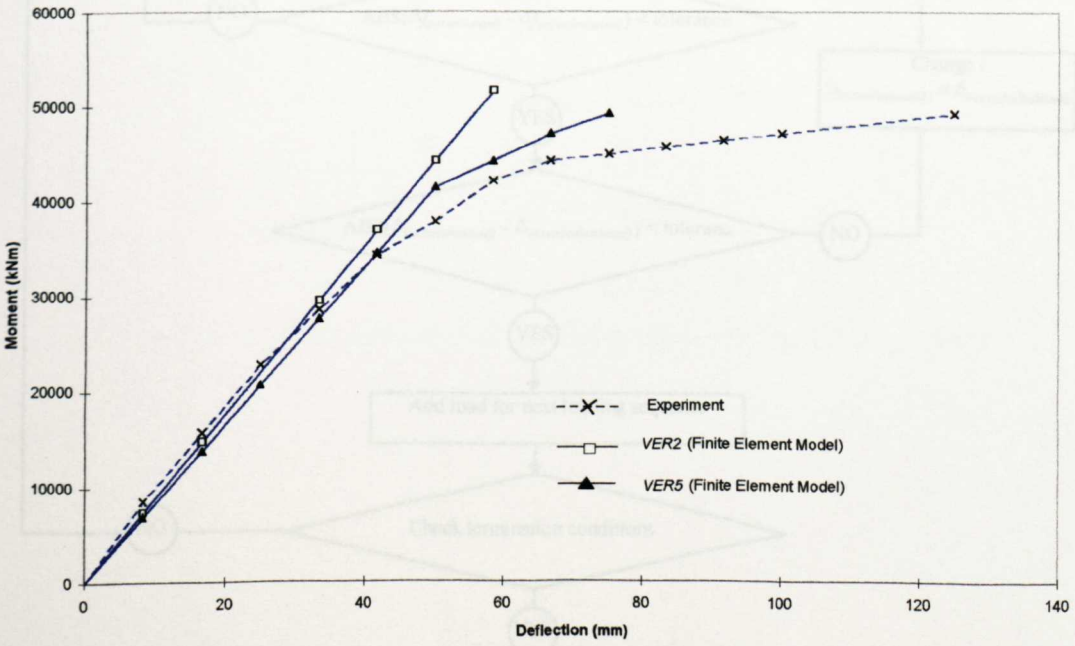

Figure 4.7 : Moment-deflection curves for beam taken from full scale test conducted by Takebayashi et al (1993)

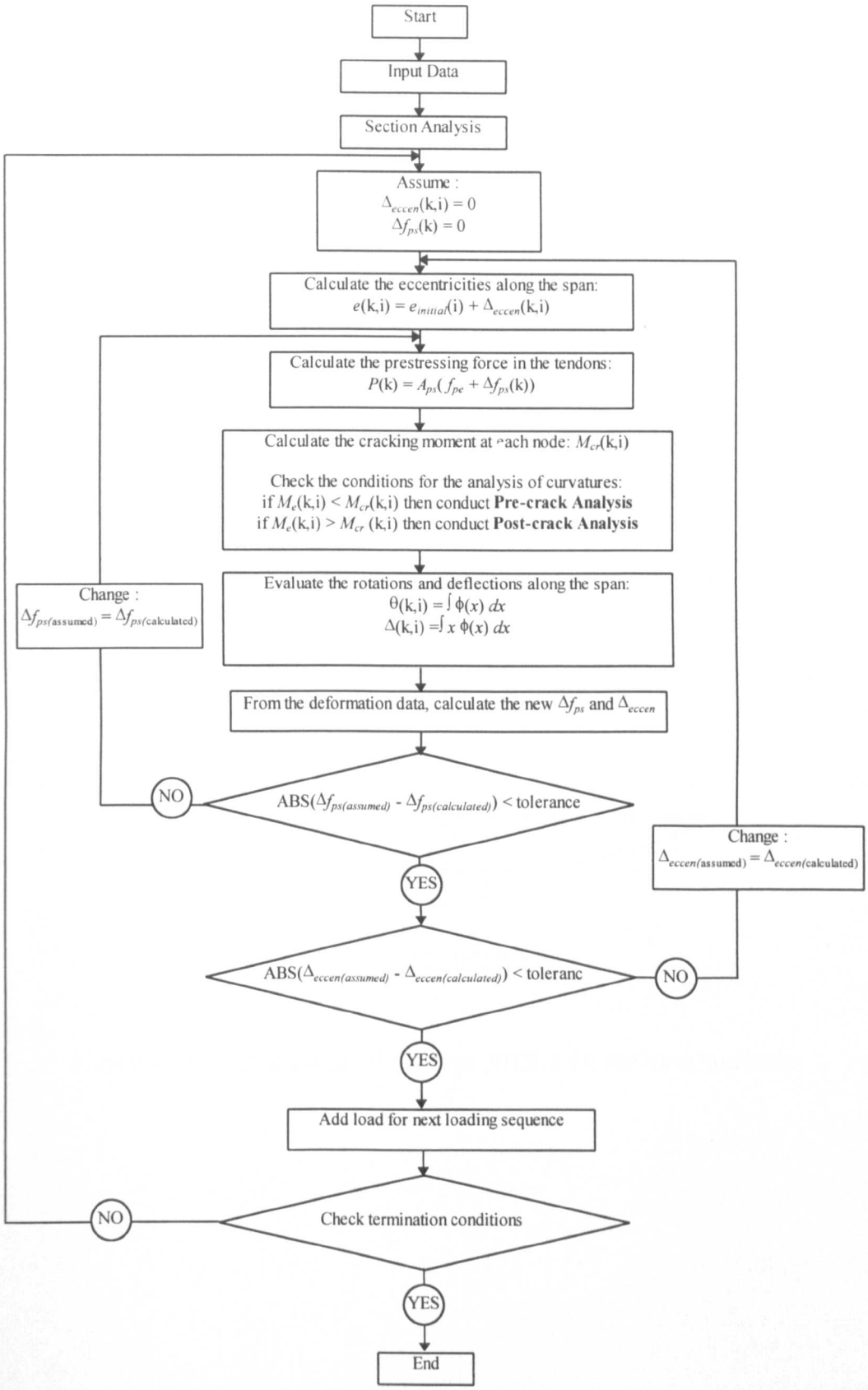

Figure 4.8 : Flowchart showing the global algorithm of the proposed models

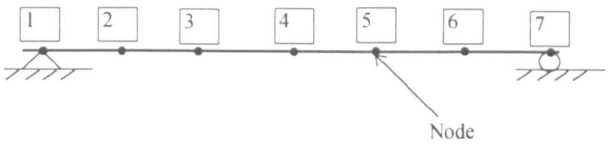

Figure 4.9 : Definition of nodes along the idealised beam

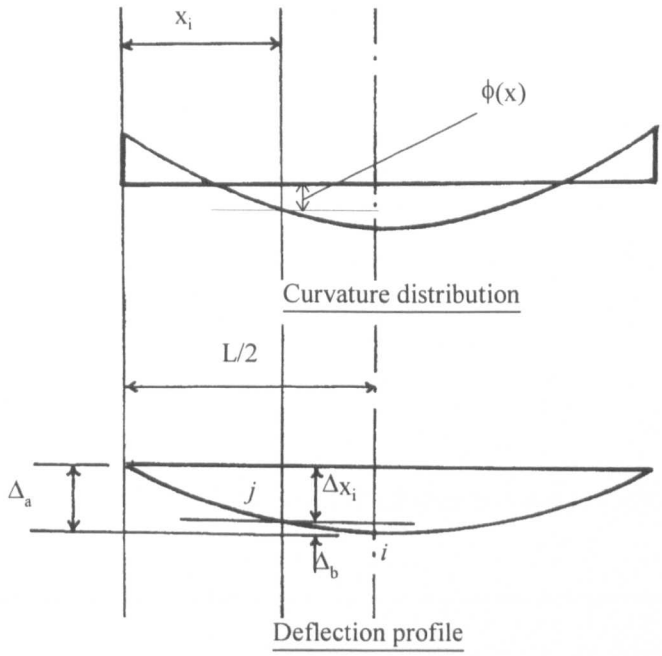

Figure 4.10 : Curvature and deflection profiles for the idealised beam

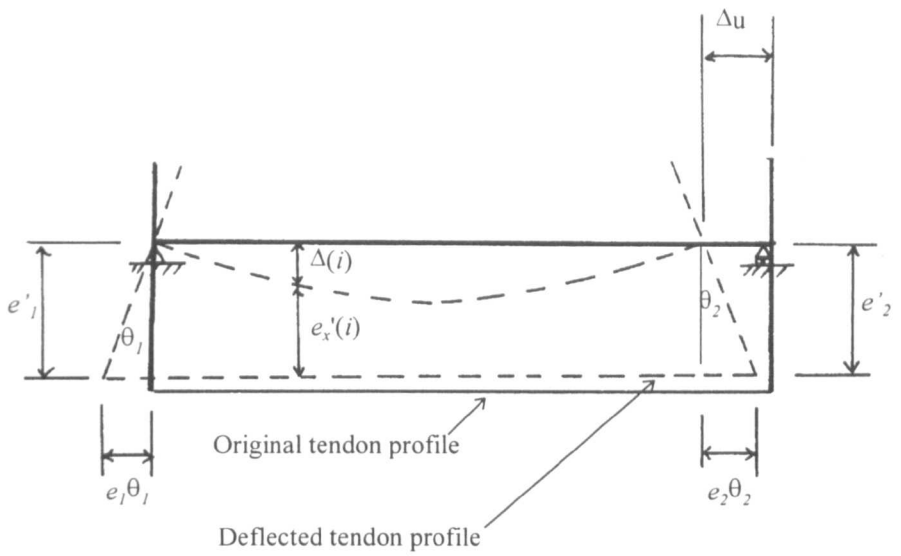

Where:

e_1=	the eccentricity of the tendons at anchorage 1
e_2=	the eccentricity of the tendons at anchorage 2
e_1'=	the new eccentricity of tendons at anchorage 1
e_2'=	the new eccentricity of tendons at anchorage 2
θ_1,θ_2=	rotations at anchorages 1 and 2 respectively
$e_x(i)$=	the eccentricity of the tendons at point *i* due to rotations at the anchorages only
e_x'(i)=	new eccentricity of tendons at point *i*
$\Delta(i)$=	vertical deflection at point *i*

Figure 4.11 : Evaluation of the change in eccentricity

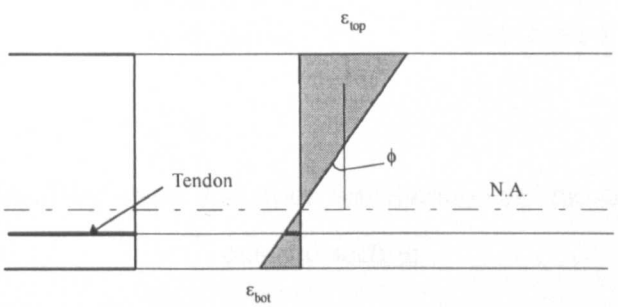

Figure 4.12 : Strain distribution along the depth of a section before cracking

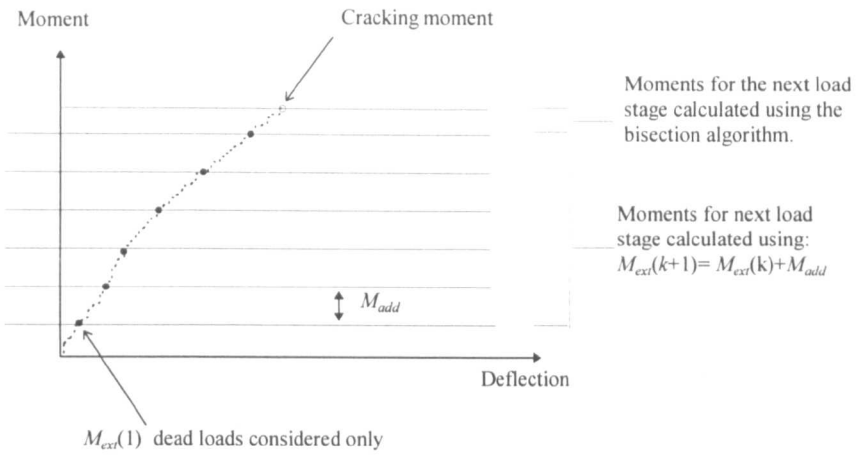

Figure 4.13 : Moment-deflection diagram up to the onset of cracking

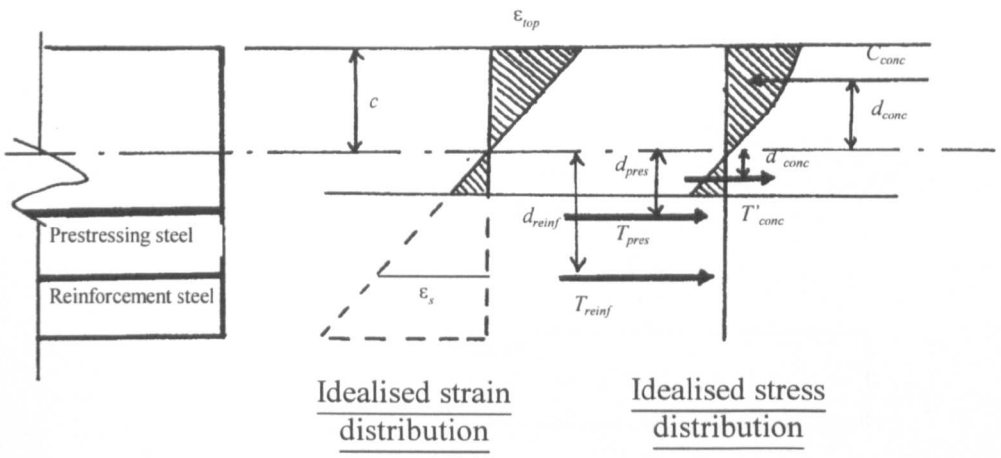

Figure 4.14 : Idealised stress and strain distribution over the depth of a typical cracked section

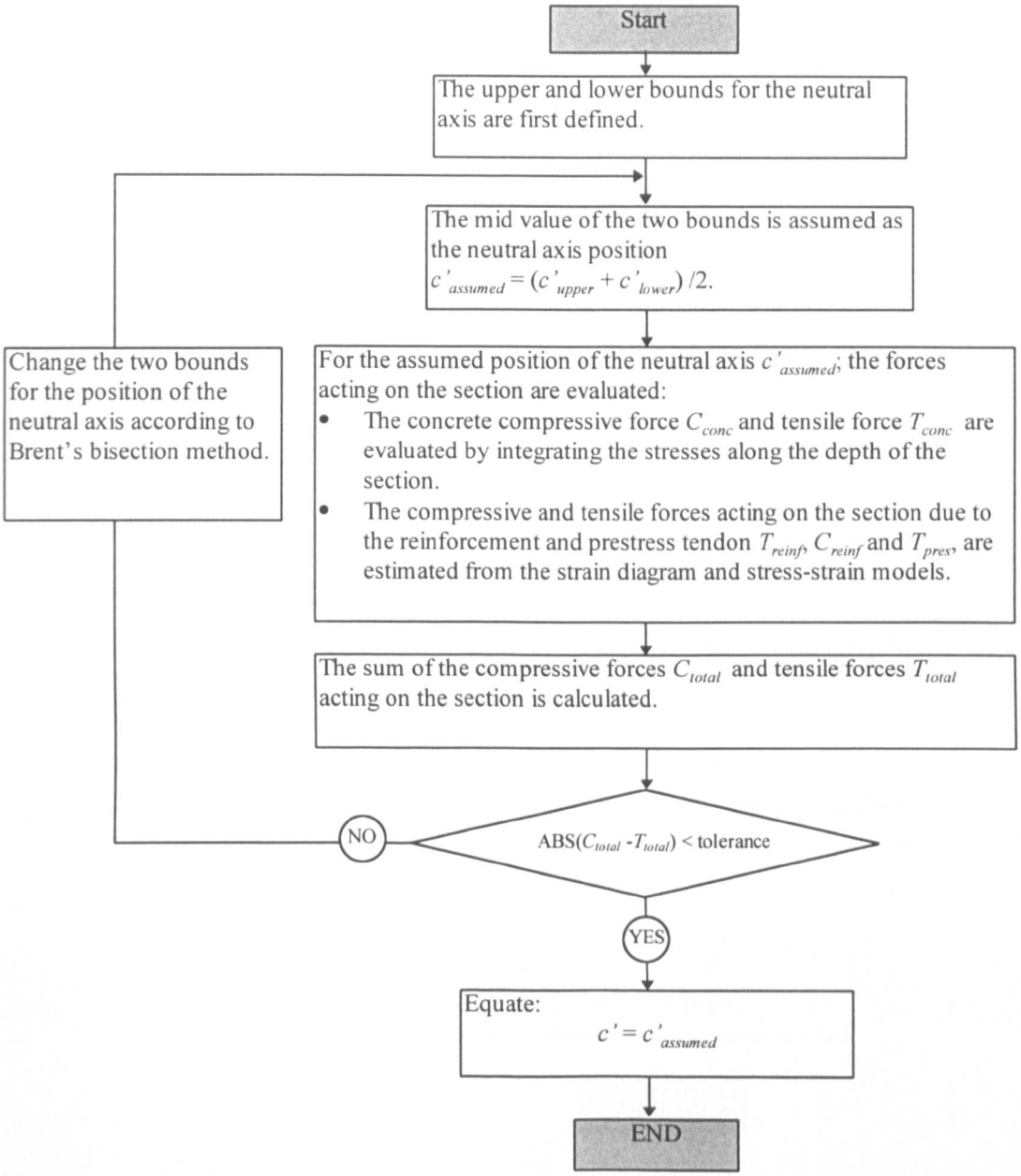

Figure 4.15 : Flowchart illustrating the force equilibrium algorithm used in the computer programmes

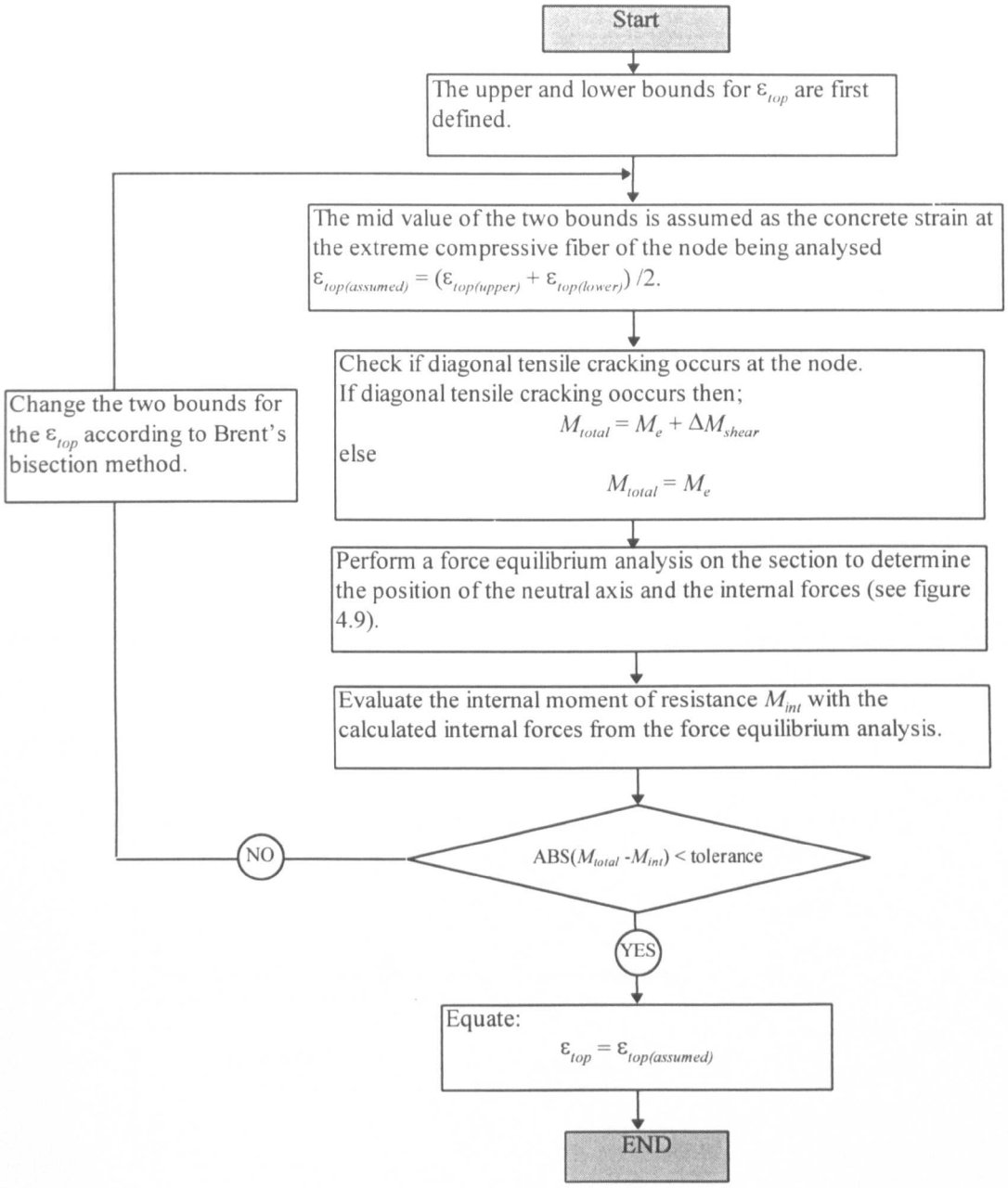

Figure 4.16 : Flowchart illustrating the moment equilibrium algorithm used in the computer programmes

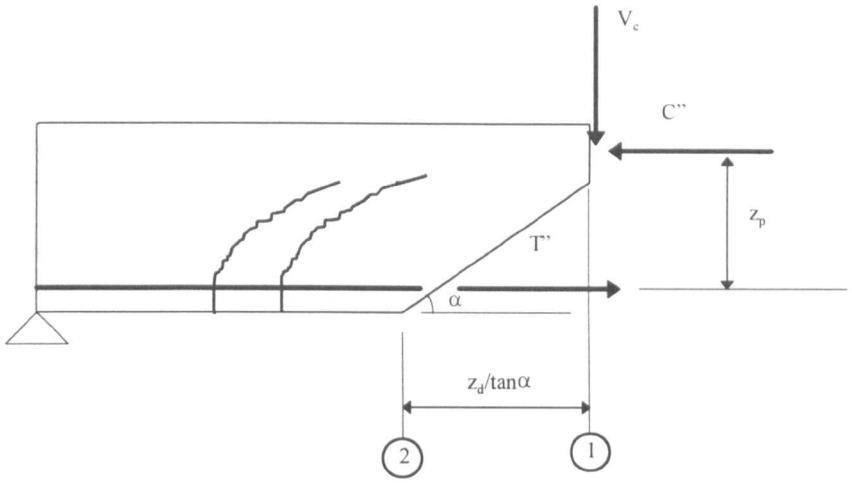

Figure 4.17 : Shear failure mechanism for a beam without web reinforcement

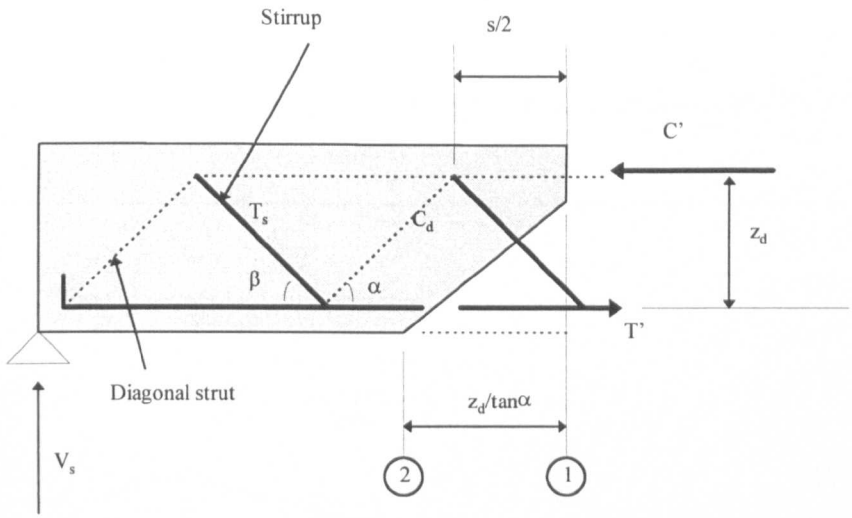

Figure 4.18 : Shear failure mechanism for a beam with web reinforcement

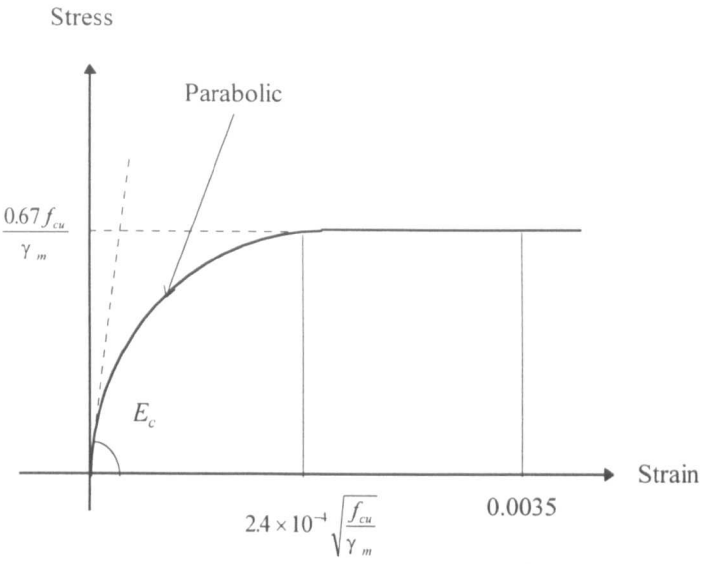

where

$$E_c = 5.5\sqrt{\frac{f_{cu}}{\gamma_m}} KN / mm^2$$

Figure 4.19 : The stress-strain curve for concrete taken from BS8110 (1985)

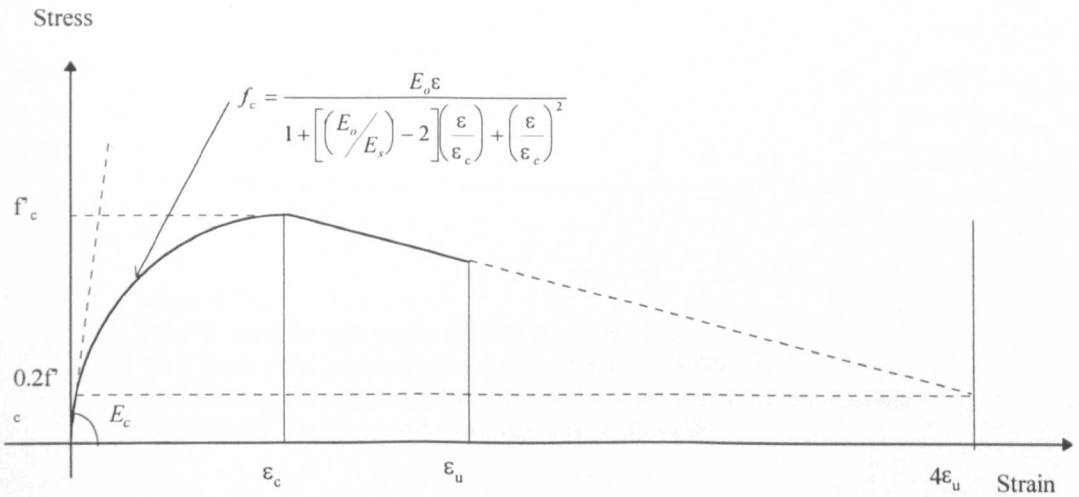

where

$$E_c = 33w^{1.5}\sqrt{f'_c}\, lb / in^2$$

Figure 4.20 : The stress-strain model for concrete suggested by Saenz (1964)

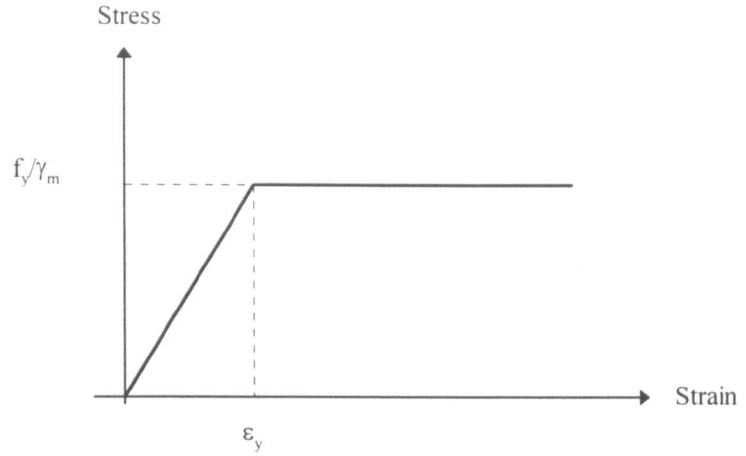

Figure 4.21 : The stress-strain model for steel reinforcement recommended in BS8110 (1985)

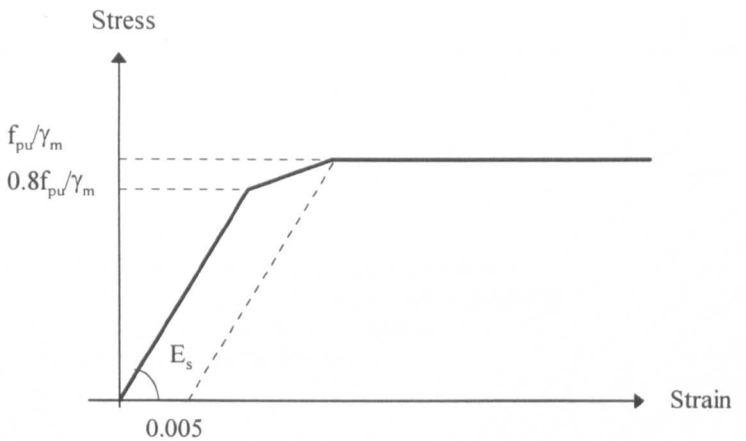

where E_s:
205 KN/mm^2 for wire section two of BS 5896 : 1980
195 KN/mm^2 for strand section three of BS 5896 : 1980
206 KN/mm^2 for rolled or rolled stretched and tempered bars to BS 4486
165 KN/mm^2 for rolled and stretched bars to BS 4486

Figure 4.22 : The stress-strain model for prestressing steel recommended in BS8110 (1985)

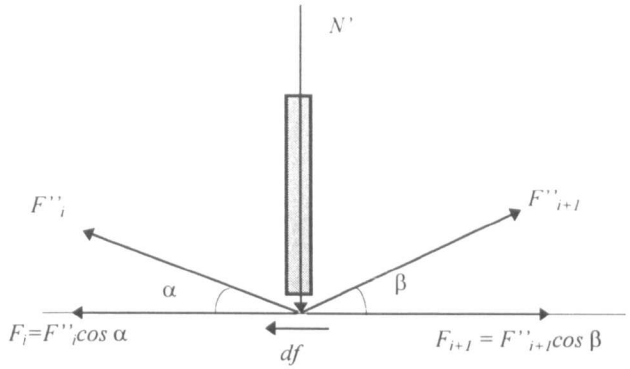

Figure 4.23 : Forces acting at a deviator

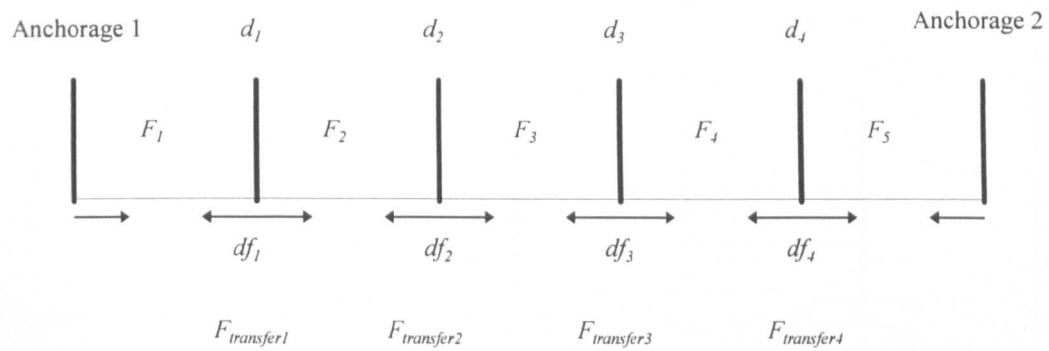

F_i = horizontal prestress force
df_j = frictional resistance generated at deviators
$F_{transferj}$ = horizontal transfer force to maintain equilibrium
i = Subcript to denote deviator spacing
j = Subscript to denote deviator

Figure 4.24 : Force redistribution diagram

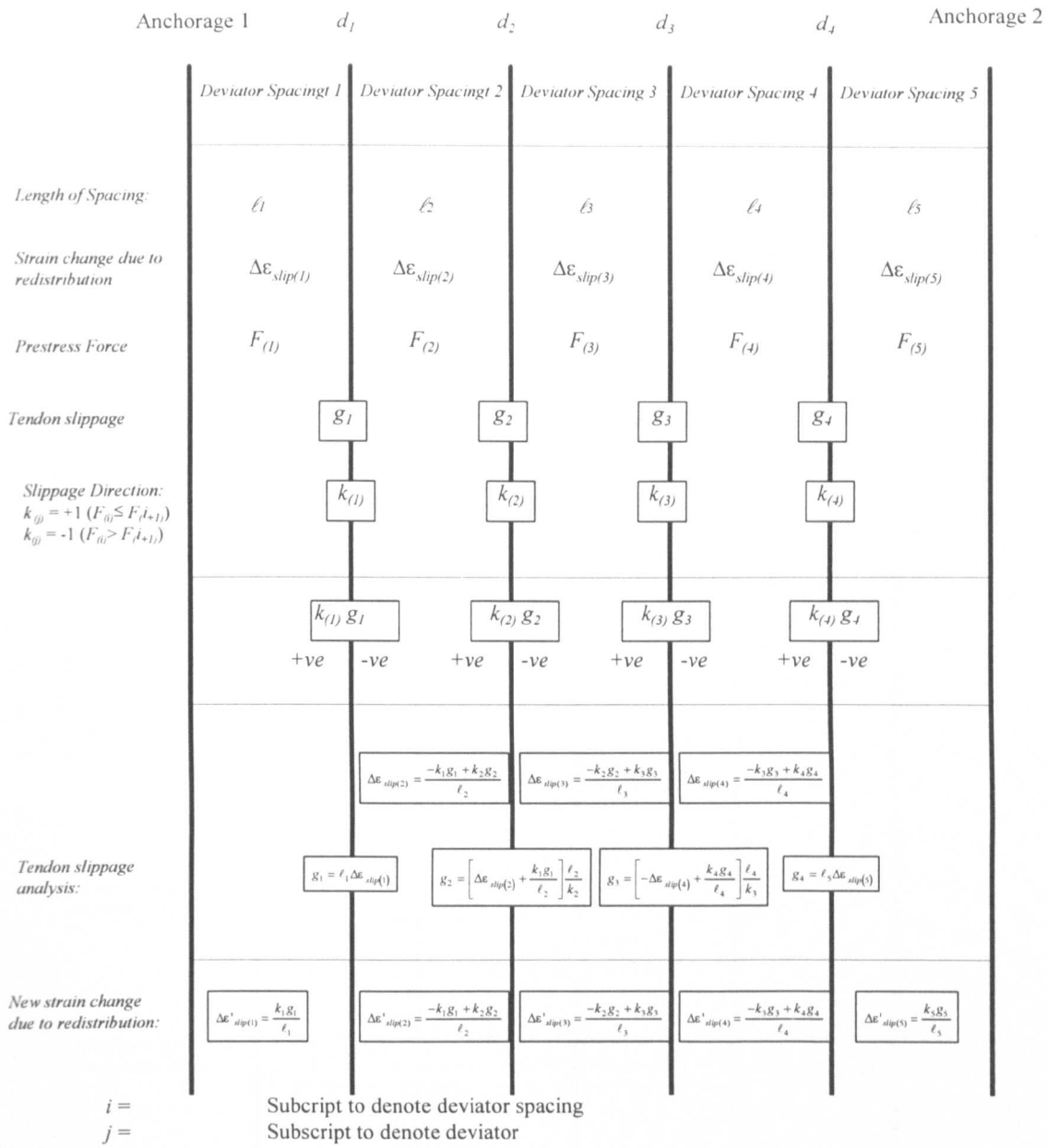

Figure 4.25 : Tendon slip redistribution analysis for beams with an even number of deviators

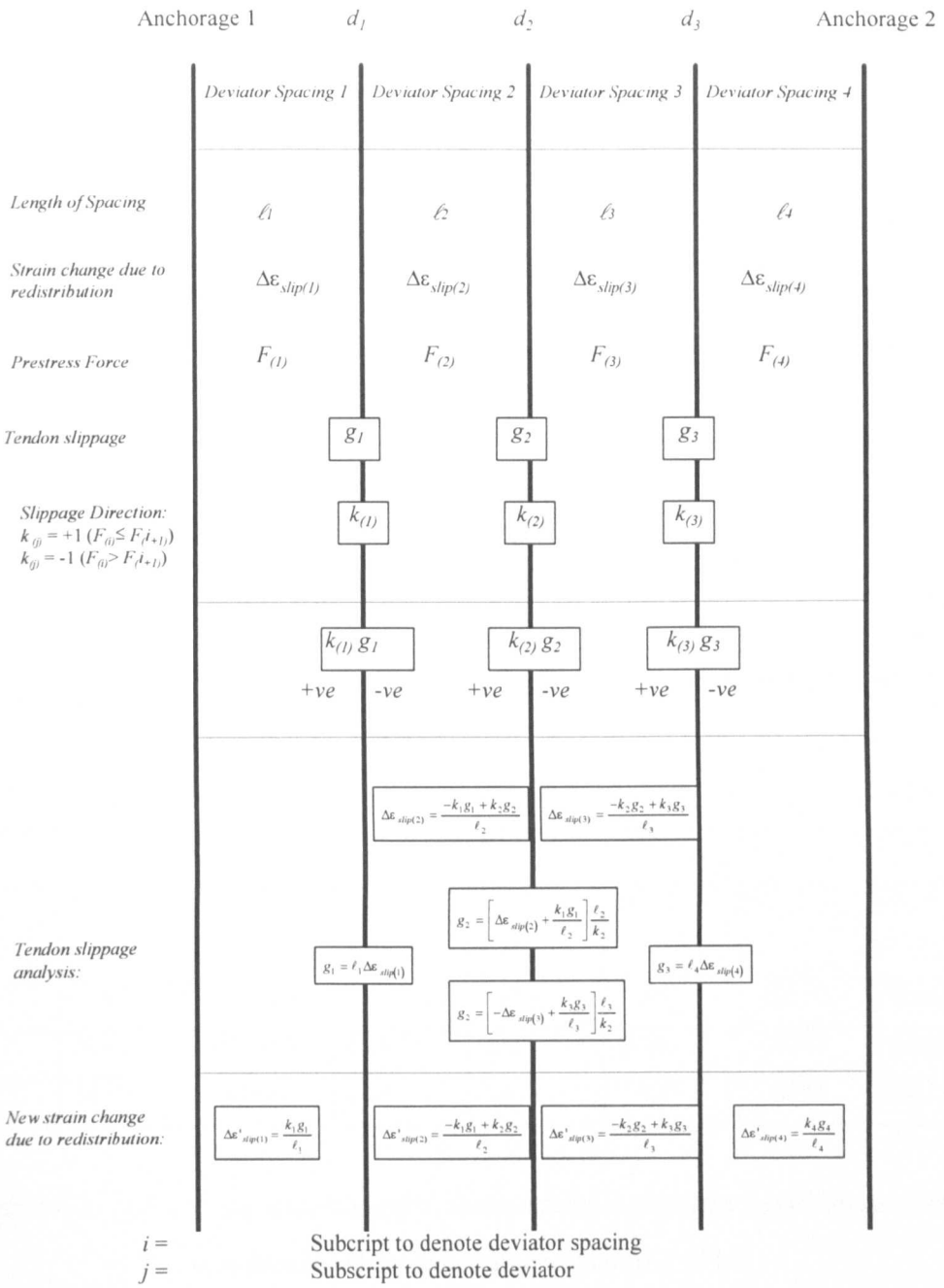

Figure 4.26 : Tendon slip redistribution analysis for beams with an odd number of deviators

f'_c(ksi)	Ascending Portion				Descending Portion			
	A1	B1	C1	D1	A2	B2	C2	D2
5	1.50886	-0.5292	-0.4911	0.47080	0.78813	-0.0503	-1.2118	0.94970
7	1.40631	-0.6998	-0.5936	0.30016	0.37260	-0.0185	-1.6274	0.98141
9	1.35586	-0.7697	-0.6441	0.23024	0.22156	-0.0095	-1.7784	0.99041

Table 4.1: Coefficients for the concrete model adopted by Naaman and Harajli (1985)

Grade	f_y(ksi)	E_s(ksi)	ε_y	E_{sh}(ksi)	ε_{sh}	f_{su}(ksi)	ε_{su}
60	60.0	29760.0	0.0020	1222.0	0.0091	98.6	0.00730

Table 4.2: Constitutive model values for grade 60 steel recommended by Naaman and Harajli (1985).

Grade	f_{pu} (ksi)	E_{ps} (ksi)	ε_{pu}	f_{py} (ksi)	N	K	Q
270	278.0	27890.0	0.069	243.5	7.344	1.0618	0.01174
235	244.0	29300.0	0.087	222.0	8.060	1.0325	0.00625
160	160.0	28790.0	0.041	141.8	7.100	1.0041	0.01750

Table 4.3: *Q,K,N* coefficients used in the prestressing tendon constitutive model recommended by Naaman and Harajli (1985).

Chapter 5

Verification of Models

5.1 General

The proposed non-linear analytical models designed for simulating the flexural behaviour of externally post-tensioned structures up to the ultimate limit state have been presented in Chapter Four. Before these non-linear models can be used for any practical purpose, they first need to be validated by showing that the results obtained from them are in close agreement with those from reported experiments. This process for verifying the authenticity of the computer models was conducted in the investigation and is presented in this chapter.

A total of seventeen beams tested by Yaginuma and Kitada (1987, 1988, 1989) and Zhang *et al* (1993) were used for the verification process. A brief description of these beams and the reasons why they were used are presented in Section 5.2. Although all these beams were simply supported and prestressed with external tendons, they had different cross sectional properties (rectangular or T-shaped), loading patterns (point load at mid-span or two equi-distant point loads), tendon profiles (straight or deviated), span-depth ratios (values ranged from 12 - 32) and non-prestressed reinforcement ratios. These were selected to ensure that the non-linear analytical models were valid for a wide range of beam parameters.

In Section 5.3, a detailed discussion is presented on the comparison between the results obtained from the proposed computer models and the experiments. Note that all analyses conducted here were performed using the Silicon Graphic computer Challenge XL MIPS 4400 CPU. The relationships used for making this comparison included the moment-deflection and the moment-change in prestress (Δf_{ps}) relationships. The ratio of the maximum moment predicted by the non-linear models to the maximum moment measured in experiments (M_{pred}/M_{exp}) was also used here

indicate the degree of accuracy obtained from using these non-linear models to predict the ultimate moment capacities of these externally prestressed beams.

The termination of an analysis conducted with the proposed models is denoted here as either complete or premature. Complete termination refers to the termination of an analysis due to one of the following conditions:

- the strain in the concrete fiber at the critical section has reached the specified ultimate concrete strain (i.e. 0.0035)
- the tensile strength of the steel has reached the specified ultimate strength.

Premature termination on the other hand refers to the termination of an analysis due to the occurrence of numerical convergence problems. Although complete terminations were achieved for most of the beams simulated in the verification process, several of the analyses failed prematurely. The cause and effects of these convergence problems encountered with the proposed models and the measures employed here to rectify or minimise them are discussed in Section 5.4.

Tension stiffening refers to the increased stiffness in a flexural member due to tension being carried by the concrete between cracks. In the proposed models, nodes are defined along the span of the beam and a sectional analysis is performed at each node to determine its curvature. In the sectional analysis, it is assumed that the concrete is fully cracked in the tensile zone whenever the stress exceeds the flexural tensile strength of the concrete. This, however, is not an accurate assumption if tension stiffening is to be considered in the analysis. Section 5.5 presents a discussion on the significance of tension stiffening and whether it should be incorporated into the algorithm of the proposed non-linear models.

When shear and flexural stresses act simultaneously at a section and the shear forces applied at the section exceeds the shear strength provided by the concrete, diagonal tensile cracking occurs. Diagonal tensile cracking causes additional deformation in the flexural member, referred to as shear deformation. Naaman and Alkhairi (1993) reported that the effects due to this shear deformation may be significant when assessing the stress increase in unbonded tendons at the ultimate limit state for beams with a span-depth ratio less than 24.

The additional deformations due to the occurrence of diagonal tensile cracking is modelled in the analytical models using the truss mechanism introduced by Park and Paulay (1975). However, the truss mechanism was developed mainly for reinforced concrete structures and the estimated shear strength V_c was based on the empirical equations suggested in the codes of practice (i.e. either ACI (1983) or BS8110 (1985)). Section 5.6 discusses the applicability of using this methodology to reflect the effects of shear deformation in the analytical models and the significance of considering it in the flexural analysis of externally prestressed structures.

5.2 Experimental Data

As part of the verification process, it is necessary to show that the results obtained from the proposed computer models are in close agreement with those given in experimental tests. However, before such a comparison can be made, an appropriate set of experimental beams should first be identified from reported research investigations on externally prestressed beams. These selected beams should generally satisfy the following conditions:

1) They should be simply supported and prestressed with external tendons.
2) There should be enough information provided in the experimental data to enable them to be simulated by the proposed computer models.
3) The experimental data should possess clear output results of the beams, e.g. moment-deflection and moment-change in prestress relationships, to enable a comparison to be made between them and the computer derived results.

A total of seventeen externally prestressed beams were found suitable for the verification process. Ten of these beams were reported by Yaginuma and Kitada (1987, 1988, 1989), the rest by Zhang *et al* (1993) [1]. Table 5.1 gives a list of the beams used for the verification process together with their key parameters. Further information of these beams may be found in Appendix A. From Table 5.1, it was observed that the parameters influencing the flexural behaviour of externally

[1] Note that an attempt was made by the author to contact the above researchers for the technical reports of their experimental works, but without success.

prestressed beams discussed in Chapter Three, i.e. cross sectional properties, loading patterns, tendons profiles, span-depth ratios and non-prestressed reinforcement ratios, were all varied in these beams. This gives an additional advantage of ensuring that the proposed models were validated with a set of beams that had a wide range of design parameters.

The beams of Yaginuma and Kitada (1987, 1988, 1989) were all rectangular in shape and loaded to failure using a single point load applied at the mid-span. For some of these beams the initial prestress force was not directly reported by Yaginuma and Kitada but indicated in the following statement: '*the prestress was 8 N/mm^2 at the bottom of the specimen*'. For such beams it nas been assumed that the stress at the extreme concrete fiber at the mid-span was 8 N/mm^2 when prestress was first applied to the structure. The initial prestress force F was then determined by back-calculating using Equation (4.11).

Although some details of the material properties (e.g. yield strength, ultimate strength, etc.) for concrete, passive reinforcement and prestressing steel were reported by Yaginuma and Kitada, they failed to provide information about the stress-strain profiles of these materials. Therefore, the constitutive model recommended by Saenz (1964) was used for concrete and those by Naaman and Harajli (1985) were used for the prestressing steel and the passive reinforcement.

Yaginuma and Kitada (1987) tested six beams to study the influence of the amount of passive reinforcement on the flexural behaviour of externally prestressed structures. Three of the test beams were prestressed externally and had enough information provided to enable them to be used for the verification process. The three beams were denoted Beams OA-1, OB-1 and OC-1, and were very similar to each other except for their reinforcement ratios which were 0.57%, 0.98% and 1.92% respectively (see Table 5.1).

Yaginuma and Kitada (1988) tested six simply supported beams to failure. Only two of these beams, denoted Beams OS-1 and OL-1 were used for the verification process because they were prestressed with external tendons and sufficient information was available to simulate their behaviour. Design specifications for Beams OS-1 and OL-1 were found to be very similar except for their span-depth ratios, which were 24 and

42 respectively. Yaginuma and Kitada (1988) intentionally chose such a large difference because they wanted to study the influence of span-depth ratio on the flexural behaviour of these structures.

Ten beams were tested by Yaginuma and Kitada (1989), out of which six were prestressed with external tendons. However, only five of these beams, denoted Beams OA88-2, OB88-1, OC88-1, OC88-2 and OD88-1 were found to be suitable for use in the verification process. These beams were all very similar to each other in terms of span-depth ratios, cross-sectional properties and loading conditions, but had different combinations of initial prestress force, prestressed and non-prestressed reinforcement ratios (see Table 5.1).

Some properties of the prestressing steel used for Beams OA88-2, OB88-1, OC88-1, OC88-2 and OD88-1 were reported by Yaginuma and Kitada (1989). From these reported values it was found that the behaviour of these tendons was best represented by Grade 160 (f_{pu} = 1103 N/mm^2) prestressing steel. Yaginuma and Kitada (1987, 1988) on the other hand did not give any information about the prestressing steel properties for Beams OS-1, OL-1, OA-1, OB-1 and OC-1, but instead reported that '*PC tendons (SBPR95/110)*' were used for these beams. The author was however unable to establish the nature of '*PC tendons (SBPR95/110)*' described by them and, therefore had to assume that Grade 160 prestressing steel (f_{pu} = 1103 N/mm^2) were also used for these beams.

Zhang *et al* (1993) tested a total of ten T-shaped, simply supported, externally prestressed beams to failure. Two loading patterns were employed on these beams:

- a single point load applied at mid-span (denoted Load Type 1)
- two equal point loads placed equi-distant from the supports (denoted Load Type 2).

Seven of the beams tested by Zhang *et al* (1993) were considered suitable for use in the verification process (see Table 5.1). Four of these, denoted Beams A1-2, A2-1, A2-2 and A3-2, were prestressed with external tendons over their full length without any deviators; the other three beams, denoted B1-2, B2-2 and B3-2 were prestressed with deviated external tendons. The profiles of the tendons used for these beams are shown in Appendix A. Although all the seven beams had about the same span-depth

ratio and initial prestress force, they were subjected to different loading conditions (Load Type 1 or 2) and possessed different non-prestressed reinforcement ratios (see Table 5.1).

The properties of the concrete, the prestressing steel and passive reinforcement were also not clearly defined by Zhang *et al* (1993) and had to be estimated for the verification process. For the concrete, the stress-strain relationship introduced by Saenz (1964) was used, since the only property reported about this material was its actual strength f'_c. In the case of the prestressing steel, the only information available about them was that: ϕ25 mm threaded steel bars with a modulus of elasticity of 175 GPa were used for Beams A1-2, A2-1, A2-2, and A3-2 and, ϕ5 mm wires with a modulus of elasticity 200 GPa were used for Beams B1-2, B2-2 and B3-2. For the ϕ25 mm threaded steel bars, their ultimate strength was taken to be 1030 N/mm^2 as recommended by the Macalloy Bar Systems Design Data and, the model introduced in BS8110 (1985) was used to represent their constitutive relationship. The stress-strain relationship recommended by Naaman and Harajli (1985) was used for the ϕ5 mm prestressing wires and, their ultimate strength was assumed to be 1655 N/mm^2 (Naaman (1982)). Finally, although the ultimate strength and modulus of elasticity of the reinforcement steel were given as 340 MPa and 200 GPa respectively by Zhang *et al*, the stress-strain relationship for this material was not reported by them. Hence, the constitutive relationship for reinforcement steel recommended by Naaman and Harajli (1985) was used.

5.3 Computer vs. Experimental Results

The flexural behaviour of the beams described in Section 5.2 were simulated to failure using the proposed non-linear analytical models. All the simulations were performed by defining twenty nodes along the span of the beams. This number of nodes was selected because it was generally found that a large number not only produced very similar results but also increased the computational time required for the analysis to an unacceptable level, and the use of fewer nodes generally caused the ultimate moments of the beams to be slightly over-estimated (e.g. as shown in Figures D.1 and D.2 in Appendix D for Beams OA-1 and OC88-1 respectively).

The moment-deflection and moment-change in prestress relationships derived from these analyses were then used, where appropriate, to validate the non-linear models by comparing them with the experimental data. Unfortunately, since the technical reports for the experimental beams were unobtainable, these curves could not be plotted with the actual values measured in the experiments. As a result, the experimental curves were reproduced here by employing the 'grid method'. In the grid method, equally spaced horizontal and vertical lines were first plotted to form a grid system on the graphs presented by Yaginuma and Kitada (1987, 1988, 1989) and Zhang *et al* (1993). Several grid-points were then defined along the profile of the experimental curves and, their numerical co-ordinates estimated from the plotted grid. These co-ordinates enabled the profile of the experimental curves to be re-plotted together with the analytically derived curves, thus allowing a better visual comparison to be made between the two curves.

5.3.1 Beams tested by Yaginuma and Kitada (1987, 1988, 1989)

Figures 5.1 to 5.10 compare the experimental and analytical mid-span deflections. From these figures, it can be seen that a good level of precision was attained by the analytical models for these beams, which had different span-depth ratios, initial prestress force, and non-prestressed and prestressed reinforcement ratios. It was, however, not possible to make a comparison between the analytical and experimental moment-change in prestress relationships for these beams because the curves were not presented clearly by Yaginuma and Kitada.

Figures 5.1 and 5.2 illustrate the experimental and analytical moment-deflection curves for Beams OS-1 and OL-1 respectively. The two beams were similar to each other except for their span depth ratios, which were 24 and 42 for Beams OS-1 and OL-1 respectively. It was observed from these figures that the proposed analytical models can be used accurately to predict the trend of the moment-deflection behaviour of these beams over their full range. The three distinct stages of behaviour which were described by Tao and Du (1985) to be present in the moment-deflection response of unbonded prestressed structures with an adequate amount of non-prestressed reinforcement were also noted to be exhibited by the analytical curves derived for Beams OS-1 and OL-1. The three stages were namely the uncracked stage, the

cracked stage and a third stage representing the behaviour of the beam after the yielding of non-prestressed reinforcement (see Figure 5.1).

From Figure 5.1 it was noted that the analytical curve for Beam OS-1 showed close agreement with the experimental curve throughout the uncracked stage. However, a higher cracking moment of about five percent was predicted by the numerical model and this over-estimation caused the analytical curve to over-estimate the $M/f_{cu}bd^2$ values of the beam (the largest difference being about five percent) in the cracked stage up to yielding of the reinforcement. After the reinforcement had yielded, the analytical curve exhibited a sharp drop in stiffness, where the beam deflections were noted to be relatively high for small increases in external loads. Near the predicted ultimate condition, the analytical curve was observed to show a small decrease in strength before terminating at $M/f_{cu}bd^2 = 0.1184$. The maximum $M/f_{cu}bd^2$ value estimated by the numerical model for Beam OS-1 was 0.119, which was 0.901 of the experimental maximum value (Table 5.2 (a)).

A total of forty-five load sequences were analysed for Beam OS-1 before the analysis was terminated due to the concrete compressive fiber at the critical section attaining the pre-set ultimate strain value (i.e. 0.0035). The whole analysis took approximately twenty-three hours of computer time (see Table 5.2 (a)). The analysis of this beam took such a long time to complete because several 'limiting points' (discussed in Section 5.4) were encountered in the analysis after the non-prestressed reinforcement had yielded. Whenever a limiting point was encountered in the analysis, the non-linear model had been programmed to reduce the load increment for the next loading sequence to prevent numerical convergence problems. This reduction in loads is cumulative and, since numerous limiting points were encountered for the analysis of Beam OS-1, the increase in moments predicted for each subsequent loading stage near ultimate was therefore very small.

The comparison between the analytical and experimental curves for Beam OL-1 is shown in Figure 5.2. The total computer time taken for the analysis was about ten hours and complete termination was achieved for this beam (i.e. the compressive strain of the concrete at the critical section had reached the ultimate strain value specified (0.0035)). The maximum $M/f_{cu}bd^2$ determined by the analytical model was

0.99 of the experimentally reported maximum value (Table 5.2 (a)). The trend of the analytical curve can also be seen to correlate well with the experimental curve for the three stages of the beam behaviour. At the pre-crack stage, the analytical curve under-estimates the experimental moment-deflection response by about fifteen percent. After cracking, although the stiffness of the analytical curve was similar to that shown for the experimental curve, higher $M/f_{cu}bd^2$ values (approximately five percent) were predicted by the analytical model up to the estimated ultimate limit state. It should be noted that the cracking moment predicted for this beam was initially over-estimated by about twenty percent in an earlier non-linear analysis conducted with the numerical model. The beam was then re-analysed again with a reduced modulus of rupture f_r defined for the concrete and, as shown in Figure 5.2, the over-estimation of the cracking moment was effectively reduced to only about five percent.

The moment-deflection relationships for Beams OA88-2, OB88-1, OC88-1, OC88-2 and OD88-1 are shown in Figures 5.3 to 5.7 respectively, and the results summarised in Table 5.2 (a). Although these beams had different combinations of prestress force, prestressed reinforcement ratios and non-prestressed reinforcement ratios, the deflection responses predicted by the proposed models showed excellent agreement with the experimental data. The average M_{pred}/M_{exp} obtained for these beams with the numerical models was also found to be about 0.943 with a standard deviation of 0.046 (Table 5.3), which was considered satisfactory here. That such excellent correlations were possible for these beams was partly due to the provision of adequate information by Yaginuma and Kitada (1989) about their experimental set-up and test results.

Figure 5.3 shows that the analytical curve predicted for Beam OA88-2 was closely related to the experimental curve at the uncracked and cracked stages. Although, the cracking moment for this beam was under-estimated by the analytical model by about fifteen percent, the stiffness of the analytical curve after cracking was in good agreement with the experimentally derived curve. Yielding of reinforcement, on the other hand, was estimated to occur at about $M/f_{cu}bd^2 = 0.10$ by the numerical model, which was about ten percent higher than that shown for the experimental curve. After yielding of the reinforcement, the analytical curve under-estimated the response of the experimental curve by about ten percent and indicated a maximum $M/f_{cu}bd^2$ value of 0.117, which was about 0.943 of the experimental value. The termination condition

for the analysis of this beam was complete (i.e. ultimate concrete strain 0.0035 was attained at the critical section) and the computing time taken for it was about 5.5 hours.

Figure 5.4 shows the comparison between the analytical and experimental curves for Beam OB88-1. Before the occurrence of cracking, it was noted that the analytical curve of Beam OB88-1 under-estimated the stiffness of the experimental curve by about thirty percent (see Figure 5.4). However, after cracking, the numerically derived curve exhibited a slightly higher stiffness and converged towards the experimental curve. The yielding of the reinforcement was also noted to occur at a higher moment (about ten percent) for the analytical curve and after which the analytical curve was found to be almost horizontal. This large change in beam deflection without much change in the $M/f_{cu}bd^2$ value was also observed for the experimental curve, but at a $M/f_{cu}bd^2$ value approximately ten percent lower. The maximum moment ratio M_{pred}/M_{exp} was 1.017 for this beam and total computing time taken for the analysis was about 4.5 hours before it terminated due to the concrete compressive strain at the critical section attaining the ultimate value specified for concrete (0.0035).

Figure 5.5 shows the experimental and analytical curves for Beam OC88-1 and, both curves in the figure were observed to be very closely related to each other before and after the occurrence of cracking. However, the analysis of the beam terminated immediately after the reinforcement started to yield, due to the concrete compressive fiber at the critical section attaining the ultimate strain specified (0.0035). The maximum $M/f_{cu}bd^2$ value predicted by the numerical model was 0.259, and this was about ten percent lower than that observed for the maximum experimental value (see Table 5.2(a)). The total computer time taken for the analysis of this beam was about 5.5 hours and forty-six load sequences were evaluated by the numerical model.

Beam OC88-2 was similar to Beam OC88-1 except for the amount of initial prestress force applied to the structure. While Beam OC88-1 was initially prestressed with a force equal to 80 kN, the initial prestress force applied to Beam OC88-2 was about 160 kN (see Table 5.1). It was noted that the overall trend of the experimental moment-deflection response for Beam OC88-2 was nearly the same as that for Beam

OC88-1 (see Figures 5.5 and 5.6), but Beam OC88-2 exhibited a higher maximum $M/f_{cu}bd^2$ value (i.e. 0.293) than Beam OC88-1 (i.e. 0.276). The numerical analysis for Beam OC88-2 over-estimated the moment-deflection response by about five percent throughout the uncracked and cracked stages and terminated before the yielding of the reinforcement. The termination of the analysis was due to the concrete compressive strain at the critical section reaching 0.0035, which was the specified ultimate strain for the concrete. The maximum $M/f_{cu}bd^2$ value measured in the experiment was found to be about fourteen percent higher than the numerically predicted maximum value (Table 5.2(a)).

Beam OD88-1 had the highest amount of non-prestressed reinforcement in this series of beams tested by Yaginuma and Kitada (1989) and, the analytical and experimental moment-deflection curves derived for it are shown in Figure 5.7. From the figure, it was observed that there was no distinct kink along the experimental and analytical moment-deflection curves to distinguish between the uncracked and cracked stages of the beam behaviour. This was because of the high non-prestressed reinforcement ratio which caused the reduction in stiffness for the beam after cracking to be less profound. It was also observed that the analytical curve over-predicted the profile of the experimental moment-deflection relationship by approximately twenty percent over the full range. Since this large over-estimation of the beam response was only observed for Beam OD88-1 in this series, it was therefore believed that it may be due to some error in the experimental data reported by Yaginuma and Kitada (1989) about the beam. The analysis terminated when the concrete strain at the critical section reached the specified ultimate strain of 0.0035 and, a maximum $M/f_{cu}bd^2$ value of 0.277 was estimated by the numerical model, which was 0.945 of the experimentally measured maximum value. Note that the numerical model took about four hours of computer time to analyse forty-four load sequences for this beam (Table 5.2(a)).

Beams OA-1, OB-1 and OC-1 were all identical except for their non-prestressed reinforcement ratios which were 0.57%, 0.98% and 1.92% respectively (see Table 5.1). The moment-deflection relationships for these beams are shown in Figures 5.8 to 5.10 and, their results are summarised in Table 5.2 (b). It can be observed from these figures that the externally prestressed beams with higher reinforcement ratio generally yield higher flexural strengths but lower deflections at the ultimate limit

state. The theoretical ultimate condition was successfully predicted by the numerical model for all these beams, since the analyses conducted on them all terminated due to the concrete compressive fiber at the critical section reaching the specified ultimate strain for concrete (0.0035). The average numerically derived maximum moment to the experimental maximum moment (i.e. M_{pred}/M_{exp}) for these beams was found to be conservative at 0.865 with a standard deviation of 0.030 (see Table 5.3).

The moment-deflection curves for Beam OA-1 are shown in Figure 5.8 and, the three stages described by Tao and Du (1985) were predicted successfully by the numerical model. Total computer time taken for the analysis was about three hours and, forty-two load sequences were predicted by the model. Comparing the analytical and experimental curves plotted in Figure 5.8, it was observed that the two curves showed very good correlation within the cracked and uncracked stages of the beam behaviour. However, after yielding of the reinforcement, the stiffness of the analytical curve decreased resulting in a near horizontal line, while the experimental curve showed a slow increase in moment up to a maximum value of 17.750 tf.m. As the predicted maximum moment was 15.508 tf.m., the ratio of the analytical and experimental maximum moments for this beam was thus found to be 0.874 (Table 5.2(b)).

The numerically derived moment-deflection curve for Beam OB-1 (Figure 5.9) showed very close agreement with the experimental curve before and after the occurrence of cracking. The analysis was terminated after analysing forty-two load sequences and the termination of the analysis occurred just when the reinforcement started to yield. It was also observed that a relatively flat contour was first indicated by the experimental curve at about 20 tf.m., before showing a small increase in moment up to a maximum value of 21.25 tf.m. This increase in moment may be due to strain hardening occurring in the reinforcement, which consequently caused the predicted maximum moment to be under-estimated by about ten percent.

Figure 5.10 shows the numerically predicted and experimentally derived moment-deflection relationships for Beam OC-1. Although it was observed that the analytical curve showed close agreement with the experimental results at the uncracked stage, the occurrence of cracking was under-estimated by approximately twenty percent. It was further observed that after cracking, the analytical curve under-estimated the

stiffness of the experimental curve and terminated at lower maximum moment of 23.168 tf.m. From Figure 5.10, it can be seen that, when the numerical model reached its maximum, the moment measured from the experiment was about eight percent higher (i.e. about 25 tf.m.). After this, the experimental curve exhibited a sudden large increase in stiffness and the maximum moment measured for the beam was 28.125 tf.m., which was about twenty percent higher than the numerically predicted maximum value. It was, however, uncertain what contributed to the large increase in the stiffness of the deflection response observed for the experimental beam near the ultimate conditions. The numerical model analysed a total of fifty load sequences for Beam OC-1 and the whole analysis took about five hours of computer time.

5.3.2 Beams tested by Zhang *et al* (1993)

Figures 5.11 to 5.14 show the computer predicted and experimentally derived moment-deflection and moment-change in prestress responses for Beams A1-2, A2-1, A2-2 and A3-2. All these beams were T-shaped, simply supported and prestressed with externally prestressed steel bars with no deviators placed along their lengths (see Appendix A). The key parameters varied in these beams were the loading pattern (either Load Type 1 or 2) and the non-prestressed reinforcement ratio (see Table 5.1).

The numerically derived moment-deflection curves for Beams A1-2, A2-1, A2-2 and A3-2 were generally found to be in good agreement with the experimental curves before cracking. However after cracking, the predicted stiffness of the moment-deflection curves for these beams were observed to decrease sharply and under-estimated the experimental moments. It is believed that the discrepancies observed between the analytical and experimental results may be due to an inaccurate interpretation of the material properties used for the simulation of these beams caused by insufficient information provided (see Section 5.2).

Figures 5.11(a) and 5.11(b) show the moment-deflection and moment-change in prestress responses for Beam A1-2 respectively. From Figure 5.11(a), it was noted that the analytical curve was in close agreement with the experimental curve until the occurrence of cracking. After cracking, the analytical curve indicated a sudden loss in stiffness and under-estimated the moments of the beam by about twenty percent. The

stiffness of the analytical curve was observed to be slightly higher than the experimental curve after the non-prestressed reinforcement yielded and, the under-estimation of the moment was consequently decreased from twenty percent to about fifteen percent. It was also observed that even though Beam A1-2 had the lowest reinforcement ratio for this series (i.e. Beams A1-2, A2-1, A2-2 and A3-2), the experimental curve exhibited a smooth curve from cracking to ultimate and no kinks were found along the curve to distinguish the occurrence of first cracking and yielding of the reinforcement. These points were however observed in the experimental deflection relationships for Beams A2-1 and A2-2, which had higher reinforcement ratios. This observation was not consistent with the deflection responses observed for the beams tested by Yaginuma and Kitada (Section 5.2), where only beams with large reinforcement ratios exhibited such a smooth transition from the cracking to the ultimate condition.

The analysis for Beam A1-2 took approximately eight hours of computer time and, terminated prematurely due to convergence problem encountered in obtaining a stable solution for the change in prestress (see Table 5.2(c)). Despite the convergence problem encountered, the numerical analysis was still able to predict about 0.863 of the maximum experimental value. The convergence problem was observed at load sequence thirty-one where the change in prestress Δf_{ps} calculated for each iteration seemed to diverged from the assumed value instead of converging towards it and, this convergence problem is discussed further in Section 5.4.

Figure 5.11(b) shows the analytical and experimental moment-change in prestress curves for Beam A1-2. From the figure, it was observed that the analytical change in the prestress curve conservatively under-estimated the experimental results by about thirty percent up to the predicted maximum moment. This under-estimation of the change in prestress was however insignificant when compared to the large initial prestress force applied to the structure. Observations made previously about the trends of the analytical and experimental moment-deflection curves were also noted for the moment-change in prestress curves, that is, the slope of the analytical moment-change in prestress curve for Beam A1-2 also decreased sharply after first cracking and was slightly higher than the experimental curve after the reinforcement had yielded.

Figures 5.12 (a) shows the moment-deflection response for Beam A2-1, and from the figure, it was noted that both the cracking moment and the yielding of the reinforcement moment was under-estimated by the numerical analysis by as much as thirty percent. This under-estimation was believed to be due to the low modulus of rupture f_r assumed for the concrete in the numerical analysis and, the agreement between the two curves may be improved by using a higher f_r value (as performed for Beam OL-1). However available information was used here for the simulation of the beams rather than fixing the values to obtain a better correlation with the experimental results. The analysis terminated prematurely due to convergence problems encountered in deriving a stable solution for the change in prestress (see Section 5.4). However, Table 5.2(c) shows that the M_{pred}/M_{exp} obtained for Beam A2-1 was found to be 0.897, which was considered reasonable given the fact that the termination condition for this beam was premature. The analysis of this beam took about two hours of computer time and forty load sequences were analysed. The moment-change in prestress relationships for Beam A2-1 are shown in Figure 5.12(b) and, their trends were found to be very similar to those observed for the moment-deflection responses shown in Figure 5.12(a).

Figure 5.13(a) shows the moment-deflection response for Beam A2-2. Before the occurrence of cracking, the analytical curve was noted to over-estimate the experimental deflection response by about ten percent. However, the cracking moment of the beam was under-estimated by the analytical model by about fifteen percent and, the trend of the analytical curve was in good agreement with the experimental curve after the occurrence of cracking. It is believed that increasing the modulus of rupture f_r of the concrete will improve the agreement between the two curves. Figure 5.13(b) showed that for a given change in prestress in the tendons, the moment derived was under-estimated by about fifteen to twenty percent throughout the whole loading history. Conversely, the implied change in prestress was over-estimated by about one hundred percent for a given moment. The complete analysis of Beam A2-2 terminated prematurely after six hours due to convergence problems encountered in deriving a stable solution for the change in prestress in the tendons (Section 5.4). However, the predicted maximum moment was found to be about 0.961 of the maximum experimental moment.

Figures 5.14(a) and 5.14(b) illustrate the moment-deflection and moment-change in prestress relationships for Beam A3-2. For the moment-deflection curves, it was observed that the numerical model estimated the profile of the experimental curve accurately over its full range, except for a slight under-estimation of the deflection response after the occurrence of cracking, where the maximum difference between the two curves was observed to be about ten percent. The analysis of this beam terminated prematurely due to convergence problems (Section 5.4) and produced a maximum moment of about 0.942 of the experimental value. Figure 5.14(b) showed that the numerically derived moment-change in prestress relationship under-estimated the experimental results by about twenty percent after the beam had cracked.

Figures 5.15 to 5.17 show the moment-deflection and moment-change in prestress relationships for beams B1-2, B2-2 and B3-2. These beams were very similar to Beams A1-2, A2-1, A2-2 and A3-2 except that steel wires were used instead of steel bars for the external tendons and, these steel wires were deflected along their lengths by two deviators. Three analytical models (i.e. EXT5, EXT7 and EXT9) were used here to simulate the flexural behaviour of these beams, each with a different assumption used for the frictional behaviour of the tendons at the deviators. Hence, the three analytical curves derived from these models for each beams were denoted:

1) **EXT5 curve**

   This curve is derived from the analytical model EXT5 where the tendons were assumed to be fixed at the deviators. Thus no redistribution of forces due to tendon slippage was allowed in the analysis.

2) **EXT7 curve**

   Derived from the analytical model EXT7 where the frictional behaviour at the deviators and the redistribution of stresses due to tendon slippage were taken into account in the analysis. It was assumed here that steel ducts were placed at the deviators where tendons come in contact with the structure. Hence, the friction coefficient at the deviators was assumed to be 0.3, as recommended by BS8110 (1985) for the contact between lightly rusted strand and lightly rusted steel.

3) **EXT9 curve**

Computed with analytical model EXT9 where the tendons were allowed to slip freely at the deviators.

From Figures 5.15(a), 5.16(a) and 5.17(a), some common characteristics about the numerically derived moment-deflection curves were noted. At the pre-cracked stage, the three numerically derived moment-deflection curves for these beams were observed to be nearly equal to each other. After cracking, the EXT5 and the EXT9 moment-deflection curves formed the upper and lower bound of the moment-deflection response respectively. The EXT7 moment-deflection curves lie between these two bounds and were observed to be very closely related to the EXT5 curves immediately after cracking before converging towards the EXT9 at higher loads. This indicated that when the beams were analysed with the EXT7 analytical model, the external tendons did not slip at the deviators until a little after the occurrence of cracking. Slippage of the tendons at the deviators caused the stresses in the tendons between the deviators to redistribute, consequently resulting in higher deflections predicted for these beams near ultimate.

Figure 5.15(b), 5.16(b) and 5.17(b) show the moment-change in prestress relationships for Beams B1-2, B2-2 and B3-2 respectively. It was generally observed from these figures that the curves obtained from the EXT9 model exhibited a higher gradient at the pre-cracked stage than the other two analytical curves. This greater slope was due to the assumption made in the EXT9 model about the tendons slipping freely at the deviators. For a given moment before cracking, the deflections of these beams computed with the three numerical models were found to be nearly the same (see Figures 5.15(a), 5.16(a), 5.17(a)). Since the stress increase in tendons is dependent on the deflection of the beam, all three analytical models should therefore theoretically give the same stress increments. However, because the tendons were assumed to slip freely at the deviators in the EXT9 model, the redistribution of stresses caused smaller stress increments to be estimated. The EXT7 moment-change in prestress curves on the other hand had the same profile as the EXT5 curves at the pre-cracked stage, indicating that no slippage of tendons occurred for these beams at this stage (as noted in the moment-deflection curves discussed earlier). After cracking, the EXT9 moment-change in prestress curves exhibited a larger decrease in the gradient than that shown for the EXT5 curves, due to the larger deflections

estimated for the beams. This caused the two moment-change in prestress curves to converge towards each other near the maximum load condition. The EXT7 moment-change in prestress curves for these beams deviated away from the EXT5 curves when tendon slippage was first predicted to occur and, their slopes were observed to be nearly the same as that exhibited by the EXT9 curves.

Figure 5.15(a) shows the experimental and the three analytical moment-deflection responses for Beam B1-2. All three numerically derived curves over-estimated the deflection response by about twenty percent before the occurrence of cracking. After cracking, the EXT5 curve indicated a loss in stiffness and was thereafter found to be closely related to the experimental curve. The analysis of the beam with EXT5 analytical model took approximately fifteen hours to complete before terminating due to the concrete strain at the extreme compressive fiber at the critical section attaining the ultimate strain specified (0.0035). The theoretical ultimate moment predicted by this model was 226.438 kNm, which was only about two percent smaller than the experimentally measured value (Table 5.2 (d)). The slopes of the EXT7 and EXT9 curves also decreased after cracking but to a greater degree than that of the EXT5 curve and their moments under-estimated the experimental curve by about twelve and fifteen percent respectively. The analysis conducted with EXT7 model took about eight hours and the maximum moment estimated by it was about 0.94 of the experimental maximum; the EXT9 analysis took about six hours with a maximum moment representing about 0.92 of the experimental value. Note that the termination conditions for both analyses were complete (i.e. ultimate concrete strain was attained at the critical section).

Figure 5.15 (b) shows the moment-change in prestress relationships for Beam B1-2. The EXT9 curve over-estimated the experimental curve (approximately five percent) at the uncracked stage, but due to the reduction of its gradient after cracking, it under-estimated the experimental curve by approximately eighteen percent throughout the cracked stage. The EXT5 moment-change in prestress curve under-estimated the experimental curve by about twenty percent, twenty-four percent and fifteen percent before cracking, after cracking and yield of the reinforcement respectively. As for the EXT7 curve, it under-estimated the experimental curve by about twenty percent before cracking and about twenty-five to thirty percent after cracking.

Figures 5.15 (a) and 5.15 (b) reveal that the curve obtained assuming that the tendons were fixed at the deviators (the EXT5 curve) gave the best agreement to the experimental curve. This indicates that no slippage of the tendons had probably occurred throughout the entire loading history of Beam B1-2, therefore implying that the tendons were fixed at the deviators although this was not explicitly stated by Zhang *et al* (1993).

Figures 5.16 (a) and 5.16 (b) show the moment-deflection and moment-change in prestress curves obtained from the experiment and the three numerical models mentioned above for Beam B2-2. Their numerically derived results are summarised in Table 5.2 (d). The analyses conducted with the EXT5, EXT7 and EXT9 models all terminated completely (i.e. due to the concrete compressive strain at the critical section reaching the specified ultimate strain value) and the analyses took approximately nine, twenty-four and three hours respectively (see Table 5.2(d)).

From Figure 5.16 (a), it can be seen that the three analytical curves over-estimated the deflection response of the test beam by about twenty percent before the occurrence of cracking. After cracking, the EXT7 curve gives the best representation of the experimental curve up to ultimate at a maximum moment of 223.024 kNm. This estimated maximum moment was only 0.5 % higher than the measured ultimate moment. The EXT5 curve was observed to form the upper bound of the solution and over-estimated the deflection response of the experimental curve by about ten percent. The maximum moment analysed by the EXT5 analytical model was 233.834 kNm, which was five percent higher than the experimental maximum moment. The EXT9 curve on the other hand gave the lower bound of the solution and, under-estimated the experimental moment-deflection response by about three percent.

Figure 5.16 (b) illustrates that the EXT9 curve over-estimated the experimental moment-change in prestress response by approximately fifteen percent before cracking and under-estimated it by approximately five percent after the reinforcement had yielded. The slope of the EXT9 curve was also observed to be slightly higher than the experimental curve and the two curves converged towards each other near ultimate. The EXT5 and EXT7 moment-change in prestress curves, however can be seen to be the same before cracking but under-estimate the experimental curve by

approximately fifteen percent. These two analytical curves diverge away from each other just a little after the occurrence of cracking. The slope of the EXT5 moment-change in prestress response was higher than that for the EXT7 analysis and converged towards the experimental curve near ultimate (see Figure 5.16 (b)). The EXT7 curve however under-estimated the experimental curve by about fifteen percent throughout the rest of the loading history after the occurrence of cracking.

Finally, the experimental and numerical moment-deflection and moment-change in prestress curves for Beam B3-2 are shown in Figure 5.17 (a) and 5.17 (b) respectively. The results obtained from the three analytical models are also presented in Table 5.2 (d). All the analyses conducted on this beam (using analytical models EXT5, EXT7 and EXT9) were observed to have terminated prematurely due to convergence problems encountered in obtaining a stable solution for the change in prestress (Section 5.4). However, despite these premature terminations, the maximum moment predicted using the EXT5, EXT7 and EXT9 models were satisfactory at 1.050, 0.953 and 0.937 of the experimental maximum value respectively (see Table 5.2 (d)). It was also noted from Figure 5.17 (a) that the experimental curve indicated a sudden increase in stiffness when the moment reached about 214 kNm and terminated at a maximum moment of about 230 kNm. Both EXT5 and EXT7 models took a relatively long time to analyse the flexural behaviour of this beam, about fifteen and ten hours respectively, while EXT9 took only two hours.

Figure 5.17 (a) shows that the three analytical moment-deflection curves were nearly coincidental with the experimental curve before cracking. However, after cracking, all three curves indicated a reduction in stiffness and deviated from each other. The EXT7 curve is seen to give the best agreement with the experimental curve and, although the analysis terminated prematurely, the calculated maximum moment was only about five percent below the measured value. The EXT5 curve over-estimated the experimental deflection response by about five percent and the numerical EXT9 curve under-estimated it by about seven percent, thus forming the upper and lower bounds to the experimental curve.

Figure 5.17 (b) shows the moment-change in prestress relationships for Beam B3-2. The numerical EXT9 curve over-estimated the experimental results by about eight

percent at the uncracked stage and under-estimated it by about eight percent at the cracked stage and ten percent at the stage after the reinforcement steel has yielded. The numerical EXT7 and EXT5 moment-change in prestress curves both under-estimated the experimental curve by about thirty percent before cracking occurred. After slippage of the tendons, the EXT7 curve exhibited a lower stiffness and deviated from the EXT5 curve, thereby under-estimating the experimental curve by about twenty percent.

5.4 Convergence Problems

Several convergence problems were encountered by the proposed analytical models when they were used to simulate the flexural behaviour of the beams used for the verification process. These convergence problems were mainly due to the highly non-linear nature of the problem and either cause the analysis of these beams to terminate prematurely or take up an extensive amount of computing time to yield the required results. Although Alkhairi and Naaman (1993) and Virlogeux (1983) who conducted numerical studies on externally post-tensioned structures (see Chapter Two) also reported encountering these numerical problems in their models, they did not propose any methods to solve them. This section describes the numerical problems encountered with the proposed non-linear models in the verification process and the methods employed here to solve these problems.

In the proposed numerical models, the change in prestress Δf_{ps} and the eccentricity variations Δ_{eccen} of the tendons are estimated from the deformed shape of the structure. However, for a given load stage, these two variables must first be known before the deformation of the beam can be determined. As such, iterative methods involving two iteration levels, one for each variable, have to be employed to determine the change in prestress and the eccentricity variations of the tendons. The procedure adopted here is to first estimate the deformation of the beam for the present load stage, using the Δf_{ps} and Δ_{eccen} from the previous load stage. With the calculated deflections and end rotations, Δf_{ps} and Δ_{eccen} are then computed again and compared to the earlier assumed values. This process is repeated until the assumed and calculated values are within a specified tolerance. Unfortunately, the calculations for Δf_{ps} and Δ_{eccen} did not always converge to a solution due to numerical problems which caused premature

terminations (e.g. accuracy of the computer despite using double precision for analysis, degree of tolerance desired, limiting points, etc.).

In an earlier version of the proposed analytical models, fixed tolerances were used for both the Δf_{ps} and Δ_{eccen} values to check the closeness of the calculated and assumed values. However, several beams analysed with these models were observed to terminate prematurely at early loading stages and only about two-thirds of their whole moment-deflection responses were predicted. This was found to be due to the large range of possible change in prestress Δf_{ps} analysed for these beams near ultimate (typical change in prestress Δf_{ps} at the ultimate conditions derived for the beams used in the verification process ranged from 30 N/mm^2 to 800 N/mm^2) which may cause the use of a fixed value tolerance (e.g. 0.001 N/mm^2) to be reasonable for the analysis of some beams but unattainable for others. Hence, percentage tolerances were used instead for the iteration of Δf_{ps} in the proposed models to prevent premature terminations of this nature from occurring. The equation used to check the percentage tolerance is given in Equation 5.1.

$$\frac{\Delta f_{ps(calculated)} - \Delta f_{ps(assumed)}}{\Delta f_{ps(assumed)}} \times 100 < tolerance\% \quad \text{.....(5.1)}$$

Percentage tolerances were not used for the iteration check of the eccentricity variation Δ_{eccen} because of the small values involved which may cause other numerical problems in the analysis. It was found that using a fixed value tolerance of 0.000001 m for Δ_{eccen} was generally satisfactory for these beams.

Although effective, the use of a percentage tolerance for Δf_{ps} did not help to extend all the analyses of the beams simulated in the verification process up to the theoretical ultimate limit state (i.e. an ultimate concrete strain of 0.0035 at the extreme compressive fiber of the critical section). This was partly due to the level of the tolerance used for these analyses. From a study conducted by the author, it was noted that the success of an analysis performed with the proposed non-linear model was critically dependent on the percentage tolerance specified for Δf_{ps}. If the tolerance specified was too high, erroneous results were produced. On the other hand, if the tolerance used was too low, no solutions were derived due to convergence problems. For the beams tested by Yaginuma and Kitada (1987, 1988, 1989), using a percentage

tolerance of 0.01% for Δf_{ps} in the models was generally found to yield satisfactory results. However, for the beams tested by Zhang *et al* (1993), this tolerance for Δf_{ps} was found to be unattainable for the load stages near ultimate conditions and usually resulted in premature terminations of the analyses. By relaxing the tolerance to 0.02% for these beams, better results were obtained closer to the theoretical ultimate limit state.

However, Beams A1-2, A2-1, A2-2, A3-2 and B3-2 extracted from Zhang *et al* (1993) still terminated prematurely when the percentage tolerance for Δf_{ps} was reduced to 0.02% and, increasing this percentage tolerance further did not yield better results. By studying the value of Δf_{ps} evaluated for each iteration in the last loading sequence before the analysis was terminated prematurely, the value computed was found to oscillate between two extreme values which were slowly diverging instead of converging to a solution. It was deduced that this numerical problem was caused by the poor initial estimate of the change in prestress Δf_{ps} in the tendons for the particular loading sequence. As Virlogeux (1983) stated: '*convergence is not monotonous; when the stress variation is under-estimated, forces will be over-estimated and from them deformations; this leads to over-estimating the stress variation of unbonded tendons at the further step. This will later cause convergence problems (at ultimate limit state) when the structure response to stress variations is too important, i.e. when structure has become too flexible, due to plastifications.*'.

Several methods were applied here to solve this convergence problem caused by poor initial estimate of the change in prestress. These methods included using a routine that estimated a higher initial change in prestress Δf_{ps} used for each loading stage, by linearly extrapolating a value from the two previous loading stages (see Figure 5.18), instead of using the Δf_{ps} from previous load stage as first initial estimate. Figure 5.18 shows that the change in prestress at Point *D* can be estimated from a straight line plotted from Points *A* and *B* (denoting two previous loading stages) and, this derived Δf_{ps} is closer to the actual value (denoted by Point *C*) than the change in prestress of the immediate previous loading stage (i.e. Point *B*). However, problems were encountered when a sudden small increase in stiffness is exhibited by the beam near ultimate, as shown in Figure 5.19, which caused the derived Point *D* to over-estimate the actual change in prestress of the beam, thereby causing convergence problems to

occur in the analysis. Since it is very difficult to make good initial estimates for Δf_{ps} near the ultimate conditions, and since the average M_{pred}/M_{exp} obtained for the five beams which failed prematurely were 0.923 with a standard deviation of 0.037, the results derived from these analyses were considered reasonably acceptable here.

Another convergence problem that was encountered in the earlier versions of the models was that due to the '*limiting points*' detected along the moment-deflection responses of the externally prestressed beams analysed. Crisfield (1991) defined these limiting points as the points located along the moment-deflection curve where the curve suddenly becomes horizontal or exhibits a sudden loss in strength. He reported that these points can cause severe convergence problems to numerical methods if they are not handled properly. In the proposed numerical models, this is especially true since the evaluation of the deflection response for a given loading stage depends critically on the curvatures of the nodes defined along the span of the whole beam. Hence, if the reinforcement ratio is high, whenever cracking of the concrete or yielding of the non-prestressed reinforcement occurs at a node away from the critical section, a sudden reduction in the stiffness of the overall beam will result. This loss in stiffness near ultimate conditions consequently produces a limiting point in the moment-deflection curve and, if any of the loading stages falls at one of these limiting points, convergence problems will occur.

The method employed here to solve the limiting point convergence problem is to avoid any analysis at these points. If a loading stage is found to be at one of these limiting points, the analytical models have been programmed to skip this problem by adding more load to the structure and analyse another moment-deflection point further up the curve. This method of skipping through the limiting points in the moment-deflection curve is denoted as the '*skip-through*' method.

In the skip-through method, if no solution is obtained for the change in prestress Δf_{ps} after a pre-set maximum number of iterative cycles (e.g. typically 20 to 40 cycles), the external loads used for the present loading sequence are first reduced. The reduction is implemented by reducing the strain increment made at the top concrete fiber of the critical section by half. This process of reducing the additional external loads is repeated until a satisfactory solution for Δf_{ps} is derived. However, if the strain increment imposed at the extreme top concrete fiber of the critical section has been

reduced four times consecutively without producing a stable solution, the analytical models assume that a limiting point has been encountered along the moment-deflection curve. The analysis will then skip through the problem moment-deflection point by doubling the initial strain increment imposed at the top concrete fiber. This will consequently increase the external loads to be placed on the structure and reduce the possibility of premature termination from occurring in the analysis.

One major disadvantage of the skip-through method is that it may cause the analysis to take an exceptionally large amount of computer time to yield the ultimate results. An example of this would be Beam OS-1 the analysis of which took approximately twenty-three hours to complete using the EXT3 model due to the numerous limiting points encountered in the analysis.

5.5 Tension Stiffening

All the beams described above were used to study the significance of considering the effects of tension stiffening in the proposed non-linear analytical models. These beams were simulated again with the EXT4 model, where tension stiffening was taken into account in the analysis using the method recommended by Ghali (1993) and CEB-FIP Model Code (1978) (see Section 4.5.2), and compared with the results analysed earlier with the EXT3 model. However, only the results of Beams OS-1, OL-1, OA-1, OB-1 and OC-1 are presented here, since observations made on the other beams were all very similar.

Figures 5.20 to 5.24 show a comparison between the moment-deflection responses obtained from the non-linear analyses conducted on Beams OS-1, OL-1, OA-1, OB-1 and OC-1 respectively, with and without the effects of tensioning stiffening considered. From these figures, the two numerical curves were observed to be the same before the occurrence of cracking and, after cracking, the numerical curve obtained from the analysis with tension stiffening considered exhibited a stiffer response. The two numerical curves were then observed to converge towards each other after the yielding of the non-prestressed reinforcement and, nearly the same maximum moments were estimated by the two analytical models, i.e. EXT3 and EXT4 models (see Table 5.4).

Figures 5.20 to 5.24 showed that after the cracking of the concrete but before the yielding of non-prestressed reinforcement, the two numerical curves derived from the analyses conducted with and without the tension stiffening effects considered, differed from each other by only about three to four percent. However, the computational time required for analysing these structures with the tension stiffening effects considered was in average found to be about two times more than that when these effects were ignored (Table 5.4). Hence it was considered more desirable to ignore the effects of tension stiffening in the proposed analytical models because it not only helps to save the computational time required for the analysis, but also yields slightly more conservative results (by about three to four percent) for the flexural response of these structures.

5.6 Shear Deformations

All the beams used in the verification process were re-analysed again with the non-linear models, but this time with the routine that incorporated the effects of shear deformations introduced by Park and Paulay (1975) removed. However, only the curves derived for Beams OS-1, OL-1, OA88-2, OC88-1, OC88-2, B1-2 and B2-2 are presented here because they indicated some interesting results. Figures 5.25 to 5.31 show the moment-deflection curves derived from analyses conducted with and without the effects of shear deformations considered for these beams.

Figure 5.25 shows the deflection responses for Beam OS-1, with and without the shear deformations considered. It can be observed that the two numerical curves are equal at the uncracked and cracked stages, but deviate from each other near the onset of yielding of the steel reinforcement, with a maximum difference of about six percent. Near ultimate, the two curves converge and the ratio of the maximum moments derived from the two numerical analyses (M_2/M_1) was near unity (see Table 5.5). The time taken for the analysis without considering the shear deformations decreased greatly from about twenty-three hours (when shear deformations were considered) to eight hours. This large reduction in time was due to the less computational work required in the skip-through method when a limiting point was encountered.

The two numerically derived curves for Beam OL-1 (with a high span-depth ratio of 32) shown in Figure 5.26 were coincident throughout the whole loading history. This shows that the effects of diagonal tensile cracking due to shear has no influence on the flexural analysis of externally post-tensioned structures with high span-depth ratios (also pointed out by Naaman and Alkhairi (1993)). The time taken for the analysis where shear deformation was ignored was approximately nine hours, which was only about an hour less than when the effects were considered (Table 5.5). Both numerical analyses conducted on the beam terminated completely due to the concrete compressive strain at the critical section reaching the specified ultimate strain (0.0035).

Figure 5.27 shows the experimental and the two analytical moment-deflection responses (with and without shear deformation) for Beam OA88-2. Similar to the observations made from Figure 5.25 for Beam OS-1, the two analytical curves were similar to each other at both the uncracked and cracked stages of the beam behaviour and deviated from each other when the non-prestressed reinforcement started yielding. The difference between the two curves after the yielding of the non-prestressed reinforcement was about two percent. Although the two numerical analyses terminated completely (concrete strain 0.0035 attained at the critical section) and the ratio of their maximum moments (M_3/M_1) calculated was near unity, the deflection of the beam predicted at ultimate when shear deformations were considered was about forty percent higher at 16 mm.

Figure 5.28 shows the experimental and two numerically derived moment-deflection curves for Beam OC88-1. The two numerically derived curves diverged from each other at about $M/f_{cu}bd^2 = 0.105$ with that neglecting the effects of shear deformations over-estimating the gradient of the experimental curve by as much as eighteen percent, the other by only about three percent. The ultimate moments evaluated by both numerical analyses were found to be nearly the same (about 74 kNm) but at a deflection some twenty-five percent higher when shear deformation effects were considered. Time taken by the analysis where diagonal tensile cracking was neglected was four hours, which was 0.72 of that required by the analysis including shear deformation (Table 5.5).

Figure 5.29 shows the moment-deflection responses for Beam OC88-2. From the figure, similar observations can be made about the trend of the two numerically derived curves as for those described for Beam OC88-1. The two analytical curves were in close agreement with each other until $M/f_{cu}bd^2$ was about 0.103, after which the two curves deviated from each other. A stiffer response of about twenty percent was observed for the curve where shear deformations were not taken into account, while only a slight over-estimation of about three percent was noted for the curve where shear deformations were considered. Again the ultimate moments derived from both analyses were approximately equal and the deflections estimated at ultimate for both analyses differed by about eighteen percent. The time taken to analyse Beam OC88-2 with the proposed models with the shear deformations neglected was about four hours (Table 5.5).

Although, Beams OA88-2 and OC88-2 were quite similar to each other, except for their non-prestressed reinforcement ratio, the two numerically derived curves (with and without shear deformation considered) derived for these beams differed by about two and thirteen percent respectively. This indicated that the amount of non-prestressed reinforcement does influence the degree to which the effects of shear deformations have on these externally prestressed beams. That is, the higher the amount of non-prestressed reinforcement, the higher the degree of influence the shear deformations has on the beams. The reason for this is as follows: the $M/f_{cu}bd^2$ value at which the two beams indicated a loss in stiffness due to shear deformation was about 0.10 and, the shear near mid-span at this load stage for both beams was about 23 kN. The non-prestressed reinforcement of Beam OA88-1 had already yielded at this load level and, the $M_{max}/f_{cu}bd^2$ value achieved at ultimate was only approximately 0.11 with a maximum computed shear of about 24.67 kN. In the case of Beam OC88-2, because of the higher non-prestressed reinforcement ratio, the $M_{max}/f_{cu}bd^2$ and maximum shear values were estimated to be about 0.26 and 54.67 kN respectively. Since the amount of apparent moment to be added to the structure due to shear deformation (ΔM_{shear}) is directly proportional to the amount of shear acting on a node in the structure (see Equation 4.40), neglecting shear deformation in the analysis for Beam OC88-2 will thus greatly under-estimate the deflections of the beam.

Figures 5.30 and 5.31 show the comparison between the moment-deflection relationships obtained when considering and neglecting the effects of shear deformations for Beams B1-2 and B2-2 respectively. Although the span-depth ratios of these beams were both equal to 11 (which was less than 24, a value given by Naaman and Alkhairi (1993) in which above this value the shear deformations has not much influence on the structure), the effects of shear deformation did not seem to have any influence on their flexural behaviour, since both numerically derived curves were the same throughout the whole loading history. The reason for this was that these beams were loaded under Load Type 2 (i.e. two equal point loads placed equi-distant from supports), which caused the shear forces acting on the structure near the regions of high bending moments to be relatively low. Hence the effects of shear deformations were very limited in these beams.

5.7 Concluding Remarks

The purpose of this chapter was to show that the computer models proposed in Chapter Four can be used accurately to predict the flexural behaviour of externally prestressed structures up to ultimate. This was carried out by performing simulations with the proposed analytical models on seventeen experimental beams reported by Yaginuma and Kitada (1987, 1988, 1989) and Zhang *et al* (1993) and, showing that the results derived from these models are in close agreement with the experiments.

Most of the beams simulated in the verification process produced results which were in good agreement with the experiments. The numerically derived moment-deflection curves were generally found to be within ten to twenty percent of the experimental curves over the full load range to failure. The numerically derived moment-change in prestress relationships for these beams were, on the other hand, found to greatly under-estimate the experimental values, sometimes by as much as thirty percent. This, however, was considered to be negligible, since the change in prestress is often very small compared to the initial prestress applied to the structure. As for the ultimate moments predicted by the proposed analytical models, the average ratio of the maximum predicted moment to the maximum experimental moment (M_{pred}/M_{exp}) obtained for all the seventeen beams was satisfactory at 0.927 with a standard deviation of 0.051 (see Table 5.3). This degree of accuracy obtained was considered

to be excellent, considering the fact that five of these beams failed prematurely due to convergence problems (i.e. Beams A1-2, A2-1, A2-2, A3-2 and B3-2).

The simulations conducted on Beams A1-2, A2-1, A2-2 and A3-2, however, did not yield very satisfactory results and substantial variations were observed after the occurrence of cracking between the analytical and experimental moment-deflection and moment-change in prestress relationships. These variations were believed to be caused by poor interpretation of the prestressing steel material properties used for the analyses as a result of insufficient information. Also the simulation of Beam OL-1 conducted with the proposed model was only found to be satisfactory (giving an over-estimation of five percent instead of twenty percent) after reducing the modulus of rupture of the concrete specified for the analysis. From these, it was concluded that the accuracy of the results obtained from the proposed analytical models is dependent on the properties specified for the concrete, non-prestressed reinforcement and prestressing steel.

Several convergence problems were initially encountered with the proposed models when they were used to simulate the complete flexural response of the seventeen beams used for the verification process. These numerical problems caused some of the earlier analyses conducted on these beams to terminate prematurely. Most of these numerical problems were solved by either using the skip-through method (for limiting point convergence problems) or reducing the degree of tolerance used for checking the iteration of the change in prestress Δf_{ps}. However, the analysis of Beams A1-2, A2-1, A2-2, A3-2 and B3-2 still terminated prematurely due to the difficulty in making good initial estimates of the change in prestress for loading sequences near the ultimate conditions. Although several numerical methods were employed to solve this problem, about only eighty-five to ninety percent of the experimental moment-deflection response was predicted for these beams. This degree of accuracy obtained for these beams were considered to be acceptable here.

For those beams without any deviators placed along their length, the total time taken by the proposed models to analyse their flexural behaviour to the ultimate limit state was found to be between two and five hours. Beams OS-1 and OL-1, however, took longer (twenty-three and ten hours respectively) than the other beams, due to several

limiting points being encountered during the analysis. As for the beams with deviators (Beams B1-2, B2-2 and B3-2), different computational times were recorded for the different analytical models employed (i.e. EXT5, EXT7 or EXT9). The time taken for analysing these beams ranged from nine to fifteen hours when the EXT5 model was used and, between eight to twenty-four hours for the EXPRE7 model. The EXT9 model, however, required the least amount of computational time ranging from two to six hours. Since the average maximum moments for B1-2, B2-2 and B3-2 derived with the EXT9 model was in average found to be 0.947 with a standard deviation of 0.029, as compared to that obtained with EXT7 which was 0.967 with a standard of deviation of 0.027; it is therefore considered more desirable to use the EXT9 model for structures with deviators located along their span.

When the effects of tension stiffening were considered, the analytical time required was found to be about twice the values mentioned above. Since it was generally observed that the moments derived from analyses conducted with and without tension stiffening differed by about only three to four percent after cracking, it was therefore considered more desirable to neglect the effects of tension stiffening in the proposed analytical models. This will not only help to save on computational time required, but will also give slightly more conservative results for the flexural behaviour of these structures.

It was also found that the effects due to shear deformations should be considered in the flexural analysis of externally prestressed structures and can be modelled satisfactorily by using the truss mechanism introduced by Park and Paulay (1975). This is because shear deformations seemed to have varying degrees of influence on the flexural behaviour of these beams and, if not considered may sometimes cause the flexural responses to be greatly over-estimated. The amount of influence in which shear deformations have on the flexural behaviour was noted to be dependent on the span-depth ratio, non-prestressed reinforcement ratio and external loading patterns.

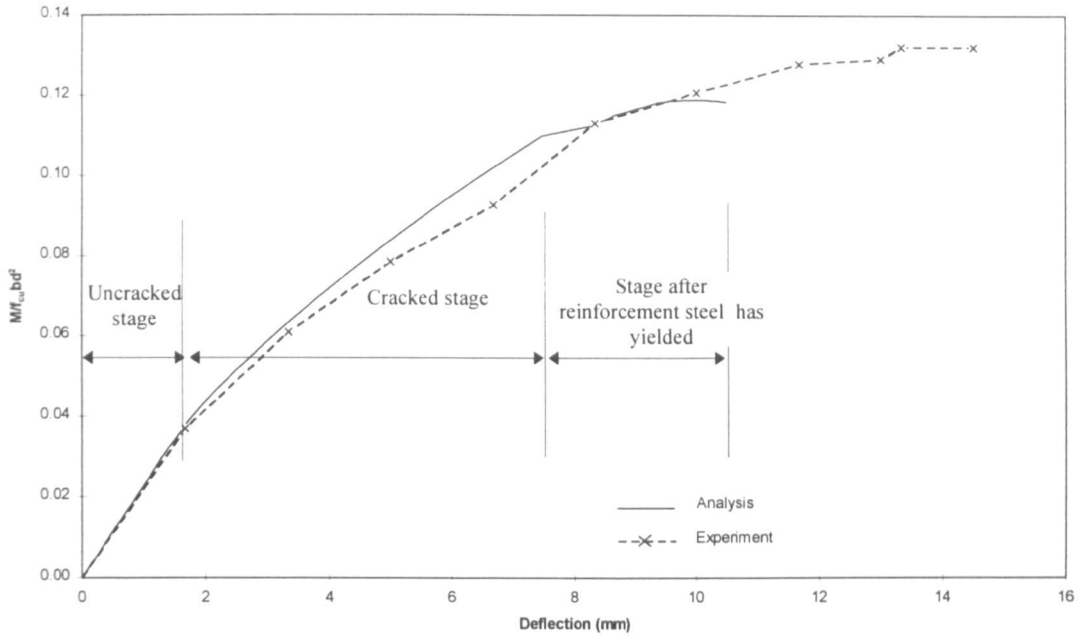

Figure 5.1: Moment-deflection relationship,
Beam OS-1 (Yaginuma and Kitada (1988))

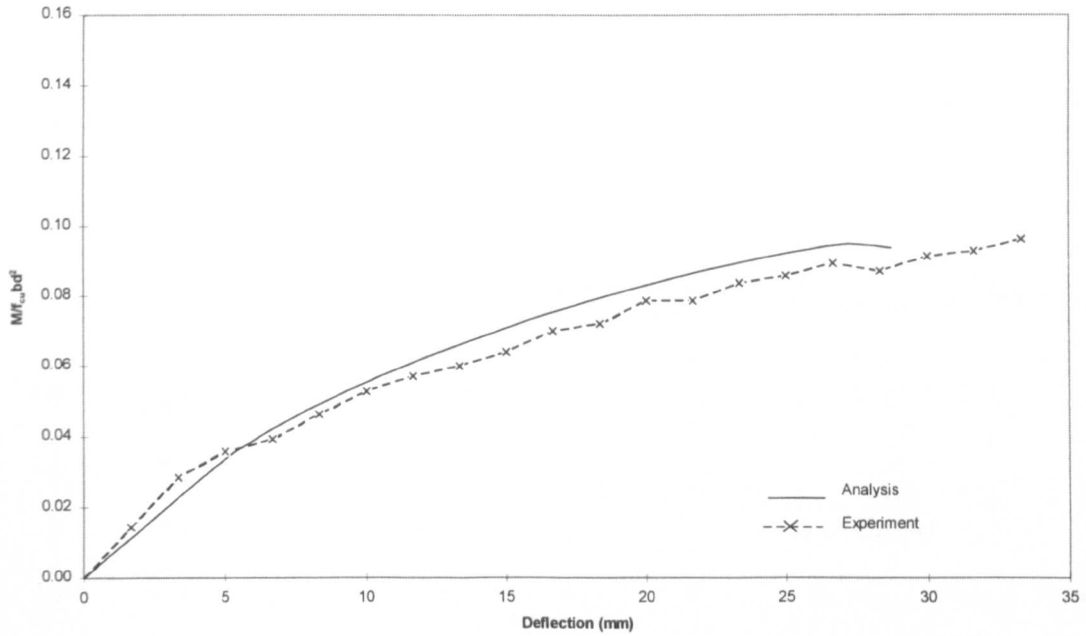

Figure 5.2: Moment-deflection relationship,
Beam OL-1 (Yaginuma and Kitada (1988))

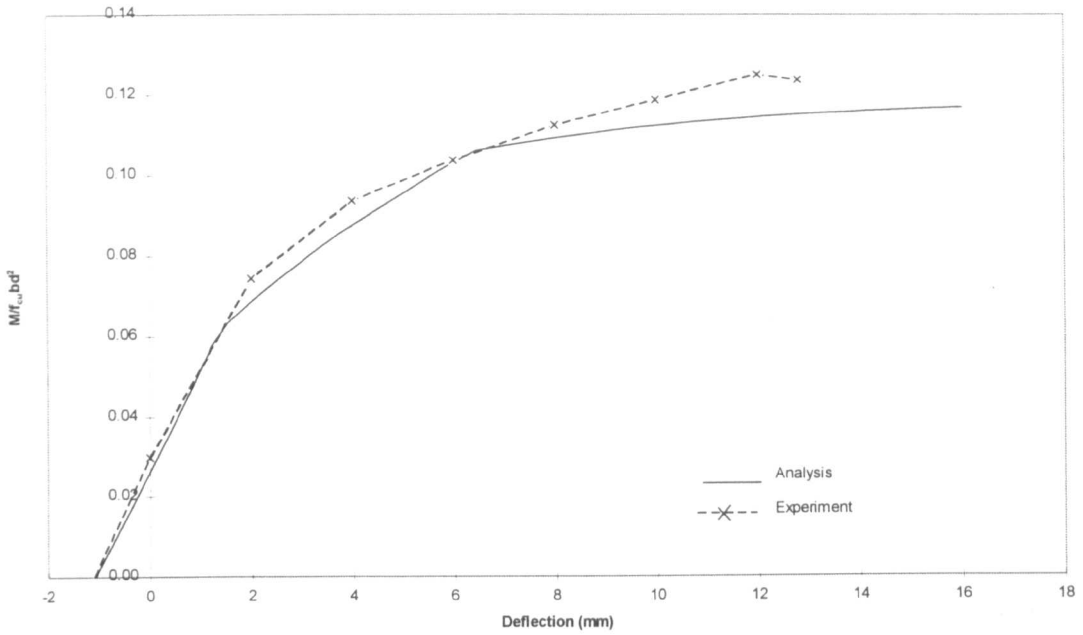

Figure 5.3: Moment-deflection relationship,
Beam OA88-2 (Yaginuma and Kitada (1989))

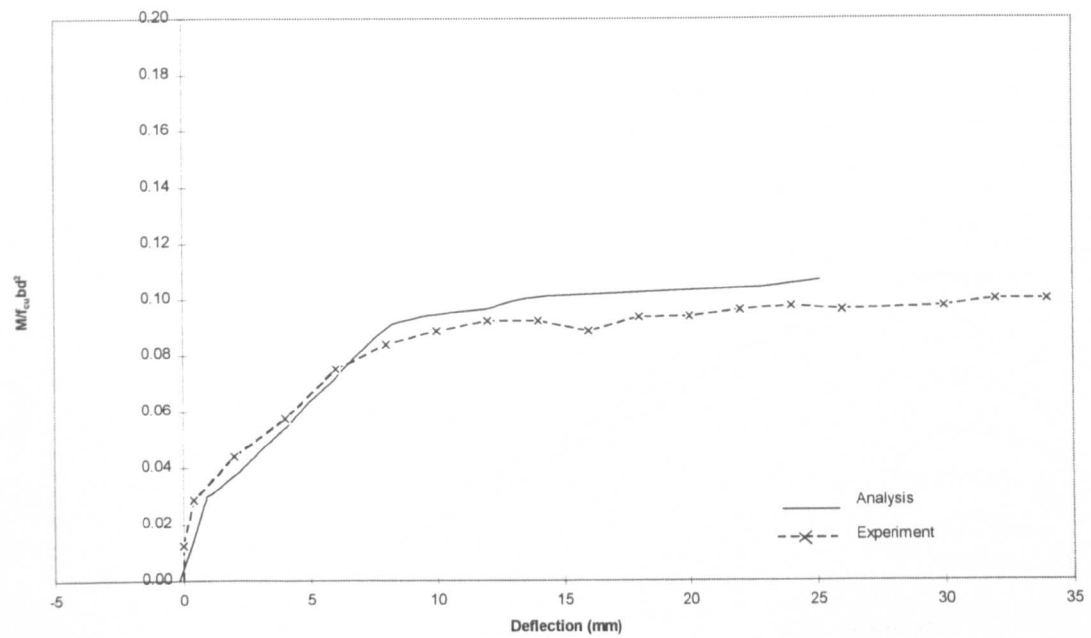

Figure 5.4: Moment-deflection relationship,
Beam OB88-1 (Yaginuma and Kitada (1989))

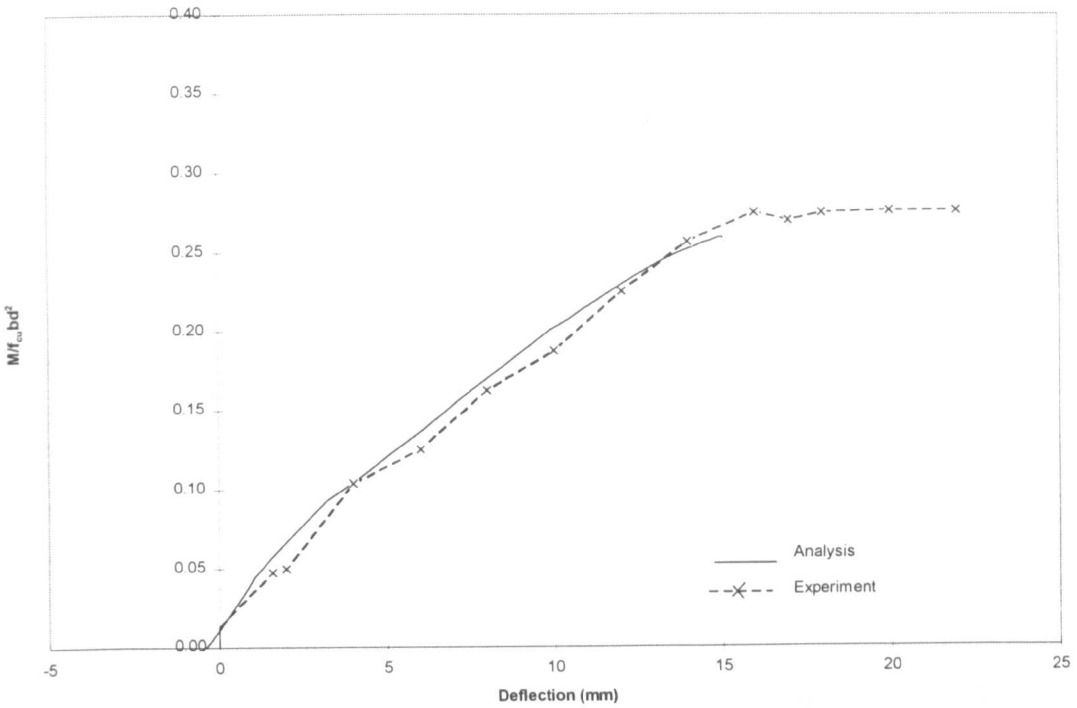

Figure 5.5: Moment-deflection relationship,
Beam OC88-1 (Yaginuma and Kitada (1989))

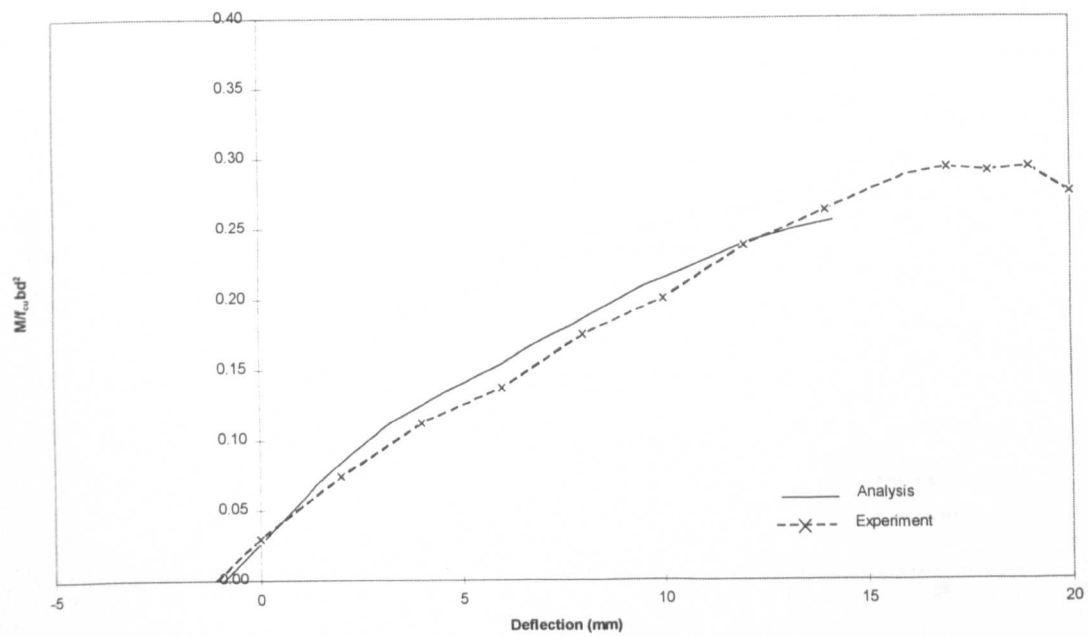

Figure 5.6: Moment-deflection relationship,
Beam OC88-2 (Yaginuma and Kitada (1989))

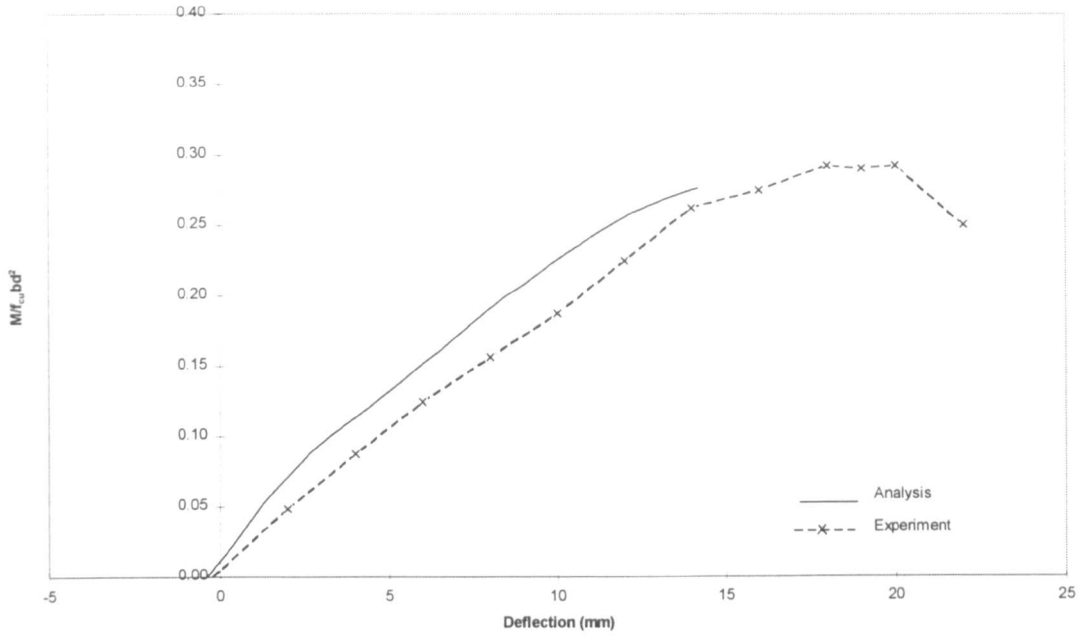

Figure 5.7: Moment-deflection relationship,
Beam OD88-1 (Yaginuma and Kitada (1989))

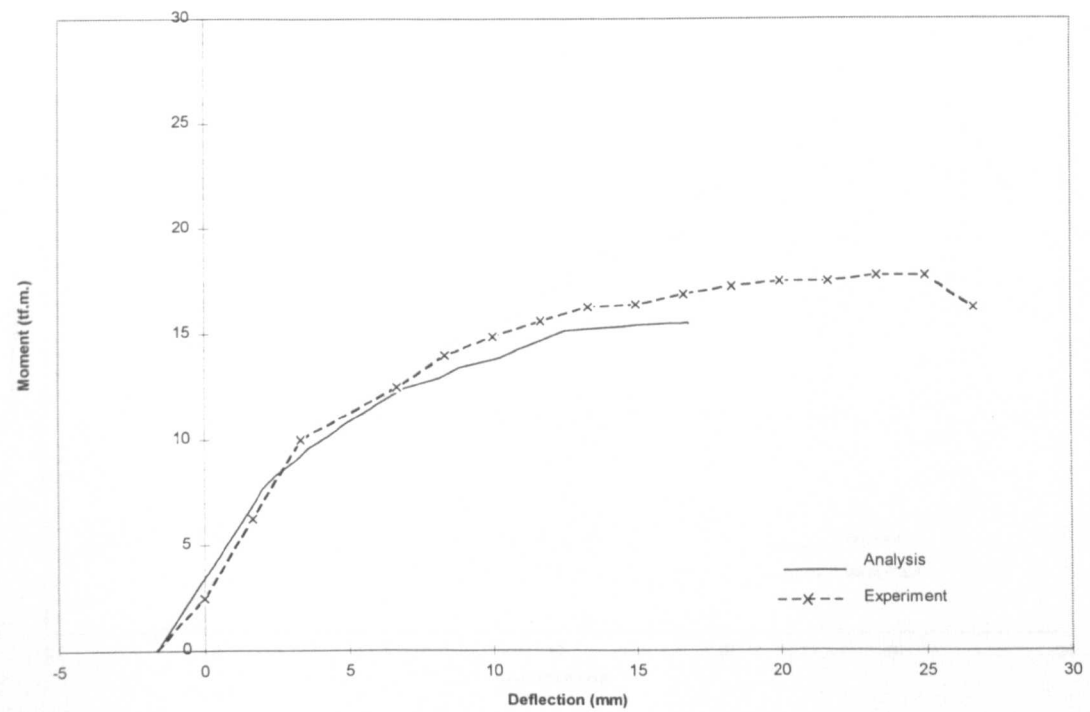

Figure 5.8: Moment-deflection relationship,
Beam OA-1 (Yaginuma and Kitada (1987))

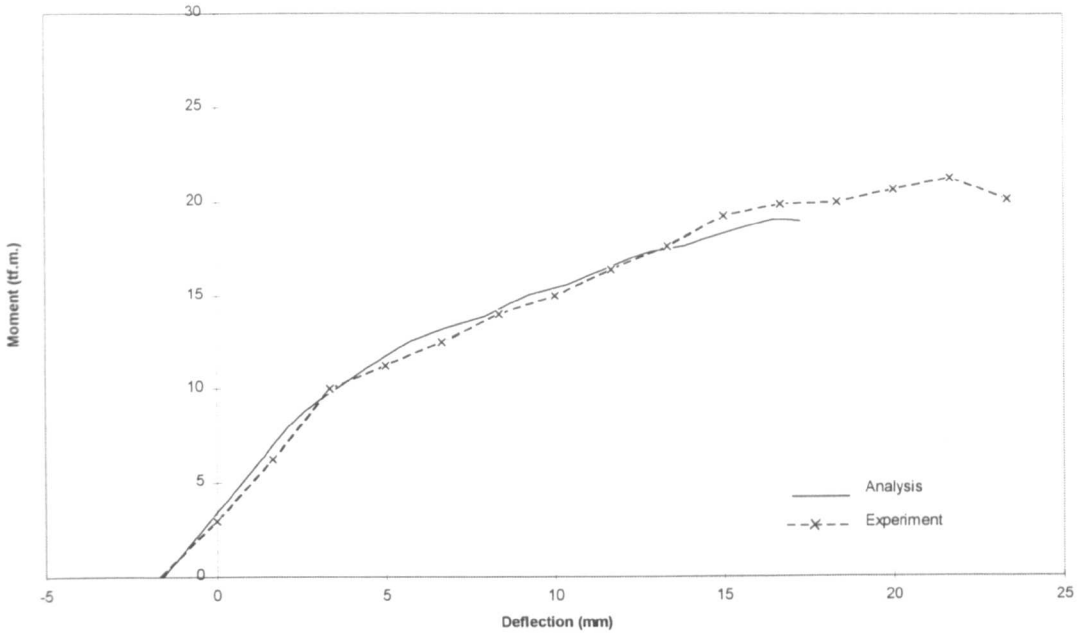

Figure 5.9: Moment-deflection relationship,
Beam OB-1 (Yaginuma and Kitada (1987))

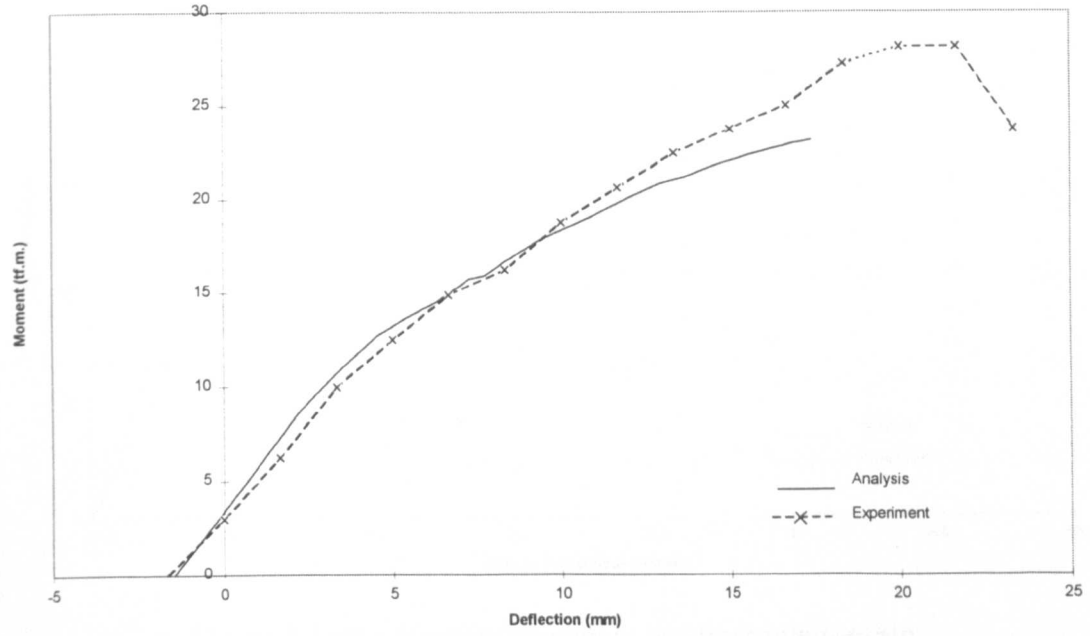

Figure 5.10: Moment-deflection relationship,
Beam OC-1 (Yaginuma and Kitada (1987))

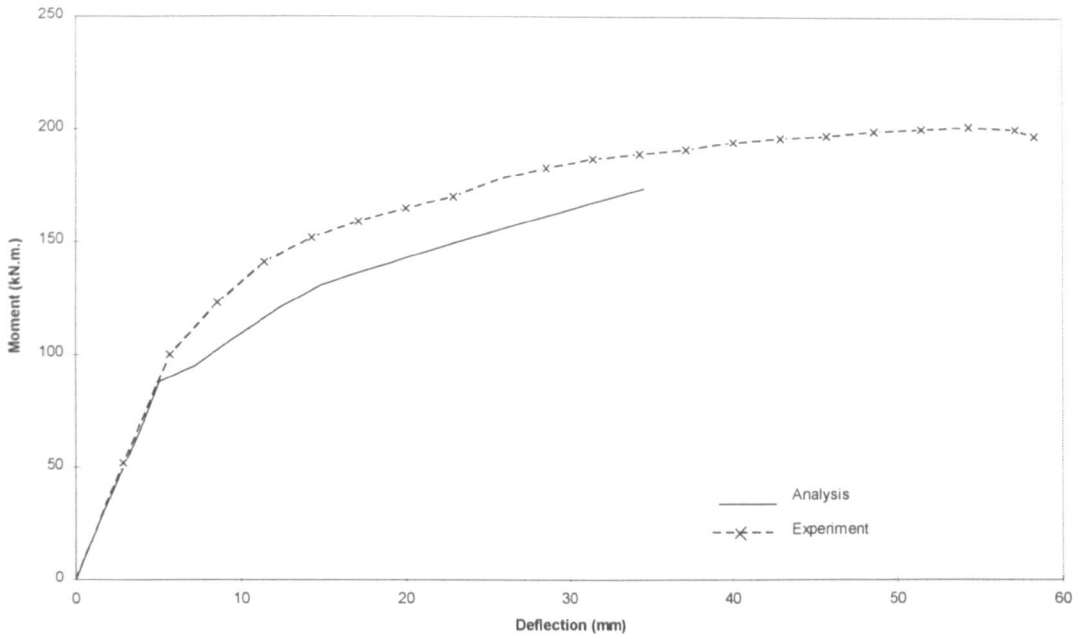

Figure 5.11(a): Moment-deflection relationship,
Beam A1-2 (Zhang *et al* (1993))

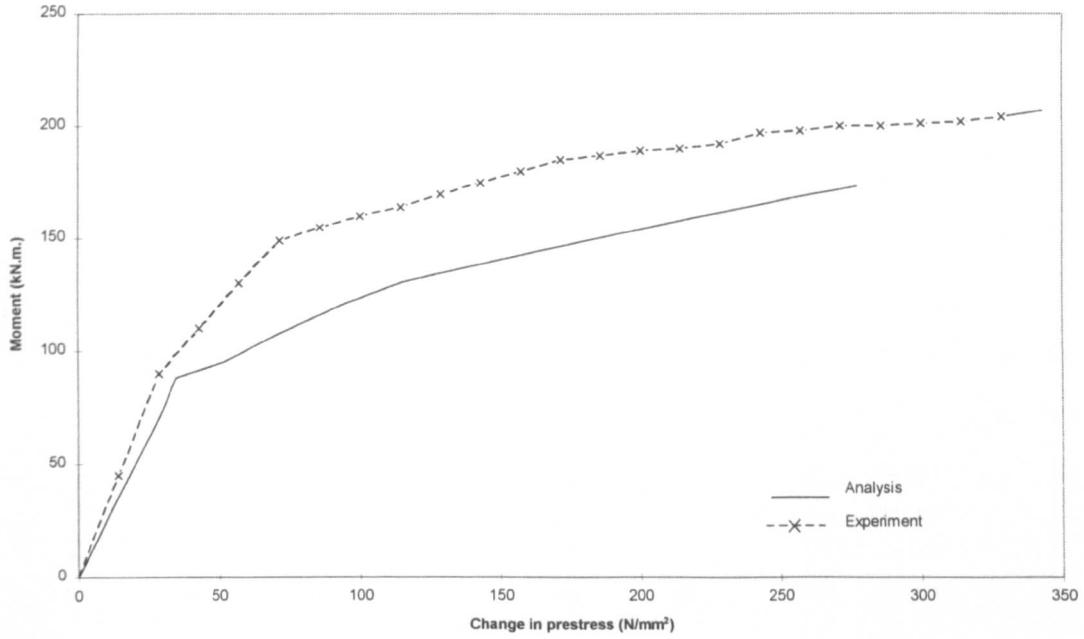

Figure 5.11(b): Moment-change in prestress relationship,
Beam A1-2 (Zhang *et al* (1993))

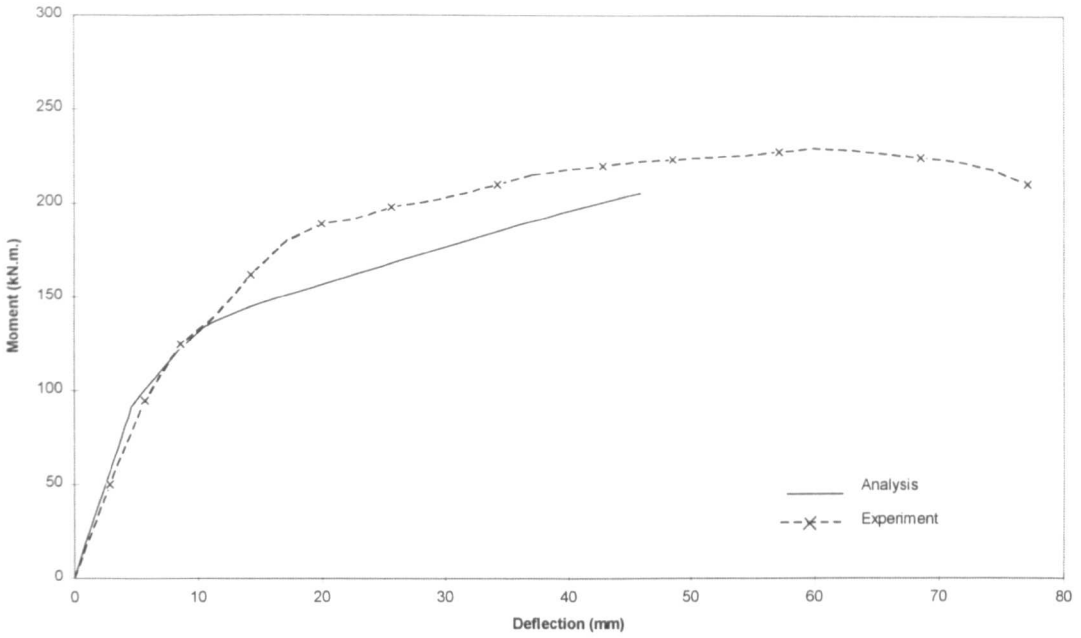

Figure 5.12(a): Moment-deflection relationship,
Beam A2-1 (Zhang *et al* (1993))

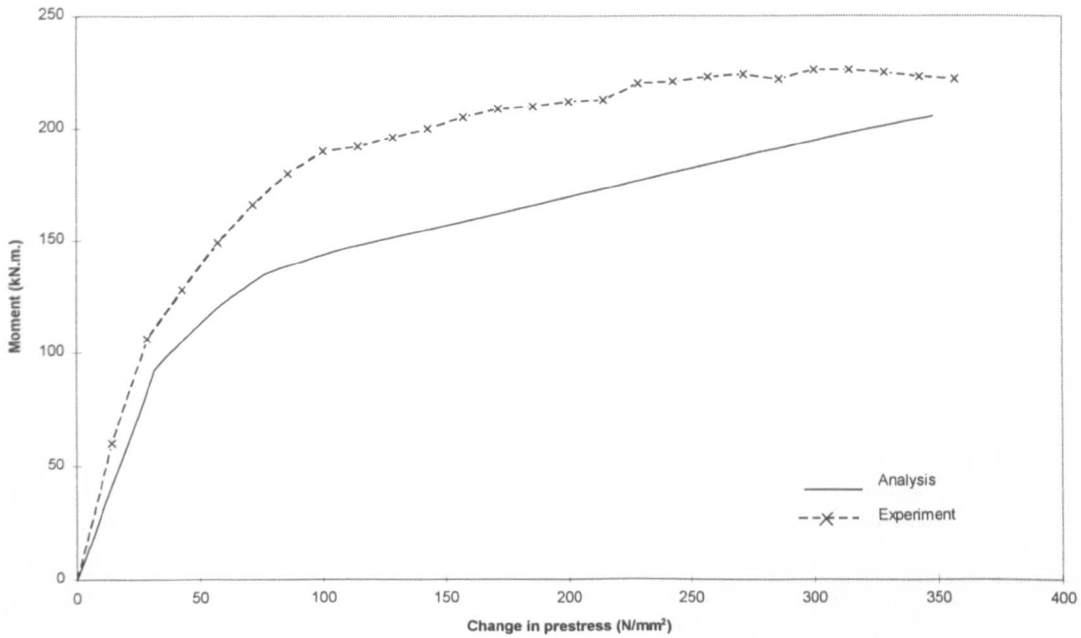

Figure 5.12(b): Moment-change in prestress relationship,
Beam A2-1 (Zhang *et al* (1993))

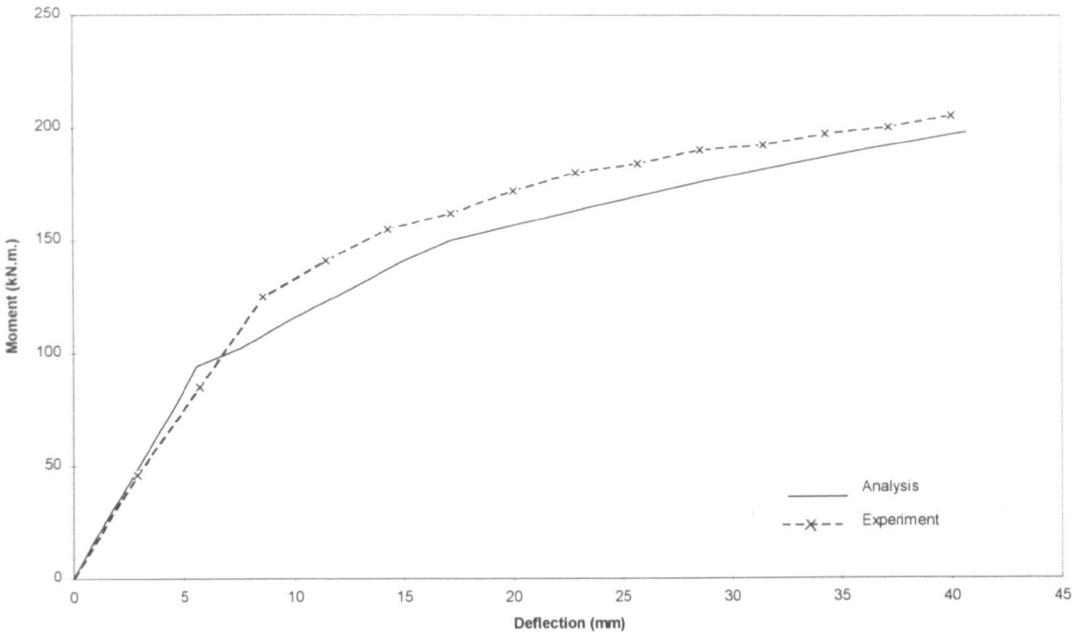

Figure 5.13(a): Moment-deflection relationship,
Beam A2-2 (Zhang *et al* (1993))

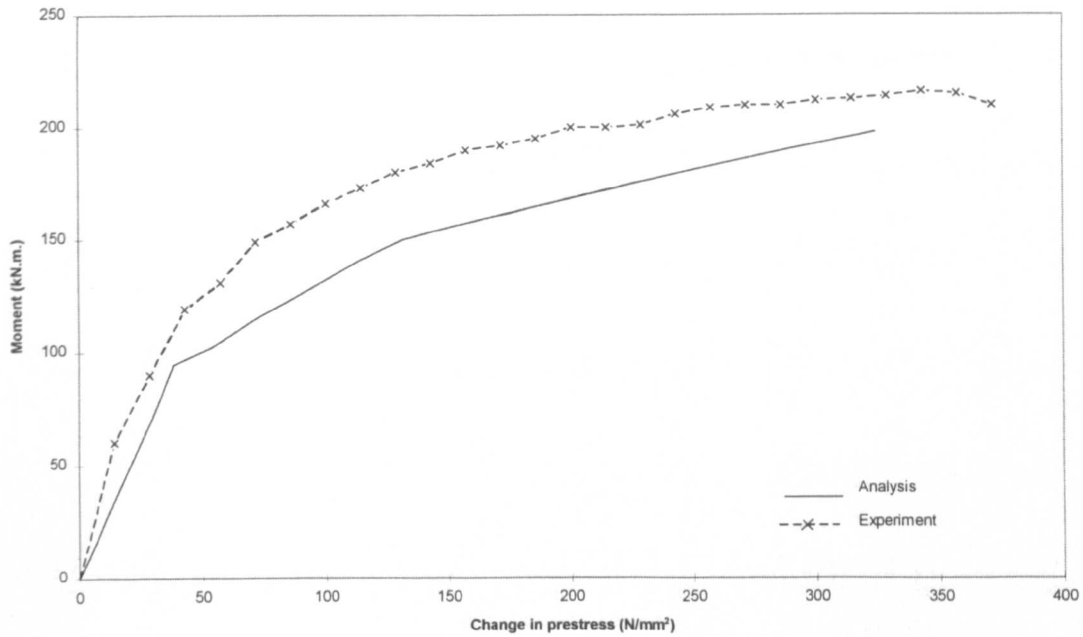

Figure 5.13(b): Moment-change in prestress relationship,
Beam A2-2 (Zhang *et al* (1993))

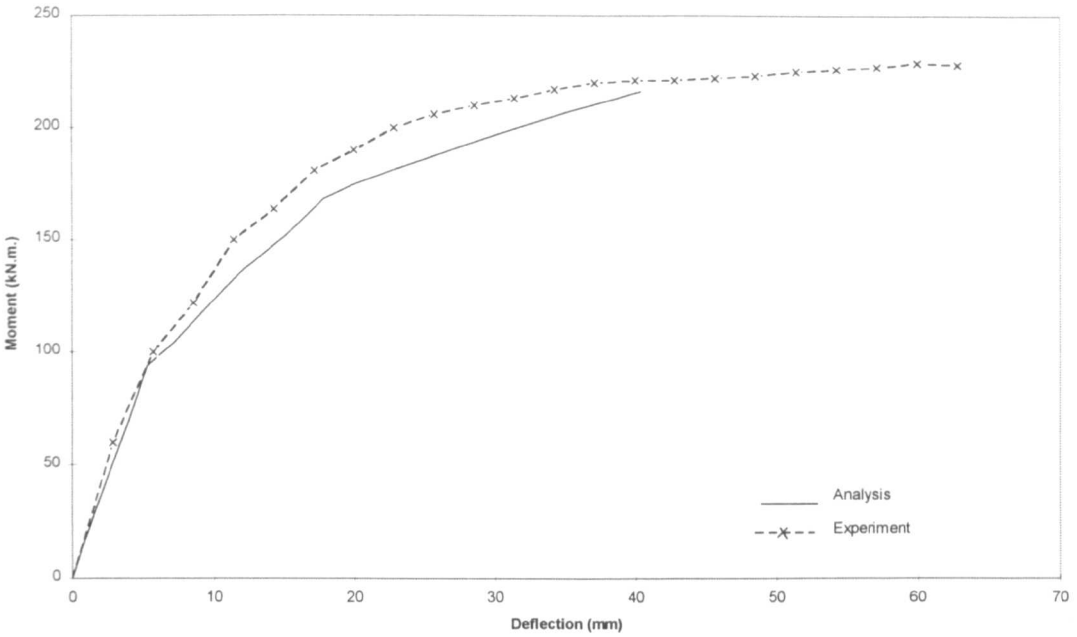

Figure 5.14(a): Moment-deflection relationship,
Beam A3-2 (Zhang *et al* (1993))

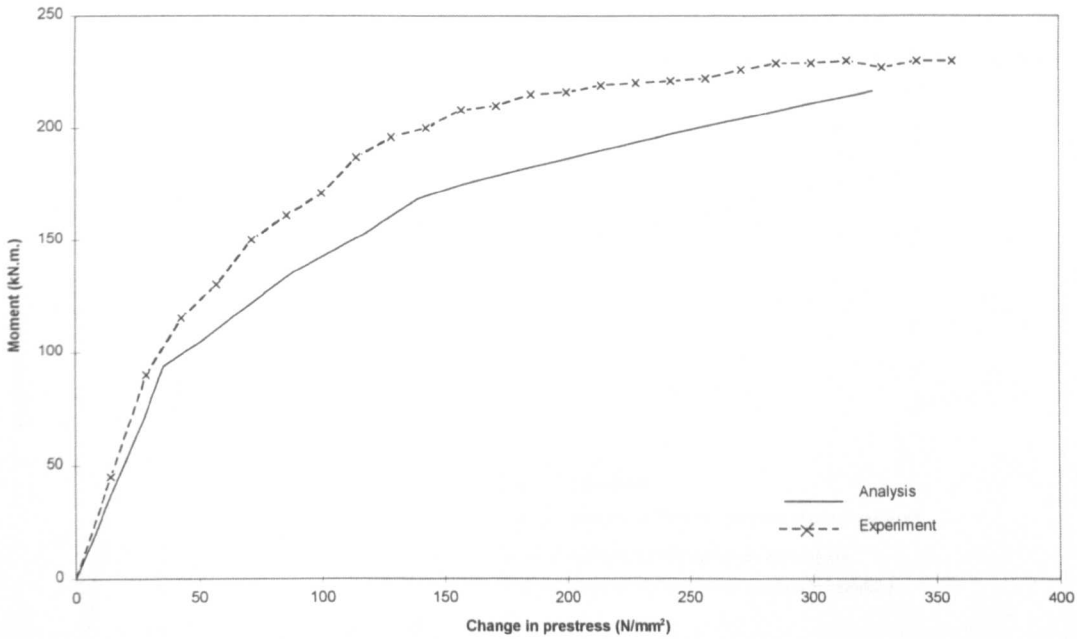

Figure 5.14(b): Moment-change in prestress relationship,
Beam A3-2 (Zhang *et al* (1993))

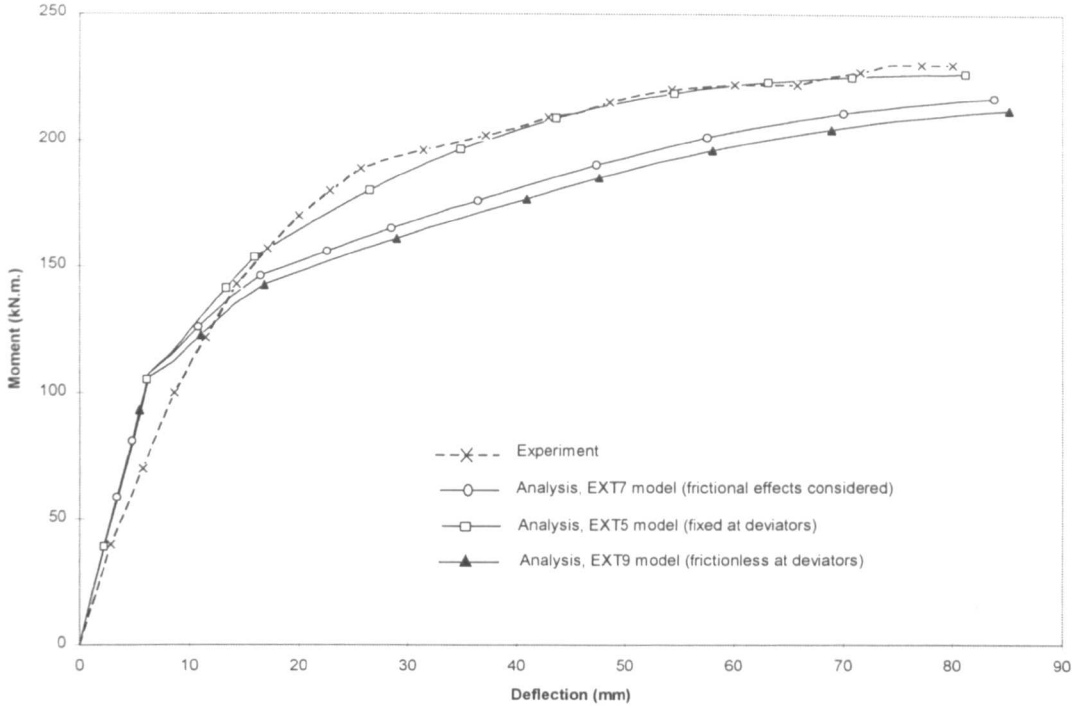

Figure 5.15(a): Moment-deflection relationships,
Beam B1-2 (Zhang *et al* (1993))

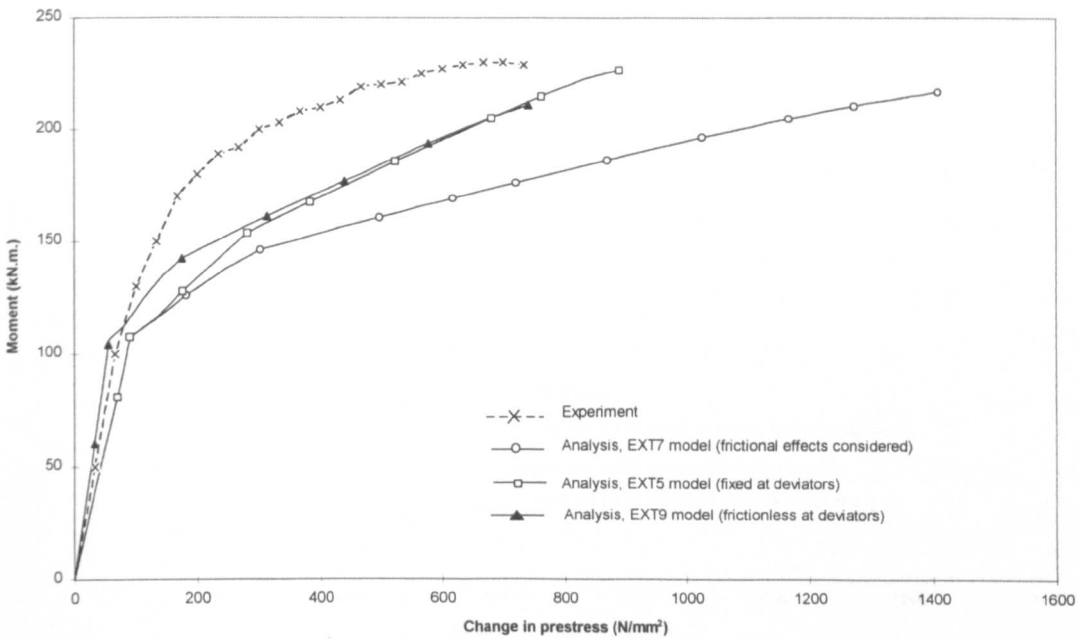

Figure 5.15(b): Moment-change in prestress relationships,
Beam B1-2 (Zhang *et al* (1993))

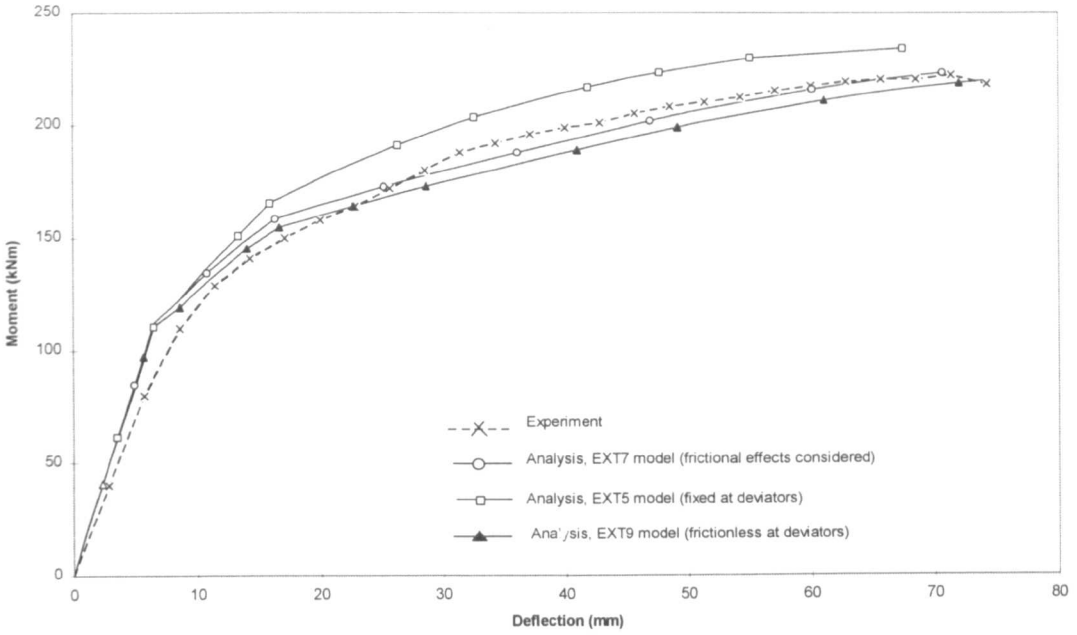

Figure 5.16(a): Moment-deflection relationships,
Beam B2-2 (Zhang *et al* (1993))

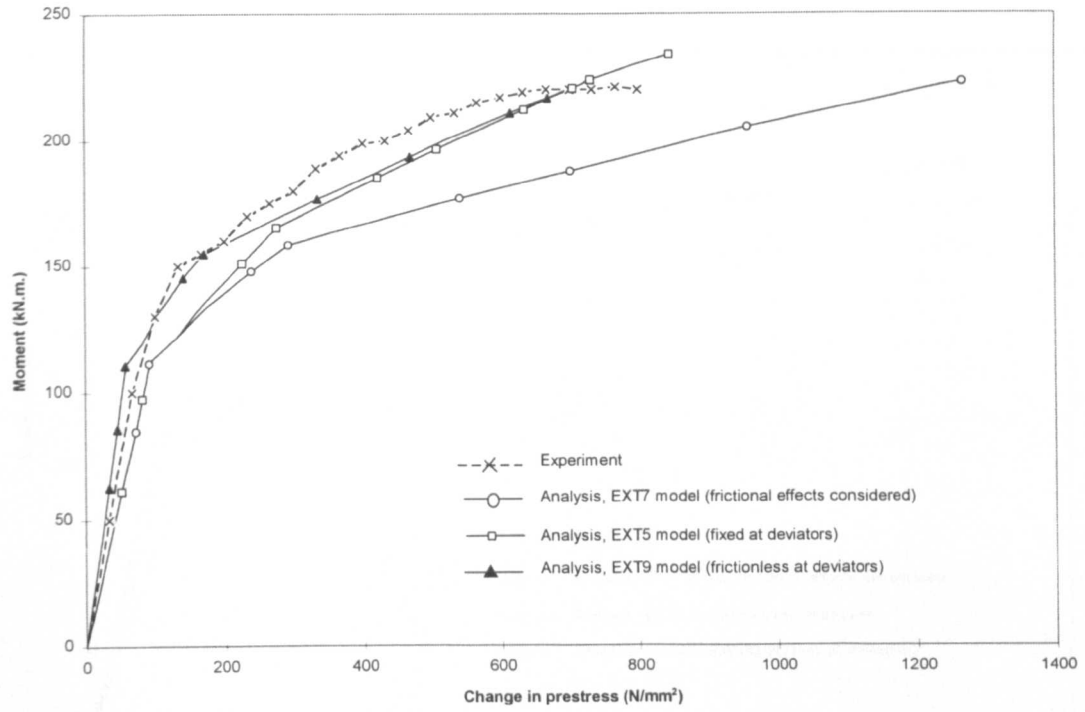

Figure 5.16(b): Moment-change in prestress relationships,
Beam B2-2 (Zhang *et al* (1993))

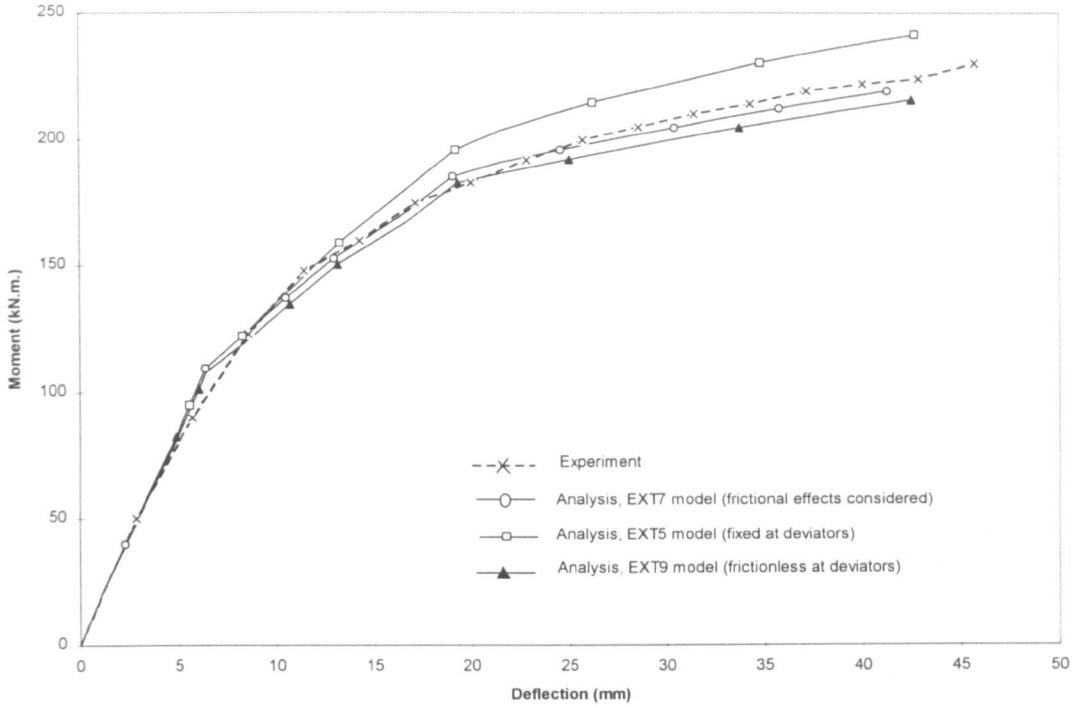

Figure 5.17(a): Moment-deflection relationships,
Beam B3-2 (Zhang *et al* (1993))

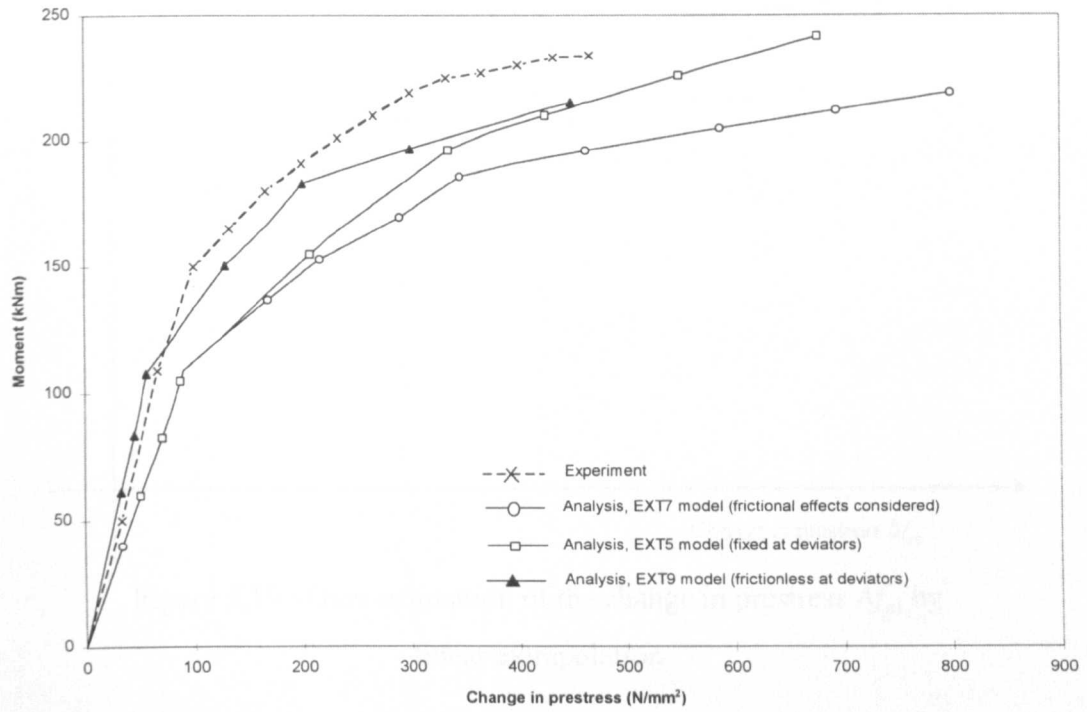

Figure 5.17(b): Moment-Change in prestress relationships,
Beam B3-2 (Zhang *et al* (1993))

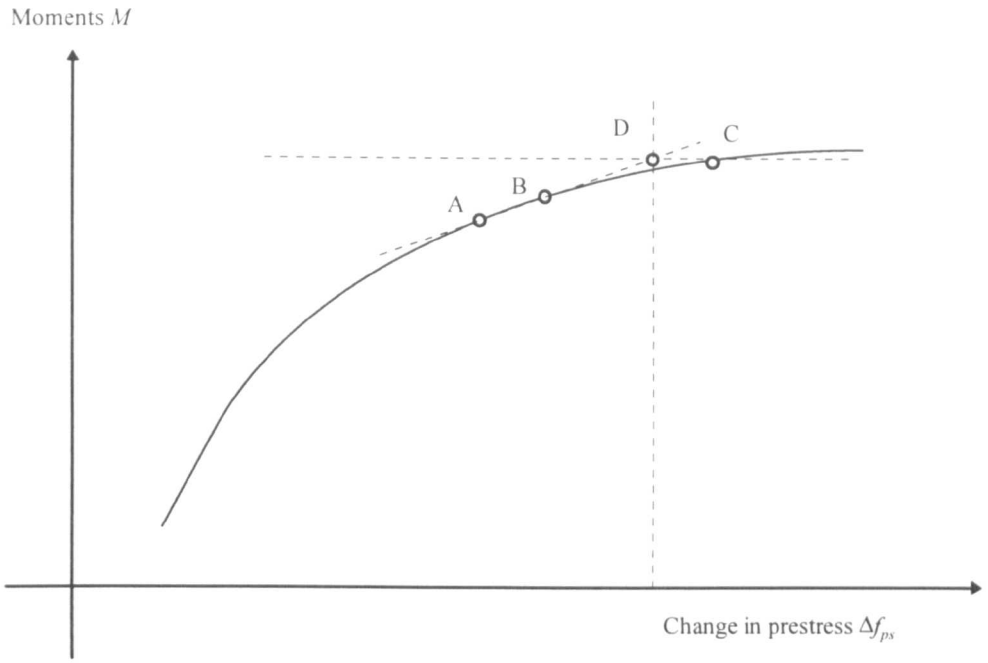

Figure 5.18 : Linear extrapolation of the change in prestress Δf_{ps}

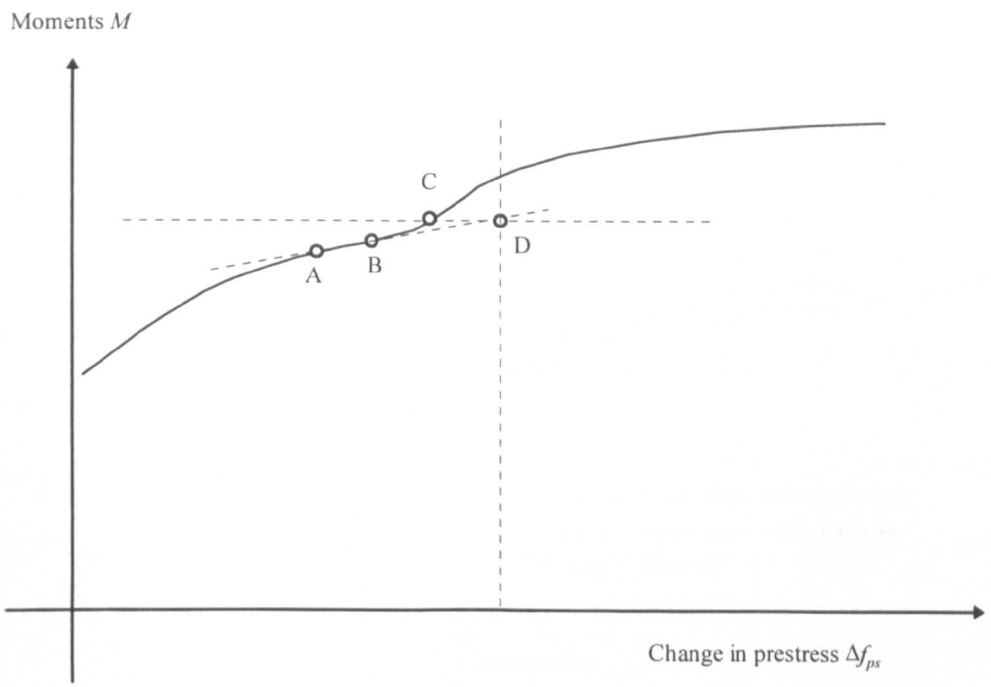

Figure 5.19 : Over-estimation of the change in prestress Δf_{ps} by linear extrapolation

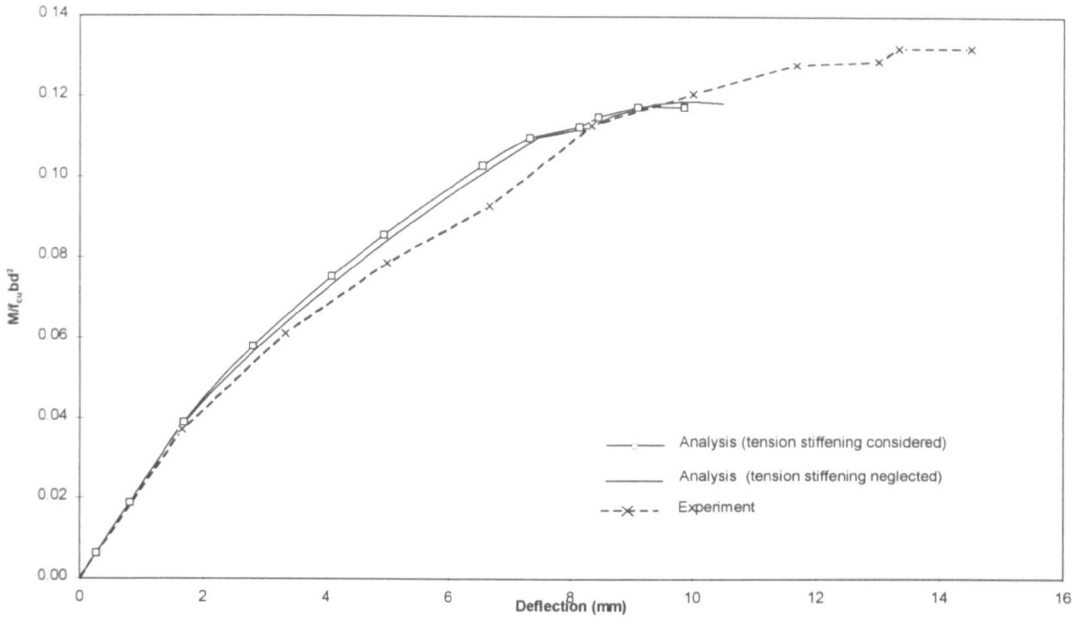

Figure 5.20 : Moment-deflection relationships for Beam OS-1 considering the effects of tension stiffening

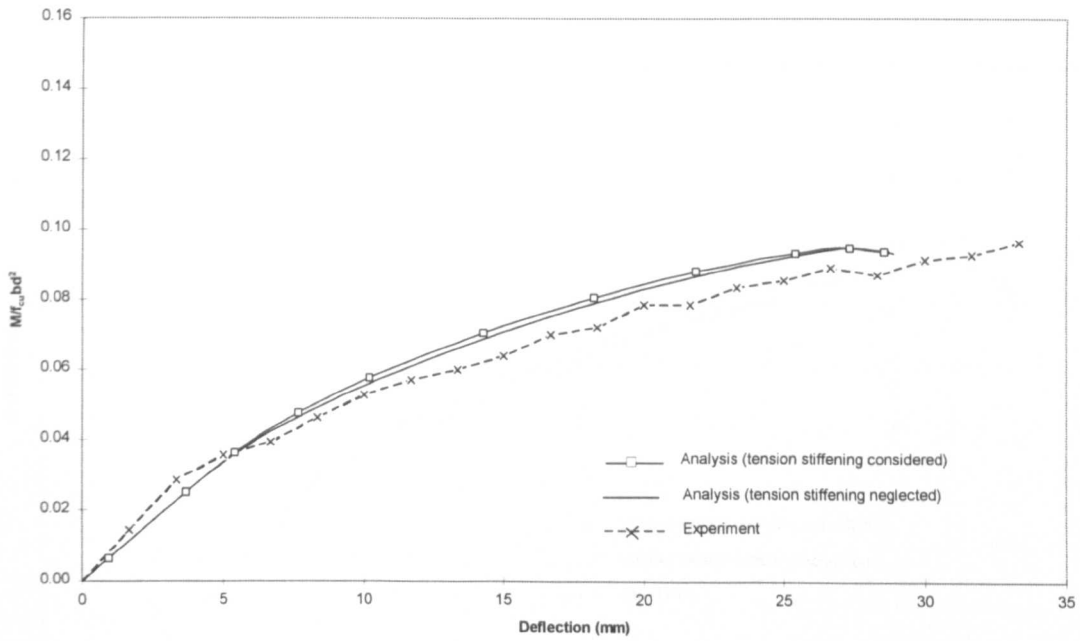

Figure 5.21 : Moment-deflection relationships for Beam OL-1 considering the effects of tension stiffening

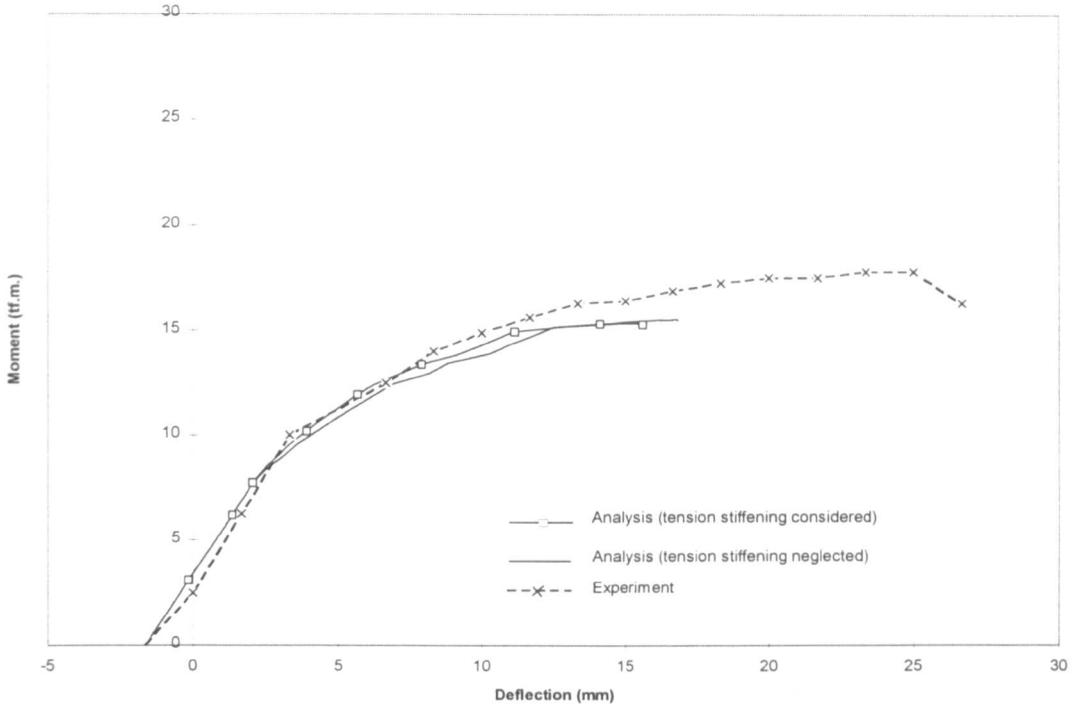

Figure 5.22 : Moment-deflection relationships for Beam OA-1 considering the effects of tension stiffening

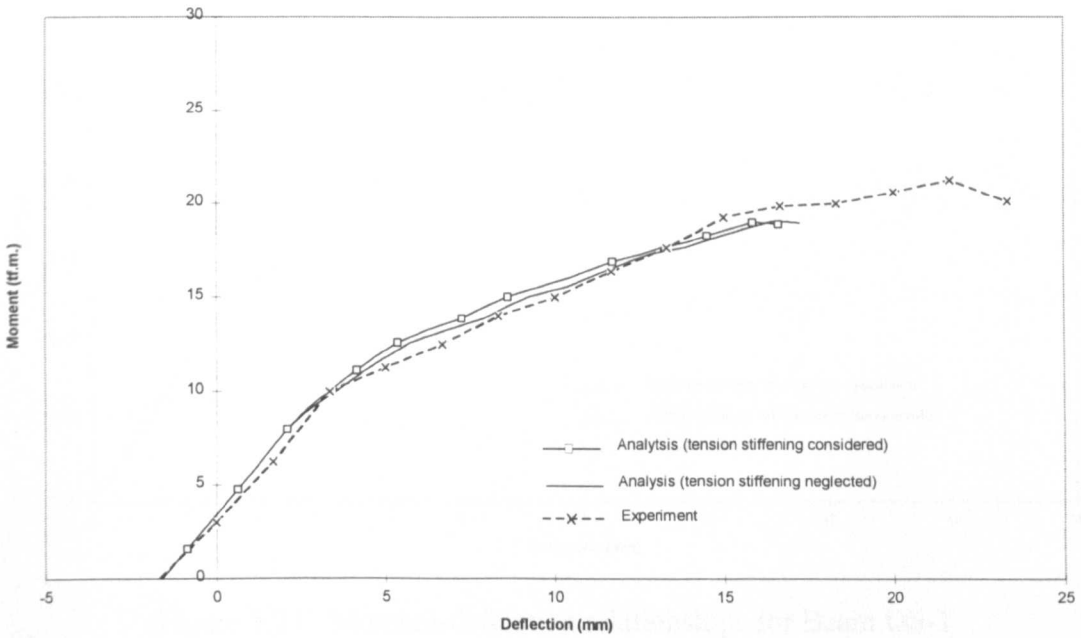

Figure 5.23 : Moment-deflection relationships for Beam OB-1 considering the effects of tension stiffening

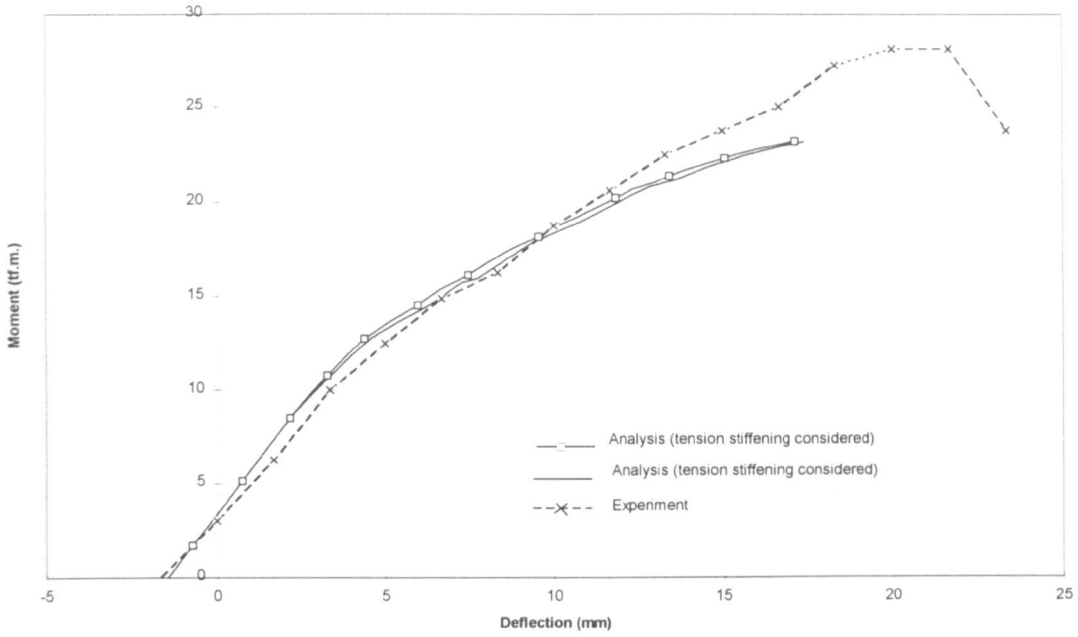

Figure 5.24 : Moment-deflection relationships for Beam OC-1 considering the effects of tension stiffening

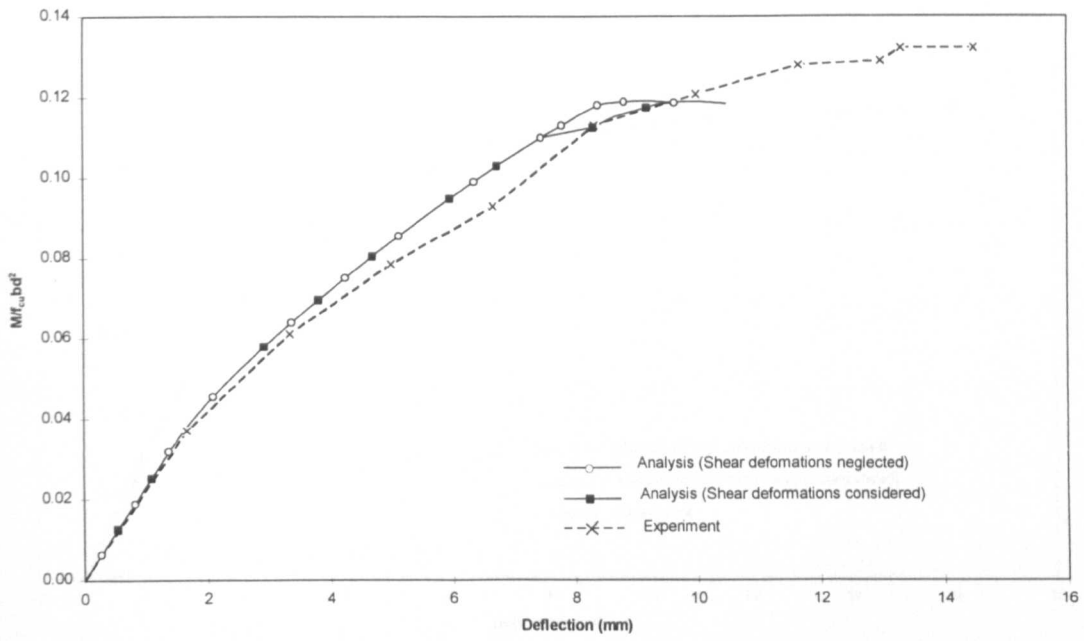

Figure 5.25 : Moment-deflection relationships for Beam OS-1 neglecting the effects of shear deformations

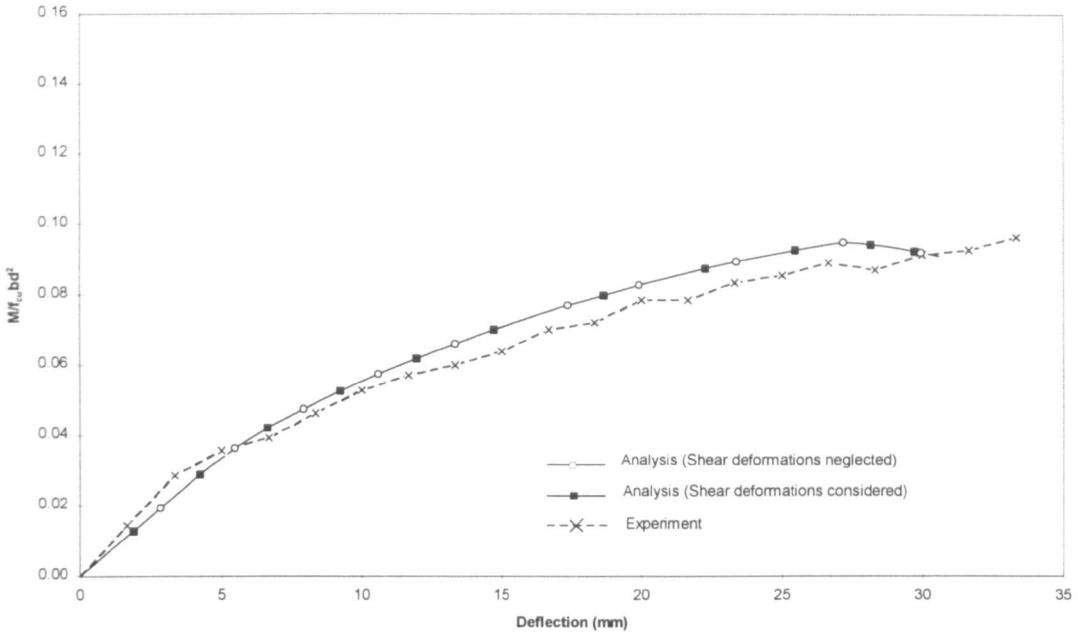

Figure 5.26 : Moment-deflection relationships for OL-1 neglecting the effects of shear deformations

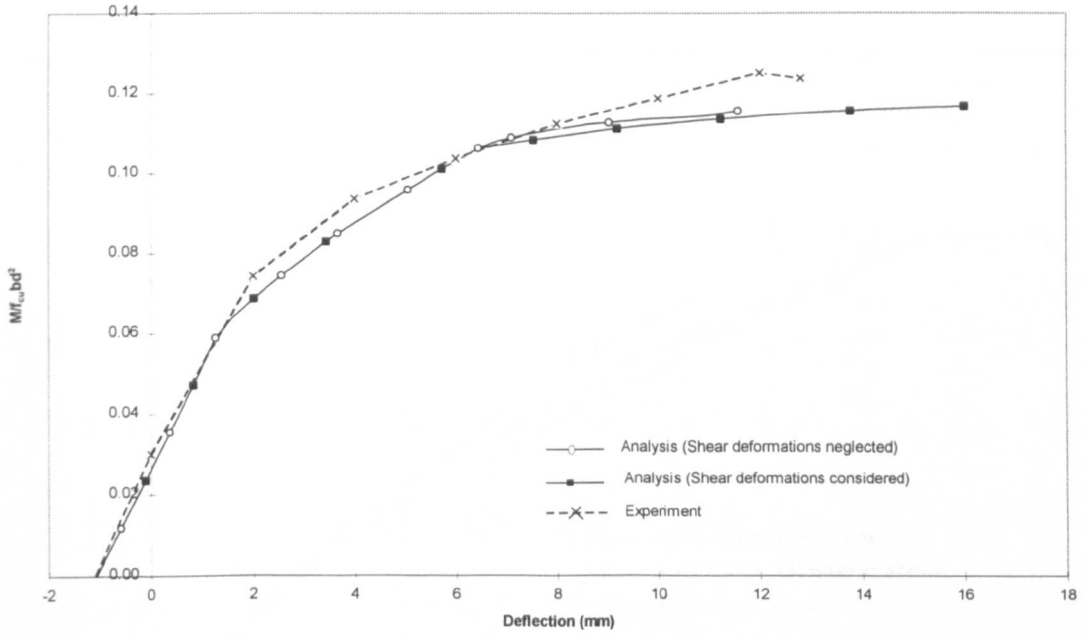

Figure 5.27 : Moment-deflection relationships for Beam OA88-2 neglecting the effects of shear deformations

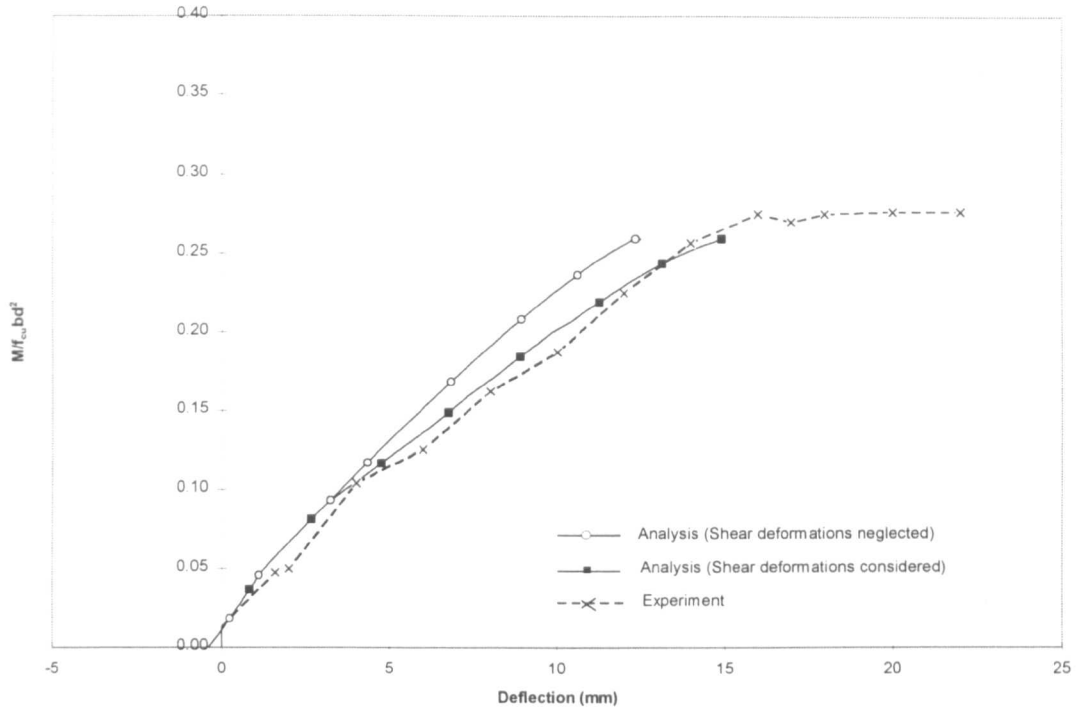

Figure 5.28 : Moment-deflection relationships for Beam OC88-1 neglecting the effects of shear deformations

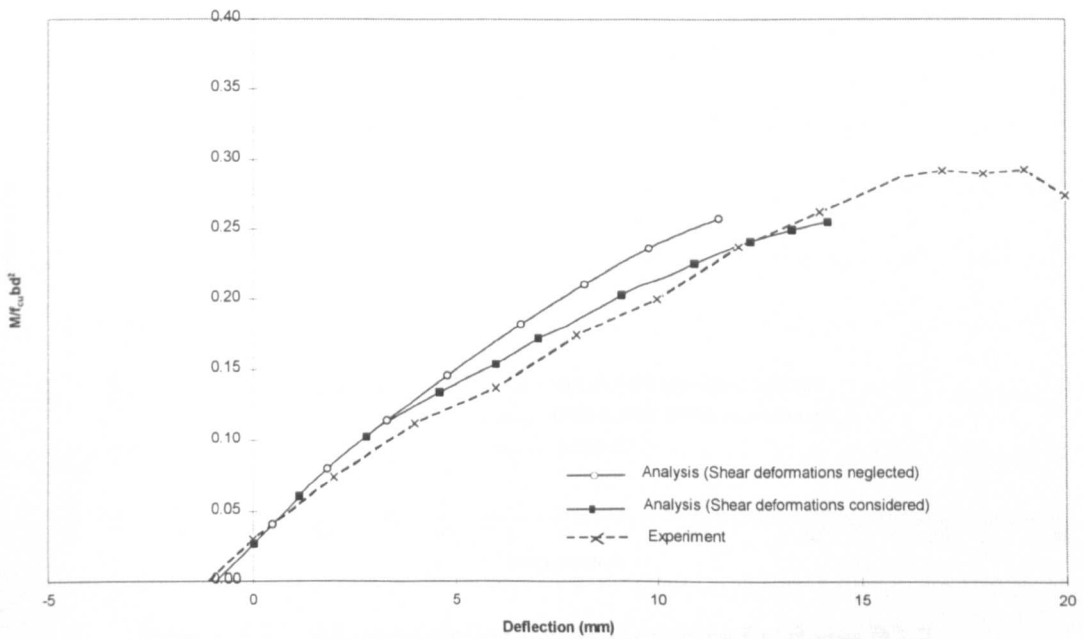

Figure 5.29 : Moment-deflection relationships for Beam OC88-2 neglecting the effects of shear deformations

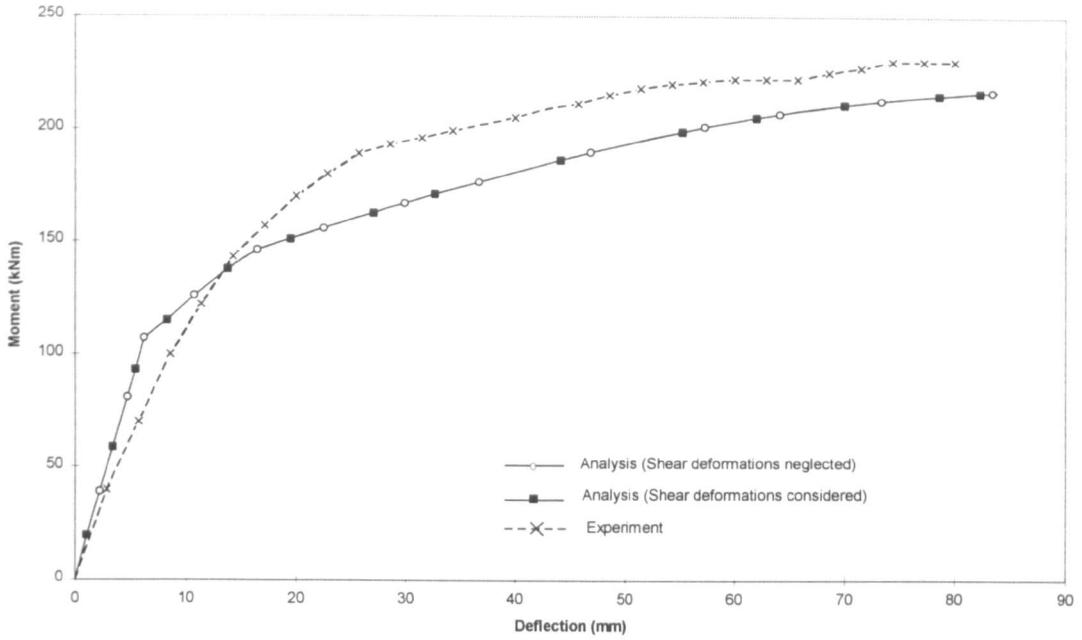

Figure 5.30 : Moment-deflection relationships for Beam B1-2 neglecting the effects of shear deformations

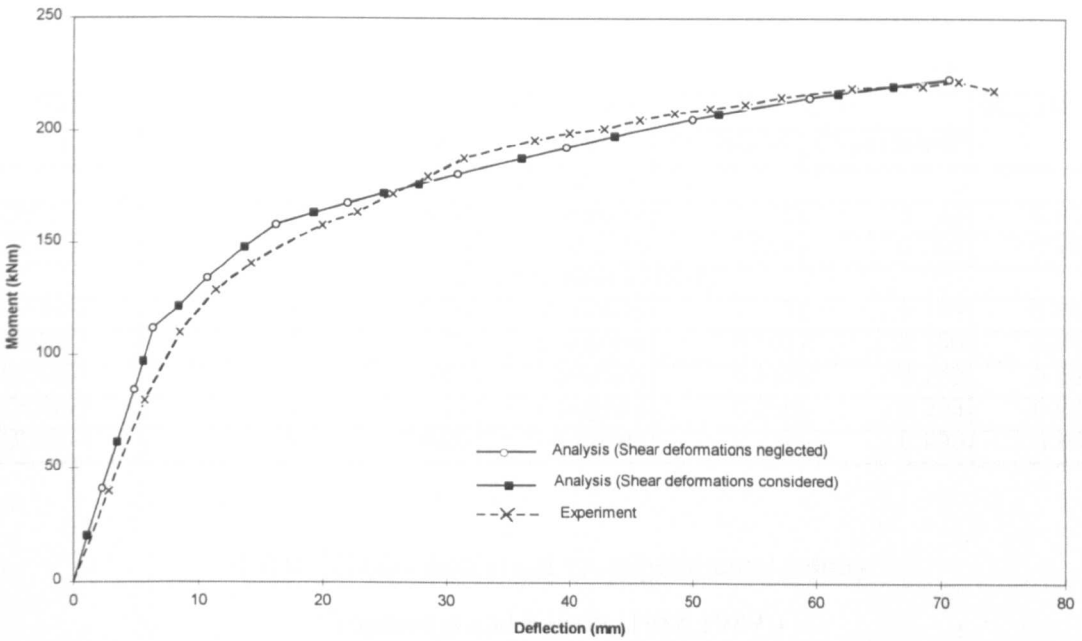

Figure 5.31 : Moment-deflection relationships for Beam B2-2 neglecting the effects of shear deformations

Beam No.	Profile Type*	Load Type**	L/d_{ps}	L_{free}/d_{ps}	A_s (mm^2)	A_s% (%)	A_{ps} (mm^2)	P_e (kN)
Yaginuma and Kitada (1988)								
OS-1	1	1	24.00	N.A.	56.65	0.94	132.95	25
OL-1	1	1	42.00	N.A.	56.65	0.94	132.95	28
Yaginuma and Kitada (1989)								
OA88-2	1	1	17.00	N.A.	157.10	0.44	265.50	160
OB88-1	1	1	17.00	N.A.	256.60	0.71	132.95	40
OC88-1	1	1	17.00	N.A.	981.70	2.73	265.50	80
OC88-2	1	1	17.00	N.A.	981.70	2.73	265.50	160
OD88-1	1	1	17.00	N.A.	1321.04	3.67	132.95	80
Yaginuma and Kitada (1987)								
OA-1	1	1	15.00	N.A.	567.06	0.57	830.95	435
OB-1	1	1	15.00	N.A.	981.70	0.98	830.95	435
OC-1	1	1	15.00	N.A.	1924.23	1.92	830.95	435
Zhang *et al* (1993)								
A1-2	1	2	14.00	N.A.	157.08	0.45	981.74	320
A2-1	1	1	14.00	N.A.	235.62	0.67	981.74	320
A2-2	1	2	14.00	N.A.	235.62	0.67	981.74	330
A3-2	1	2	14.00	N.A.	358.14	1.02	981.74	330
B1-2	2	2	13.00	7.20	157.08	0.42	392.70	320
B2-2	2	2	13.00	7.20	201.06	0.54	392.70	330
B3-2	2	2	13.00	7.20	402.12	1.07	392.70	320

* Refer to Figures A.2(b) and A.2(c) in Appendix A for arrangement of Load Type 1 and 2 respectively.
** Refer to Figures A.2(d) and A.2(e) in Appendix A for arrangement of Tendon Profile 1 and 2 respectively.

Table 5.1: Experimental beams used for verification process

Beam No.	No. of Load Sequence	Computing Time (hrs)	Termination Condition	$M_{ult}/f_{cu}bd^2$		M_{pred}/M_{exp}
				Analytical	Experiment	
Yaginuma and Kitada (1988)						
OS-1	45	23.00	complete	0.119	0.132	0.901
OL-1	42	10.00	complete	0.095	0.096	0.990
Yaginuma and Kitada (1989)						
OA88-2	46	5.50	complete	0.117	0.124	0.943
OB88-1	46	4.50	complete	0.102	0.100	1.017
OC88-1	46	5.50	complete	0.259	0.276	0.937
OC88-2	44	5.00	complete	0.256	0.293	0.872
OD88-1	45	4.00	complete	0.277	0.293	0.945

Table 5.2 (a) : Analytical vs. experimental results

(Yaginuma and Kitada (1988,1989))

Beam No.	No. of Load Sequence	Computing Time (hrs)	Termination Condition	M_{ult} (tf.m)		M_{pred}/M_{exp}
				Analytical	Experiment	
Yaginuma and Kitada (1987)						
OA-1	42	3.00	complete	15.508	17.750	0.874
OB-1	42	3.50	complete	19.057	21.250	0.897
OC-1	50	5.00	complete	23.168	28.125	0.824

Table 5.2 (b) : Analytical vs. experimental results

(Yaginuma and Kitada (1987))

Beam No.	No. of Load Sequence	Computing Time (hrs)	Termination Condition	M_{ult} (kN.m)		M_{pred}/M_{exp}
				Analytical	Experiment	
Zhang *et al* (1993)						
A1-2	34	3.00	premature	173.530	201.000	0.863
A2-1	40	2.00	premature	205.400	229.000	0.897
A2-2	33	2.00	premature	197.097	205.000	0.961
A3-2	30	3.00	premature	216.272	229.670	0.942

Table 5.2 (c) : Analytical vs. experimental results Beams A1-2, A2-1, A2-2 and A3-2

(Zhang et al (1993))

Beam No.	Analytical Model	No. of Load Sequence	Computing Time (hrs)	Termination Condition	M_{ult} (kN.m)		M_{pred}/M_{exp}
					Analytical	Experiment	
Zhang *et al* (1993)							
B1-2	EXT5	47	15.00	complete	226.438	230.000	0.985
B1-2	EXT7	49	8.00	complete	216.738	230.000	0.942
B1-2	EXT9	46	6.00	complete	211.938	230.000	0.921
B2-2	EXT5	45	9.00	complete	233.834	222.000	1.053
B2-2	EXT7	49	24.00	complete	223.024	222.000	1.005
B2-2	EXT9	47	3.00	complete	219.724	222.000	0.990
B3-2	EXT5	34	15.00	premature	241.449	230.000	1.050
B3-2	EXT7	30	10.00	premature	219.149	230.000	0.953
B3-2	EXT9	29	2.00	premature	215.449	230.000	0.937

Table 5.2 (d) : Analytical vs. experimental results Beams B1-2, B2-2 and B3-2

(Zhang et al (1993))

Beams:	M_{pred}/M_{exp}	
	Average	Standard Deviation
Yaginuma and Kitada (1987, 1988, 1989)		
OS-1 and OL-1	0.945	0.044
OA88-2, OB88-1, OC88-1, OC88-2 and OD88-1	0.943	0.046
OA-1, OB-1 and OC-1	0.865	0.030
Zhang *et al* (1993)		
A1-2, A2-1, A2-2 and A3-2	0.916	0.038
B1-2, B2-2 and B3-2 (EX17)	0.967	0.027
All beams	**0.927**	**0.051**

Table 5.3: Average and standard deviation of M_{pred}/M_{exp} for beams used in verification process

Beam	Computing Time (hrs)		T_2/T_1	M_{ult} (kNm)		M_2/M_1
	T_1	T_2		M_1	M_2	
OS-1	23.00	37.00	1.61	3.004	2.976	0.991
OL-1	10.00	16.50	1.65	2.409	2.402	0.997
OA-1	3.00	8.00	2.67	155.079	153.479	0.990
OB-1	3.50	7.00	2.00	190.562	189.962	0.997
OC-1	5.00	9.00	1.80	231.690	231.989	1.001
		Average	1.95		**Average**	1.00

Where
T_1 = time taken to conduct the analysis neglecting the tension stiffening effects
T_2 = time taken to conduct the analysis with the tension stiffening effects
M_1 = M_{ult} analysed neglecting the tension stiffening effects
M_2 = M_{ult} analysed with the tension stiffening effects.

Table 5.4: Comparing the computer time and M_{ult} derived from analyses conducted with and without the tension stiffening effects considered

Beam	Computing Time (hrs)		T_3/T_1	M_{ult} (kNm)		M_3/M_1
	T_1	T_3		M_1	M_3	
OS-1	23.00	8.00	0.35	3.004	3.008	1.001
OL-1	10.00	9.00	0.90	2.409	2.401	0.997
OA88-2	5.50	3.00	0.55	33.305	32.944	0.989
OC88-1	5.50	4.00	0.73	73.922	73.972	1.001
OC88-2	5.00	4.00	0.80	72.842	73.412	1.008
B1-2 (EXT7)	8.00	10.00	1.25	216.738	216.538	0.999
B2-2 (EXT7)	24.00	8.00	0.33	223.024	222.520	0.998
		Average	0.70		**Average**	1.00

Where

T_1 = time taken to conduct the analysis with the shear deformations

T_3 = time taken to conduct the analysis neglecting shear deformations

M_1 = M_{ult} analysed with the shear deformations

M_3 = M_{ult} analysed neglecting the shear deformations.

Table 5.5: Comparing the computer time and M_{ult} derived from analyses conducted with and without the shear deformations considered

Chapter 6

Parametric Study

6.1 General

Several parameters that influence the ultimate behaviour of externally post-tensioned structures have been discussed in Chapter Three. From the discussion, it is evident that the influences of these parameters are still not fully understood by many engineers and researchers. Hence, as part of the investigation, a parametric study was conducted to examine in more detail the effects which some of these parameters have on externally prestressed structures. This chapter describes how the parametric study was conducted and the results and conclusions derived from it.

Six typical externally prestressed structures, denoted Beams T1 to T6, were designed here for the parametric study and are described in Section 6.2. The span-depth ratio, non-prestressed reinforcement ratio, amount of prestressed reinforcement and initial prestress force of these beams were then varied and, simulations conducted on them with the proposed non-linear models for their flexural behaviour up to ultimate. Thus resulting in over a hundred simulations conducted for the investigation.

Due to the large number of parameters considered in the investigation, the study was divided into two parts. The first part of the study (Section 6.3) considered the effects of the following parameters on the flexural behaviour of externally prestressed structures: the non-prestressed reinforcement ratio (Section 6.3.1), span-depth ratio (Section 6.3.2) and the initial prestress force and amount of prestressed reinforcement (Section 6.3.3). In the second part of the parametric study, the effects of incorporating deviators along the span of these structures are investigated (Section 6.4). The difference in flexural behaviour between beams having deflected and straight tendon profiles is discussed in Section 6.4.1. Finally, the effects of the frictional behaviour at

the deviators and the free length to depth ratio on the ultimate behaviour of such structures are investigated in Section 6.4.2 and Section 6.4.3 respectively.

6.2 Beams used for the Parametric Study

Six typical externally prestressed beam configurations were selected for the parametric study, denoted Beams T1 to T6. Beam T1 was based on the simply supported externally prestressed structure used in the Bangkok Second Stage Expressway (Hewson (1993)) and the others were variations of this main design. These beams were designed in accordance to BS5400 Part 2 and Part 4 (1990), and the design guidelines for externally prestressed structures by the UK DoT BA 58/94 (1995) and BD 58/94 (1995). The non-prestressed reinforcement ratios, span-depth ratios, initial prestress force, amount of prestressed reinforcement and properties of the deviators (if applicable) for these beams were then varied and the appropriate non-linear analytical models were used to predict their flexural behaviour up to failure. This resulted in over a hundred simulations which formed the basis for this parametric study (performed using Silicon Graphic computer Challenge XL MIPS 4400 CPU).

In the design of Beams T1 to T6, the service and ultimate loading conditions were first evaluated according to the HA and HB loading requirements given in BS 5400 Part 2 (1990). The service limit states of these beams were then checked with the specifications stated in BS 5400 (Part 4) for Class 2 prestressed structures and their ultimate moment of resistance were estimated using the following assumptions given in BA 58/94 (1995) and BD 58/94 (1995) :

- zero stress increase in the tendons, $\Delta f_{ps(ult)} = 0.0$ N/mm^2
- zero eccentricity variation of the tendons, $\Delta_{eccen(ult)} = 0.0$ mm.

All the six beams were simply supported box-girders with a deck width of 10.5 m. However, since transverse behaviour is not within the scope of this study, the box-girders were modelled as equivalent I-section beams for simplicity. The first five of these beams were prestressed with external tendons with a straight profile, while Beam T6, was prestressed with tendons with a deflected profile.

Beam T1 had an overall length of 45 m and an overall depth of 3 m. A prestress force of 57,406 kN was initially applied to this structure and the initial eccentricity of the

tendons was 372 mm from the centroid of the beam cross-section. Beams T2 and T3 were 25m in length with an overall depth of 1.5 m and had identical cross-sections. Although these two beams were prestressed with a similar amount of initial prestress force (i.e. 27,233 kN and 24,457 kN respectively), the initial eccentricity of the tendons were varied, being 380 mm for Beam T2 and 560 mm for Beam T3. The cross-sections of Beams T4 and T5 were also similar to each other and they both had an overall length of 25 m and depth of 2.5 m. The initial prestressing force applied to Beams T4 and T5 were 28,879 kN and 29,093 kN respectively with initial tendon eccentricities of 600 mm and 300 mm respectively. Finally, the overall span of Beam T6 was 45 m while its overall depth was 2.4 m. The external tendons were prestressed with an initial prestress force of 81,450 kN and deflected along the structure by two deviators (located at 10.7 m from both supports). For comprehensive information on the values of the parameters used in all the parametric studies given in this chapter refer to Appendix B and C.

6.3 Parametric Study: Straight Tendons

A preliminary discussion of the effects of span-depth ratio, non-prestressed reinforcement ratio, initial prestress force and amount of prestressed reinforcement on the flexural behaviour of externally prestressed structures has already been presented in Chapter Three. From the discussion it was evident that the nature and extent of influence which these parameters have on the flexural behaviour of such beams are still not fully understood. Hence, in the first part of the parametric study, an investigation was conducted into these parameters to gain a better understanding on their effects.

Two terms that are used frequently in the text to describe the ultimate behaviour of these externally post-tensioned structures need to be defined here first to avoid confusion, i.e. the *maximum moment* (M_{max}) and *material limit moment* ($M_{(limit)}$). The term *material limit moment* $M_{(limit)}$ is used here to refer to the theoretical ultimate moment of the beam associated with either a specified concrete strain at the extreme compressive fiber (i.e. 0.0035) or the ultimate strength specified for the non-prestressed or prestressed reinforcement. The other term M_{max} refers to the maximum moment corresponding to the exhaustion of the bending moment capacity, i.e. $dM/d\Delta$

= 0. For externally prestressed structures, these two moments may sometimes be coincidental to each other as shown in Figure 6.1, in which case both moments may be used to describe the ultimate capacity of the beam. However, the maximum moment M_{max} may also sometimes be observed to be higher than the material limit moment $M_{(limit)}$ due to the large reduction in the eccentricity of the tendons at higher load levels caused by second-order effects (see Figure 6.2).

In practice, the maximum moment M_{max} is usually the term used to describe the ultimate carrying capacity of the externally prestressed beams (e.g. Yaginuma and Kitada (1987, 1988, 1989) and Zhang *et al* (1993)) and, hence, the value of M_{max} for the various parameters considered here was first determined. However, without the availability of either finite element software or non-linear analytical models (such as the proposed models), designers may sometimes be required to use the simplified approach introduced in the codes of practices (e.g. BS5400, AASHTO, etc.) to evaluate the ultimate capacity of such beams. This approach normally involves limiting the extreme top concrete fiber strain at failure to an ultimate strain value (e.g. 0.0035) and performing a sectional analysis at the critical section with the assumption that the stress increase in the tendons is equal to a recommended value. For internally bonded prestressed structures, this method will usually yield the ultimate capacity, but as explained above, they may yield lower results which correspond to the material limit moment condition for externally prestressed structures (see Figure 6.2). Since one of the purposes of conducting this study is to investigate if the stress increase and eccentricity variation of the external tendons recommended in the codes of practices are acceptable for practical purposes, the variations of the material limit moments $M_{(limit)}$, change in prestress $\Delta f_{ps(limit)}$ and eccentricity variations $\Delta_{eccen(limit)}$ for the parameters investigated (e.g. prestressed and non-prestressed reinforcement ratios, initial prestress force and span-depth ratios) were thus also considered in the parametric study.

6.3.1 Amount of Non-prestressed Reinforcements

A total of thirty-six simulations were conducted with the proposed analytical models (described in Chapter four) to study the effects of non-prestressed reinforcement on the ultimate flexural response of externally prestressed beams. The analytical

simulations were performed on Beams T1 to T5 (described in Section 6.2), but with varying non-prestressed reinforcement ratios A_s% specified in their designs. The range of reinforcement ratios used for this study varied from 0.15% to 4.00%, which were the maximum and minimum allowable values given in BS 5400 (1990). It should be noted that the term reinforcement ratio A_s% used here is in accordance with that described in BS5400 Part 4 (1990):

$$A_s\% = \frac{A_s 100}{b_a d} \quad \text{.....(6.1)}$$

where

b_a = the breadth of section or the average breadth excluding the compression flange for non-rectangular sections

d = the effective depth to the tension reinforcement.

Figures 6.3 to 6.6 show the moment-deflection relationships for Beams T1 to T5 respectively with different reinforcement ratios. In Figure 6.3, which illustrates the deflection response for Beam T1 with different A_s%, it was observed that when low reinforcement ratios were used (e.g. A_s% = 0.15%) the moment-deflection response was characterised by a sudden loss in strength immediately after cracking, followed by an increase in strength until the maximum moment condition was reached which was only about two percent higher than the cracking moment. After reaching maximum moment condition, the curve then showed a steady decrease in moment to the material limit condition as the beam deflection increased. For higher reinforcement ratios (e.g. A_s% = 2.4% and 4%), the moment-deflection responses did not show a sudden decrease in moment after the occurrence of cracking, but instead exhibited an increase in moment with reduced stiffness. After the curves reached the maximum moment condition, they then exhibited a relatively horizontal response indicating very small changes in moments with large deflections up to the material limit condition.

Figure 6.4 shows deflection responses for Beam T2 with different A_s% from which it can be seen that all the curves indicated a higher maximum moment M_{max} than the material limit moment $M_{(limit)}$ (maximum difference about twenty percent). At lower reinforcement ratios (e.g. A_s% = 0.15%, 0.5% and 0.7%), failure was observed to

occur immediately after the occurrence of cracking for the beam. This was because after cracking, a single large crack was developed at the critical section, thereby causing the beam to behave as a shallow tied arch rather than a flexural member. However, due to the reduction in eccentricity of the tendons caused by second-order effects, the tied arch mechanism could not support loads which are higher than those placed on the structure at cracking, thus causing the beam to collapse. This 'snap-through' failure was observed to be avoided by placing more non-prestressed reinforcement in the beam. The moment-deflection curves for Beam T2 with higher reinforcement ratios (A_s% = 2.4% and 4%) exhibited an increase in moment after cracking up to the yielding of the non-prestressed reinforcement. After the reinforcement had yielded, the curves showed a decrease in moment until the material limit condition was reached.

The design of Beam T3 was very similar to Beam T2, except for the initial position of the tendons from the centroid of the section. In Figure 6.5, the snap-through failure described for Beam T2 was also observed for Beam T3 with the lower reinforcement ratios (i.e. A_s%= 0.15% and 0.5%). When more non-prestressed reinforcement was specified, the deflection response was found to be greatly improved. The moment-deflection relationships for Beam T3 with higher reinforcement ratios (i.e. A_s% = 2.4% and 4%) showed a reduction in the stiffness after cracking, but the moments continued to increase up to the maximum condition. When the maximum moment was attained, the curves then exhibited a slight decrease in strength and produced a material limit moment which was about five percent lower than the maximum moment.

The moment-deflection responses for Beam T4 with different reinforcement ratios are shown in Figure 6.6. From the figure, it can be observed that for lower reinforcement ratios (i.e. A_s% = 0.3% and 0.5%), the moment-deflection curves exhibited a sudden large drop in strength after cracking, indicating the formation of a tied arch mechanism. The tied arch mechanism caused large deflections to occur in the beam, to generate the required tensile force in the external tendons, until the beam failed due to concrete crushing at the critical section. The material limit moments for these curves were noted to be only slightly higher than the cracking moments (less than two percent for A_s% = 0.3% and less than fifteen percent for A_s% = 0.5%). When higher

reinforcement ratios were specified in Beam T4, the moment-deflection curve exhibited an increase in moment up to failure, where reductions in stiffness occurred after first cracking and after yield of the reinforcement. It was also noted that all the moment-deflection curves for this beam shown in Figure 6.6 exhibited a maximum moment which is equal or similar to the material limit moment.

Figure 6.7 shows the deflection responses for Beam T5 with different reinforcement ratios. The figure shows that snap-through failure will occur in this beam if the reinforcement ratios are too low (e.g. $A_s\%$ = 0.3%). Increasing the amount non-prestressed reinforcement for Beam T5 will prevent such failure from occurring and improve the flexural response of the beam up to failure. The material limit moments for Beam T5 with different reinforcement ratios were also found to be only slightly lower than the maximum moments (not more than five percent).

Figure 6.8 shows the variation of the maximum moment M_{max} with the reinforcement ratio $A_s\%$ for Beams T1 to T5. It was observed from the figure that increasing the amount of reinforcement ratio will generally cause an increase in the maximum moment capacity of these structures. The relationships between the maximum moment and the reinforcement ratio were also observed to be near linear. The gradients (m) which were estimated using the Least Squares Method, were estimated to be about 22,646 kNm/%, 12,646 kNm/% and 11,961 kNm/% for Beams T1, T4 and T5 respectively and these values were considered relatively high as compared to the gradients evaluated for Beams T2 and T3, which were 2,723 kN/% and 3,395 kN/% respectively (see Figure 6.8). This shows that although increasing the amount of non-prestressed reinforcement in externally post-tensioned structures will generally increase their flexural performance, the rate of maximum moment increase with reinforcement ratios varies greatly for different beam configurations.

Figure 6.9 shows the material limit moment $M_{(limit)}$ - reinforcement ratio $A_s\%$ relationships for Beams T2 to T5. It should be noted that the material limit moment - reinforcement ratio relationship for Beam T1 was not plotted in Figure 6.9 because the material limit condition could not be predicted by the analytical model for this beam due to convergence problems encountered in the analysis (see Section 5.4). The curves shown in Figure 6.9 show that the increase in material limit moment with the

increase in reinforcement ratio was relatively small until the reinforcement ratio reached about 1.2%. From a reinforcement ratio of 1.2% to 4% it was found that increasing the area of reinforcement generally caused a near linear increase in the material limit moments.

Figure 6.10 shows the relationships between the change in prestress at the material limit condition $\Delta f_{ps(limit)}$ with the reinforcement ratios for Beams T2 to T5. All the curves show an increase in the change in prestress $\Delta f_{ps(limit)}$ as the non-prestressed reinforcement ratio is increased up to about 1.2%, where the change in prestress remained relatively constant for higher reinforcement ratios. This explains why Ramos and Aparicio (1996) found that Δf_{ps} at the ultimate limit state does not change much for different reinforcement ratios, since the A_s% values used in their parametric studies were relatively high.

The variation of eccentricity at the material limit condition $\Delta_{eccen(limit)}$ with the reinforcement ratios A_s% for Beams T2 to T5 are shown in Figure 6.11. From the figure, it can be observed that the overall trends of the $\Delta_{eccen(limit)}$ - A_s% relationships for the four beams were very similar to those described for the $\Delta f_{ps(limit)}$ - A_s% curves. The curves showed an increase in $\Delta_{eccen(limit)}$ as A_s% is increased up to about 1.2%, after which, the increase of reinforcement ratio in these beams does not seem to cause significant changes to $\Delta_{eccen(limit)}$.

The variation of $\Delta f_{ps(limit)}$ and $\Delta_{eccen(limit)}$ with reinforcement ratio can be explained by examining the changes in the profile of the curvature distributions along the span for beams having different reinforcement ratios. Figure 6.12 illustrates the curvature distributions for Beam T5 at the material limit condition for three different reinforcement ratios, i.e. 0.15%, 1.2% and 4%. From the figure, it can be observed that, when very little non-prestressed reinforcement is placed in the beam (i.e. 0.15%), the curvature distribution of the beam is characterised by a very large curvature developed at the critical section with a relatively small plastic hinge length. When more non-prestressed reinforcement is specified in the beam, the plastic hinge length increases while the curvature at the critical section of the beam decreases (Figure 6.13 shows the curvature - A_s% relationships at the material limit condition for Beams T2 - T5). These changes in the shape of the curvature distributions cause the deflection

estimated at the material limit condition to vary with the A_s%, as shown in Figure 6.14. Since both $\Delta f_{ps(limit)}$ and $\Delta_{eccen(limit)}$ are dependent on the deflected profile of the structure, the variation of $\Delta f_{ps(limit)}$ and $\Delta_{eccen(limit)}$ with the reinforcement ratio will therefore follow the same trend as the deflection - A_s% curves shown in Figure 6.14, i.e. an increase in values up to about 1.2% before remaining constant for higher A_s%.

6.3.2 Span-Depth Ratio

This section describes the investigation conducted on the effects of span-depth ratio on the ultimate behaviour of externally post-tensioned structures. A total of about fifty simulations were conducted in this study with the proposed analytical models applied to Beams T1 to T5, with a range of different overall lengths to produce a series of beams with different span-depth ratios. It should be noted that the reinforcement ratios adopted for these beams were relatively small, ranging from 0.15% to 0.5% (see Table 6.1). These analyses were then supplemented with a small number of beams with higher reinforcement ratio (i.e. A_s% = 3%) to cover the full range of reinforcement ratios.

Figure 6.15 shows the change in prestress in the external tendons at the material limit condition $\Delta f_{ps(limit)}$ with span-depth ratio L/d_{ps} for Beams T1 to T5. From the figure, it can be observed that $\Delta f_{ps(limit)}$ does not vary much with the span-depth ratio for all five beams, since the gradients obtained for these curves using the Least Square Method were found to be less than 0.53 N/mm^2 for Beams T1 to T5 respectively. The reason for this lack of influence is due mainly to the low reinforcement ratios used for these beams. The equilibrium of forces at a section is maintained by satisfying Equation (6.2).

$$C_{conc} - T_{reinf} - T_{conc} - T_{pres} = 0 \quad \text{.....(6.2)}$$

Since the non-prestressed reinforcement ratios for Beams T1 to T5 are low and the tensile contribution from concrete is usually negligible, the two forces T_{reinf} and T_{conc} in Equation (6.2) do not play a major role in maintaining equilibrium at the critical section at the material limit condition. The two primary forces used to maintain the equilibrium of forces at the critical section are thus the compressive force C_{conc} acting on the concrete and the prestressing force T_{pres}. When the top concrete fiber strain

reaches the ultimate strain value (i.e. taken as 0.0035 in this investigation), the estimated compressive force C_{conc} was found to be nearly the same for all beams irrespective of their span length. As such, the increase in prestress force ΔT_{pres} from the initial stressing level (and thus the change in prestress in the tendons Δf_{ps}) remains nearly constant for these beams.

If the amount of reinforcement in these beams is increased, the effect of span-depth ratio on the change in prestress at the material limit condition will also increase. Figure 6.16 shows that when the reinforcement ratio of Beam T5 was increased from 0.3% to 3%, the gradient of the $\Delta f_{ps(limit)}$ - L/d_{ps} relationship reversed from 0.0253 N/mm^2 to -6.0358 N/mm^2 respectively. This is because increasing the span-depth ratio in these beams generally caused higher deflections to occur, thereby increasing the curvature of the sections within the plastic hinge length. With higher reinforcement area, the increased curvature in these sections will induce higher tensile forces in the non-prestressed reinforcement T_{reinf} and lower compression force acting on the concrete C_{conc}. As a result, the prestress force T_{pres} (which is the same throughout the whole span) reduces to maintain equilibrium at these sections.

Figure 6.17 shows that the change in eccentricity of the tendons at the material limit condition $\Delta_{eccen(limit)}$ increases non-linearly as the span-depth ratio increases for all the five beams investigated. As explained earlier, the increase in stress at the material limit condition for all beams with low reinforcement ratio was almost the same irrespective of span length. This increase in stress $\Delta f_{ps(limit)}$ in the tendons is generated through the lengthening of the external tendons between the anchorages ($\Delta \ell_{ps}$) as the beam deforms. Since the strain increase in tendons $\Delta \varepsilon_{ps}$ is evaluated from Equation (6.2), a larger elongation ($\Delta \ell_{ps}$) is therefore required for beams with longer free spanning tendons (ℓ_{ps}) to yield the same amount of strain increase $\Delta \varepsilon_{ps}$ (and consequently stress increase Δf_{ps}) in the tendons. This larger elongation is produced by the beams through greater deformation, which consequently causes the change in tendon eccentricity to increase as the span-depth ratio increases.

$$\Delta \varepsilon_{ps} = \Delta \ell_{ps} / \ell_{ps} \quad \text{(6.2)}$$

Figure 6.18 shows a comparison between the $\Delta_{eccen(limit)}$ - L/d_{ps} relationships for Beam T5 with two extreme reinforcement ratios (i.e. 0.3% and 3%). From the figure, it is

observed that higher reinforcement ratio causes the rate of change between $\Delta_{eccen(limit)}$ and L/d_{ps} to increase as L/d_{ps} is increased.

Figure 6.19 shows the material limit moment $M_{(limit)}$ - span-depth ratio L/d_{ps} relationships for Beams T1 to T5. From the figure, it can be seen that the predicted $M_{(limit)}$ decreases non-linearly as the span-depth ratio increases. Since it was shown earlier that the stress increase at the material limit condition remained fairly constant when the span-depth ratio was varied, the reduction of $M_{(limit)}$ must therefore be caused mainly by the eccentricity variations of the tendons. Figure 6.20 shows that when more non-prestressed reinforcement was incorporated into the beam (i.e. A_s% increased to 3%), higher values of $M_{(limit)}$ were obtained and the rate of change of the $M_{(limit)}$ - L/d_{ps} relationship decreases as L/d_{ps} increases.

Figure 6.21 shows the maximum moment M_{max} - span-depth ratio L/d_{ps} relationships for Beams T1 to T5. The profiles of the five curves shown in Figure 6.21 were observed to be nearly similar to the $M_{(limit)}$ - L/d_{ps} curves shown in Figure 6.19, that is, the moment decreases non-linearly as the span-depth ratio increases. However, the M_{max} - L/d_{ps} curves for Beams T1 and T2 seemed to indicate a reduction in the rate of decrease for values of L/d_{ps} above 20. This is because when L/d_{ps} was lower than 20 for Beams T1 and T2, their maximum moments were found to be equal to their estimated material limit moments. However, when their span-depth ratios were greater than 20, the maximum moment of the beams was attained before the concrete strain reached the ultimate value at the critical section, hence the maximum moment was higher than the material limit moment (see Figure 6.22).

6.3.3 Initial Prestress Force and Amount of Prestressed Reinforcement.

The term initial prestress force used here refers to the initial residual prestress force applied to the structures after taking all losses into consideration. About thirty-four simulations were conducted on Beams T1 to T5 with the proposed non-linear models to study the effects of the initial prestress force and amount of prestressed reinforcement on the flexural performance of externally prestressed structures at ultimate. This section describes the results obtained from this study.

Figure 6.23 shows the relationships between the maximum moment M_{max} and the initial prestress force for Beams T1 to T5. Note that the areas of prestressing steel were kept constant whilst the initial stressing levels were varied for these beams. It was observed that the maximum moment of these beams increases linearly with the amount of initial prestress force applied to them. The gradients for the M_{max} - initial prestress force curves, evaluated using the Least Squares Method, ranged from 0.716 kNm/kN to 1.299 kNm/kN as shown in Figure 6.23. The relationships between the material limit moment $M_{(limit)}$ and initial prestress force for Beams T1 to T5 were also found to be increasing linearly in Figure 6.24. The figure also shows that the gradients obtained for each of the $M_{(limit)}$ - initial prestress force curves corresponded very closely with those derived for the M_{max} - initial prestress force curves, with a maximum difference of about sixteen percent. The reason for this close relationship is because as the initial prestress forces in these beams are increased, the increase in the maximum and material limit moments are found to be almost equal. An example of this is illustrated in Figure 6.25, which shows the moment-deflection relationships for Beam T1 with an initial prestress force of 33,255 kN, 57,406 kN and 66,730 kN. When the initial prestress force was increased from 33,255 kN to 57,408 kN, the increase in the maximum moment was about fifty-four percent and the increase in the material limit moment was about fifty percent and, when it was increased from 57,406 kN to 66,730 kN, both maximum and material limit moments were increased by approximately eighteen percent.

Figures 6.26 and 6.27 show that both the change in prestress $\Delta f_{ps(limit)}$ and the eccentricity variation $\Delta_{eccen(limit)}$ at the material limit condition reduce as the initial prestress forces for the beams are increased. This reduction in $\Delta f_{ps(limit)}$ and $\Delta_{eccen(limit)}$ with the increase in initial prestress force is due to the beams attaining the ultimate concrete strain (0.0035) at the extreme concrete compressive fiber of the critical section at lower loading levels. This resulted in lower deflections and smaller changes in prestress and eccentricity for these beams at the material limit condition when a higher initial prestress force was involved. It was also noted that the reduction of both $\Delta f_{ps(limit)}$ and $\Delta_{eccen(limit)}$ with the increase in initial prestress force was very varied for these beams.

Figure 6.28 shows the relationship between the maximum moment and the initial prestress force for Beam T1 with two different span-depth ratios, i.e. 26.615 and 14.786. The two curves shown in Figure 6.28 indicate that the maximum moment M_{max} increases linearly with the initial prestress force, higher maximum moments being obtained for the curve with the smaller span-depth ratio (i.e. 14.786). This is observed to be consistent with the findings derived from Figure 6.21, where the maximum moment of the beam was found to decrease as the span-depth ratio is increased. It can also be seen that the two curves plotted in Figure 6.28 were almost parallel, where the gradient for the span depth ratio 26.615 and 14.786 curves were 1.163 kNm/kN and 1.299 kNm/kN respectively. This shows that the rate of increase of the maximum moment with the initial prestress force is quite similar for a beam with only its span-depth ratio varied. Figure 6.29 shows the $M_{(limit)}$ - initial prestress force relationship for Beam T1 for the same two span-depth ratios together with their respective gradients.

For Beam T4, Figure 6.6 shows that the M_{max} is coincidental with M_{limit}, hence, Figure 6.30 shows the M_{max}/M_{limit} - initial prestress force relationships for Beam T4 with span-depth ratios of 15.385 and 8.00. Similar to the trends observed in Figure 6.28 for Beam T1, the M_{max}/M_{limit} increases linearly with the initial prestress force and the gradients of the two curves were nearly parallel to each other (i.e. 1.063 kNm/kN and 1.135 kNm/kN). Figure 6.31 and 6.32 show the variation of the change in prestress at the material limit condition with the initial prestress force for Beams T1 and T4 respectively with different span-depth ratios. The change in tendon prestress at the material limit condition was observed to decrease as the initial prestress force increased. Also, both the $\Delta f_{ps(limit)}$ - initial prestress force curves with different span-depth ratios were nearly coincidental. This is in agreement with the observation made in Section 6.3.2 about the change in prestress at the material limit condition not varying much with the span-depth ratio of the beam.

Figures 6.33 and 6.34 show the relationships between the eccentricity variation $\Delta_{eccen(limit)}$ of the tendons with the initial prestress force applied to the structure for Beams T1 and T4 respectively with different span-depth ratios. It was noted that $\Delta_{eccen(limit)}$ decreases as the initial prestress force increases, but at a greater rate for beams with a larger span-depth ratio.

When the reinforcement ratio of Beam T5 was increased from 0.3% to 3%, the variations of the $M_{max}/M_{(limit)}$ with the initial prestress force for the two different reinforcement ratios are compared in Figure 6.35. The ultimate moment capacity was observed to increase with the initial prestress force for both curves, but the A_s% = 3% curve had a lower gradient than the A_s% = 0.3% curve. Hence increasing the initial prestress force in externally prestressed structures with relatively low reinforcement ratios (e.g. 0.3%) would yield greater improvement in the strength capacity than when an equivalent increase was applied on the same structure but containing more reinforcement (e.g. 3%).

Figure 6.36 shows the relationship between the change in prestress at the material limit condition for Beam T5 with reinforcement ratios of 3% and 0.3%. Both curves indicate that the change in prestress at the limit moment condition decreases as the initial prestress force increases. However for the A_s% = 3% curve, the rate of decrease in the change in prestress $\Delta f_{ps(limit)}$ - initial prestress force curve was larger than that observed for the A_s% = 0.3% curve.

Figure 6.37 compares the relationships between the change in eccentricity at the material limit condition and the initial prestress force for Beam T5 with reinforcement ratios of 0.3% and 3%. Both curves were observed to show a decrease in $\Delta_{eccen(limit)}$ as the initial prestress force was increased in the beam.

Figure 6.38 shows the moment-deflection relationships derived for Beam T1 with two prestressing steel areas, i.e. A_{ps} = 53,200 mm^2 and A_{ps} = 79,800 mm^2. Both curves exhibited similar relationships before the occurrence of cracking; the A_{ps} = 53,200 mm^2 curve indicated a cracking moment which was five percent higher than the A_{ps} = 79,800 mm^2 curve This small difference in the cracking moments was due to the slightly different residual initial prestress force applied to the structure due to losses. After cracking the A_{ps} = 53,200 mm^2 curve indicated a smaller stiffness and exhibited a maximum moment of about 59,619 kNm when the mid-span deflection was about 100 mm, after which, the curve showed a loss in strength as the beam deflected further as it approached the material limit condition. The A_{ps} = 79,800 mm^2 curve on the other hand showed a small increase in strength with large deflections after the occurrence of cracking. It achieved a maximum strength of about 59,844 kNm, which

was only about 0.3 % higher than the maximum moment exhibited by the other curve, when the beam mid-span deflection was about 244 mm.

The moment-deflection curves for Beam T2 with two different prestressing steel areas, i.e. A_{ps} = 26,600 mm^2 and 53,200 mm^2 are shown in Figure 6.39. Both curves exhibited a similar trend before the occurrence of cracking. The cracking moment of the A_{ps} = 26,600 mm^2 curve was about 19,032 kNm, which was about four percent higher than the cracking moment of the A_{ps} = 53,200 mm^2 curve. After cracking, the A_{ps} = 26,600 mm^2 curve indicated a large drop in strength and the maximum moment achieved after this was only about 18,424 kNm, hence, the maximum moment capacity of this curve was its cracking moment. The A_{ps} = 53,200 mm^2 curve exhibited a similar large drop in strength after cracking but showed an increase in strength as the beam deformed to produce a maximum moment of about 19,809 kNm, which was about four percent higher than the A_{ps} = 26,600 mm^2 curve.

Figure 6.40 shows the moment-deflection curve for Beam T3 with two amounts of prestressing steel reinforcement, 26,600 mm^2 and 53,200 mm^2. Both curves were found to be nearly identical before the occurrence of cracking but with the cracking moment of the A_{ps} = 26,600 mm^2 curve about six percent higher than the other curve. After cracking, the curve for the lower area of prestressing steel exhibited a loss in strength before yielding a maximum moment of about 22,604 kNm at a beam mid-span deflection of about 200 mm. The A_{ps} = 53,200 mm^2 curve showed a similar decrease in strength after cracking but the maximum moment for this curve was about 26,545 kNm, which was about fifteen percent higher than the A_{ps} = 26,600 mm^2 curve.

The moment-deflection responses for Beam T4 with different areas of prestressing steel (A_{ps} = 26,600 mm^2 and A_{ps} = 53,200 mm^2) are shown in Figure 6.41. The cracking moment for the A_{ps} = 26,600 mm^2 curve was now only two percent higher than that for the A_{ps} = 53,200 mm^2 curve. After cracking, the A_{ps} =26,600 mm^2 curve exhibited a maximum strength (49,210 kNm) which was about seventeen percent lower than the A_{ps} = 53,200 mm^2 curve (59,572 kNm).

Figure 6.42 shows the moment-deflection curves for Beam T5 with the same prestressing steel areas of 26,600 mm^2 and 53,200 mm^2. The two curves were observed to be virtually equal before the occurrence of cracking with their cracking

moments differing by only about two percent. After cracking, both curves showed a sudden loss in strength before indicating large deflections as the moments increased to maximum values. The maximum moment attained for the A_{ps} = 26,600 mm^2 curve was about 35,865 kNm which was about sixteen percent lower than the A_{ps} = 53,200 mm^2 curve (42,580 kNm).

6.4 Parametric Study: Deflected Tendons

In this section, the effects of incorporating deviators in externally prestressed structures are investigated and the results obtained from the study are discussed.

6.4.1 Deflected vs Straight Profile

The flexural behaviour of Beam T6 (described in Section 6.2) was simulated to the ultimate condition using three non-linear models that were developed here for externally prestressed structures with deviators located along their spans:

1) **EXT5** : the tendons are assumed to be fixed at the deviators.
2) **EXT7** : the frictional behaviour at the deviators is considered in the analytical model (friction coefficient taken to be 0.3)
3) **EXT9** : the tendons are assumed to slip freely at the deviators.

Figure 6.43 shows the moment-deflection responses for Beam T6 predicted with the above mentioned non-linear models. From the figure, the three analytical curves were observed to be nearly equal before the occurrence of cracking. The EXT9 curve indicated cracking at a marginally lower load than the other two curves and formed the lower bound to the flexural response of the beam. The EXT5 curve on the other hand formed the upper bound and yielded a maximum moment which was about four percent higher than the maximum moment indicated by the EXT9 curve. The EXT7 curve was observed to follow the same line as the EXT5 curve until the occurrence of tendon slippage at the deviators (when beam deflection reached about 125 mm), after which it deviated away from the EXT5 curve and moved towards the EXT9 curve. The maximum moment predicted by the EXT7 model was found to be only approximately one percent higher than the EXT9 value (see Table 6.2), but the final

deflection of EXT9 curve was about five and twelve percent greater than the EXT7 curve and EXT5 curve respectively.

Figure 6.44 compares the moment-deflection relationships derived for Beam T6 (predicted with the EXT7 model) and Beam T6(A). Beam T6(A) is identical to Beam T6 in all respects except that there are no deviators, the external tendons being anchored at both ends of the beam with a constant eccentricity of 595 mm. Before cracking, the Beam T6 curve exhibited a stiffness which was about ten percent higher than the Beam T6(A) and this percentage difference was maintained after cracking and the yielding of non-prestressed reinforcement. The maximum moment predicted for Beam T6 was approximately 102,510 kNm (see Table 6.2), which was about nine percent higher than for Beam T6(A) (92,810 kNm). However, it was noted that the compressive stress at the extreme bottom fiber of the section near the supports evaluated for Beam T6(A) before external loadings were placed on the structure (f_{ci} = 27.38 N/mm^2) exceeded the allowable stress given in BS5400 (Part 2) (1990) (20 N/mm^2). This indicated that Beam T6(A) failed to satisfy the service limit state checks given in BS5400 (Part2) (1990) and, in practice, would need to be redesigned.

6.4.2 Frictional Behaviour at Deviators

6.4.2.1 Deviation Angles at Deviators

Two externally prestressed beams, denoted Beam T6(B) and Beam T6(C), were simulated to failure with the three non-linear models listed in Section 6.4.1. Beams T6(B) and T6(C) were similar to Beam T6, except for the deviation angles of the tendons at the deviators which were 5.84° and 0° respectively (see Figures 6.45 and 6.46 for the arrangements of the tendons).

Figure 6.45 shows the moment-deflection responses for Beam T6(B) derived from the proposed analytical models. From the figure, it can be seen that the two bounding curves, EXT5 and EXT9, were very closely related to the curves shown for Beam T6 in Figure 6.43. However, the EXT7 curve indicated that slippage of tendons for Beam T6(B) first occurred when the beam deflection was about 140 mm instead of 125 mm (see Section 6.4.1). This was because increasing the angle of deviation from 4.25° to 5.84° had caused higher frictional resistance to be generated at the deviators. This

higher frictional resistance consequently prevented the tendons from slipping until the deflection of the beam reached a higher value. The difference between the maximum moments obtained for the EXT5 and EXT9 curves of Beam T6(B) was also found to be only four percent (similar to that observed for Beam T6). The maximum moment predicted by the EXT7 model for Beam T6(B) was observed to be 102,710 kNm which was less than one percent higher than that estimated for Beam T6 (i.e. 102,510 kNm) (see Table 6.2).

The moment-deflection relationships for Beam T6(C) are shown in Figure 6.46 and again show that the EXT5 and EXT9 curves are very closely related to the curves shown in Figure 6.43 for Beam T6. The difference between the maximum moments estimated by the EXT5 and EXT9 curves were also found to be about four percent. The EXT7 curve however was found to almost exactly follow the EXT9 curve (less than 0.5% difference) for the entire loading history. This was because the small deviation angle formed at the deviators due to the deflected profile of the beam did not generate enough frictional resistance to prevent frictional slippage. Hence slippage of the tendons at the deviators occurred throughout the whole loading history of the beam, thereby causing the EXT7 curve to be very closely related to the EXT9 curve (where tendons were assumed to slip freely at the deviators). The maximum moment predicted by the EXT7 model for Beam T6(C) was about 101,010 kNm (see Table 6.2), which was about one percent lower that predicted for Beam T6. This shows that a reduction in the angle of deviation at the deviators will cause the flexural strength of these beams to reduce, although the reduction was observed to be very small for this beam.

6.4.2.2 Initial Prestress Force

Figures 6.47 and 6.48 show the moment-deflection relationships for Beams T6(D) and T6(E) which were similar to Beam T6 except for their initial prestress force which was changed from 81,450 kN to 95,650 kN and 47,270 kN respectively. In Figure 6.47, where the higher initial prestress force was applied, the EXT5 and EXT7 curves are seen to be the same throughout the whole loading history. This was because the high initial prestress force had caused large frictional forces to develop at the deviators, thus preventing the tendons from slipping at these points. Since the tendons

do not slip at the deviators, the moment-deflection response will thus be identical to that predicted by the EXT5 model (where tendons are assumed to be fixed at the deviators). The trend of the EXT9 curve was also found to be very closely related to the other two curves (maximum difference in moments not exceeding one percent) and the maximum moment predicted by the EXT9 model was approximately one percent smaller than that estimated by the EXT5 and EXT7 models. This shows that although the high frictional forces generated at the deviators will prevent tendon slippages from occurring when high initial prestress forces are used, the flexural behaviour of the beam predicted using the three analytical models (i.e. EXT5, EXT7 and EXT9) did not yield very different results (less than one percent). The maximum moment predicted for Beam T6(D) with the EXT7 model was found to be thirteen percent higher than that predicted for Beam T6. This was consistent with the observations made in Section 6.3.3 where it was found that a higher initial prestress force applied to the structure will generally yield a higher ultimate strength.

Figure 6.48 shows the deflection responses of Beam T6(E) where the initial prestress force for the beam was reduced to 47,270 kN. The three analytical curves in Figure 6.48 were again observed to be very similar to each other before the onset of cracking. However after cracking, the three curves deviated from each other with the EXT5 curve indicating the highest post-cracking stiffness (upper bound) and the EXT9 curve forming the lower bound. The maximum moments predicted for this beam were 74,810 kNm and 61,730 kNm by the EXT5 and EXT9 models respectively, representing a range of about seventeen percent. The EXT7 curve was observed to run almost parallel to the EXT9 curve after the yielding of the non-prestressed reinforcement and the maximum moment predicted by this model (62,790 kNm) was about two percent higher than that predicted by the EXT9 model (61,730 kNm). This indicated that when the initial prestress force applied to the structure is relatively low, the difference between the flexural behaviour at ultimate using the two extreme assumptions at the deviators will be very large. However, the flexural strength predicted when frictional effects (where $\mu = 0.3$) were considered was found to be only two percent higher than the maximum moment capacity predicted using the assumption that the tendons slip freely at the deviators (see Table 6.2). Although it may appear that some benefit may be obtained in fixing the tendons at the deviators,

the benefit only applies to structures with small initial prestress force which is not economical for practical purposes. It was also observed that the maximum moment estimated for Beam T6(E) with the EXT7 model was about forty percent lower than that predicted for Beam T6.

6.4.2.3 Coefficient of Friction at Deviators

The coefficient of friction at the deviators used for all the analyses conducted so far in parametric study part two was taken to be 0.3, as recommended in BS8110 (1990) for the contact between lightly rusted strand and lightly rusted steel. This value was noted to give close agreement with the experimental beams used for the verification process in Chapter Five. However, the coefficient of friction is dependent on several factors (e.g. the type of materials used for the deviators) and, hence, vary greatly for different beams. This section investigates the variation of the flexural performance of externally prestressed structures when different coefficients of friction are specified at the deviators.

Beam T6(E) was used for this study because the difference in the flexural behaviour estimated using the EXT5 and EXT9 models was sufficiently large to allow a comparison to be made between the deflection responses derived when different coefficients of friction were specified at the deviators. Figure 6.49 shows the moment-deflection responses predicted for Beam T6(E) where the coefficient of friction was taken to be 0.3, 0.5 and 1.0. It can be seen that the curves derived for these three different coefficients of friction were approximately parallel to the EXT9 curve after the tendons first slipped at the deviators. The curve for the coefficient of friction equal to 1.0 indicated the greatest difference with the EXT9 curve and the maximum moment predicted with this analysis was about seven percent higher than that predicted by the EXT9 model and fourteen percent lower than that estimated with the EXT5 model.

Beam T6(F) was also used to study the effects of varying the coefficient of friction on the flexural behaviour of externally prestressed structures. This was because the difference in the ultimate strengths of this beam predicted with the EXT5 and EXT9 models was also found to be large enough for such a study to be conducted (i.e. about

eight percent). The tendon arrangement for this beam is shown in Figure 6.51. Figure 6.50 shows the deflection responses predicted for Beam T6(F) using coefficients of friction equal to 0.3, 0.5 and 1.0. The curves representing coefficients of friction 0.3 and 0.5 were observed to be closer to the EXT9 curve than they were to the EXT5 curve and their moments predicted after the yielding of non-prestressed reinforcement were noted to be only about one and three percent higher than the EXT9 curve respectively. The EXT7 curve for $\mu = 1.0$ lies between the EXT5 and EXT9 curves, with a maximum moment about five percent higher than the EXT9 value and four percent lower than the EXT5 value. The performance of both beams discussed in this section, i.e. Beams T6(E) and T6(F), would seem to indicate that allowing the tendons to slip freely at the deviators (i.e. EXT9 model) gives a conservative estimate of the flexural response of these beams (under-estimating the ultimate moment obtained using values for the coefficient of friction up to 1.0 by not more than seven percent).

6.4.3 Free length to depth ratio

For Beam T6 shown in Figure 6.43, the distance between the two deviators near the mid-span was about 23,600 mm. This distance was changed to 10,000 mm and 33,600 mm in Beam T6(F) (see Figure 6.51) and Beam T6(G) (see Figure 6.52) respectively, to study the effects of varying the free length of the tendons near mid-span on the flexural behaviour of these structures. Figure 6.51 shows the moment-deflection responses derived for Beam T6(F) which had a smaller free-length to depth ratio α_{free} of 5.87. The EXT5 curve and EXT9 curve exhibited a maximum moment of about 115,710 kNm and 106,910 kNm respectively, thus giving a difference of about eight percent between the maximum moments predicted by the two extreme analytical models. The EXT7 curve was observed to deviate from the EXT5 curve immediately after the occurrence of cracking, and predicted moments which were approximately one percent higher than that estimated by the EXT9 curve for the same deflection. The maximum moment predicted by the EXT7 model for this beam was about 108,400 kNm, which was about five percent higher than that predicted for Beam T6 (102,510 kNm) (see Table 6.2). The eccentricity variation Δ_{eccen} at the ultimate condition for Beam T6 and Beam T6(F) were calculated to be 89.68 mm and 21.88 mm respectively (see Table 6.2). This indicates that even though the two beams

were similar and had the same span-depth ratio (i.e. 23.5), Beam T6(F), which had a lower free length to depth ratio, exhibited a higher strength than Beam T6. This was because a reduction in the free length to depth ratio reduced the eccentricity variation in the tendons at the critical section, thereby increasing the flexural strength of the beam.

Figure 6.52 shows the deflection responses for Beam T6(G) and, from the figure, it can be seen that the EXT7 curve did not deviate from the EXT5 curve until the beam deflection was about 180 mm and then only marginally. This was due to the higher angle of deviation (about 7.2°) at the deviators caused by the greater separation between the deviators at mid-span (see Figure 6.52). The higher angle of deviation consequently caused higher frictional forces to be generated at the deviators which prevented the tendons from slipping. However, because of the higher eccentricity variations of tendons occurring near mid-span for this beam (142.10 mm) the maximum flexural capacity predicted using EXT7 model (98,110 kNm) was found to be nine percent and five percent lower than for Beam T6(F) and Beam T6 respectively. The difference between the maximum moments predicted by the EXT5 and EXT9 models for this beam was found to be only approximately two percent.

6.5 Concluding Remarks

Six externally prestressed beams were selected for the parametric study. Five of these beams were prestressed with straight external tendons while the last beam was prestressed with tendons with a deflected profile. The span-depth ratios, non-prestressed reinforcement ratios, amount of prestressed reinforcement, initial prestress force and frictional properties of the deviators (if applicable) of these beams were then varied and non-linear analyses conducted on them with the proposed models to determine their flexural response up to ultimate.

Two moment conditions were defined in this chapter to describe the ultimate moment capacity of these externally prestressed beams, they are the *maximum moment* condition and the *material limit moment* condition. In this study, the material limit moments for externally prestressed structures were shown sometimes to be lower than the maximum moments (sometimes by as much as twenty percent). The lower

material limit moment derived was caused by the large reduction in eccentricity of the external tendons at the material limit condition due to second-order effects.

In practice, the maximum moment should be taken as the ultimate moment capacity of the externally post-tensioned structure. However, this moment is not always easily predicted without the use of either a detailed finite element analysis or non-linear analytical models. An alternative method for estimating the ultimate moment capacity of these beams would be to adopt the simple sectional analysis recommended by several codes of practice (e.g. AASHTO, BS5400, etc.), where the top concrete fiber strain at the critical section is assumed to be equal to an ultimate strain value and the change in prestress is taken as some recommended value at the ultimate condition. This method, however, only yields the material limit moment which would often under-estimate the ultimate moment capacity.

However, it has been argued that the material limit moment can still be used to represent the ultimate moment capacity, since it is a conservative estimation of the maximum moment. Hence, the variations of the change in prestress $\Delta f_{ps(limit)}$ and eccentricity variation $\Delta_{eccen(limit)}$ at the material limit condition with the span-depth ratio, non-prestressed reinforcement, amount of prestressed reinforcement and initial prestress force were investigated to determine whether these variables can be represented by a single value or estimated by a simple expression so as to aid the computation of the material limit moment using the sectional analysis method.

For relatively low reinforcement ratios (e.g. approximately 0.15% - 0.5%), the moment-deflection responses were found to be characterised by a sudden large drop in strength immediately after cracking, followed by a slow increase in strength as the beam deflections increased rapidly up to the maximum moment condition. The sudden loss in strength after cracking was due to the development of a single crack at the critical section and the formation of a tied arch mechanism in the structure. In some beams, failure occurs immediately after the occurrence of first cracking because the tied arch mechanism developed can not support the external loads placed on the structure. Increasing the amount of non-prestressed reinforcement in these structures will not only help to prevent such instability failures from occurring but also improve their general flexural behaviour.

The maximum moment capacity M_{max} of externally post-tensioned structures was observed to increase linearly with increase in the non-prestressed reinforcement ratio. However, the rate at which the maximum moment increases with the amount of non-prestressed reinforcement was noted to vary for different beams. This indicated that increasing the amount of reinforcement in externally prestressed structures will not always produce a commensurate improvement in the flexural strength.

The change in prestress $\Delta f_{ps(limit)}$ and eccentricity variation $\Delta_{eccen(limit)}$ at the material limit condition were observed to increase as the reinforcement ratio increased up to 1.2%, however these variables remained fairly constant when A_s% ranged from 1.2% to 4%. The material limit moment $M_{(limit)}$ was also found to increase as the reinforcement ratio increased, but at a relatively low rate when A_s% was less than 1.2%. The changes in prestress ranged from 90 N/mm^2 to 600 N/mm^2 while the eccentricity variations ranged from 120 mm to 600 mm for the Beams T1 to T5 using different reinforcement ratios (ranging from 0.15% to 4%). This illustrates how these parameters varied with the amount of reinforcement specified in the beams.

The maximum moment M_{max} and material limit moment $M_{(limit)}$ decrease non-linearly with increasing span-depth ratio. For beams with higher levels of reinforcement, the reduction in strength with the increase in the span-depth ratio was noted to be greater. It was found that the change in prestress $\Delta f_{ps(limit)}$ at the material limit condition does not change significantly with an increase in the span-depth ratio for externally prestressed beams with low reinforcement ratios (about 0.314%). However, increasing the amount of reinforcement (to about 3%) causes $\Delta f_{ps(limit)}$ to decrease with an increase in the span-depth ratio L/d_{ps}. The eccentricity variation $\Delta_{eccen(limit)}$ at the material limit condition was found to increase non-linearly with the span-depth ratio L/d_{ps} and the trend of the relationship between these two variables was found to be dependent on the amount of non-prestressed reinforcement. The increase in the eccentricity variation for beams with large span-depth ratios causes the ultimate strength of these beams to decrease, a phenomenon described by Virlogeux (1988) as second-order effects. Hence, if long externally prestressed structures are required (which is common in bridge applications), incorporating deviators along the span will help reduce the loss of strength due to second-order effects.

The maximum and material limit moments for these structures were found to increase linearly as the initial prestress forces applied to the structures are increased. The rate of increase of flexural strength for increasing levels of initial prestress force was observed to be lower for beams with higher reinforcement ratios. However, it was observed earlier that increasing the level of reinforcement also increases their flexural strength, although at different rates. Hence, it is often difficult to decide upon the best combination of these parameters to be used. A trial and error analysis is thus recommended here, where various practical and economic considerations are carefully reviewed, before deciding on the best combination of reinforcement ratio and initial prestress force to be used.

Both the change in prestress and the eccentricity variation at the material limit condition were observed to decrease with an increase in the initial prestress force. However, the rates of decrease of these variables with the initial prestress force were found to be very varied for different beam configurations. For externally prestressed beams with different span-depth ratios, similar trends were obtained between the change in prestress $\Delta f_{ps(limit)}$ at the material limit condition with the initial prestress force applied to the structure. As for the eccentricity variation $\Delta_{eccen(limit)}$, the rate of decrease in $\Delta_{eccen(limit)}$ with the initial prestress force was found to be greater in beams with larger span-depth ratios. For beams with higher reinforcement ratios, the rate of decrease in the $\Delta f_{ps(limit)}$ with the initial prestress force was also noted to be higher.

Increasing the prestressing steel area while maintaining the same amount of initial prestress force will generally increase the maximum moment capacity. However, this method of increasing flexural performance was found to be uneconomical here, since the study showed that increasing the prestressing steel area by approximately fifty percent only yielded a relatively modest increase in the ultimate strength (not more than seventeen percent).

Hence from the first part of the parametric study, it was shown that the variables $\Delta f_{ps(limit)}$ and $\Delta_{eccen(limit)}$ vary greatly with parameters such as the span-depth ratio, non-prestressed reinforcement ratio, prestressed reinforcement ratio and initial prestress force. Moreover, it was observed that the influence of the above parameters on these two variables are also inter-dependent on each other. Thus, it will be very difficult (if

not impossible) to derive a single value or simple expression to represent these variables accurately for every beam considered.

Using a deflected tendon profile not only increases the ultimate flexural strength of these structures, but also enables the eccentricity of the prestress force at the ends of the member to be reduced, so as to produce acceptable final stress levels throughout the length of the beam at the service conditions. When deviators are placed in an externally prestressed structure, the frictional forces generated at the deviators may prevent the external tendons from slipping at these points. This consequently prevents the stresses in the tendons from re-distributing across the deviators and, hence, increases the flexural strength of these structures. The frictional force generated at the deviators is dependent on three factors, i.e. the angle of deviation of the tendons at the deviators, the coefficient of friction at the deviators and the initial prestress force applied to the structure. It was found from this study that increasing any of these factors will generally increase the frictional resistance generated at the deviators and consequently the maximum moment capacity. However, for all the beams considered with deflected tendons, except for Beams T6(E) and T6(F), the differences between the maximum moments analysed with the upper and lower bound models, i.e. EXT5 and EXT9, were all found to be less than about four percent. For Beams T6(E) and T6(F), although the differences of the maximum moment predicted by the EXT5 and EXT9 models were considerably greater than four percent, the maximum moments estimated with the EXT7 model using a high coefficient of friction (i.e. $\mu = 1$) was found to yield a maximum difference of only seven percent with the moments predicted by EXT9 model. Hence, assuming that the tendons slip freely at the deviators (e.g. the EXT9 model) when analysing the behaviour of these structures, should conservatively predict their ultimate response to an acceptable level of accuracy for design purposes. This assumption also simplifies the analysis of these structures, since frictional slippage and redistribution of stresses in the tendons across deviators are neglected.

Finally, the provision of deviators in externally prestressed structures helps to reduce the free length of the tendons and hence the free length to depth ratio. It was found that reducing the free length to depth ratio increases the flexural performance of these beams, even though the span-depth ratio is maintained constant. This is because a

reduction in the free length to depth ratio reduces the eccentricity variations near the critical sections, thereby increasing flexural strength.

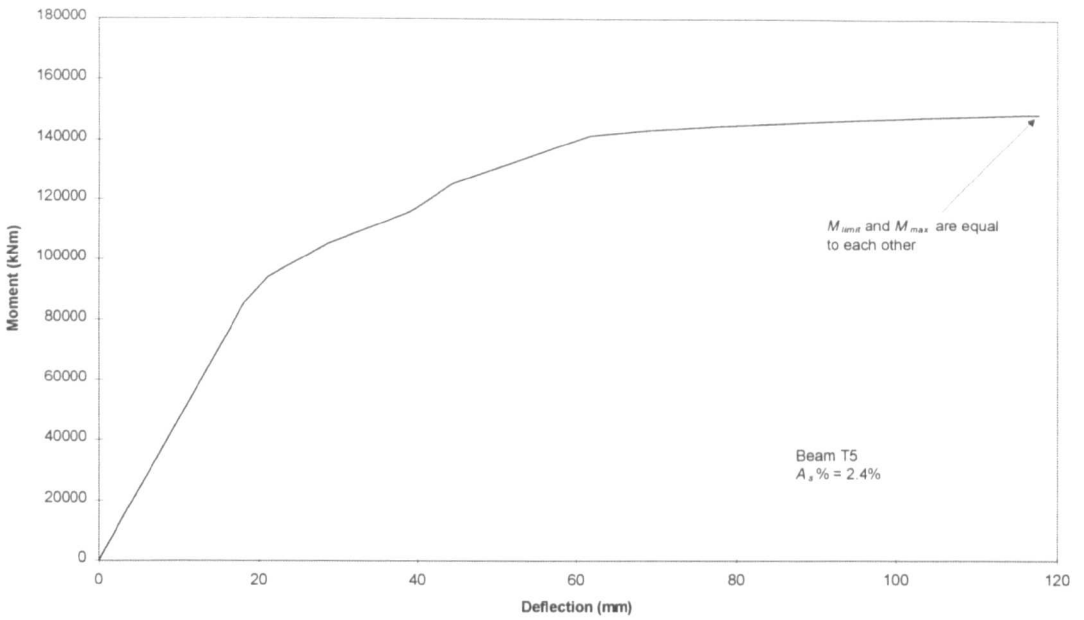

Figure 6.1: Moment-deflection response showing that M_{limit} and M_{max} can be equal to each other

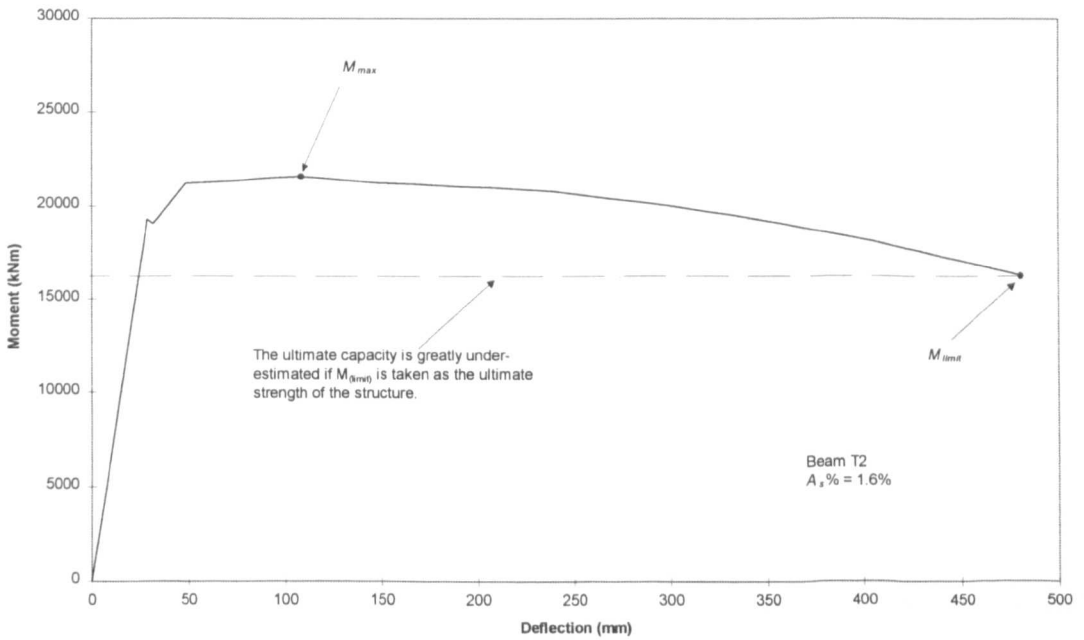

Figure 6.2: Moment-deflection response showing that M_{limit} and M_{max} can also be different from each other

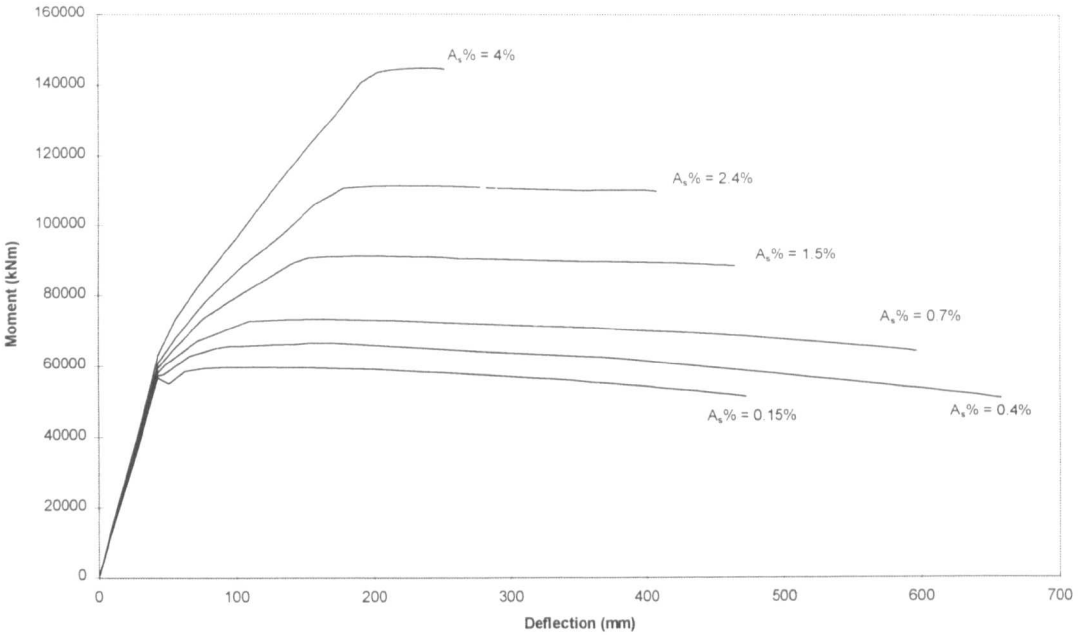

Figure 6.3: Moment-deflection responses for Beam T1 with different A_s%

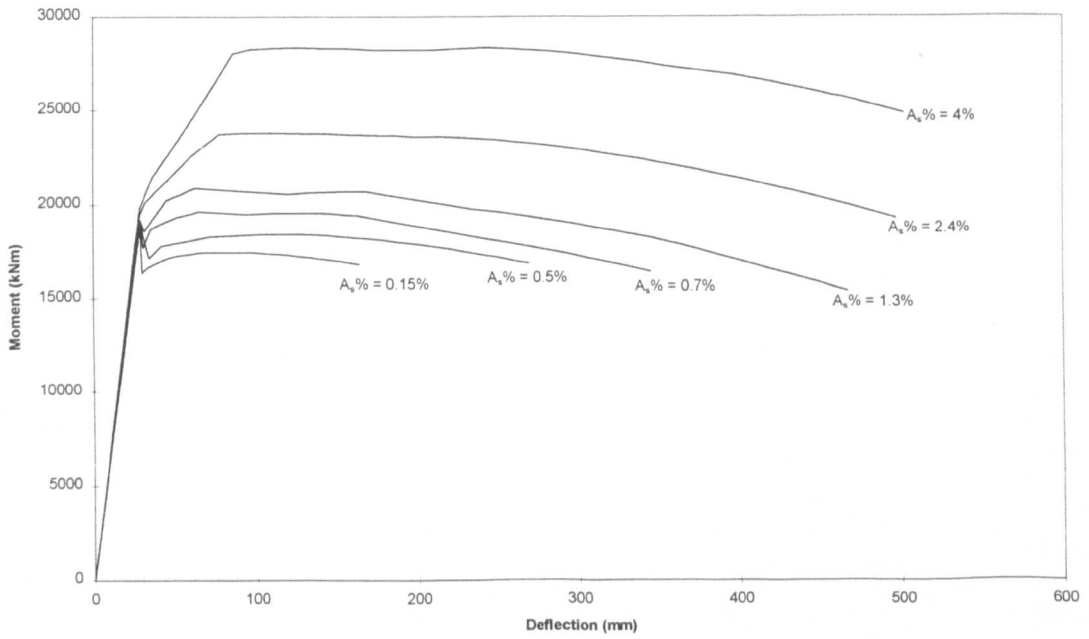

Figure 6.4: Moment-deflection responses for Beam T2 with different A_s%

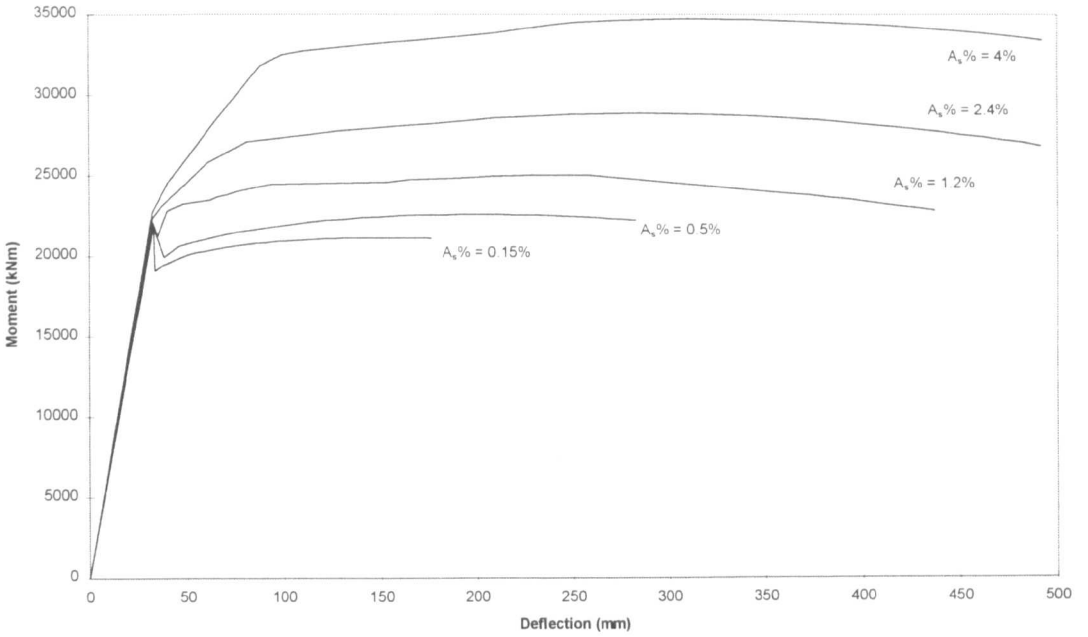

Figure 6.5: Moment-deflection responses for Beam T3 with different A_s%

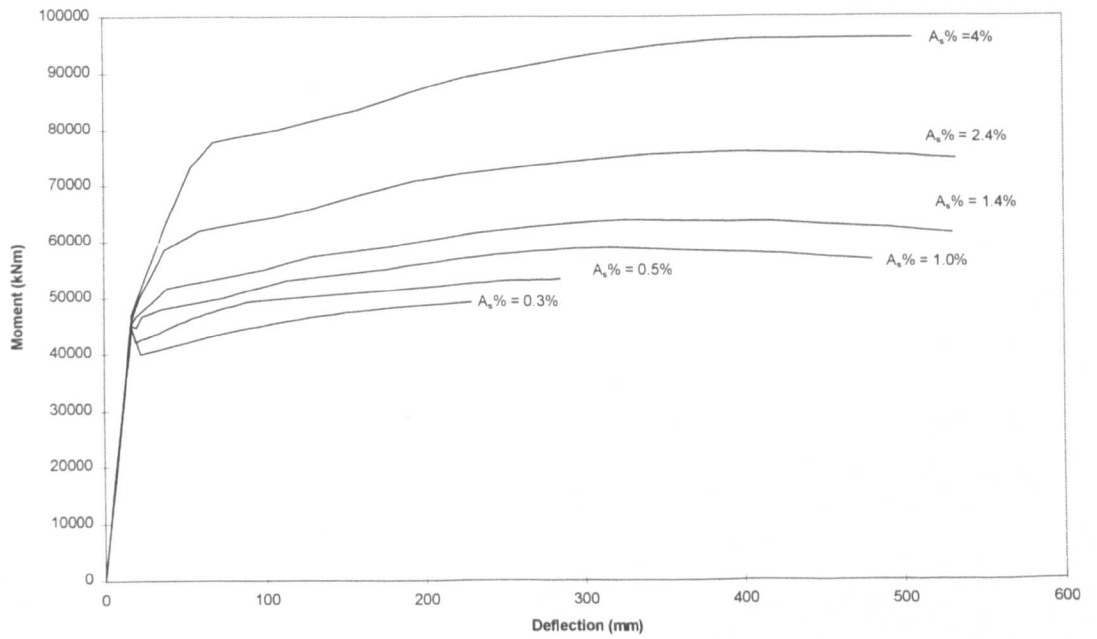

Figure 6.6: Moment-deflection responses for Beam T4 with different A_s%

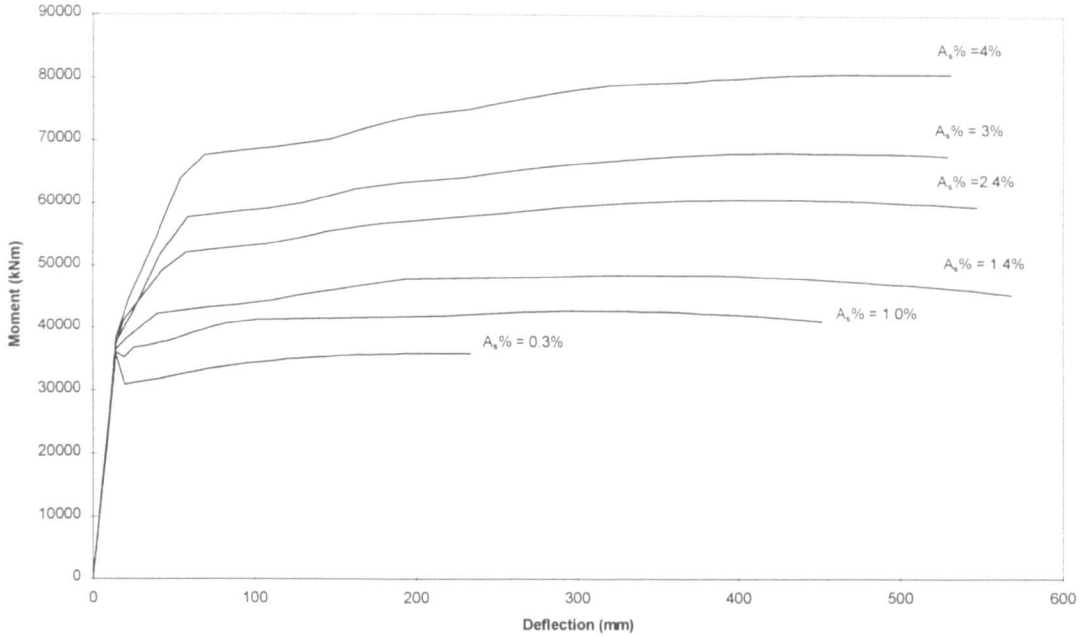

Figure 6.7: Moment-deflection responses for Beam T5 with different $A_s\%$

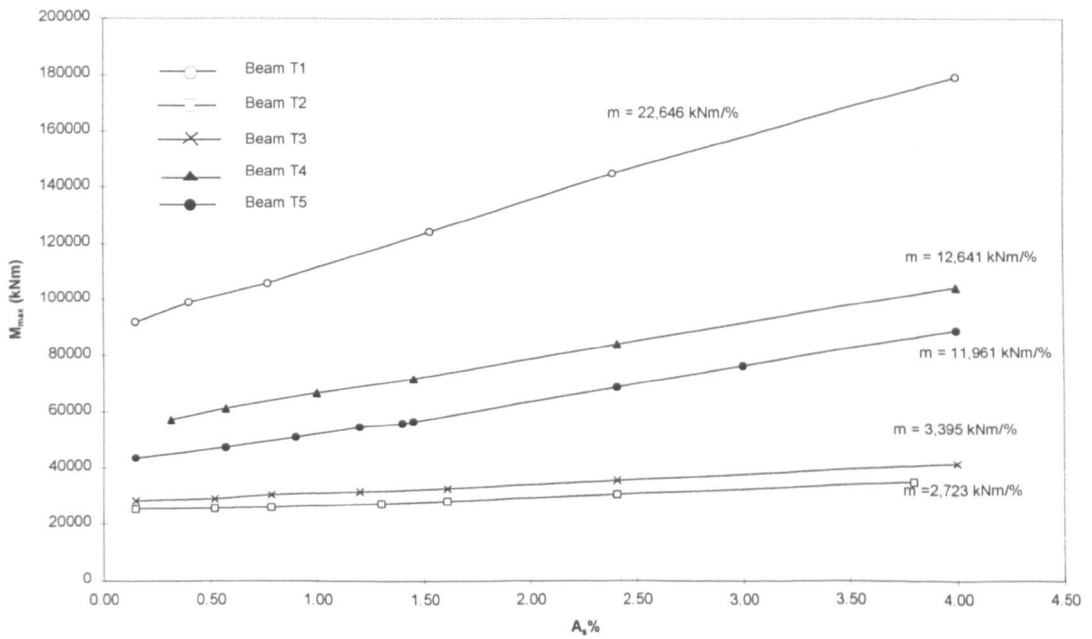

Figure 6.8: Variation of M_{max} with $A_s\%$ for Beams T1 to T5

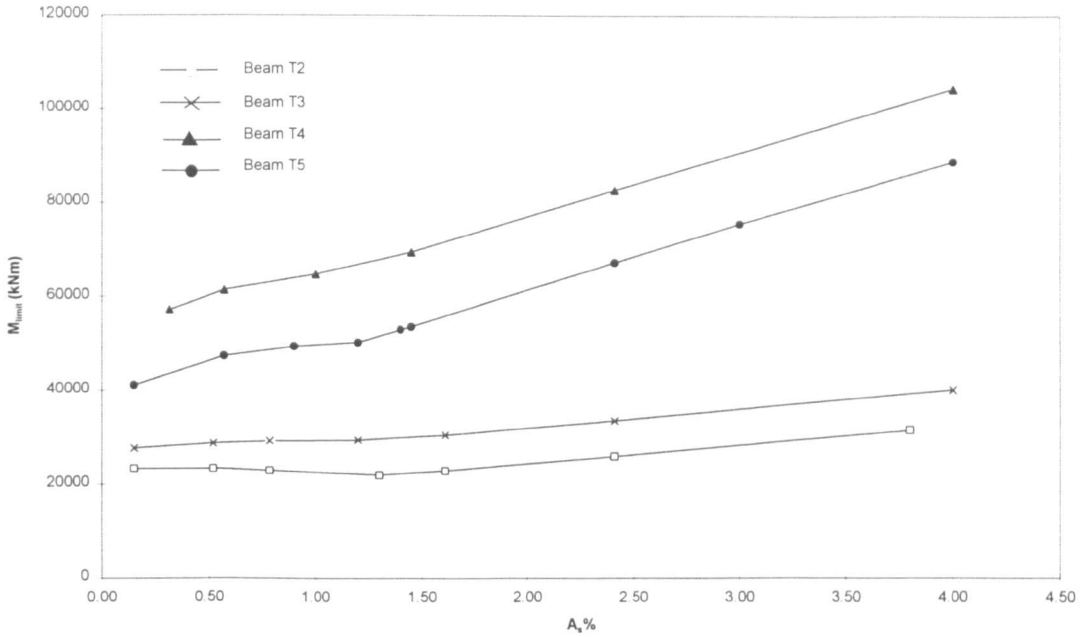

Figure 6.9: Variation of M_{limit} with A_s% for Beams T2 to T5

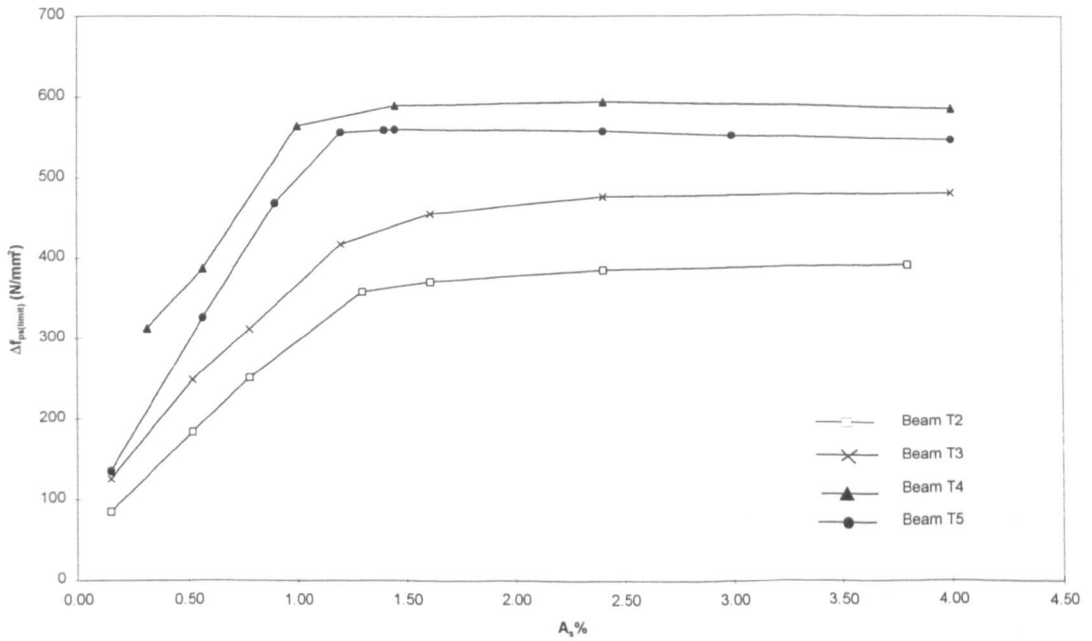

Figure 6.10: Variation of $\Delta f_{ps(limit)}$ with A_s% for Beams T2 to T5

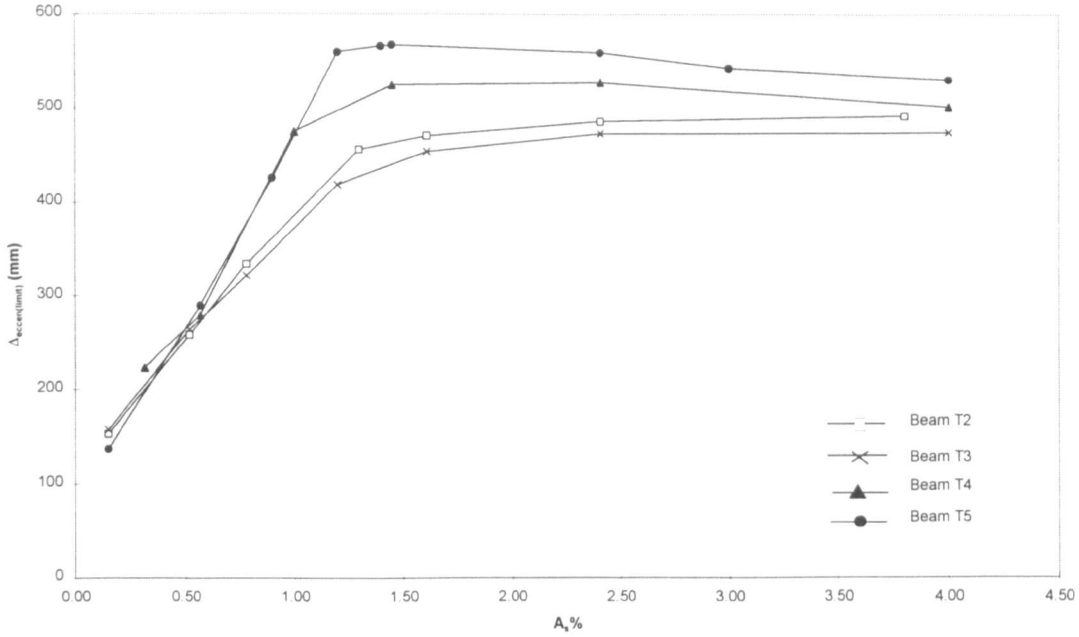

Figure 6.11: Variation of $\Delta_{eccen(limit)}$ with A_s% for Beams T2 to T5

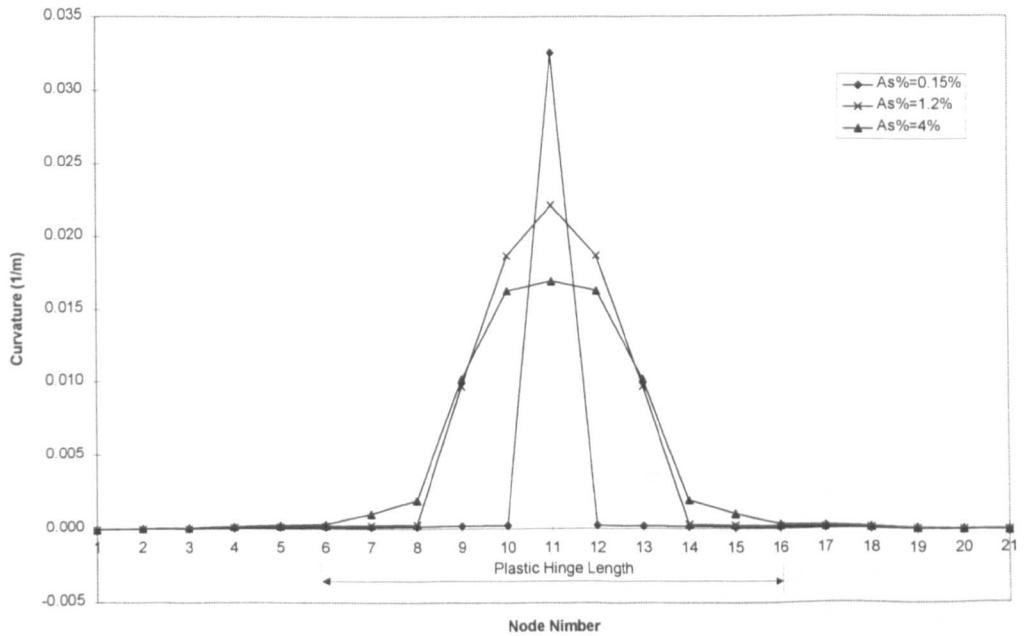

Figure 6.12: Curvature distributions for Beam T5 at the material limit condition.

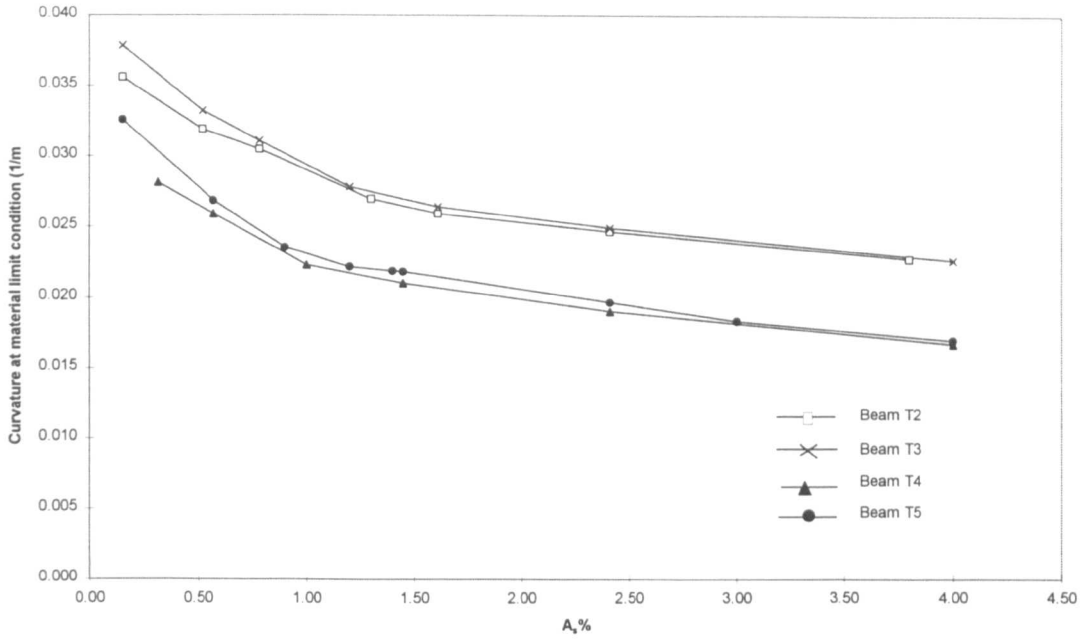

Figure 6.13: Variation of curvature at material limit condition with A_s% for Beams T2 to T5

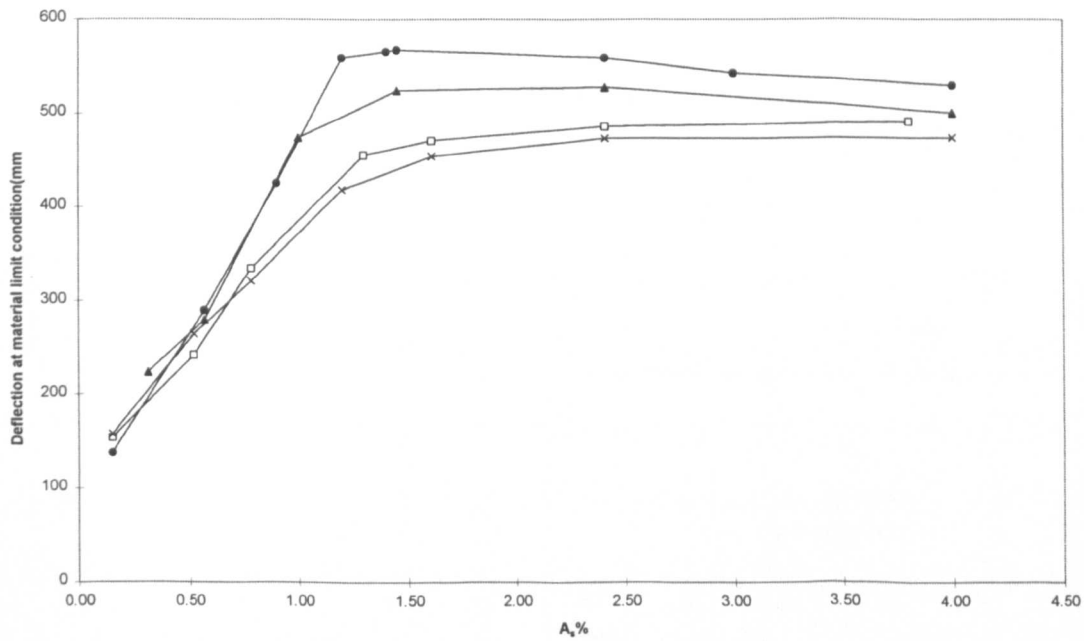

Figure 6.14: Variation of deflection at material limit condition with A_s% for Beams T2 to T5

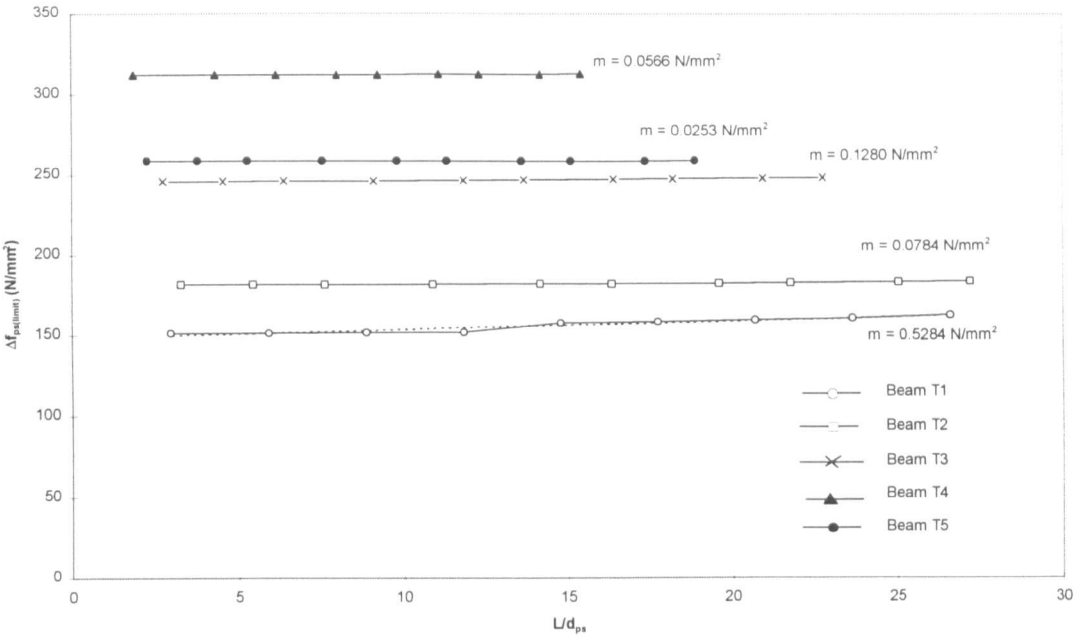

Figure 6.15: Variation of $\Delta f_{ps(limit)}$ with L/d_{ps} for Beams T1 to T5

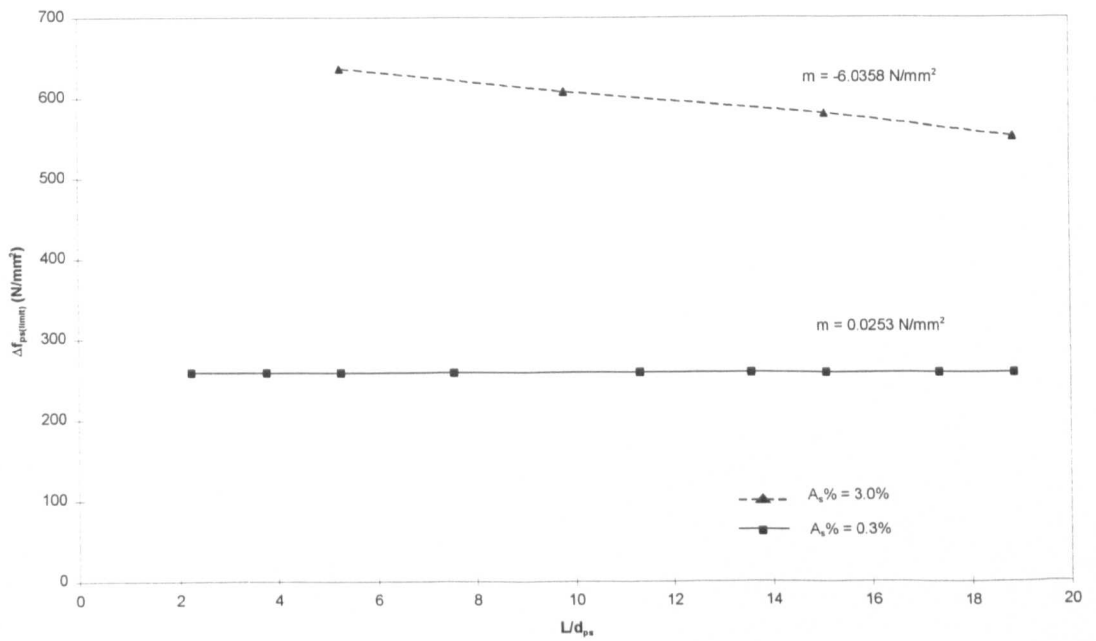

Figure 6.16: Variation of $\Delta f_{ps(limit)}$ with L/d_{ps} for Beam T5 with different A_s%

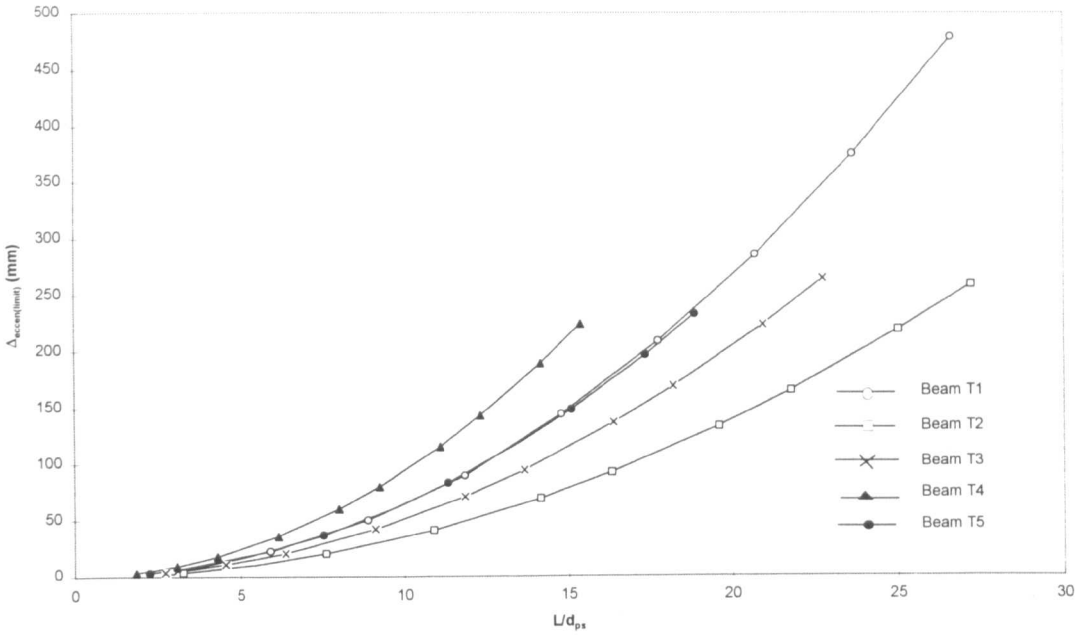

Figure 6.17 : Variation of $\Delta_{eccen(limit)}$ with L/d_{ps} for Beams T1 to T5

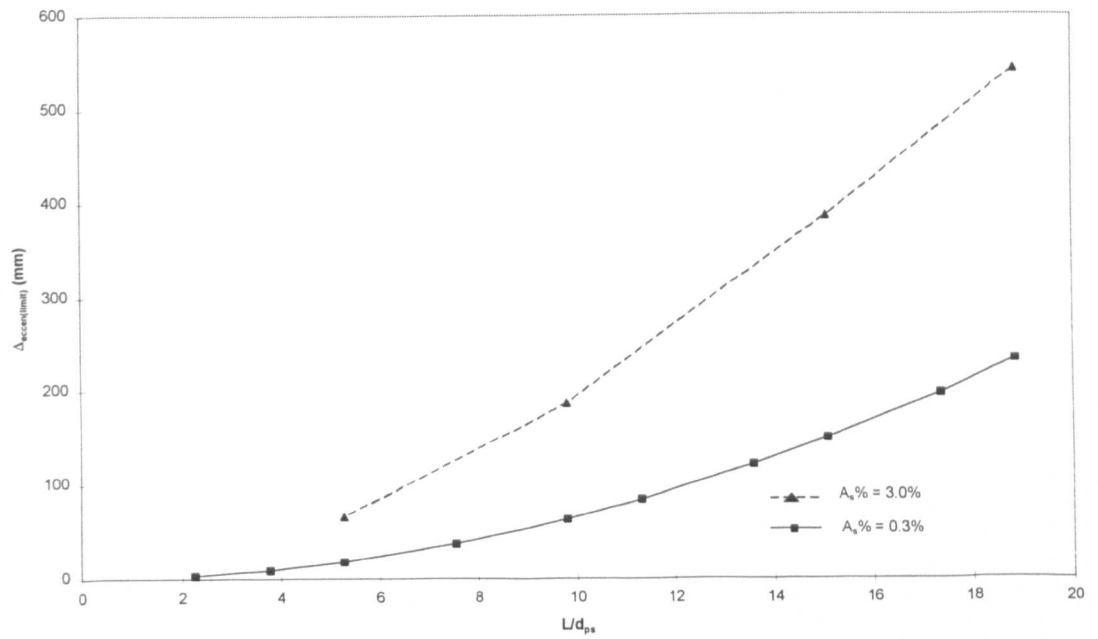

Figure 6.18: Variation of $\Delta_{eccen(limit)}$ with L/d_{ps} for Beam T5 with different A_s%

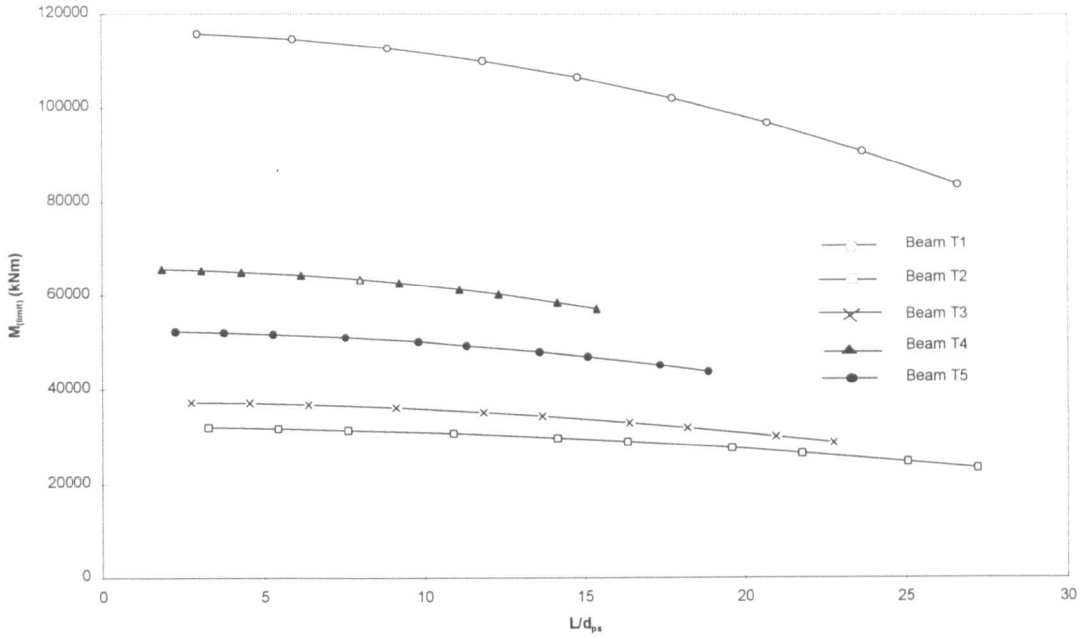

Figure 6.19: Variation of $M_{(limit)}$ with L/d_{ps} for Beams T1 to T5

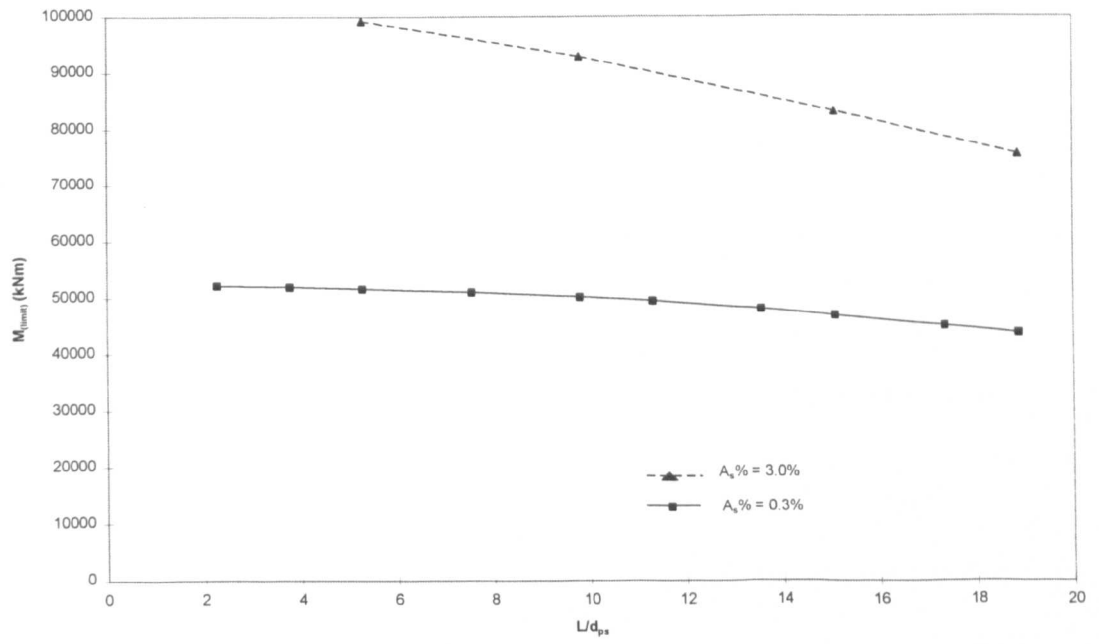

Figure 6.20: Variation of $M_{(limit)}$ with L/d_{ps} for Beam T5 with different A_s%

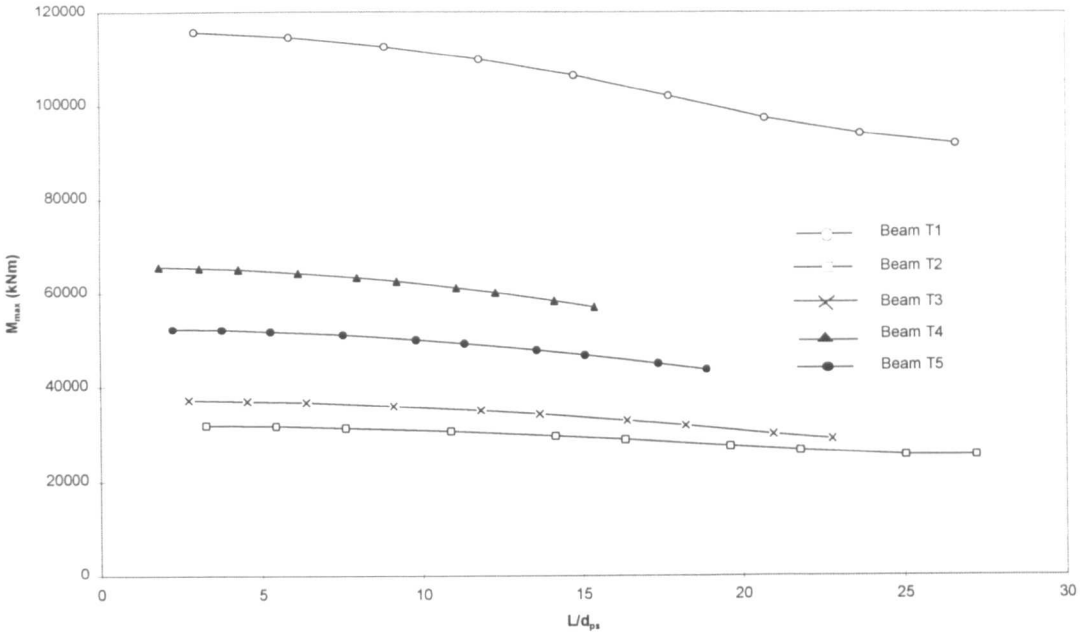

Figure 6.21: Variation of M_{max} with L/d_{ps} for Beams T1 to T5

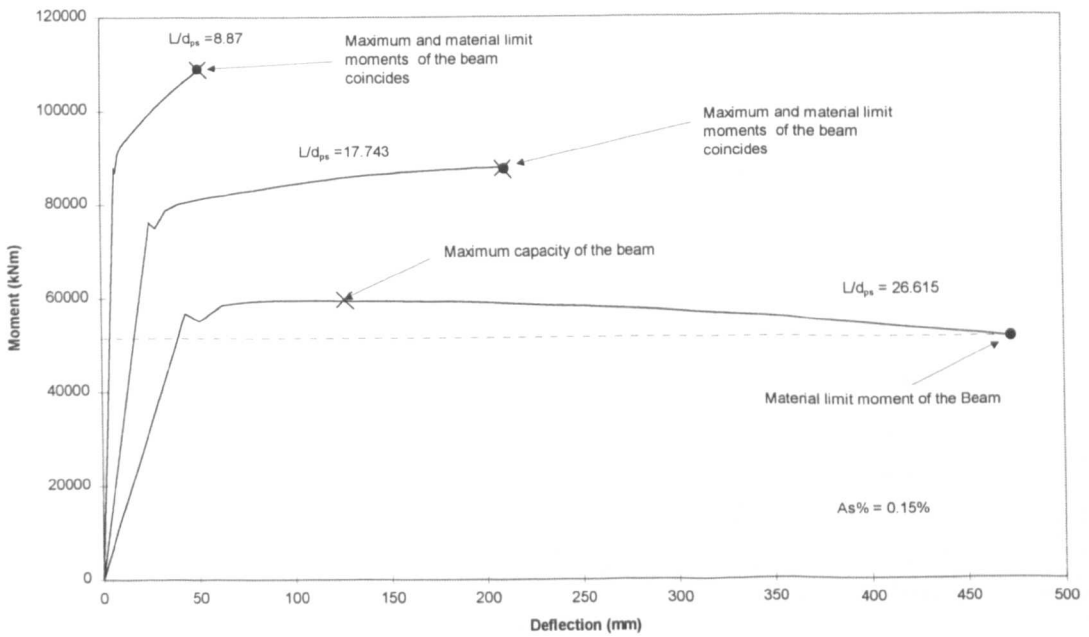

Figure 6.22: Moment-deflection curves for Beam T1 with different L/d_{ps}

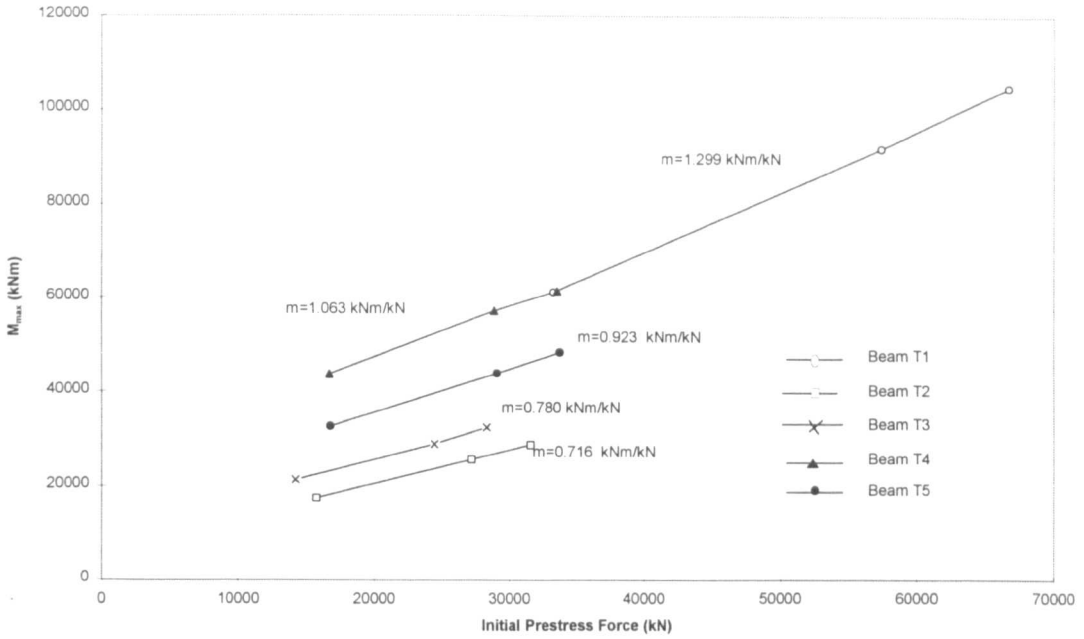

Figure 6.23: Variation of M_{max} with initial prestress force for Beams T1 to T5

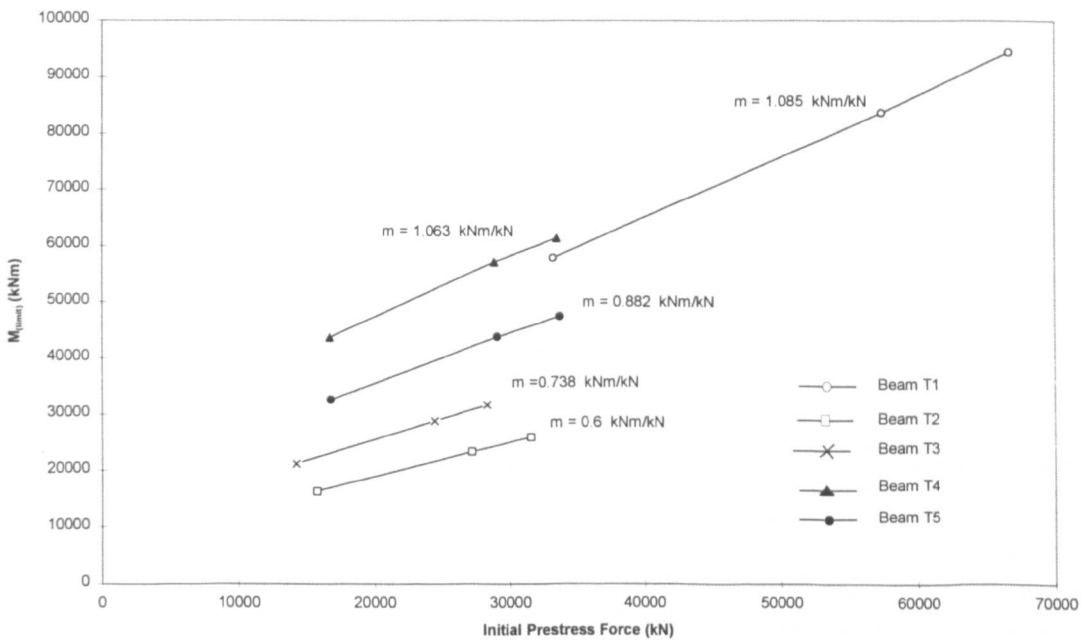

Figure 6.24: Variation of $M_{(limit)}$ with initial prestress force for Beams T1 to T5

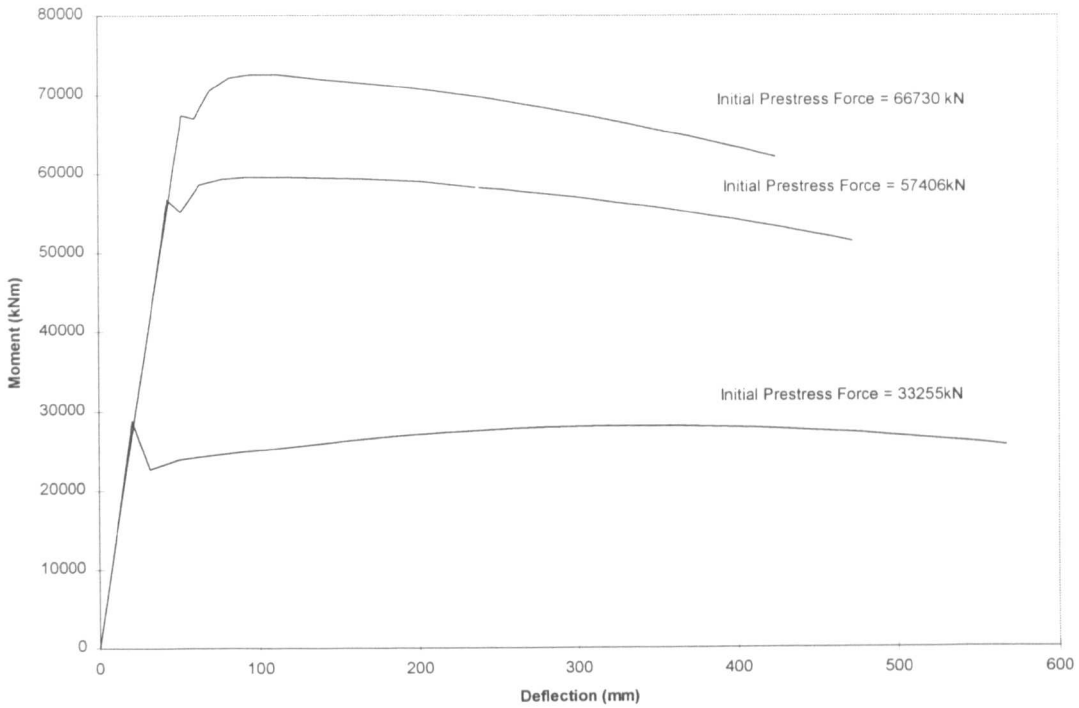

Figure 6.25: Moment-deflection relationships for Beam T1 with different initial prestress force

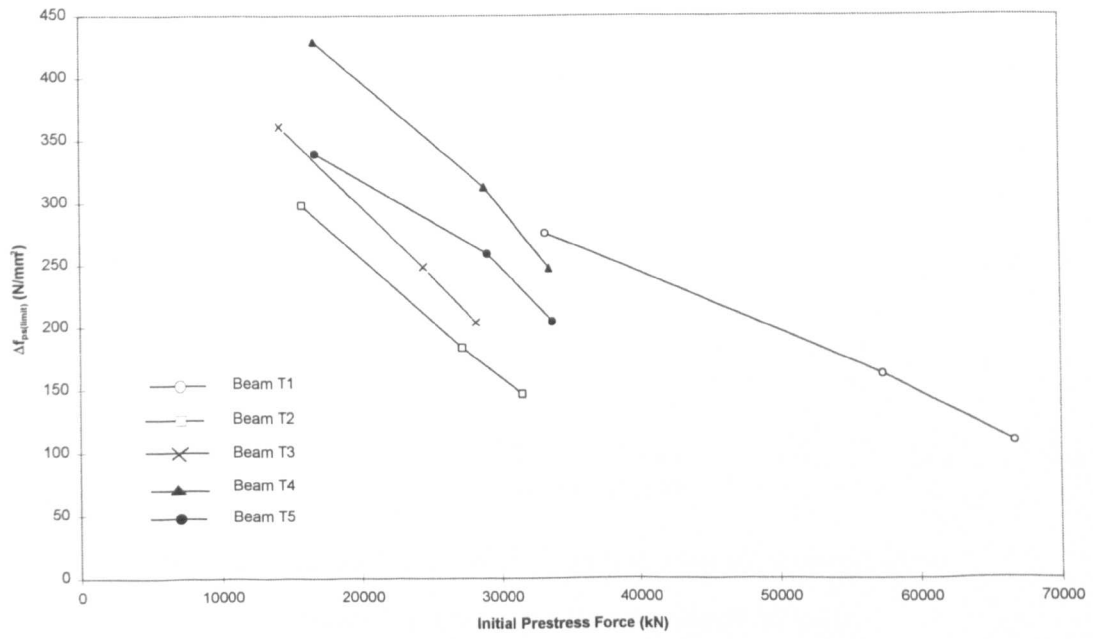

Figure 6.26: Variation of $\Delta f_{ps(limit)}$ with the initial prestress force for Beams T1 to T5

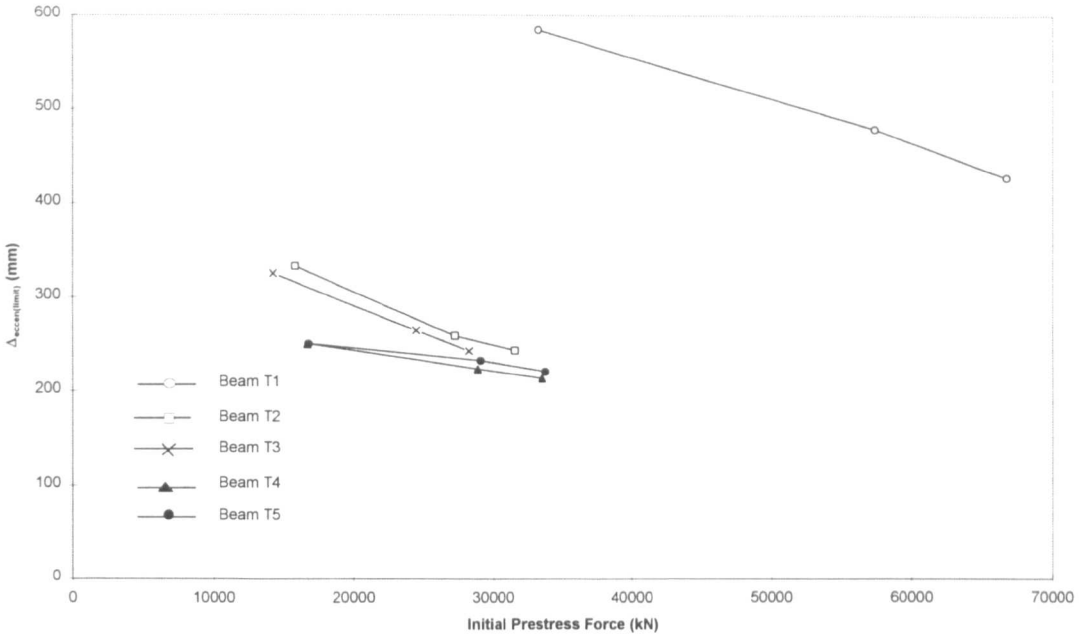

Figure 6.27: Variation of $\Delta_{eccen(limit)}$ with the initial prestress force for Beams T1 to T5

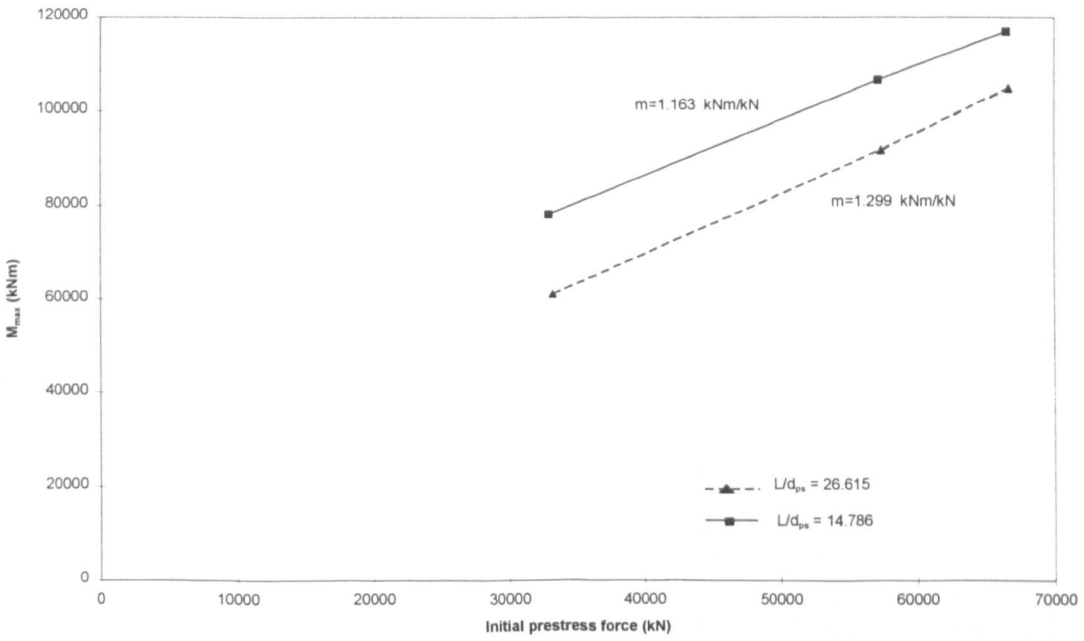

Figure 6.28: Variation of M_{max} with the initial prestress force for Beam T1 with two different values of L/d_{ps}

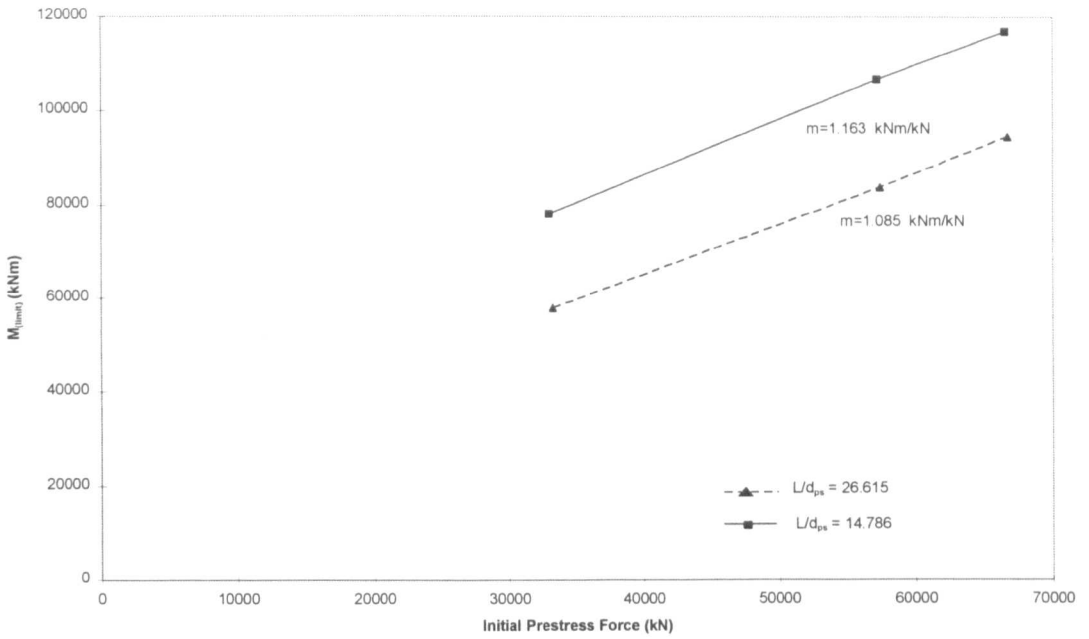

Figure 6.29: Variation of $M_{(limit)}$ with the initial prestress force for Beam T1 with two different values of L/d_{ps}

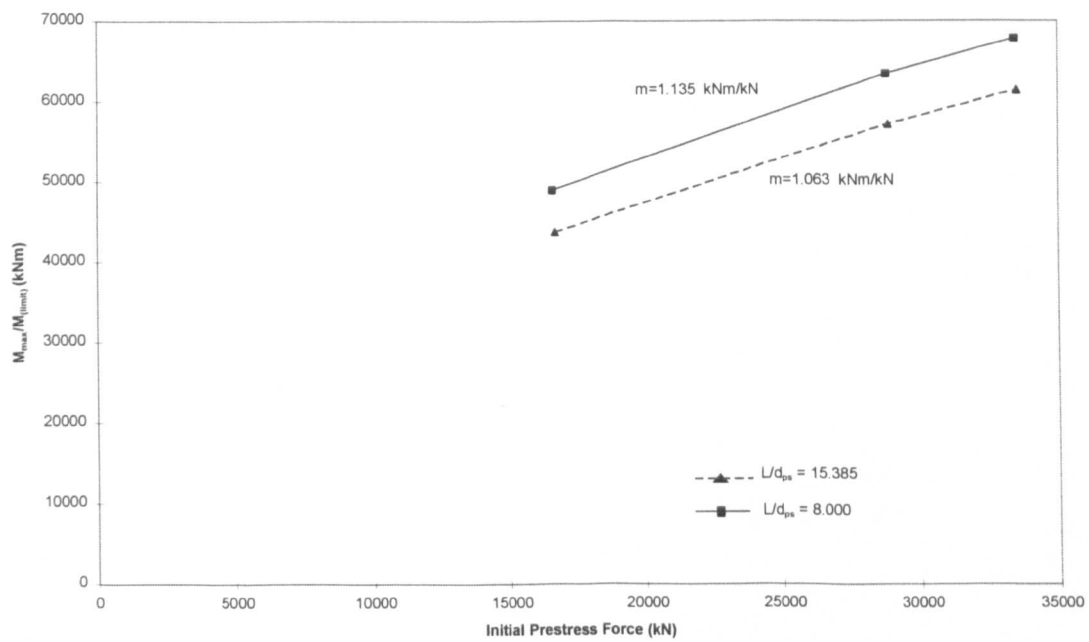

Figure 6.30: Variation of M_{max}/M_{limit} with the initial prestress force for Beam T4 with two different values of L/d_{ps}

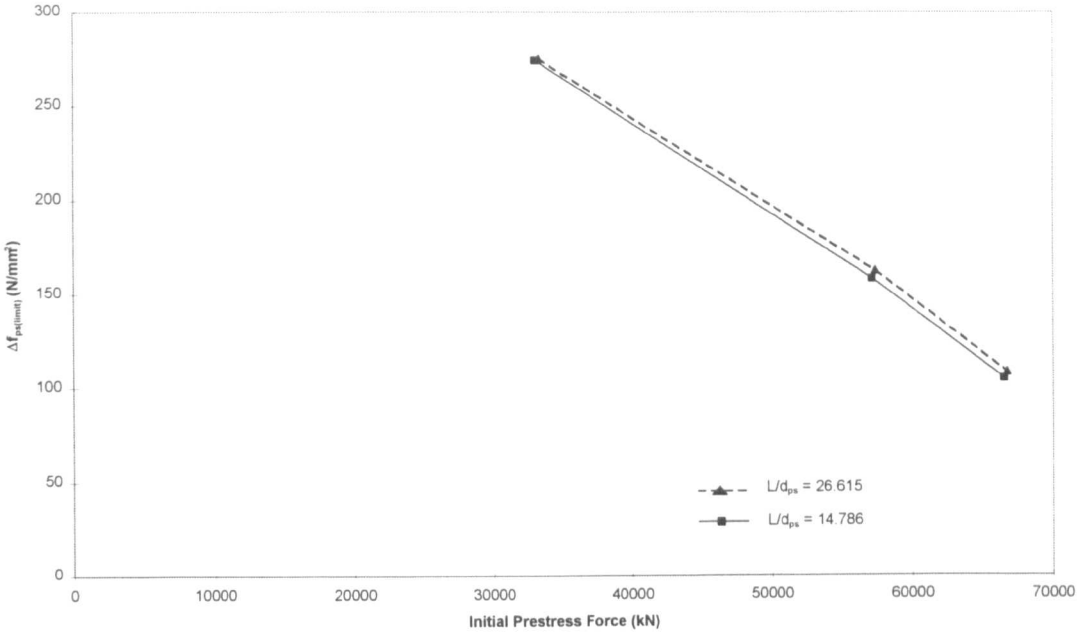

Figure 6.31: Variation of $\Delta f_{ps(limit)}$ with the initial prestress force for Beam T1 with two different values of L/d_{ps}

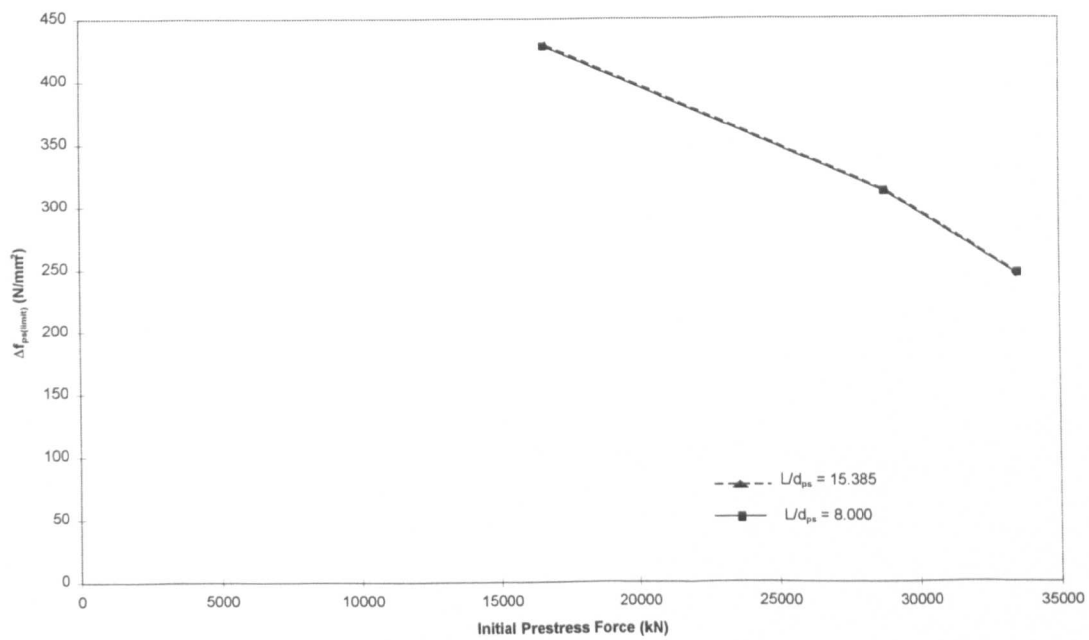

Figure 6.32: Variation of $\Delta f_{ps(limit)}$ with initial prestress force for Beam T4 with two different values of L/d_{ps}

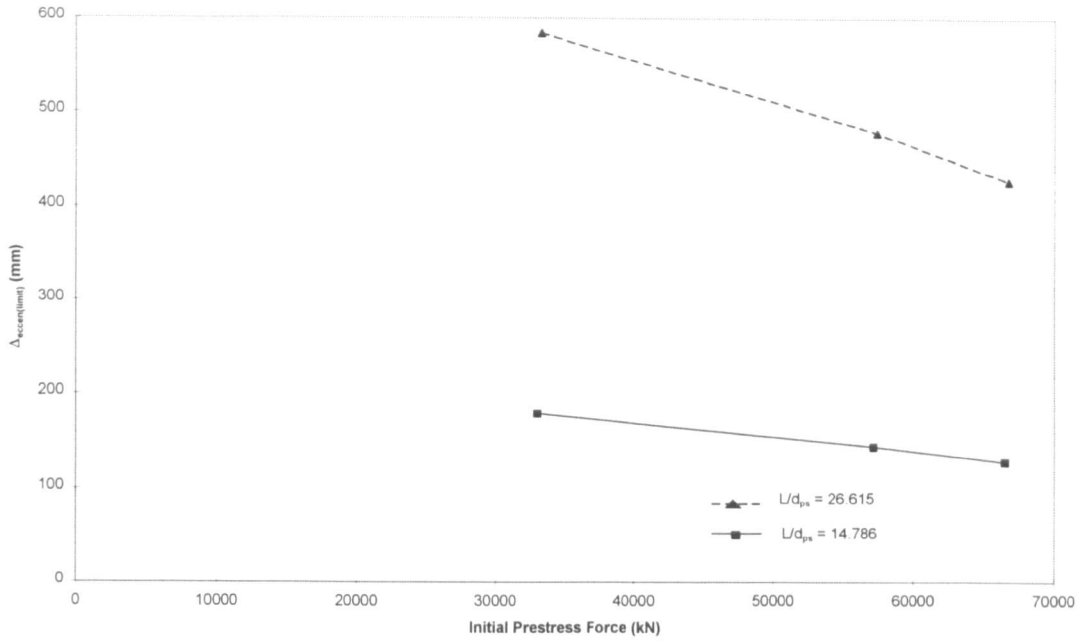

Figure 6.33: Variation of $\Delta_{eccen(limit)}$ with the initial prestress force for Beam T1 with two different values of L/d_{ps}

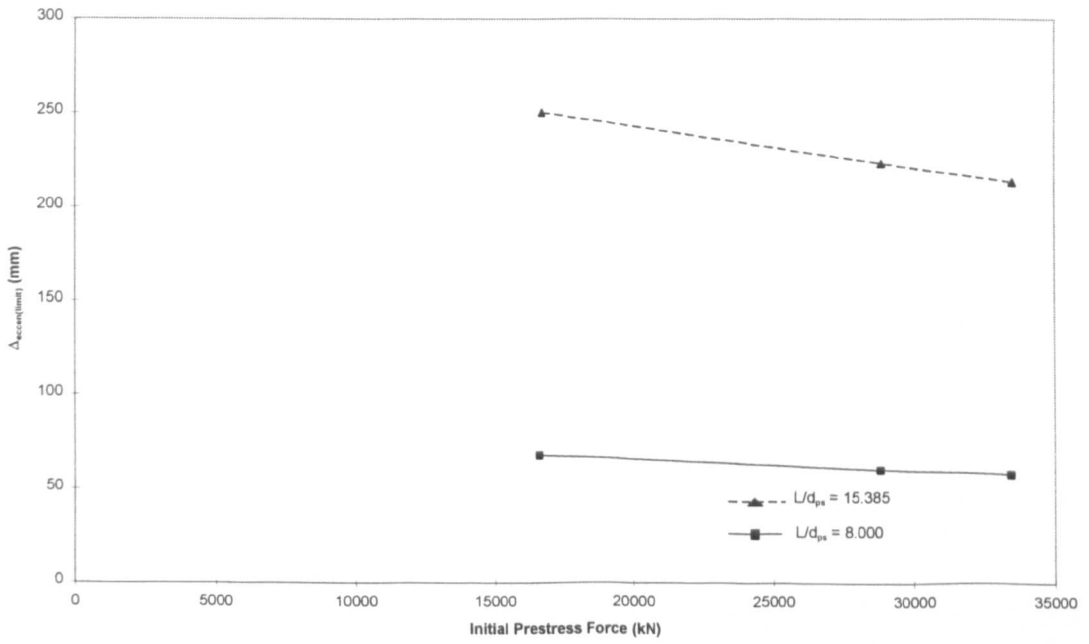

Figure 6.34: Variation of $\Delta_{eccen(limit)}$ with the initial prestress force for Beam T4 with two different values of L/d_{ps}

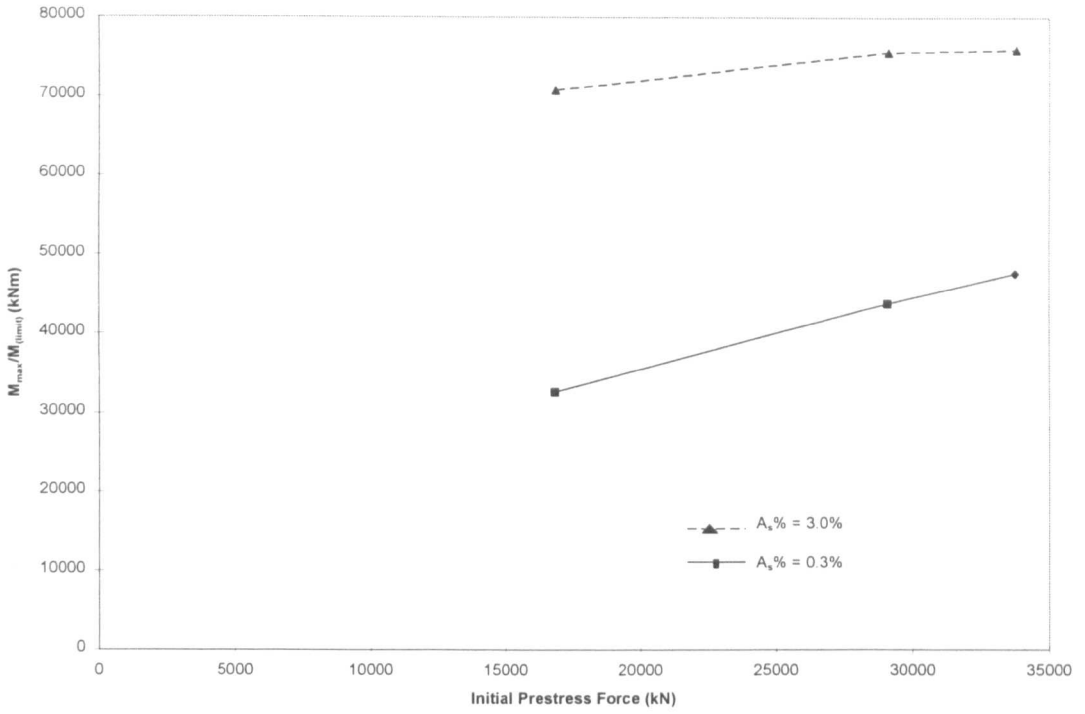

Figure 6.35: Variation of $M_{max}/M_{(limit)}$ with the initial prestress force for Beam T5 with two different values of $A_s\%$

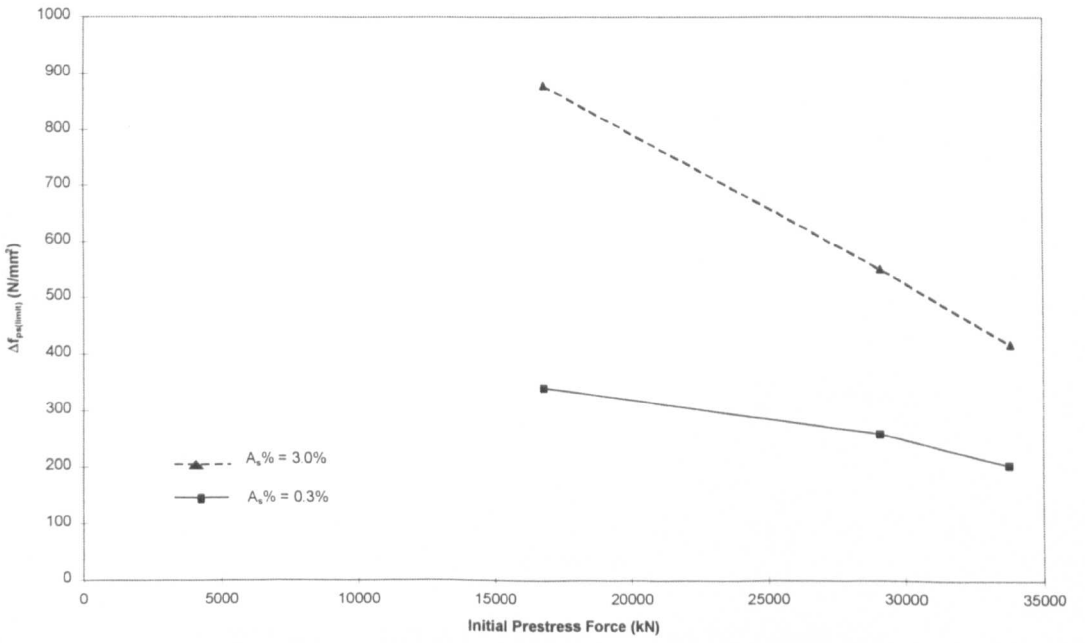

Figure 6.36: Variation of $\Delta f_{ps(limit)}$ with the initial prestress force for Beam T5 with two different values of $A_s\%$

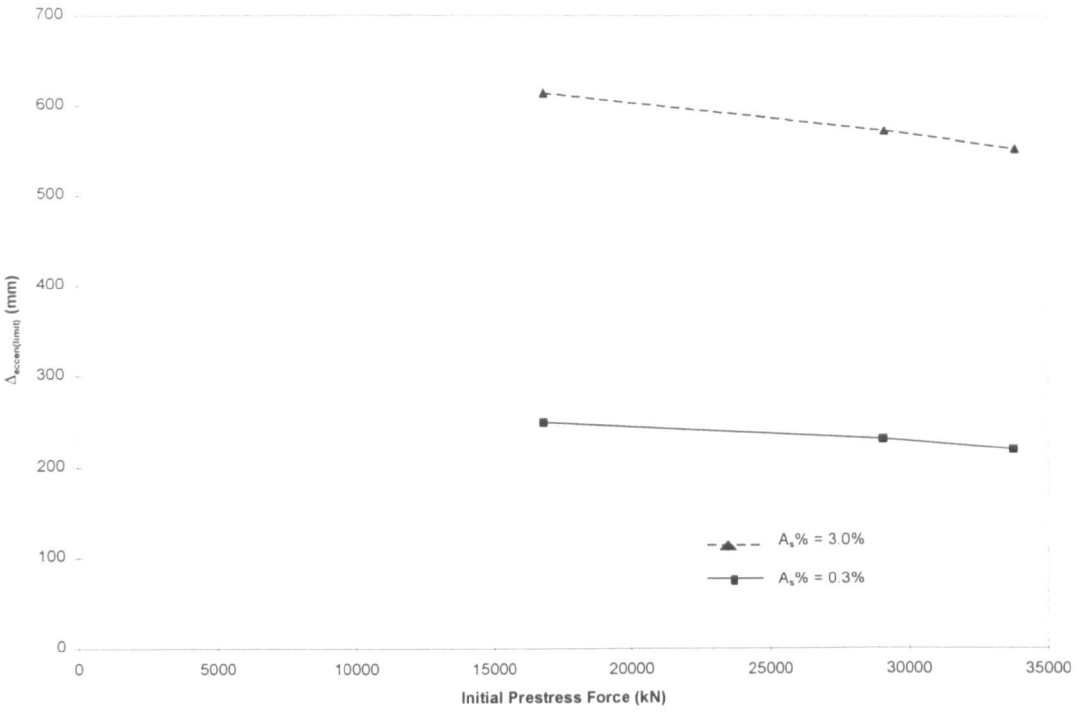

Figure 6.37: Variation of $\Delta_{eccen(limit)}$ with the initial prestress force for Beam T5 with two different values of $A_s\%$

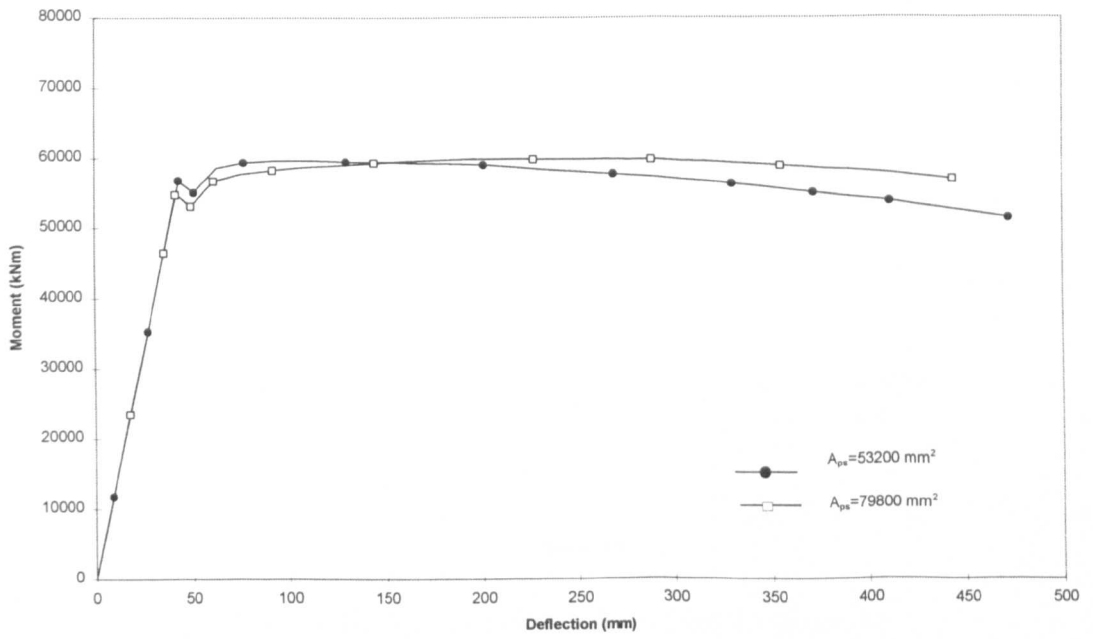

Figure 6.38: Moment-deflection curves for Beam T1 with two different values of A_{ps}

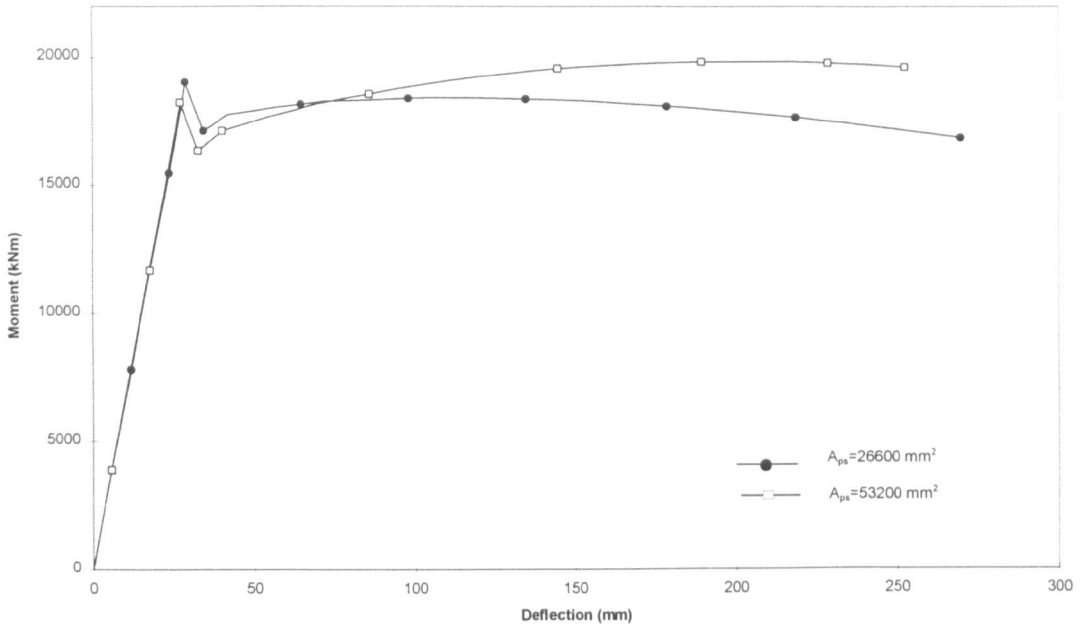

Figure 6.39: Moment-deflection curves for Beam T2
with two different values of A_{ps}

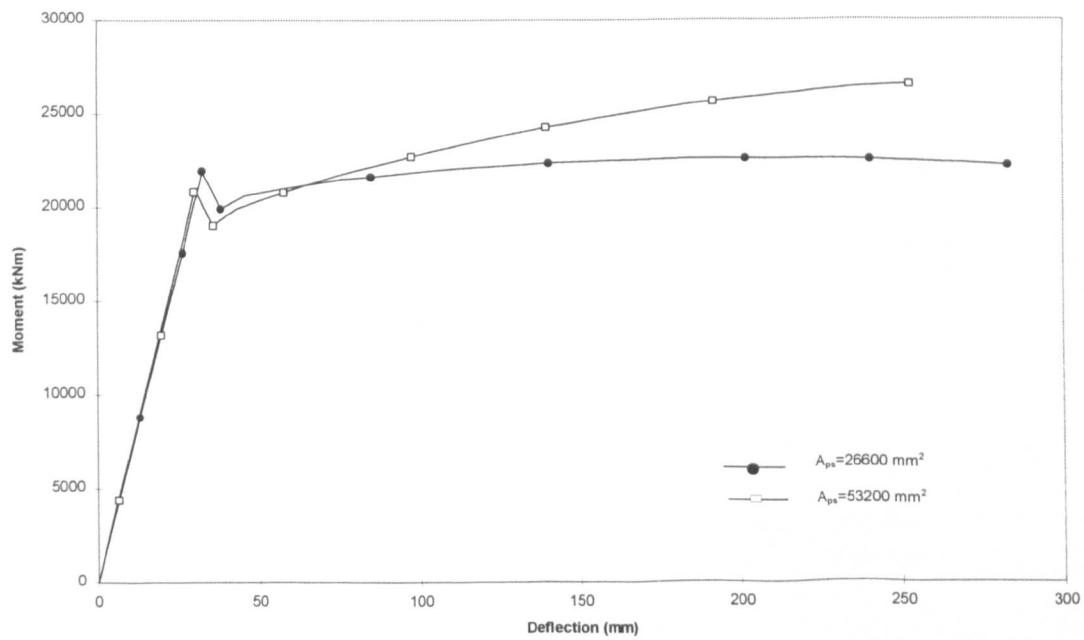

Figure 6.40: Moment-deflection curves for Beam T3
with two different values of A_{ps}

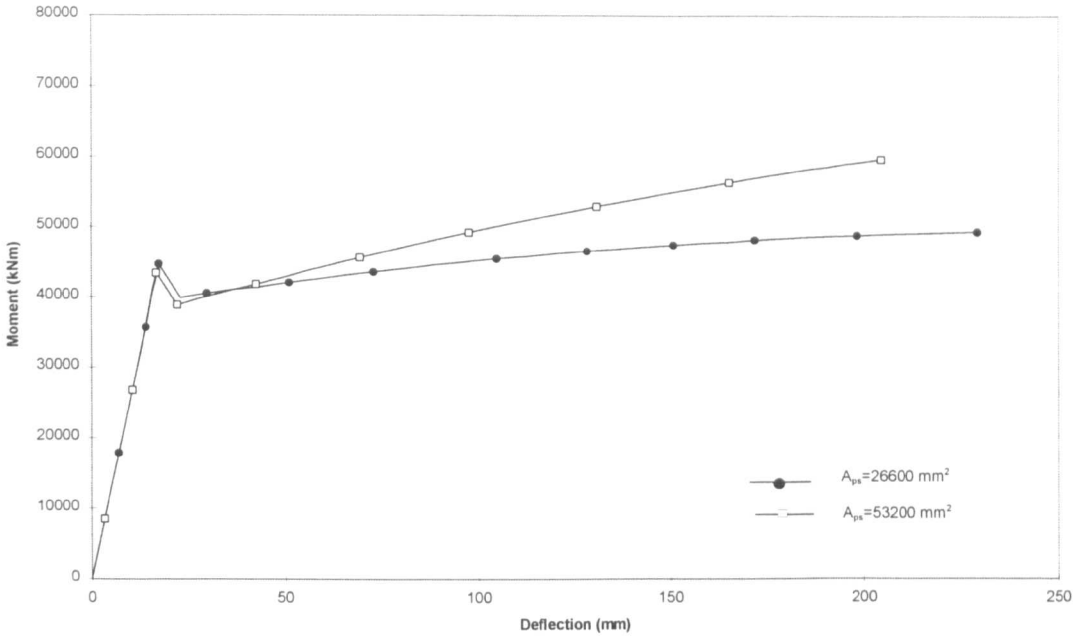

Figure 6.41: Moment-deflection curves for Beam T4
with two different values of A_{ps}

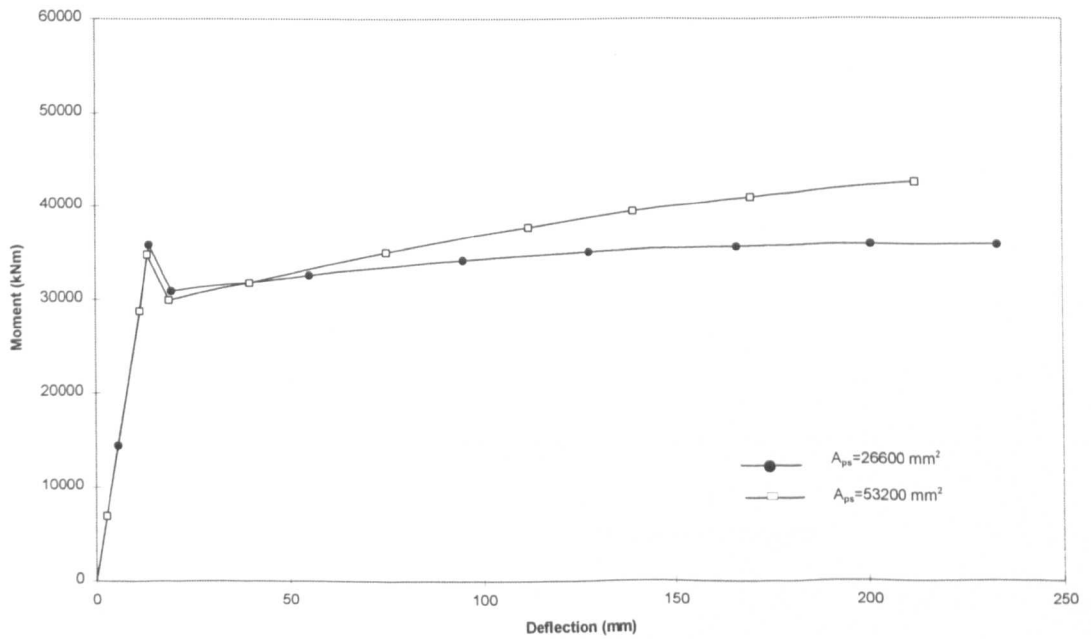

Figure 6.42: Moment-deflection curves for Beam T5
with two different values of A_{ps}

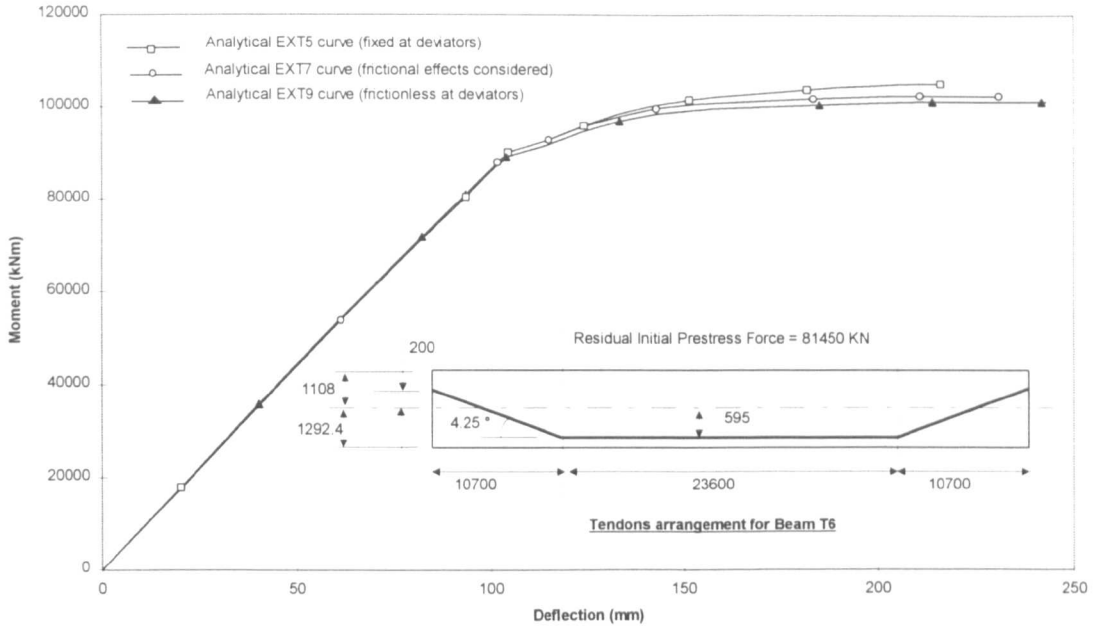

Figure 6.43: Moment-deflection curves for Beam T6

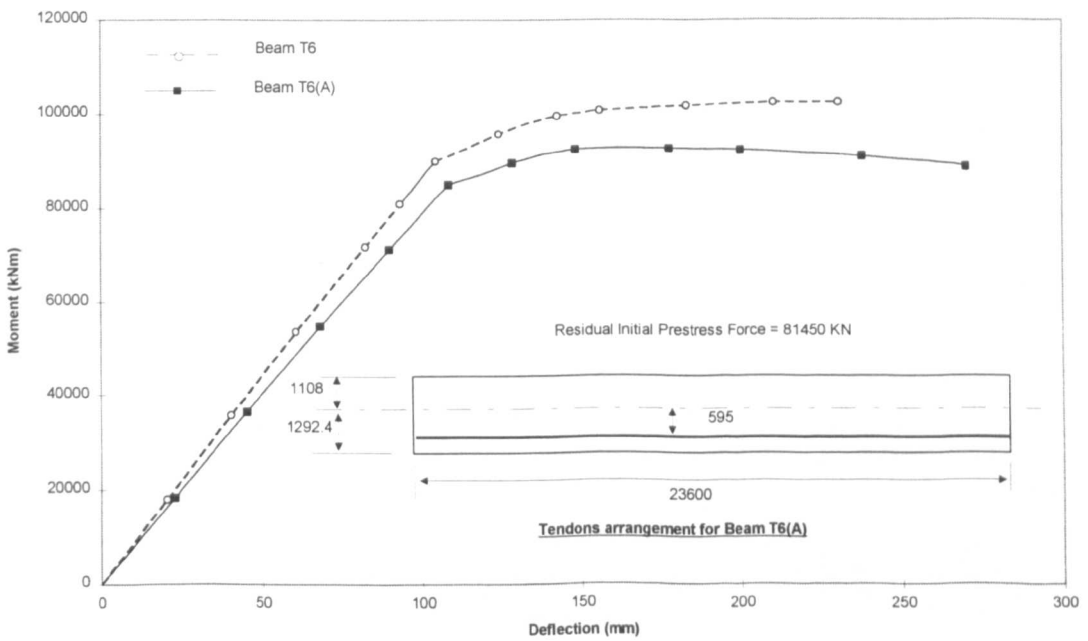

Figure 6.44: Moment-deflection curve for Beam T6(A) compared with that for Beam T6

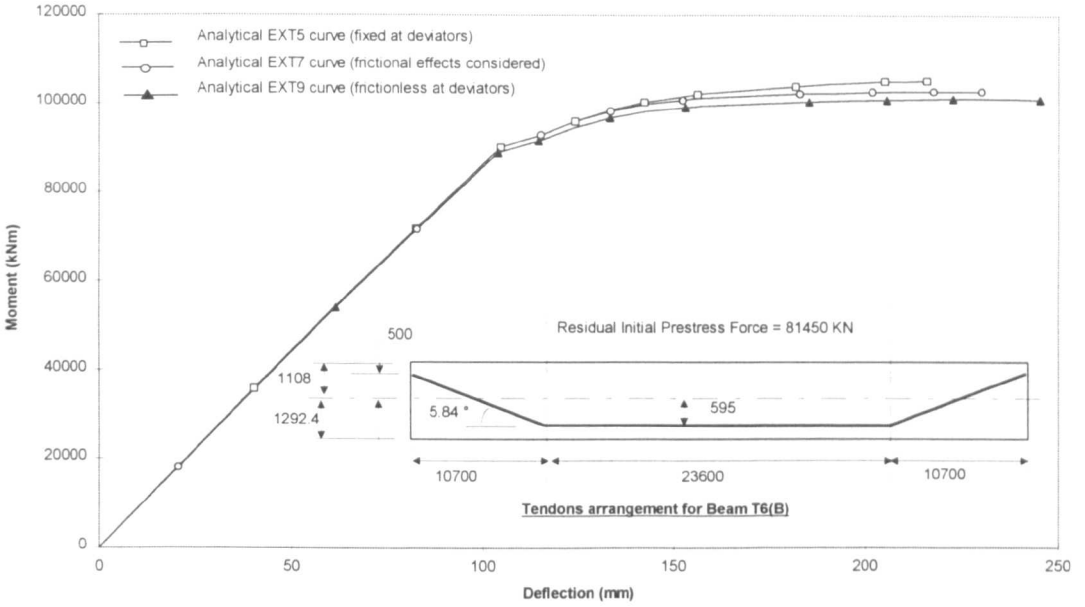

Figure 6.45: Moment-deflection curves for Beam T6(B)

(Deviation angles = 5.84°)

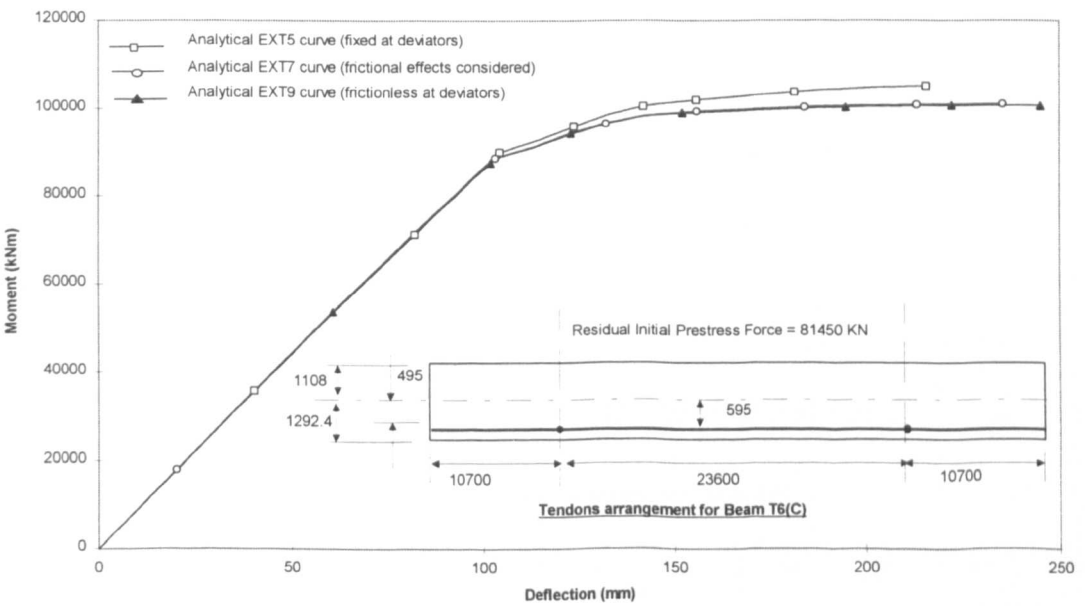

Figure 6.46: Moment-deflection curves for Beam T6(C)

(Deviation angles = 0°)

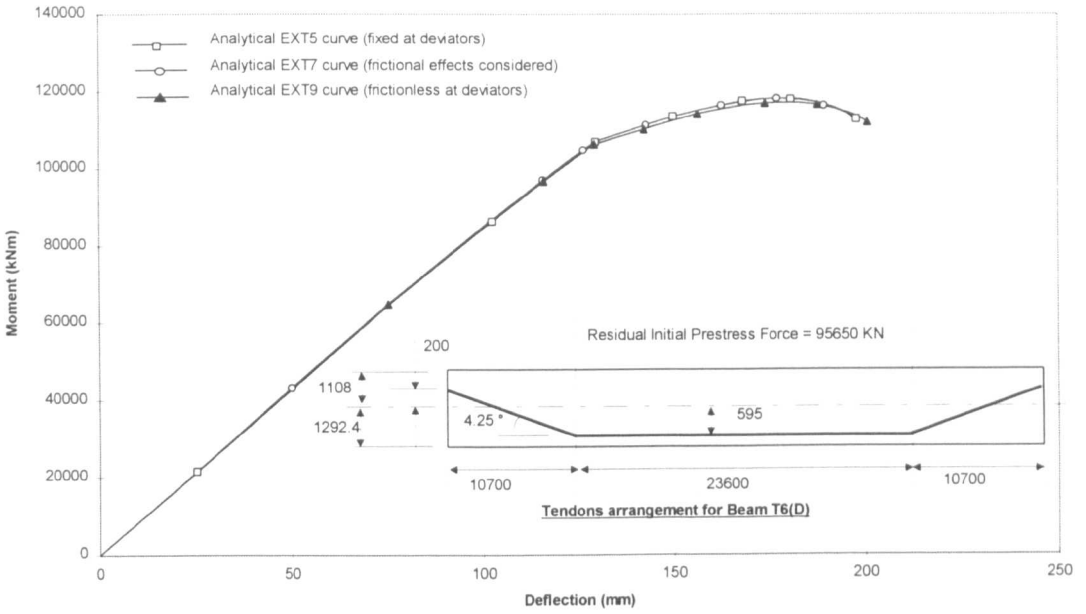

Figure 6.47: Moment-deflection curves for Beam T6(D)

(Initial prestress force = 95650 kN)

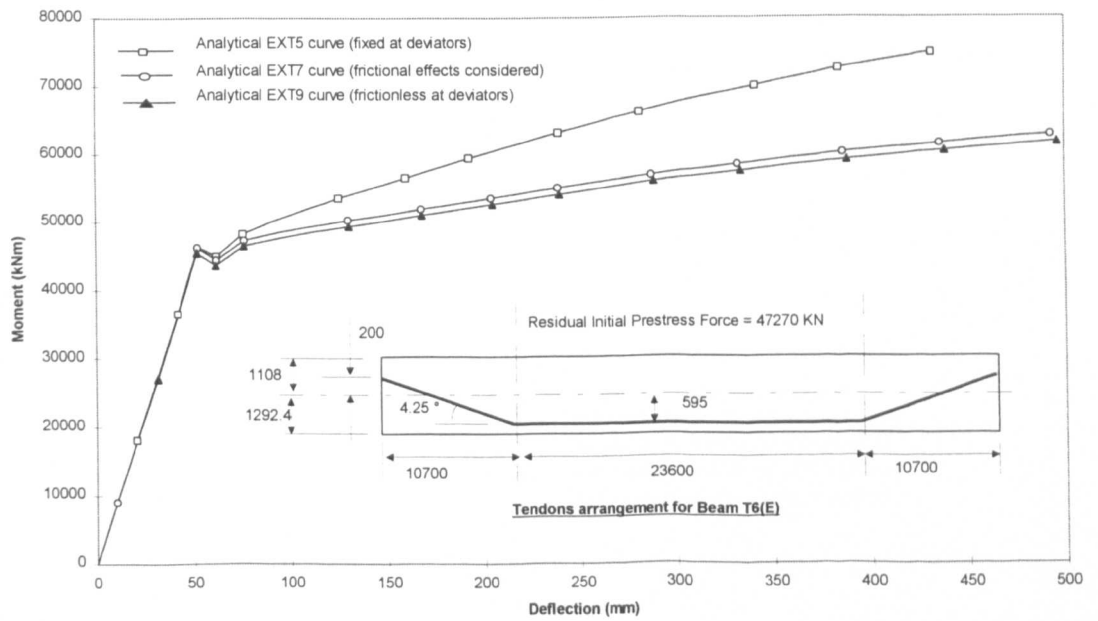

Figure 6.48: Moment-deflection curves for Beam T6(E)

(Initial prestress force = 47270 kN)

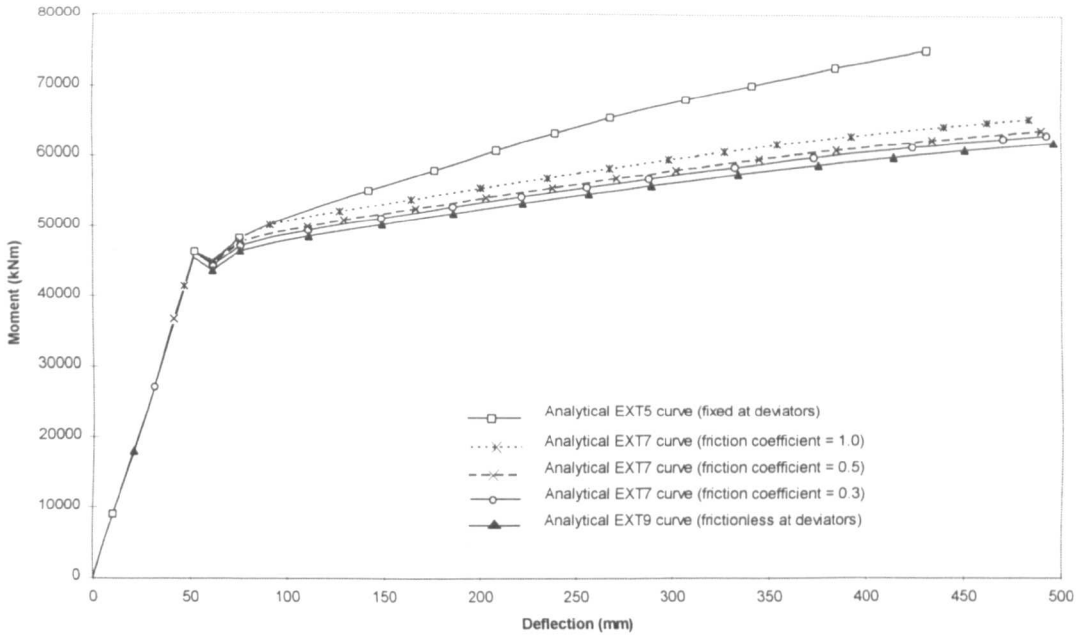

Figure 6.49: Moment-deflection curves for Beam T6(E)
with different friction coefficients

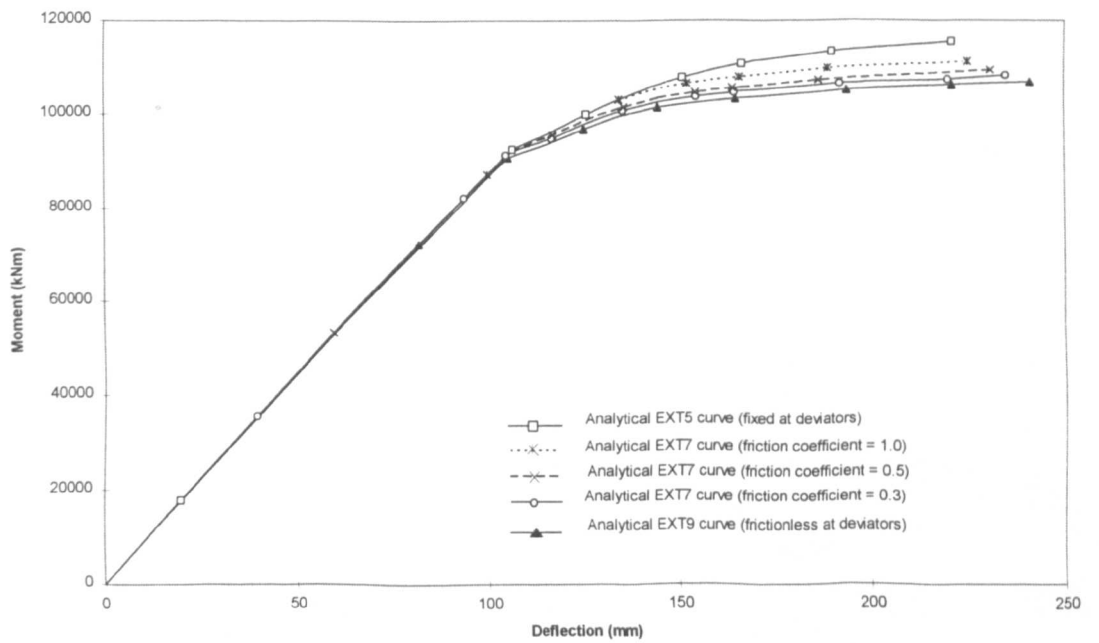

Figure 6.50: Moment-deflection curves for Beam T6(F)
with different friction coefficients

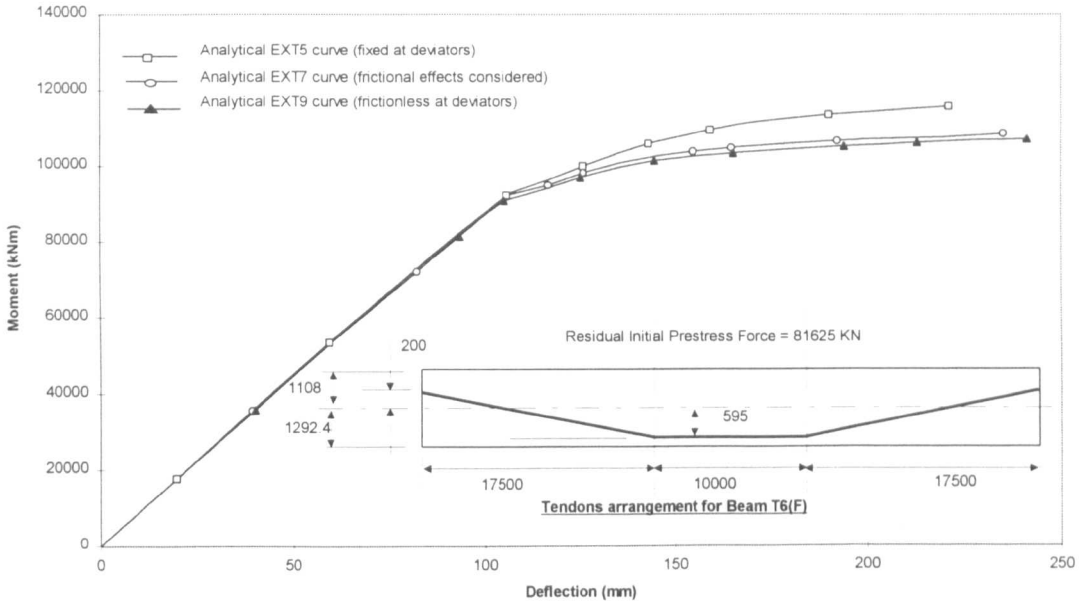

Figure 6.51: Moment-deflection curves for Beam T6(F)

(Free length to depth ratio α_{free} = 5.87)

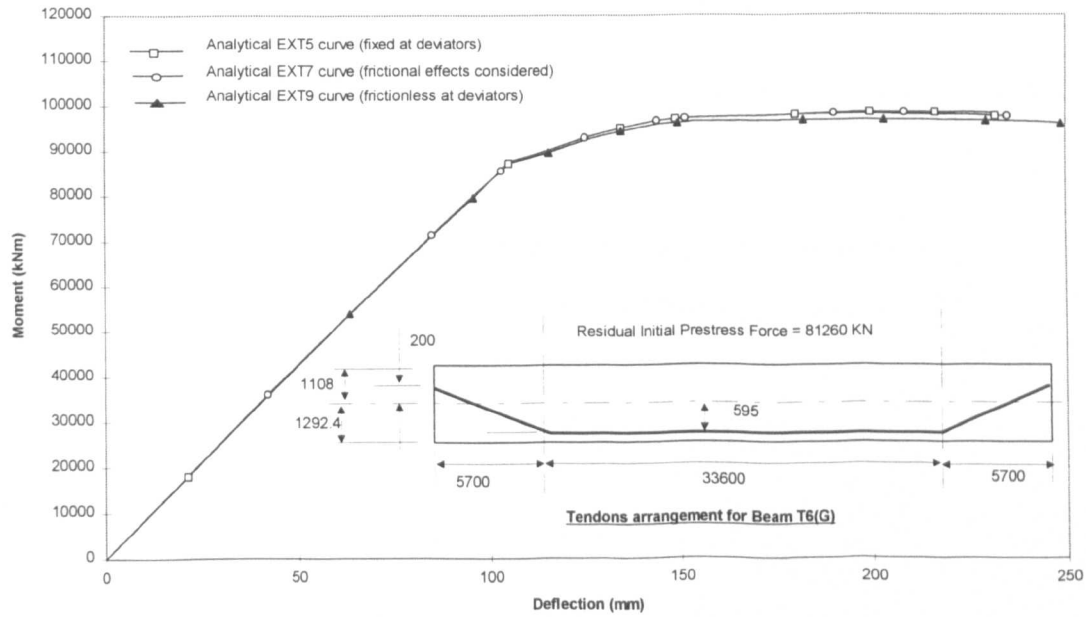

Figure 6.52: Moment-deflection curves for Beam T6(G)

(Free length to depth ratio α_{free} = 19.72)

Beam no.	Profile Type	L (m)	d_{ps} (mm)	L/d_{ps}	A_s% (%)	A_{ps} (mm^2)	P_e (kN)
T1	1	45	1689.86	26.63	0.15	53200	57406
T2	1	25	918.40	27.22	0.50	26600	27233
T3	1	25	1098.40	22.76	0.50	26600	24457
T4	1	25	1625.12	15.38	0.30	26600	28879
T5	1	25	1325.12	18.87	0.30	26600	29093
T6	2	45	1702.60	26.43	0.15	66500	81450

* Refer to Figures B.1(b) and B.1(c) in Appendix B for the arrangement of Tendon Profile 1 and 2 respectively

Table 6.1: Key parameters of Beams T1 to T6

Beam No.	M_{max} (kNm)				Δ_{eccen} (mm)		
	EXT3	EXT5	EXT7	EXT9	EXT5	EXT7	EXT9
T6	N.A.	105110	102510	101210	81.66	89.68	95.98
T6(A)	92810	N.A.	N.A.	N.A.	N.A.	N.A.	N.A.
T6(B)	N.A.	105110	102710	100910	81.66	89.11	97.01
T6(C)	N.A.	105110	101010	100610	74.09	92.62	97.70
T6(D)	N.A.	118110	118010	116910	65.68	65.97	67.31
T6(E)	N.A.	74810	62790	61730	209.00	242.00	244.00
T6(F)	N.A.	115710	108400	106910	15.73	21.88	29.87
T6(G)	N.A.	98410	98110	96810	140.20	142.10	152.40

EXT3: non-linear analytical model for beams with no deviators

EXT5: non-linear analytical model for beams with deviators where tendons are assumed to be fixed at the deviators

EXT7: non-linear analytical model for beams with deviators and the friction coefficient at the deviators are assumed to be 0.3

EXT9: non-linear analytical model for beams with deviators where the tendons are assumed to slip freely at the deviators.

Table 6.2 : Maximum moments and eccentricity variations predicted using the various proposed non-linear models

Chapter 7

Design Implementations

7.1 General

The purpose of this chapter is to check the applicability and accuracy of using different analytical methods to estimate the flexural behaviour of externally prestressed structures. The analytical methods considered in this investigation are:

- the sectional analysis method (as recommended in BD 58/94 (1995), ASSHTO (1989) and ACI (1983))
- the proposed non-linear models introduced in Chapter Four.

In Chapters One and Two, it was pointed out that the use of external post-tensioning in bridge construction was only recently encouraged in the United Kingdom by the Department of Transport. Since design rules for externally prestressed structures were not included in BS 5400 Part 4 (1990), the UK DoT commissioned Gifford and Partners to establish new design guidelines for these structures. The new rules published in BD 58/94 (1995) recommended that the ultimate strength of these beams can be estimated by performing a sectional analysis at the section of maximum moment where the stress increase in the tendons $\Delta f_{ps(ult)}$ required for the ultimate load analysis be either assumed to be zero or calculated from a non-linear analysis. In the United States, although external post-tensioning is used commonly in many bridge construction, no formal recommendations are given exclusively for the estimation of the ultimate behaviour of these structures. Instead, the design rules given in ASSHTO (1989) and ACI (1983) for internally unbonded prestressed structures were deemed also to be applicable for externally prestressed structures. Both codes recommended that the sectional analysis method may be used for predicting the ultimate flexural behaviour of these unbonded structures, provided the stress increase in the tendons is either assumed to be 103 N/mm^2 (as recommended by AASHTO (1989)) or evaluated

by using Equations (2.2) and (2.3) (as recommended by ACI (1983)). Since the recommendations given in the two codes were directed for internally unbonded prestressed structures, no reference was given about the change in eccentricity of the tendons due to second-order effects. Section 7.2 compares the ultimate moments derived from sectional analyses conducted using the guidelines given in BD 58/94 (1995), AASHTO (1989) and ACI (1983) and the proposed non-linear models and discusses the applicability of using these given guidelines for estimating the ultimate strength of externally post-tensioned structures.

7.2 Sectional Analysis

For reinforced and internally bonded prestressed concrete structures, the ultimate moment capacity can be easily determined by conducting a sectional analysis at the section of maximum moment. In the sectional analysis, the strain at the extreme compressive fiber of the concrete is assumed to be at an ultimate value (e.g. BS8110 (1985) recommends 0.0035) and the following assumptions are usually used to evaluate the various forces acting at the critical section (i.e. C_{conc}, T_{conc}, T_{pres}, T_{reinf}):

1) Plane section remains plane after bending.
2) The concrete will crack whenever the tensile strains in the concrete exceeds the modulus of rupture and, after cracking, the tensile force is carried by the reinforcement and the prestressing steel.
3) The constitutive relationships of the materials are known.

The evaluated forces are then balanced by adjusting the depth of the neutral axis, until force equilibrium is achieved at the critical section (i.e. Equation (5.1) is satisfied). Once equilibrium of forces is ensured, the ultimate moment capacity is then evaluated using Equation (5.2).

$$C_{conc} - T_{reinf} - T_{conc} - T_{pres} = 0 \quad \text{.....(5.1)}$$

$$M_{ult} = C_{conc}d'_{conc} + T_{conc}d_{conc} + T_{reinf}d_{reinf} + T_{pres}d_{pres} \quad \text{.....(5.2)}$$

However, problems are encountered when the sectional analysis method described above is used to evaluate the flexural behaviour of externally prestressed structures. This is because the change in prestress $\Delta f_{ps(ult)}$ above the initial stressing level (which determines the amount of prestress force in the tendons T_{pres}) and, the eccentricity

variations $\Delta_{eccen(ult)}$ of the tendons due to second-order effects (which determines the position of the tendons d_{pres}) are both not easily estimated by just considering the stress and strain distribution across the critical section. In fact, due to the lack of bond between the concrete and the external tendons, these two variables are found to be dependent on the deformation response of the whole beam and can only be accurately estimated if the deflected profile of the beam at the ultimate condition is known.

A study was conducted here to investigate the accuracy of using the recommendations given in BD 58/94 (1995), AASHTO (1989) and ACI (1983) for estimating the ultimate moment capacities of externally prestressed structures. In the study, the flexural strengths of the beams used in the verification process (described in Chapter Five) were first analysed with the proposed non-linear models (introduced in Chapter Four) and then with the specifications given by the three selected design codes. The evaluated ultimate moments M_{ult} and their ratio with the experimental results (M_{pred}/M_{exp}) are all tabulated in Table 7.1.

Beams OS-1 and OL-1 were nearly identical beams except for their span-depth ratios, which were 24 and 40 respectively. When these beams were analysed with the proposed non-linear models, the predicted maximum moments were found to be 0.902 and 0.990 of the experimental beams respectively. For Beam OS-1 the maximum moment evaluated using BD 58/94 was under-estimated by about ten percent and, over-estimated by AASHTO and ACI by approximately fifteen and twelve percent respectively. AASHTO and ACI over-estimated the maximum moments because they did not take into account the large loss in lever arm caused by eccentricity variations of the tendons due to the relatively high span-depth ratio of Beam OS-1 (i.e. 24). Although eccentricity variation was also neglected in BD 58/94, the over-conservative assumption of using zero stress increase in tendons at ultimate caused the derived ultimate moments to be under-estimated instead. In the case of Beam OL-1 because the span-depth ratio was further increased, the ultimate capacity was over-estimated by twenty-five percent, sixty-three percent and fifty-six percent by BD 58/94, AASHTO and ACI respectively. This shows that despite the extremely conservative assumption used in BD 58/94, the ultimate capacity can also sometimes be over-estimated.

Beams OA88-2, OB88-1, OC88-1, OC88-2 and OD88-1 all had the same cross-section, loading pattern, non-prestressed reinforcement ratio and span-depth ratio but different amounts of prestressing steel and initial prestress force. The ultimate moment capacities were found to be under-estimated by approximately twenty-five to thirty-five percent when BD 58/94 was used to predict their flexural strength. AASHTO and ACI both gave better estimations of the flexural strength of these beams, under-estimating them by only approximately ten to twenty percent. However, when the proposed non-linear models were used, the flexural strengths of all these beams were only under-estimated by approximately five to thirteen percent except for Beam OB88-1 which was slightly over-estimated by two percent.

Beams OA-1, OB-1 and OC-1 were similar to each other except for the amount of non-prestressed reinforcement ratios. The proposed non-linear analytical models under-estimated the flexural strength of these beams by about thirteen, ten and eighteen percent respectively. Such a large under-estimation was predicted for Beam OC-1 because its estimated maximum flexural strength was limited by the theoretical value of ultimate compressive strain assumed for the concrete (i.e. assumed here to be 0.0035). When the stress increase in tendons was assumed to be zero (i.e. BD 58/94), the derived ultimate moment capacities for Beams OA-1, OB-1 and OC-1 were found to be under-estimated by about thirteen, eleven and twenty percent respectively which were very close to the percentages obtained for the non-linear models. The reasonably close estimation of the ultimate strengths with BD 58/94 was again due to the conservative assumption made in the analysis, that is, zero stress increase in the tendons at the ultimate condition. This assumption compensated for the over-estimation of the flexural strength due to neglecting the eccentricity variation of the tendons. Both AASHTO and ACI on the other hand over-estimated the ultimate strengths of these beams by approximately three to seven percent. This was because the eccentricity variations of the tendons at ultimate were not taken into account by these codes and the recommended values for $\Delta f_{ps(ult)}$ were not small enough to compensate for the over-estimation of the flexural strength. It was also noted that the over-estimation of the flexural strength increases as the non-prestressed reinforcement ratios increases. This is because higher reinforcement ratios generally cause higher deflections at ultimate for these beams (see Chapter Six), and this consequently causes

larger changes in the eccentricity of the tendons. Since the eccentricity variations were neglected by these codes, higher flexural strengths were thus predicted.

Beams A1-2, A2-1, A2-2 and A3-2 were tested by Zhang *et al* (1993) and although they were quite similar to each other, they had different loading patterns and non-prestressed reinforcement ratios (see Appendix A). When zero stress increase was assumed for the estimation of the ultimate strength of these beams (i.e. BD 58/94) , the maximum moment predicted was on average found to be 0.74 of the experimentally determined maximum value. Using the $\Delta f_{ps(ult)}$ values recommended by AASHTO and ACI, the maximum moment estimated was found to be approximately 0.89 and 0.86 of the experimentally measured values respectively. As for the maximum moments estimated by the non-linear models, despite the premature terminations encountered due to convergence problems, they were on average found to be 0.92 of the experimentally measured values.

Beams B1-2, B2-2 and B3-2 were also tested by Zhang *et al* (1993) and had deflected tendon profiles. The maximum moments predicted for these beams using the EXT9 model (where tendons were assumed to slip freely) are shown in Table 7.1. The average M_{pred}/M_{exp} obtained for these beams using the EXT9 model was found to be 0.95 with a standard deviation of 0.03. When a fixed value of 103 N/mm^2 (ASSHTO) and the ACI equations were used to predict the ultimate moments of these beams, the average M_{pred}/M_{exp} obtained were approximately 0.83 and 0.81 of the experimental results with standard deviations of 0.08 and 0.09 respectively. BD 58/94 under-estimated the experimentally derived ultimate moments of these beams greatly by about fifteen percent to thirty-five percent.

The maximum moments derived with the proposed non-linear models gave the best representation of the experimental results, predicting an average M_{pred}/M_{exp} of approximately 0.924 with a standard deviation of only 0.050 for all seventeen beams (see Table 7.1). The non-linear models were also seen to be able to predict accurately the flexural strengths of beams with large span-depth ratios and high reinforcement ratios. It should also be noted that the experimentally determined strengths of all seventeen beams were under-estimated by the proposed non-linear models, except for Beam OB88-1 which was over-estimated by only two percent. The analytical models

therefore constantly provided accurate yet conservative values, hence safe and efficient design solutions.

The average ratio of the ultimate moment predicted with BD 58/94 to the experimental moment (M_{pred}/M_{exp}) for all the seventeen beams was found to be 0.788 with a large standard deviation of 0.141. The high variation in M_{pred}/M_{exp} values derived with BD 58/94 was due mainly to the assumptions made for $\Delta f_{ps(ult)}$ and $\Delta_{eccen(ult)}$ at ultimate. Firstly, assuming zero stress increase in the external tendons $\Delta f_{ps(ult)}$ at ultimate is a very conservative assumption, since it has been shown in previous chapters that the increase in prestress at ultimate is dependent on the deformation response of the structure and may sometimes be a value considerably higher than zero. Hence, this assumption will greatly under-estimate the flexural strength of externally prestressed structures. Secondly, the variations in eccentricity $\Delta_{eccen(ult)}$ due to second-order effects were neglected in the analysis. Conversely, this will cause the ultimate strength of the beams to be over-estimated especially for beams with large span-depth ratios or non-prestressed reinforcement ratios. Thus solutions of varying accuracy are derived when the recommendations given by BD 58/94 (1995) are used to predict the ultimate flexural strength of these beams.

When a fixed value 103 N/mm^2 was used as the stress increase in tendons at ultimate, as recommended by AASHTO, the average M_{pred}/M_{exp} was found to be a commendable 0.951 but with a large standard deviation of 0.202. Such a large variation in results was again due to the assumptions made for the values of $\Delta f_{ps(ult)}$ and $\Delta_{eccen(ult)}$. Firstly, although a stress increase in tendons of 103 N/mm^2 was considered to be conservative by AASHTO for internally unbonded prestressed structures, it has been shown earlier in Chapter Six that the stress increase in tendons at ultimate for externally prestressed structures is dependent on several parameters and is too variable to be accurately represented by a single value. Secondly, the eccentricity variations $\Delta_{eccen(ult)}$ were again neglected in the analysis which may cause the ultimate flexural strength of these beams to be sometimes greatly over-estimated (e.g. the ultimate moment capacity of Beam OL-1 was over-estimated by about sixty-three percent). Although ACI proposed two equations (i.e. Equations (2.2) and (2.3)) for estimating the prestress change in tendons at ultimate, the results obtained from using these recommendations were also found to be very varied. The average

M_{pred}/M_{exp} derived with ACI was found to be 0.936 with a standard of deviation of 0.190. The reasons for the large variation in results obtained with the ACI codes are similar to those for the ASSHTO recommendations.

Beams T1 to T6 described in Section 6.2 were also used to check the reliability of applying the sectional analysis method for predicting the ultimate moment capacities of externally post-tensioned structures. Beams T1 to T5 had straight external tendons with no deviators placed along their span, while Beam T6 had external tendons which were deflected by two deviators placed within the span. In the parametric study (see Chapter Six), the flexural behaviour for all the six beams were simulated up to failure with the appropriate non-linear computer models. Since it was shown earlier that these analytical models can accurately predict the maximum flexural response of externally prestressed structures (within eight percent), it was thus assumed here that the results obtained from these analytical models reflected the actual behaviour of Beams T1 to T6.

The ultimate moment capacities of these beams were then estimated using the recommendations given by BD 58/94 (1995), AASHTO (1989) and ACI (1983), and compared to the ultimate moments obtained from the analytical models. The ultimate moments derived from these analyses M_{ult} and their ratios with the moments derived from the non-linear models ($M_{ult(code)}/M_{ult(analytical)}$) are presented in Table 7.2. From Table 7.2, it can be seen that the average $M_{ult(code)}/M_{ult(analytical)}$ derived from BD 58/94, ASSHTO and ACI were 0.817, 0.888 and 0.873 respectively with large standard deviations of 0.096, 0.109 and 0.105 respectively.

The ultimate strengths of Beams T1 to T6 were then calculated using three different analytical approaches, denoted *Method 1 to 3* respectively. All three methods involved conducting a sectional analysis at the section of maximum moment, but with different assumptions used to define $\Delta f_{ps(ult)}$ and $\Delta_{eccen(ult)}$.

- **Method 1**

  The ultimate flexural strength of the beams was estimated assuming zero values for the stress increase in the tendons and the eccentricity variation due to second-order effects. This method simulated the case in which the ultimate moment

capacity of externally prestressed structures are estimated based on the recommendations given in BD 58/94 (1995).

- **Method 2**

  In Method 2, the stress increase in tendons at the ultimate conditions was taken to be equal to $\Delta f_{ps(limit)}$ derived from the proposed analytical models, but the change in eccentricity of the tendons was neglected in the sectional analysis. This method simulated the case in which the Δf_{ps} at the limit moment condition (where the top compressive strain of the concrete at the critical section is equal to 0.0035) can be accurately predicted using some recommended equation but not the eccentricity variations of the tendons.

- **Method 3**

  Finally, the third method assumed that $\Delta f_{ps(ult)}$ and $\Delta_{eccen(ult)}$ at the ultimate conditions were equal to $\Delta f_{ps(limit)}$ and $\Delta_{eccen(limit)}$ respectively, obtained from analyses conducted with the proposed analytical models. This method simulated the case where both the stress increase and eccentricity variations of the tendons at the material limit condition can be estimated accurately and used in the sectional analysis to predict flexural strength.

Table 7.3 shows the ultimate moments computed from these three analytical approaches.

In Method 1, the $M_{ult(method)}/M_{ult(analytical)}$ derived for Beams T1 to T6 ranged from 0.67 to 0.932, with an average value of 0.817 and a standard deviation of 0.096. Since Method 1 employed the same assumptions as those given by BD 58/94 (1995), the average value and standard deviation of $M_{ult(method)}/M_{ult(analytical)}$ computed was therefore equal to the $M_{ult(model)}/M_{ult(analytical)}$ derived for BD 58/94 in Table 7.2. The reasons for the large variations in results obtained with this method of analysis were the same as those explained earlier for the BD 58/94 method.

Method 2 used the $\Delta f_{ps(limit)}$ predicted by the proposed non-linear models but neglected the variations in eccentricity of the tendons to estimate the ultimate flexural strength of Beams T1 to T6. This analytical approach is typical of the methods proposed by several codes of practices (e.g. ACI (1983), AASHTO (1989)) and researchers (e.g. Naaman (1994)), where the expressions for estimating $\Delta f_{ps(ult)}$ are stated but no guidelines are given for the variations in eccentricity of the tendons caused by second-

order effects. From Table 7.3, it was noted that $M_{ult(method)}/M_{ult(analytical)}$ obtained for the six beams using Method 2 were relatively high with an average value of 1.008 and a standard deviation of 0.094. In some cases, the moment capacity of the beams were noted to be over-estimated by up to thirteen percent (i.e. Beam T3). This indicated that the ultimate strength of an externally post-tensioned structure may be non-conservative when more accurate estimates for the stress increases in tendons are considered while the eccentricity variations of the external tendons are neglected in the sectional analysis.

In Method 3, both $\Delta f_{ps(ult)}$ and $\Delta_{eccen(ult)}$ were taken to be equal to $\Delta f_{ps(limit)}$ and $\Delta_{eccen(limit)}$ which were derived from analyses conducted with the proposed non-linear models. The average $M_{ult(method)}/M_{ult(analytical)}$ obtained from this method was about 0.795 with a standard deviation of 0.044. The ultimate moments were under-estimated by about twenty percent when this approach was used because Method 3 produced estimations for the material limit moment M_{limit} instead of the maximum moment capacity M_{max} (explained in Chapter Six). However, the results obtained from this method produced the least variation. This therefore indicated that, even though $\Delta f_{ps(limit)}$ and $\Delta_{eccen(limit)}$ can be accurately estimated, the maximum moment capacity predicted using sectional analysis may still be under-estimated if the material limit moment is lower than the maximum moment.

7.3 Concluding Remarks

In this chapter, the applicability and relative accuracy of using sectional analysis (BD 58/94 (1995), AASHTO (1989) and ACI (1983)) and non-linear analysis (proposed analytical model) to predict the ultimate flexural behaviour of externally prestressed structures were investigated.

When sectional analysis is used to determine the ultimate flexural response of externally prestressed structures, the change in prestress $\Delta f_{ps(ult)}$ and eccentricity variations $\Delta_{eccen(ult)}$ of the tendons at ultimate need to be estimated first. BD 58/94 (1995) recommends a zero stress increase, but gives no guidelines for the estimation of the eccentricity variations $\Delta_{eccen(ult)}$. It was found that using the specifications given by BD 58/94 (1995) generally under-estimated the flexural strength of these beams

(often by as much as twenty percent). However, because $\Delta_{eccen(ult)}$ was not considered in the analysis, it was found that the flexural strength can still be sometimes over-estimated, despite the use of the conservative assumption $\Delta f_{ps(ult)} = 0$.

Great variations in the accuracy of the results were observed when the American codes of practice, i.e. AASHTO (1989) and ACI (1983), were used to estimate the flexural strength of externally prestressed structures. For AASHTO (1989), $\Delta f_{ps(ult)}$ was recommended to be of a fixed value, i.e. 103 N/mm^2 while, ACI (1983) suggested two equations (i.e. Equations (2.2) and (2.3)) for the estimation of $\Delta f_{ps(ult)}$. However, as shown in Chapter Six, because $\Delta f_{ps(ult)}$ varies greatly for different externally prestressed beams and is dependent on several parameters which are inter-dependent on each other, it could not realistically be represented by a single value or a simple expression for all cases considered. It should be noted that the flexural response of externally prestressed beams can be greatly over-estimated by these two codes of practice, especially for beams with high span-depth ratio and non-prestressed reinforcement, because they do not take into account the loss of lever arm in the analysis due to second-order effects.

It was also shown here that even if the stress increase $\Delta f_{ps(ult)}$ and eccentricity variations $\Delta_{eccen(ult)}$ can be accurately estimated and used for the sectional analysis, the derived ultimate moment capacity of the beam can still be greatly under-estimated. This is because the calculated moment derived from such an analysis is actually the material limit moment and, as shown in Chapter Six, there is a possibility for the material limit moment to be very much smaller than the maximum moment capacity of the beam. Hence it is concluded here that, although the sectional analysis suggested in the codes of practice is easy to apply, it does not always give an accurate estimation for the ultimate strength of externally prestressed structures.

The proposed non-linear model was shown here to give the best estimation for the ultimate strength of these externally prestressed beams (under-estimating it by less than eight percent with the least variation). Hence, it is proposed here that non-linear models of the type introduced in Chapter Four be used for the prediction of ultimate flexural behaviour in order to ensure safe yet economical design of externally prestressed structures.

Beam no.	$M_{ult}/f_{cu}bd^2$					M_{pred}/M_{exp}			
	Experiment	BD 58/94	AASHTO	ACI	Analytical	BD 58/94	AASHTO	ACI	Analytical
OS-1	0.132	0.117	0.152	0.148	0.119	0.889	1.152	1.120	0.902
0L-1	0.096	0.121	0.157	0.150	0.095	1.259	1.632	1.558	0.990
OA88-2	0.124	0.088	0.101	0.103	0.117	0.710	0.815	0.828	0.944
OB88-1	0.100	0.076	0.084	0.088	0.102	0.760	0.844	0.875	1.020
OC88-1	0.276	0.192	0.220	0.221	0.259	0.697	0.797	0.802	0.938
OC88-2	0.293	0.191	0.237	0.235	0.256	0.651	0.809	0.802	0.874
OD88-1	0.293	0.204	0.262	0.263	0.277	0.695	0.894	0.898	0.945
	M_{ult} (kNm)					M_{pred}/M_{exp}			
	Experiment	BD 58/94	AASHTO	ACI	Analytical	BD 58/94	AASHTO	ACI	Analytical
OA-1	177.500	153.856	182.800	182.700	155.080	0.867	1.030	1.029	0.874
OB-1	212.500	188.116	222.960	223.457	190.570	0.885	1.049	1.052	0.897
OC-1	281.680	223.288	301.200	301.397	231.680	0.793	1.069	1.070	0.822
A1-2	201.000	141.908	175.878	169.934	173.530	0.706	0.875	0.845	0.863
A2-1	229.000	156.519	192.014	184.770	205.400	0.683	0.838	0.807	0.897
A2-2	205.000	159.031	184.337	175.086	197.097	0.776	0.899	0.854	0.961
A3-2	229.670	181.183	219.731	212.239	216.272	0.789	0.957	0.924	0.942
B1-2	230.000	148.960	170.198	165.879	211.938	0.648	0.740	0.721	0.921
B2-2	222.000	162.640	181.862	175.095	219.724	0.733	0.819	0.789	0.990
B3-2	230.000	196.059	215.748	214.588	215.449	0.852	0.938	0.933	0.937
				Average		**0.788**	**0.951**	**0.936**	**0.924**
				Standard Deviation		**0.141**	**0.202**	**0.190**	**0.050**

Table 7.1: The ultimate moments derived for beams used in verification process.

Beam no.	M_{ult} (kNm)				$M_{ult(code)}/M_{ult(analytical)}$		
	Model	BD 58/94	AASHTO	ACI	BD 58/94	AASHTO	ACI
T1	91901	80698	89045	87749	0.878	0.969	0.955
T2	25556	23816	26077	25553	0.932	1.020	1.000
T3	29129	26181	28962	28317	0.899	0.994	0.972
T4	57132	38298	42538	41846	0.670	0.745	0.732
T5	43787	31399	34808	34252	0.717	0.795	0.782
T6	134100	108270	108037	106650	0.807	0.806	0.795
			Average		**0.817**	**0.888**	**0.873**
			Standard Deviation		**0.096**	**0.109**	**0.105**

Table 7.2: Comparing the ultimate moments derived for Beams T1 to T6.

Beam no.	M_{ult} (kNm)				$M_{ult(method)}/M_{ult(analytical)}$		
	Model	Method 1	Method 2	Method 3	Method 1	Method 2	Method 3
T1	91901	80697	93705	66640	0.878	1.020	0.725
T2	25556	23816	27797	20037	0.932	1.088	0.784
T3	29129	26181	32773	24962	0.899	1.125	0.857
T4	57132	38298	56047	48307	0.670	0.981	0.846
T5	43787	31399	43924	34141	0.717	1.003	0.780
T6	134100	108270	111134	104765	0.807	0.829	0.781
			Average		0.817	1.008	0.795
			Standard Deviation		0.096	0.094	0.044

Note:

Method 1: Conducted with $\Delta f_{ps(ult)} = 0$ and $\Delta_{eccen(ult)}$ not considered.

Method 2: Conducted with $\Delta f_{ps(ult)}$ = evaluated from proposed models and $\Delta_{eccen(ult)}$ not considered.

Method 3: Conducted with $\Delta f_{ps(ult)}$ and $\Delta_{eccen(ult)}$ evaluated from proposed models.

Table 7.3: Comparing moments derived for Beams T1 to T6 using different method of analysis.

Chapter 8

Conclusions and Recommendations for Future Work

8.1 Conclusions

Due to the corrosion problems encountered with conventional internally bonded post-tensioned structures, the Department of Transport in the United Kingdom has, until very recently, discouraged the use of these structures for the construction of new bridges. As a preferred alternative, the UK DoT has suggested that externally post-tensioned structures be used instead, the principal reasons for this being that they allow easy maintenance and monitoring of tendons for corrosion problems. The flexural behaviour of externally prestressed structures is however very different from internally bonded ones due to the lack of bond between the tendons and the concrete. As such, this research investigation is concerned with the ultimate flexural response of externally prestressed structures and the following are the principal conclusions derived from the study:

1) The study revealed that the design of externally prestressed beams is often controlled by the ultimate limit state behaviour, hence an accurate method used to predict the ultimate strength is essential for deriving safe and economical design of such structures.

2) The finite element method was found to be unattractive for use as a design or research tool for the estimation of the ultimate behaviour of externally prestressed structures. Large amounts of computing power and time were found to be required to derive reasonably good solutions for relatively simple elastic models. The problem is likely to be exacerbated by the introduction of non-linear material models and the need to consider concrete cracking,

opening of joints, large deflections and redistribution of prestress due to slippage at the deviators.

3) The eight non-linear analytical models utilising the strain compatibility concept proposed here were found to show excellent correlation to the experimental results in terms of moment-deflection and moment-change in prestress relationships over the full range. They also predicted the maximum flexural strength of externally prestressed beams conservatively with an average error of only eight percent and with very small variations. Hence they are recommended to be used for the estimation of the flexural response of these structures to collapse.

4) Using the recommendations given by BD 58/94 (1995) to predict the ultimate flexural strength of externally prestressed beams would generally under-estimate the ultimate strength by about twenty percent, although it is also possible in some cases (e.g. beams with very high span depth ratio) to over-estimate the ultimate strength because second-order effects are not considered.

5) The design recommendations given by AASHTO (1989) and ACI (1983) were found to give reasonably good estimation for the flexural strength of such beams. However, large variations in the results were noted as the methods tended to over-estimate the ultimate behaviour for beams with large span-depth ratios and reinforcement ratios.

6) The ultimate moment capacity derived for an externally post-tensioned beam using sectional analysis method can still be under-estimated even when accurate values for the change in prestress and the eccentricity variation at the material limit conditions are used. This is because the derived material limit moment is sometimes lower than the maximum capacity of the beam.

7) The effect of shear deformation was found to have varying degrees of influence on the flexural performance of externally prestressed structures and can be satisfactorily considered in the analytical models by using the displaced moment concept introduced by Park and Paulay (1975).

8) Tension stiffening effects can be neglected in the proposed analytical models because an improvement in accuracies of approximately three to four percent is not justified by an increase in the computing time by a factor of two.

9) The frictional slippage model introduced here provides a rational method for considering slippage of tendons and re-distribution of stresses between deviators in the analytical models.

10) For beams with deviators incorporated along their span, the assumption that the tendons are slipping freely at the deviators would produce a conservative estimate for the flexural strength of externally prestressed structures with minimum variations in the results, and require very little additional computing time to produce the solutions.

11) For externally prestressed beams with low reinforcement ratios (e.g. 0.15% to 0.5%), a tied arch mechanism forms immediately after the occurrence of first cracking. In some beams, the formation of such a mechanism may lead to instantaneous collapse. Increasing the amount of reinforcement in these beams will improve their overall flexural performance and prevent this type of failure from occurring.

12) Although increasing the amount of non-prestressed reinforcement will generally lead to an increase in the flexural strength of externally prestressed structures, the rate of increase was noted to be different for different beam configurations.

13) The maximum moment decreases with increases in the span-depth ratio for structures with no deviators placed in their span. The rate of decrease of the maximum moment with the increase of span-depth ratio was found to be greater for beams with higher non-prestressed reinforcement ratios. Incorporating deviators along the span of these structures would reduce the loss of flexural strength by controlling the high changes in the eccentricity of the tendons.

14) It was also observed that structures having lower free length to depth ratios at their critical sections exhibited higher moment capacities.

15) Higher levels of initial prestress force were generally found to increase the strength of externally prestressed structures. The increase in flexural strength with an increase in initial prestress force is, however, dependent on the amount of non-prestressed reinforcement specified in the structure, being lower for beams with higher reinforcement ratios. Hence it is usually very difficult to decide on the most efficient combination of prestressing force and non-prestressed reinforcement ratio to be used.

16) Increasing the prestressing steel area in externally prestressed structures without changing the initial prestress force applied to the structure causes an increase in the flexural strength. However, the improvement was found here to be too small to be considered economical for practical purposes.

17) It was observed that the values of change in prestress and eccentricity variation at the material limit condition vary too greatly with parameters such as span-depth ratio, non-prestressed reinforcement ratio, prestressed reinforcement and initial prestressing force. The influence of these parameters was also found to be inter-dependent on each other. Hence it is very difficult (if not impossible) to introduce a single value or simple expression to estimate these variables accurately for all the cases considered.

8.2 Recommendations for Future Work

The following investigations are recommended as a useful extension to this investigation:

1) As continuous structures are more commonly used for bridge construction than simply supported structures, the proposed non-linear models described in Chapter Four should be extended to evaluate continuous externally post-tensioned structures. The derived analytical model would need to be verified by comparing its results with those obtained from experimental investigations.

2) In the present investigation, it was found that premature termination of the analysis was possible when the proposed non-linear models were used to estimate the flexural response of some externally prestressed structures (see Section 5.4). This premature termination was due mainly to the large beam

deflections occurring near ultimate conditions which makes estimating the stress increment in the external tendons very difficult. Hence further study is required to understand more about this numerical problem and to suggest a more robust algorithm to be included into the proposed models.

3) The non-linear models should be extended to allow segmental concrete elements with dry or epoxy coated joints to be analysed. This will require the development of additional routines to model crack formation and the opening of joints between the segments. Such a study is considered to be useful because this method of bridge construction is used extensively in modern bridge construction.

4) In the present investigation, it was found that the change in prestress and the eccentricity variation at the material limit state cannot be accurately represented by a single value or estimated by a simple equation for all cases of beam configuration considered. However, since the values of these variables were found to be related to the deflection response of these structures, it may be possible to produce some design charts that allow these values to be predicted accurately. This would involve extensive simulations of many externally prestressed beams with different beam configurations using the proposed non-linear models. Such a development would permit the simple sectional analyses currently favoured by design codes to be used to provide more cost effective solutions.

References

AASHTO (1983), 'Standard Specifications for Highway Bridges', American Associate of State Highway and Transportation Officials, Thirteenth Edition, Washington, D.C.

AASHTO (1989), 'Guide Specifications for Design and Construction of Segmental Concrete Bridges', American Association of State Highways and Transportation Officials, United States.

ACI 318-83 (1983), 'Building Code Requirements for Reinforced Concrete (ACI 318-83)' , ACI Committee, American Concrete Institute, Detroit, Michigan, pp. 111.

Ahmad, S.H. (1981), 'Properties of Confined Concrete Subjected to Static and Dynamic Loading', PhD Thesis, Department of Materials Engineering, University of Illinois at Chicago, March 1981, pp. 342.

Alkhairi, F.M. (1991), 'On the flexural behaviour of concrete beams prestressed with unbonded internal and external tendons', PhD dissertation, University of Michigan, Ann Arbor, Mich.

BA 58/94 (1995), 'The Design of Concrete Highway Bridges and Structures with External and Unbonded Prestressing', The Department of Transport, Volume 1, Section 3, Part 10, United Kingdom, November.

Balaguru, P.N. (1981), 'Increase of stress in unbonded tendons in prestressed concrete beams and slabs', Canadian Journal of Civil Engineers, Vol. 8, pp. 262-268.

Baker, A.L.L. (1949), 'A Plastic Theory of Design for Ordinary Reinforced and Prestressed Concrete, Including Moment Redistribution in Continuous Members', Magazine of Concrete Research, London, Vol. 1, No. 2, June, pp. 57-66.

Baker, A.L.L. (1951), 'Recent Research in Reinforced Concrete and its Application to Design', Journal, Institute of Civil Engineers, London, Vol. 35, No. 4, February, pp. 262-329.

BD 58/94 (1995), 'The Design of Concrete Highway Bridges and Structures with External and Unbonded Prestressing', The Department of Transport, Volume 1, Section 3, Part 9, United Kingdom, November.

Billig, K. (1960), 'Structural Concrete', Macmillan & Co. Ltd., New York, pp 334 - 363.

Burns, N.H., Helwig, T. and Tsujimoto, T. (1991), 'Effective Prestress Force in Continuous Post-Tensioned Beams with Unbonded Tendons', ACI Structural Journal, Vol. 88, No. 1, January-February, pp. 84-90.

BS8110 (1985), 'Structural Use of Concrete', British Standards Institution, clause 4.3.7.3, London.

BS5400 (Part 2) (1990), 'Part 2: Specification for loads', British Standards Institutions.

BS5400 (Part 4) (1990), 'Part 4: Code of practice for design of concrete bridges', British Standards Institutions.

Campbell, T.I. and Chouinard, K.L. (1991), 'Influence of Non-prestressed Reinforcement on Strength of Unbonded Partially Prestressed Concrete Members', ACI Structural Journal, Vol. 88, No. 5, September-October, pp. 546-551.

Canadian Standard Association (1984), 'Design of concrete structures for buildings', CAN3-A23.3-M84, Rexdale, Ontario.

CEB-FIP (1978), 'Model Code for Concrete Structures (MC-78)', Lausanne, 1978

Chen W.F. (1982), 'Plasticity in reinforced concrete', McGraw-Hill Book Co., New York.

Chirgwin, B.H., Plumpton, C., 'A course of mathematics for Engineers and Scientists', Vol. 3, Pergarmom Press, Oxford, 1978.

Cooke, N., Park, R. and Yong, P. (1981), 'Flexural Strength of Prestressed Concrete Members with Unbonded Tendons', PCI Journal, November-December, pp. 52-80.

Crisfield, M.A. (1991), 'Non-linear finite element analysis of solids and structures', John Wiley and Sons, Singapore, pp. 253-333.

Dutch Code (1984), 'Voorschriften Beton VB', (NEN 3880), Part H, Section 503.1.3.

German Code (1980), 'Spannbeton, Bauteile mit Vorspannung ohne Verbund', (DIN 4227), Teil 6, Entwurf.

Ghali, A. (1993), 'Deflection of Reinforced Concrete Members: a Critical Review' ACI Structural Journal, July-August, Vol. 90, No. 4, pp. 364-373.

Gifford, F.W. (1954), 'The Design of Simply Supported Prestressed Concrete Beams for Ultimate Loads', Proceedings, Institution of Civil Engineers, London, Part III, Vol. 3, No. 1, April, pp. 125-143.

Harajli, M.H. (1990), 'Effect of Span-Depth Ratio on the Ultimate Steel Stress in Unbonded Prestressed Concrete Members', ACI Structural Journal, Vol. 87, No. 3, May-Jun, pp. 305-312.

Harajli, M.H. and Hijazi, S.M. (1991), 'Evaluation of the Ultimate Steel Stress in Partially Prestressed Concrete Members', PCI Journal, Vol. 36, No. 1, January-February, pp. 62-81.

Harajli, M.H. and Kanji M.Y. (1992), 'Service load behaviour of concrete members prestressed with unbonded tendons', Journal of Structural Engineering, Vol. 118, No. 9, September, pp. 2569-2589.

Hewson, N. (1992), 'The use of dry joints between precast segments for bridges', Proceedings of the Institution of Civil Engineers and Engineering, November, pp. 177-184.

Hewson, N.R. (1993), 'The use of external tendons for the Bangkok Second Stage Expressway', Structural Engineer, Vol. 71, No. 23-24, December, pp 412-215.

Hindi, A., MacGregor, R., Kreger, M.E. and Breen, J.E. (1995), 'Enhancing Strength and Ductility of Post-Tensioned Segmental Box Girder Bridges', ACI Structural Journal, Vol. 92, No. 1, January and February.

I'vanyi, G., Buschmeyer, W. and Muller, R.A. (1985), 'Additional strains in unbonded tendons during loading', Magazine of Concrete Research, Vol. 37, No. 137, March, pp. 39-43.

Jackson, P. (1994), 'Design rules for Unbonded Prestress,' The society of Concrete Bridge Development Group, Durable Post-Tensioned Concrete Bridges Seminar, 18 May, pp. 65-72.

Janney, J.R., Hognestad, E. and McHenry, D. (1956), 'Ultimate Flexural Strength of prestressed and Conventionally Reinforced concrete beams', ACI Journal, Proceedings Vol. 52, No. 6, February, pp. 601-620.

Jungwirth, D., Breidenbruch, R., Hochreither, H and. Nutzel, O. (1993), 'External Prestressing', FIP Symposium'93, Kyoto, Japan, Oct., pp. 853-860.

Lacroix, R. and Jartoux, P. (1994), 'The Intermediate Blocking Device for External Prestressing: A New Development of Unbonded Tendons with Protection by Soft Materials', FIP-XIIth Congress, FIP' 94 Symposium, Washington, pp. 83-85.

Lin, T.Y.and Burns, N.H. (1982), 'Design of prestressing structures', Third edition, John Wiley and Sons, New York.

MacGregor, R.J.G. and Kreger M.E. (1989), 'Strength and Ductility of a Three-span Externally Post-Tensioned Segmental Box-Girder Model' PhD dissertation, University of Texas at Austin.

MacGregor, R.J.G., Kreger, M.E., Breen, J.E. (1989), 'Strength and Ductility of a Three-Span Externally Post-Tensioned Segmental Box-Girder Bridge Model', Research Report 365-3F, Project 3-5-85/8-365, Centre for Transportation Research, Bureau of Engineering Research, The University of Texas at Austin, January.

Mattock, A.H., Yamakazi, J. and Kattula, B.T. (1971), 'Comparative Study of Prestressed Concrete Beams, With and Without Bond', ACI (Proceedings American Concrete Institute), Vol. 68, No. 2, February, pp. 116-125.

Mojtahedi, S. and Gamble, M.L. (1978), 'Ultimate Steel Stresses in Unbonded Prestressed Concrete', Proceedings of the ASCE, Vol. 104, No. ST7, July, pp. 1159-1165

Mosley, W.H. and Bungey, J.H. (1990), 'Reinforced Concrete Design', Fourth edition, Macmillan, Hong Kong, pp 367-372

Muller, J. and Gauthier, Y. (1990), 'Ultimate Behaviour of Precast Segmental Box Girders with External Tendons', ACI, SP-120: External Prestressing in Bridges, American Concrete Institute (ACI), Detroit, Michigan, pp. 355-374.

Naaman, A.E. (1982), 'Prestressed Concrete and Design, Fundamentals', McGraw Hill, United States.

Naaman, A.E. (1990), 'A new methodology for the analysis of beams prestressed with external tendons', External Prestressing in Bridges; SP120-16, A.E.Naaman and J.E. Breen, eds., the American Concrete Institute (ACI), Detroit, Mich., pp. 339-354.

Naaman, A.E. and Alkhairi, F.M. (1991), 'Stress at Ultimate in Unbonded Post-tensioning Tendons: Part 1 - Evaluation of the state-of-the-art', ACI Structural Journal, Vol. 88, No. 5, pp. 641-651.

Naaman, A.E. and Alkhairi, F.M. (1991), 'Stress at Ultimate in Unbonded Post-tensioning Tendons: Part 2 - Proposed Methodology', ACI Structural Journal, Vol. 88, No. 6, pp. 683-692.

Naaman, A.E. and Alkhairi, F.M. (1993), 'Analysis of Beams Prestressed with unbonded Internal or External Tendons', Journal of Structural Engineers, ASCE, Vol. 119, No. 9, September, pp. 2680-2699.

Naaman, A.E. and Harajli, M.H. (1985), 'Evaluation of Ultimate Steel Stress in Partially Prestressed Flexural Members', PCI Journals, Sept.-Oct., pp. 54-81.

Naaman, A.E. (1994), 'The new AASHTO recommendations on reinforcement limits for reinforced, prestressed, and partially prestressed concrete (RN 120), FIP Symposium, XIIth International Congress, Washington, May-June, pp. G52-G57.

Park, R. and and Paulay, T. (1975), 'Reinforced concrete structures', John Wiley & Sons , New York.

Powell, L.C., Breen, J.E.and Kreger, M.E. (1988), 'State of the Art Externally Post-Tensioned Bridges with Deviators', Research Report 365-1, Centre for Transportation Research, Bureau of Engineering Research, The University of Texas at Austin, June.

Press, W.H., Teukolsky, S.A., Vetterling, W.T., Flannery, B.P. (1986), 'Numerical Recipes in FORTRAN, The Art of Scientific Computing', Second Edition, Cambridge University Press, USA.

Raiss, M. (1995), 'Post-tensioned concrete bridges: the UK debate', Concrete, Mar./Apr., pp. 23-26.

Ramos, G. (1994), 'Mordelisation du comportement en servicio, prerotura y rotura de puentes de hormigon con pretensado exterior', PhD dissertation, E.T.S. Ingenieros de Caminos, Canales y Puertos, Universidad Politecnica de Cataluna, Barcelona, Spain.

Ramos, G. and Aparicio, A.C. (1995), 'Ultimate Behaviour of Externally Prestressed Concrete Bridges', Structural Engineering International, Vol.5, No. 3, pp. 172-177.

Ramos, G. and Aparicio, A.C. (1996), 'Ultimate Analysis of Monolithic and Segmental Externally Prestressed Concrete Bridges', ASCE, Journal of Bridge Engineering, Vol. 1, No. 1, February, pp. 10-17.

Ramos, G. and Aparicio, A.C. (1996), 'Flexural Strength of Externally Prestressed Concrete Bridges', Paper accepted for publishing at the ACI structural Journal.

Report No. SR479 (1991), 'Report on the instrumentation of a trial bridge span for the SES project, Bangkok, Thailand', Kumgai Gumi Co. Ltd., Unpublished report, Thailand.

Rubakantha, S. and Daly, A. (1994), 'E516A/BD: The use of unbonded tendons in bridge construction', Transport Research Laboratory, Unpublished report, U.K.

Saenz (1964), 'Discussion of equation for the stress-strain curve of concrete by Desayi and Krsihman', Journal of American Concrete Institute, Vol. 61, Sept., pp. 1229 - 1235.

Service d'Etudes Techniques des Rouutes et Autoroutes (SETRA) (1990), 'External Prestressing', Working Party Report.

Sowlat, K., Rabbat, B.G. (1987), 'Testing of Segmental Concrete Girders with External Tendons', PCI Journal, Prestressed Concrete Institute, Vol. 32, No. 2, March-April, pp. 87-107.

Sun, B.J. (1991), 'Comments on Harajli's paper: Evaluation of the Ultimate Steel Stress in Partially Prestressed Concrete Members', PCI Journal, Readers Comments, September-October, pp 91-95.

Swiss Code (1979), 'Ultimate Load Behaviour of Slabs', SIA 162, Working Party 5.

Takebayashi, T., Kitayama, H., Hewson, N.R. and Fox, P.D. (1993), ' Bangkok Second Stage Expressway The Use of External Tendons and Dry Joints with Precast Segmental Construction', FIP Symposium '93, Kyoto, Japan, October, pp. 943-950.

Takebayashi, T., Deeprasertwong, K., Honda, B.T., Umeki, H. And Kumasaka, T. (1993), 'Full Scale Testing of a Precast Concrete Segmental Bridge with External Tendons and Dry Joints', FIP Symposium '93, Kyoto, Japan, October, pp. 1145-1152.

Takebayashi, T., Deeprasertwong, K.and Leung, Y.W. (1994), 'A full-scale destructive test of a precast segmental box girder bridge with dry joints and external tendons', Proceedings for Institution of Civil Engineers and Structural and Buildings, 104, August, pp. 297-315.

Tam, A. and Pannell, F.N. (1976), ' The ultimate moment of resistance of unbonded partially prestressed reinforced concrete beams', Magazine of Concrete Research, Vol. 28, no. 97, December, pp. 203-208.

Tan, K.H. and Naaman, A.E. (1993), 'Strut-and-Tie Model for Externally Prestressed Concrete Beams', ACI Structural Journal, Vol. 90, No. 6, November, pp. 683-691.

Tao, X. And Du, G. (1985), 'Ultimate Stress of Unbonded Tendons in Partially Prestressed Concrete Beams', PCI Journal, Prestressed Concrete Institute, , Vol. 30, No. 6, Nov.-Dec., pp. 72-90.

Virlogeux, M. (1988), 'Non-linear Analysis of Externally Prestressed Structures', Proceedings of the FIP Symposium, Israel, pp 319-340.

Virlogeux, M. (1993), 'External Prestressing in Bridges', FIP Symposium'93, Kyoto, Japan, Oct., pp. 843-852.

Wang, P.T. (1977), 'Complete Stress-Strain Curve of Concrete and its Effect on Ductility of Reinforced Concrete Members', PhD Thesis, University of Illinois at Chicago Circle, Chicago, pp. 257.

Warwaruk, J., Sozen, M.A. and Siess, C.P. (1962), 'Investigation of Prestressed Reinforced Concrete for Highway Bridges, Part III: Strength and Behaviour in Flexure of Prestressed Concrete Beams', Bulletin No. 464, University of Illinois Engineering Experiment Station, Urbana, August, pp 105.

Wieland, M. (1990), 'Ultimate Load of Simply Supported Segmental Viaduct with External Post-Tensioning', Second Stage Expressway Project, Expressway and Rapid Transit Authority of Thailand, Unpublished Report.

Winkler, N. and Zenobi, G. (1993), 'External Prestressing for Bridges, Buildings and Other structures in practice', FIP Symposium'93, Kyoto, Japan, Oct., pp. 899-906.

Woodward, R.J. and Williams, F.W. (1988), 'Collapse of Ynys-y-Gwas Bridge', West Glamorgan, Proceedings of the Institution of Civil Engineers, Pt. 1, Vol. 84, August, pp. 635-669.

Wong L.H. (1993), "State-of-the-Art for External Post-tensioning", Research report 1, Unpublished report, University of Sheffield.

Wong L.H. (1994(a)), "Stress at the Ultimate in Unbonded Post-tensioned Tendons: Evaluation of the State-of-the-Art", Research report 2, Unpublished report, University of Sheffield.

Wong L.H. (1994(b)), "Preliminary Study on the Frictional Effects on Externally Post-tensioned Structures", Research report 3, Unpublished report, University of Sheffield.

Wong L.H. (1994(c)), "Study on the Stress Increase History for Externally Prestressed Structures", Research report 4, Unpublished report, University of Sheffield.

Wong L.H. (1994(d)), "Finite Element Modelling with ANSYS", Research report 5, Unpublished report, University of Sheffield.

Wong L.H. (1994(e)), "Comparative Study on the Design of Post-Tensioned Structures", Research report 6, Unpublished report, University of Sheffield.

Wong L.H. (1995(a)), "Research Manual: Ultimate Behaviour of Externally Post-Tensioned Structures", Research report 7, Unpublished report, University of Sheffield.

Wong L.H. (1995(b)), "Non-linear Analytical Model for Externally Post-tensioned Structures: EXTPRE1 (Version 1)", Research report 8, Unpublished report, University of Sheffield.

Wong L.H. (1997), "Non-linear Analytical Model Manual", Research report 9, Unpublished report, University of Sheffield.

Yaginuma, Y. And Kitada (1987), Y., 'Mechanical Behaviour of Partially Prestressed Concrete Beams with Exterior Cables', Transaction of the Japan Concrete Institute, Vol. 9, pp. 351-359.

Yaginuma, Y. And Kitada, Y. (1988), 'Influence of Span on the Behaviour of Partially Prestressed Concrete Beams with Exterior Cables', Transaction of the Japan Concrete Institute, Vol. 10, pp. 409-417.

Yaginuma, Y. And Kitada, Y. (1989), 'Flexural Behaviour of Partially Prestressed Beams with Exterior Cables', Transaction of the Japan Concrete Institute, Vol. 11, pp. 409-417.

Yaginuma, Y. (1993), 'Ultimate strength of PPC beams with Exterior Cables 'FIP Symposium '93, Japan, October, , pp. 915-926

Zhang, Z., Niu, B. and Sun, L. (1993), 'Ultimate Strength of Externally Prestressed Concrete Structures', FIP Symposium '93, Japan, pp. 907-914.

Appendix A

Beams used in Verification Process

Test Beams taken from Yaginuma and Kitada (1987,1988, 1989)

Cross-sectional properties, span detail and concrete properties:

Beam	Cross-sectional properties					Span detail		Concrete Properties		
	b_w (mm)	d (mm)	d_s (mm)	d'_s (mm)	e_{mid}	ℓ (m)	ℓ_{load} (m)	f_{cu} (N/mm^2)	f_r (N/mm^2)	E_c (KN/mm^2)
Yaginuma and Kitada (1988)										
OS-1	60	100	90	0	17	1.60	0.80	42.10	4.30	32.65
OL-1	60	100	90	0	17	2.80	1.40	42.10	4.30	32.65
Yaginuma and Kitada (1989)										
OA88-2	150	240	210	30	40	2.70	1.35	43.10	3.98	33.07
OB88-1	150	240	210	30	40	2.70	1.35	43.10	3.98	33.07
OC88-1	150	240	210	30	40	2.70	1.35	43.10	3.98	33.07
OC88-2	150	240	210	30	40	2.70	1.35	43.10	3.98	33.07
OD88-1	150	240	210	30	40	2.70	1.35	43.10	3.98	33.07
Yaginuma and Kitada (1987)										
OA-1	250	400	350	50	67	4.00	2.00	31.98	3.77	28.46
OB-1	250	400	350	50	67	4.00	2.00	31.98	3.77	28.46
OC-1	250	400	350	50	67	4.00	2.00	32.57	3.85	28.72

* See figures A.1(a) and A.1(b) for explaination of notation.

Reinforcement properties and prestress properties:

Beam	Reinforcement properties					Prestress properties				
	f_y (N/mm^2)	E_y (KN/mm^2)	A_s (mm^2)	A'_s (mm^2)	α_e	f_{py} (N/mm^2)	E_p (KN/mm^2)	A_{ps} (mm^2)	f_{pu} (N/mm^2)	JACK% %
Yaginuma and Kitada (1988)										
OS-1	460.00	205.20	56.55	0.00	6.28	977.71	198.51	132.95	1103.20	17.13
OL-1	460.00	205.20	56.55	0.00	6.28	977.71	198.51	132.95	1103.20	19.06
Yaginuma and Kitada (1989)										
OA88-2	413.00	195.00	157.10	157.10	5.90	1140.00	205.00	265.50	1170.00	51.50
OB88-1	353.00	199.00	265.60	157.10	6.03	1150.00	205.00	132.95	1170.00	25.71
OC88-1	361.00	203.00	981.70	157.10	6.14	1140.00	205.00	265.50	1170.00	25.75
OC88-2	361.00	203.00	981.70	157.10	6.14	1140.00	205.00	265.50	1170.00	51.50
OD88-1	348.00	194.00	1321.04	157.10	5.87	1150.00	205.00	132.95	1170.00	51.43
Yaginuma and Kitada (1987)										
OA-1	460.00	205.20	567.06	157.10	7.21	977.71	198.51	830.95	1103.20	47.44
OB-1	361.00	203.00	981.70	157.10	7.13	977.71	198.51	830.95	1103.20	47.44
OC-1	460.00	205.20	1924.23	157.10	7.14	977.71	198.51	830.95	1103.20	47.44

Typical cross section and beam layout:

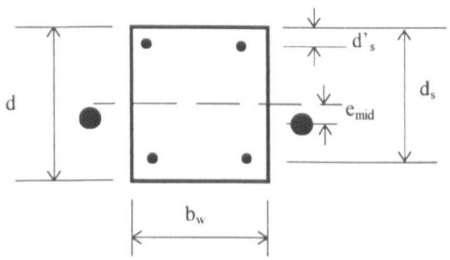

Figure A.1(a): Typical cross-section

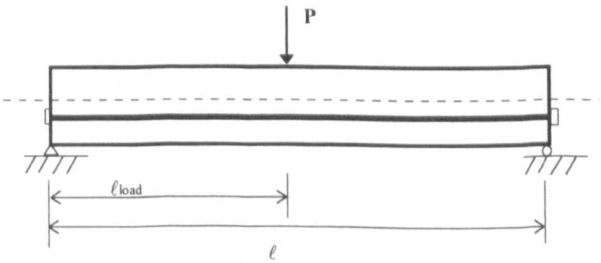

Figure A.1(b): Typical beam layout

Test Beams taken from Zhang *et al* (1993)

Cross-sectional properties, span detail and concrete properties:

Beam	Cross-sectional properties				Span detail			Concrete Properties		
	x (mm)	d_s (mm)	d'_s (mm)	e_{mid} (mm)	Load type**	Tendon profile***	ℓ (m)	f_{cu} (N/mm^2)	f_r (N/mm^2)	E_c (KN/mm^2)
Zhang *et al* (1993)										
A1-2	291.53	410.00	40.00	191.53	2	1	5.00	52.30	4.50	36.39
A2-1	290.23	370.00	40.00	190.23	1	1	5.00	49.80	4.39	35.51
A2-2	290.23	370.00	40.00	190.23	2	1	5.00	49.80	4.39	35.51
A3-2	188.33	383.70	40.00	161.67	2	1	5.00	52.60	4.52	36.50
B1-2	291.27	390.00	40.00	216.27	2	2	5.00	52.70	4.52	36.53
B2-2	290.34	410.00	40.00	215.34	2	2	5.00	52.70	4.52	36.53
B3-2	287.59	390.00	40.00	212.59	2	2	5.00	49.30	4.37	35.33

* See figure A.2(a) for explaination of notation.

** Figures A.2(b) and A.2(c) show the arrangement of Load Type 1 and 2 respectively.

*** Figures A.2(d) and A.2(e) show the arrangement of Tendon Profile 1 and 2 respectively.

Reinforcement properties and prestress properties:

Beam	Reinforcement properties					Prestress properties				
	f_y (N/mm^2)	E_y (KN/mm^2)	A_s (mm^2)	A'_s (mm^2)	α_e	f_{py} (N/mm^2)	E_p (KN/mm^2)	A_{ps} (mm^2)	f_{pu} (N/mm^2)	JACK% %
Zhang *et al* (1993)										
A1-2	340.00	200.00	157.08	235.62	5.50	977.71	198.51	981.74	1103.00	29.55
A2-1	340.00	200.00	235.62	235.62	5.63	977.71	198.51	981.74	1103.00	30.12
A2-2	340.00	200.00	235.62	235.62	5.63	977.71	198.51	981.74	1103.20	30.40
A3-2	340.00	200.00	358.14	235.62	5.48	977.71	198.51	981.74	1103.00	29.63
B1-2	340.00	200.00	157.08	235.62	5.47	1407.00	200.00	392.70	1655.00	48.68
B2-2	340.00	200.00	201.06	235.62	5.47	1407.00	200.00	392.70	1655.00	50.96
B3-2	340.00	200.00	402.12	235.62	5.66	1407.00	200.00	392.70	1655.00	49.68

Typical cross section and beam layout:

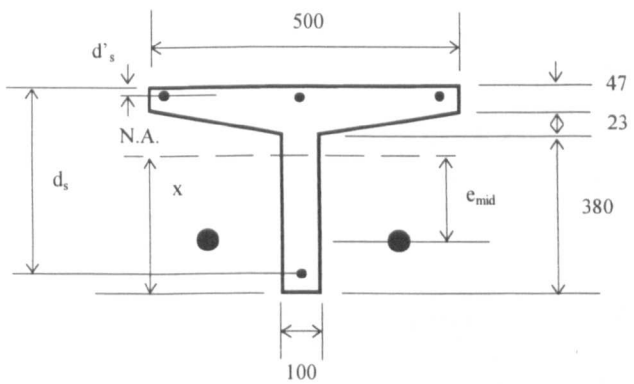

Figure A.2(a): Typical cross-section

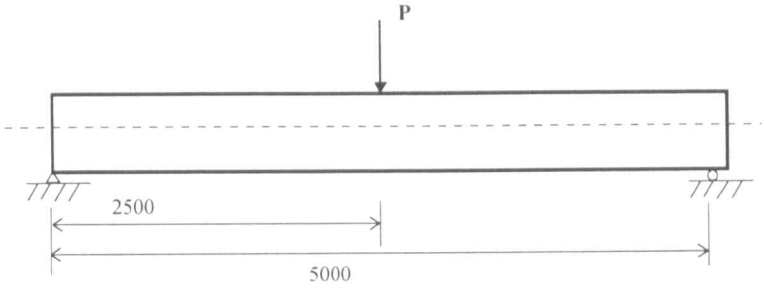

Figure A.2(b): Load Type 1

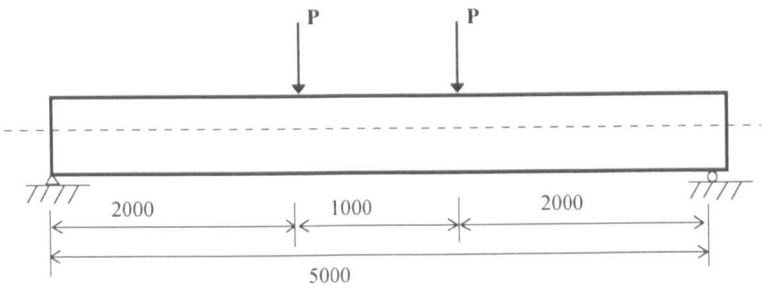

Figure A.2(c): Load Type 2

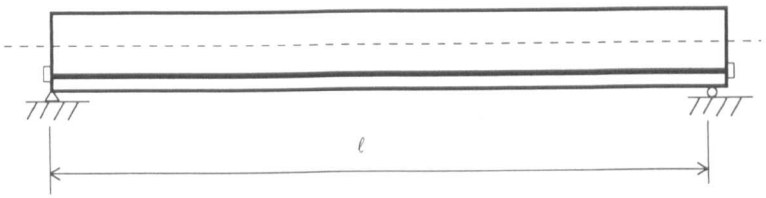

Figure A.2(d): Tendon Profile 1

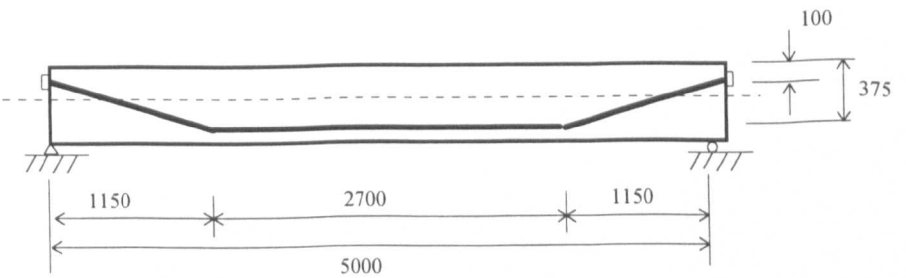

Figure A.2(e): Tendon Profile 2

Sample Input File 1

PROJECT: EXTERNAL 3
YAGINUMA TEST MODEL SERIAL 0S-1
NO. OF COORDINATE POINTS FOR INPUT (MAX. 50)
4
COORDINATES OF SECTION (ANTICLOCKWISE FROM A REFERENCE, MM)
0,0
30,0
30,100
0,100
INPUT IF VOID EXISTS (0/NO,1/YES)
0
IF EXTREME POINTS IN SECTION ARE TO BE DEFINED (0/NO,1/YES)
0
CONCRETE MATERIAL PROPERTIES MODEL DESIRED (1,2,3)
3
ULTIMATE STRAIN OF CONCRETE
0.0035
CONCRETE COMPRESSIVE STRENGTH (CUBE STR./CYLINDER STR.,N/MM^2)
42.1
MODULUS OF RUPTURE FOR CONCRETE (N/MM^2)(+VE INPUT)
4.3
STEEL MATERIAL PROPERTIES MODEL DESIRED (1,2)
2
STEEL STRENGTH (N/MM^2)
460
PRESTRESS STEEL PROPERTIES MODEL DESIRED (1,2)
2
TYPE OF PRESTRESS TYPE DESIRED (1,2,3)
3
PROPERTIES OF SPAN
SPAN (M)
1.6
NO. OF SEGMENTS FOR BEAM TO BE DIVIDED
20
CONCRETE DENSITY (KG/M^3)
2400
AUTOMATIC CALCULATION OF DEAD LOAD (YES/1,NO/0)
1
EXTERNAL LOAD TYPE (1,2,3)
2
PRESTRESS AREA (MM^2)
132.9
% JACKING FORCE (%)
17.13
PRESTRESS LOSSES (%)
0
ECCENTRICITY AT LHS ANCHORAGE (MM)
17
ECCENTRICITY AT RHS ANCHORAGE (MM)
17
DEPTH TO TENSILE REINFORCEMENT FROM TOP (MM)
90
AREA OF TENSILE STEEL (MM^2)
56.55
DEPTH TO COMPRESSIVE REINFORCEMENT FROM THE TOP (MM)
0.0
AREA OF COMPRESSIVE STEEL (MM^2)
0.0
MODULAR RATIO (ES/EC)
6.28
STRAIN INCREMENT AT POST-CRACK STATE (0.0001)
0.0001

Appendix B

Generic Beams used in Parametric Study

Typical Beams used in Parametric Study

Cross-sectional properties:

Beam	Cross-sectional properties							
	x (mm)	d (mm)	d_s (mm)	d'_s (mm)	d_b (mm)	b_b (mm)	b_w (mm)	e_{mid} (mm)
Typical beams used for parametric study								
T1	1682.14	3000.00	2890.00	110.00	350.00	4500.00	700.00	372.00
T2	963.21	1500.00	1390.00	110.00	250.00	4000.00	400.00	380.00
T3	963.21	1500.00	1390.00	110.00	250.00	4000.00	400.00	560.00
T4	1476.30	2500.00	2390.00	110.00	350.00	4000.00	400.00	600.00
T5	1476.30	2500.00	2390.00	110.00	350.00	4000.00	400.00	300.00
T6	1292.40	2400.00	2245.00	110.00	450.00	4500.00	600.00	595.00

* See figures B.1(a) for explaination of notation.

Concrete and reinforcement properties:

Beam	Concrete Properties			Reinforcement properties				
	f_{cu} (N/mm^2)	f_r (N/mm^2)	E_c (KN/mm^2)	f_y (N/mm^2)	E_y (KN/mm^2)	A_s (mm^2)	A'_s (mm^2)	α_e
Typical beams used for parametric study								
T1	60.00	4.82	38.98	460.00	205.20	3142.00	3142.00	5.26
T2	60.00	4.82	38.98	460.00	205.20	3142.00	3142.00	5.26
T3	60.00	4.82	38.98	460.00	205.20	3142.00	3142.00	5.26
T4	60.00	4.82	38.98	460.00	205.20	3142.00	3142.00	5.26
T5	60.00	4.82	38.98	460.00	205.20	3142.00	3142.00	5.26
T6	60.00	4.82	38.98	460.00	205.20	3142.00	3142.00	5.26

Prestress properties and span detail:

Beam	Prestress properties					Span Details	
	f_{py} (N/mm^2)	E_p (KN/mm^2)	A_{ps} (mm^2)	f_{pu} (N/mm^2)	JACK% %	ℓ (m)	Tendon Profile**
Typical beams used for parametric study							
T1	1678.93	192.30	53200.00	1916.80	69.10	45.00	1
T2	1678.93	192.30	26600.00	1916.80	69.14	25.00	1
T3	1678.93	192.30	26600.00	1916.80	69.14	25.00	1
T4	1678.93	192.30	26600.00	1916.80	69.14	25.00	1
T5	1678.93	192.30	26600.00	1916.80	69.14	25.00	1
T6	1678.93	192.30	66500.00	1916.80	49.68	45.00	2

** Figures B.1(b) and B.1(c) show the arrangement of Tendon Profile 1 and 2 respectively.

Typical cross section and beam layout:

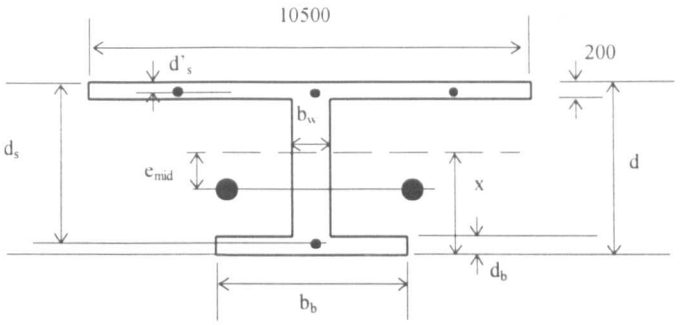

Figure B.1(a): Typical Cross-section

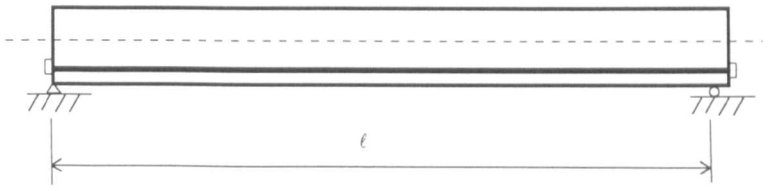

Figure B.1(b): Tendon Profile 1

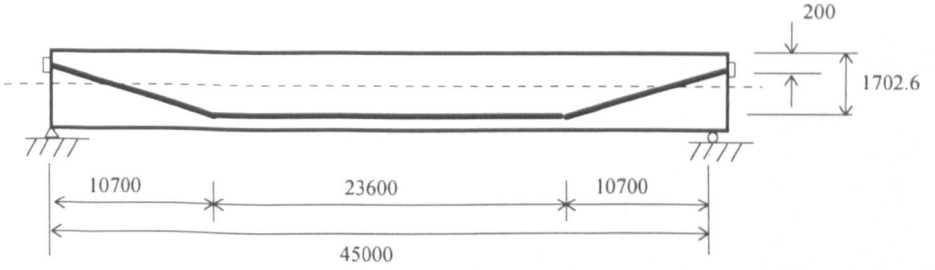

Figure B.1(c): Tendon Profile 2

Appendix C

Details of Beams referred to in Chapter Six

Beams used in Parametric Study

Notes:

1) Cross-sectional and material properties for the following beams are as given in Appendix B for typical beams unless otherwise stated.

2) All beams were analysed using the following constitutive models:

- concrete Saenz (1964)
- reinforcing steel Naaman and Harajli (1985)
- prestressing steel Naaman and Harajli (1985).

Amount of Non-prestressed Reinforcement

Figure no.	Beam No.	Beam Type	A_s (mm^2)	A_s%	L (m)	d_{ps} (mm)	L/d_{ps}	F_e (kN)	A_{ps} (mm^2)
6.3	C1T1S001	T1	3150	0.15	45	1690.76	26.62	70500	53200
	C1T1S002	T1	8400	0.40	45	1690.76	26.62	70500	53200
	C1T1S003	T1	14700	0.70	45	1690.76	26.62	70500	53200
	C1T1S004	T1	31500	1.50	45	1690.76	26.62	70500	53200
	C1T1S005	T1	50400	2.40	45	1690.76	26.62	70500	53200
	C1T1S006	T1	84000	4.00	45	1690.76	26.62	70500	53200
6.4	C1T2S001	T2	900	0.15	25	918.40	27.22	35250	26600
	C1T2S002	T2	3000	0.50	25	918.40	27.22	35250	26600
	C1T2S003	T2	4200	0.70	25	918.40	27.22	35250	26600
	C1T2S004	T2	7800	1.30	25	918.40	27.22	35250	26600
	C1T2S005	T2	14400	2.40	25	918.40	27.22	35250	26600
	C1T2S006	T2	24000	4.00	25	918.40	27.22	35250	26600
6.5	C1T3S001	T3	900	0.15	25	1098.40	22.76	35250	26600
	C1T3S002	T3	3000	0.50	25	1098.40	22.76	35250	26600
	C1T3S003	T3	7200	1.20	25	1098.40	22.76	35250	26600
	C1T3S004	T3	14400	2.40	25	1098.40	22.76	35250	26600
	C1T3S005	T3	24000	4.00	25	1098.40	22.76	35250	26600
6.6	C1T4S001	T4	3000	0.30	25	1625.12	15.38	35250	26600
	C1T4S002	T4	5000	0.50	25	1625.12	15.38	35250	26600
	C1T4S003	T4	10000	1.00	25	1625.12	15.38	35250	26600
	C1T4S004	T4	14000	1.40	25	1625.12	15.38	35250	26600
	C1T4S005	T4	24000	2.40	25	1625.12	15.38	35250	26600
	C1T4S006	T4	40000	4.00	25	1625.12	15.38	35250	26600
6.7	C1T5S001	T5	3000	0.30	25	1325.12	18.87	35250	26600
	C1T5S002	T5	10000	1.00	25	1325.12	18.87	35250	26600
	C1T5S003	T5	14000	1.40	25	1325.12	18.87	35250	26600
	C1T5S004	T5	24000	2.40	25	1325.12	18.87	35250	26600
	C1T5S005	T5	30000	3.00	25	1325.12	18.87	35250	26600
	C1T5S006	T5	40000	4.00	25	1325.12	18.87	35250	26600

Figure no.	Beam No.	Beam Type	A_s (mm^2)	A_s%	L (m)	d_{ps} (mm)	L/d_{ps}	F_e (kN)	A_{ps} (mm^2)
6.8, 6.9, 6,10, 6.11, 6.13 and 6.14.	C1T1S001	T1	3150	0.15	45	1690.76	26.62	70500	53200
	C1T1S002	T1	8400	0.40	45	1690.76	26.62	70500	53200
	C1T1S003	T1	14700	0.70	45	1690.76	26.62	70500	53200
	C1T1S004	T1	31500	1.50	45	1690.76	26.62	70500	53200
	C1T1S005	T1	50400	2.40	45	1690.76	26.62	70500	53200
	C1T1S006	T1	84000	4.00	45	1690.76	26.62	70500	53200
	C1T2S001	T2	900	0.15	25	918.40	27.22	35250	26600
	C1T2S002	T2	3000	0.50	25	918.40	27.22	35250	26600
	C1T2S003	T2	4200	0.70	25	918.40	27.22	35250	26600
	C1T2S004	T2	7800	1.30	25	918.40	27.22	35250	26600
	C1T2S005	T2	14400	2.40	25	918.40	27.22	35250	26600
	C1T2S006	T2	24000	4.00	25	918.40	27.22	35250	26600
	C1T3S001	T3	900	0.15	25	1098.40	22.76	35250	26600
	C1T3S002	T3	3000	0.50	25	1098.40	22.76	35250	26600
	C1T3S003	T3	7200	1.20	25	1098.40	22.76	35250	26600
	C1T3S004	T3	14400	2.40	25	1098.40	22.76	35250	26600
	C1T3S005	T3	24000	4.00	25	1098.40	22.76	35250	26600
	C1T4S001	T4	3000	0.30	25	1625.12	15.38	35250	26600
	C1T4S002	T4	5000	0.50	25	1625.12	15.38	35250	26600
	C1T4S003	T4	10000	1.00	25	1625.12	15.38	35250	26600
	C1T4S004	T4	14000	1.40	25	1625.12	15.38	35250	26600
	C1T4S005	T4	24000	2.40	25	1625.12	15.38	35250	26600
	C1T4S006	T4	40000	4.00	25	1625.12	15.38	35250	26600
	C1T5S001	T5	3000	0.30	25	1325.12	18.87	35250	26600
	C1T5S002	T5	10000	1.00	25	1325.12	18.87	35250	26600
	C1T5S003	T5	14000	1.40	25	1325.12	18.87	35250	26600
	C1T5S004	T5	24000	2.40	25	1325.12	18.87	35250	26600
	C1T5S005	T5	30000	3.00	25	1325.12	18.87	35250	26600
	C1T5S006	T5	40000	4.00	25	1325.12	18.87	35250	26600

Span-Depth Ratio

Figure no.	Beam No.	Beam Type	A_s (mm^2)	A_s%	L (m)	d_{ps} (mm)	L/d_{ps}	F_e (kN)	A_{ps} (mm^2)
6.15, 6.16, 6.17, 6.18, 6.19, 6.20 and 6.21.	C2T1S001	T1	3142	0.15	45	1690.76	26.62	70500	53200
	C2T1S002	T1	3142	0.15	40	1690.76	23.66	70500	53200
	C2T1S003	T1	3142	0.15	35	1690.76	20.70	70500	53200
	C2T1S004	T1	3142	0.15	30	1690.76	17.74	70500	53200
	C2T1S005	T1	3142	0.15	25	1690.76	14.79	70500	53200
	C2T1S006	T1	3142	0.15	20	1690.76	11.83	70500	53200
	C2T1S007	T1	3142	0.15	15	1690.76	8.87	70500	53200
	C2T1S008	T1	3142	0.15	10	1690.76	5.91	70500	53200
	C2T1S009	T1	3142	0.15	5	1690.76	2.96	70500	53200
	C2T2S001	T2	3142	0.52	25	918.40	27.22	35250	26600
	C2T2S002	T2	3142	0.52	23	918.40	25.04	35250	26600
	C2T2S003	T2	3142	0.52	23	918.40	25.04	35250	26600
	C2T2S004	T2	3142	0.52	18	918.40	19.60	35250	26600
	C2T2S005	T2	3142	0.52	15	918.40	16.33	35250	26600
	C2T2S006	T2	3142	0.52	13	918.40	14.16	35250	26600
	C2T2S007	T2	3142	0.52	10	918.40	10.89	35250	26600
	C2T2S008	T2	3142	0.52	7	918.40	7.62	35250	26600
	C2T2S009	T2	3142	0.52	5	918.40	5.44	35250	26600
	C2T2S010	T2	3142	0.52	3	918.40	3.27	35250	26600
	C2T3S001	T3	3142	0.52	25	1098.40	22.76	35250	26600
	C2T3S002	T3	3142	0.52	23	1098.40	20.94	35250	26600
	C2T3S003	T3	3142	0.52	20	1098.40	18.21	35250	26600
	C2T3S004	T3	3142	0.52	18	1098.40	16.39	35250	26600
	C2T3S005	T3	3142	0.52	15	1098.40	13.66	35250	26600
	C2T3S006	T3	3142	0.52	13	1098.40	11.84	35250	26600
	C2T3S007	T3	3142	0.52	10	1098.40	9.10	35250	26600
	C2T3S008	T3	3142	0.52	7	1098.40	6.37	35250	26600
	C2T3S009	T3	3142	0.52	5	1098.40	4.55	35250	26600
	C2T3S010	T3	3142	0.52	3	1098.40	2.73	35250	26600
	C2T4S001	T4	3142	0.30	25	1625.12	15.38	35250	26600
	C2T4S002	T4	3142	0.30	23	1625.12	14.15	35250	26600
	C2T4S003	T4	3142	0.30	20	1625.12	12.31	35250	26600
	C2T4S004	T4	3142	0.30	18	1625.12	11.08	35250	26600
	C2T4S005	T4	3142	0.30	15	1625.12	9.23	35250	26600
	C2T4S006	T4	3142	0.30	13	1625.12	8.00	35250	26600
	C2T4S007	T4	3142	0.30	10	1625.12	6.15	35250	26600
	C2T4S008	T4	3142	0.30	7	1625.12	4.31	35250	26600
	C2T4S009	T4	3142	0.30	5	1625.12	3.08	35250	26600
	C2T4S010	T4	3142	0.30	3	1625.12	1.85	35250	26600
	C2T5S001	T5	3142	0.30	25	1325.12	18.87	35250	26600
	C2T5S002	T5	3142	0.30	23	1325.12	17.36	35250	26600
	C2T5S003	T5	3142	0.30	20	1325.12	15.09	35250	26600
	C2T5S004	T5	3142	0.30	18	1325.12	13.58	35250	26600
	C2T5S005	T5	3142	0.30	15	1325.12	11.32	35250	26600
	C2T5S006	T5	3142	0.30	13	1325.12	9.81	35250	26600
	C2T5S007	T5	3142	0.30	10	1325.12	7.55	35250	26600
	C2T5S008	T5	3142	0.30	7	1325.12	5.28	35250	26600
	C2T5S009	T5	3142	0.30	5	1325.12	3.77	35250	26600
	C2T5S010	T5	3142	0.30	3	1325.12	2.26	35250	26600

Initial Prestress Force

Figure no.	Beam No.	Beam Type	A_s (mm^2)	A_s%	L (m)	d_{ps} (mm)	L/d_{ps}	F_e (kN)	A_{ps} (mm^2)
6.23, 6.24, 6.26 and 6.27.	C3T1S001	T1	3142	0.15	45	1690.76	26.62	40790	53200
	C3T1S002	T1	3142	0.15	45	1690.76	26.62	70500	53200
	C3T1S003	T1	3142	0.15	45	1690.76	26.62	81580	53200
	C3T2S001	T2	3142	0.52	25	918.40	27.22	20395	26600
	C3T2S002	T2	3142	0.52	25	918.40	27.22	35250	26600
	C3T2S003	T2	3142	0.52	25	918.40	27.22	40790	26600
	C3T3S001	T3	3142	0.52	25	1098.40	22.76	20395	26600
	C3T3S002	T3	3142	0.52	25	1098.40	22.76	35250	26600
	C3T3S003	T3	3142	0.52	25	1098.40	22.76	40790	26600
	C3T4S001	T4	3142	0.30	25	1625.12	15.38	20395	26600
	C3T4S002	T4	3142	0.30	25	1625.12	15.38	35250	26600
	C3T4S003	T4	3142	0.30	25	1625.12	15.38	40790	26600
	C3T5S001	T5	3142	0.30	25	1325.12	18.87	20395	26600
	C3T5S002	T5	3142	0.30	25	1325.12	18.87	35250	26600
	C3T5S003	T5	3142	0.30	25	1325.12	18.87	40790	26600

Figure no.	Beam No.	Beam Type	A_s (mm^2)	A_s%	L (m)	d_{ps} (mm)	L/d_{ps}	F_e (kN)	A_{ps} (mm^2)
6.28, 6.29, 6.31 and 6.33.	C3T1S001	T1	3142	0.15	45	1690.76	26.62	40790	53200
	C3T1S002	T1	3142	0.15	45	1690.76	26.62	70500	53200
	C3T1S003	T1	3142	0.15	45	1690.76	26.62	81580	53200
	C3T1S004	T1	3142	0.15	25	1690.76	14.79	40790	53200
	C3T1S005	T1	3142	0.15	25	1690.76	14.79	70500	53200
	C3T1S006	T1	3142	0.15	25	1690.76	14.79	81580	53200
6.30, 6.32 and 6.34.	C3T4S001	T4	3142	0.30	25	1625.12	15.38	20395	26600
	C3T4S002	T4	3142	0.30	25	1625.12	15.38	35250	26600
	C3T4S003	T4	3142	0.30	25	1625.12	15.38	40790	26600
	C3T4S004	T4	3142	0.30	13	1625.12	8.00	20395	26600
	C3T4S005	T4	3142	0.30	13	1625.12	8.00	35250	26600
	C3T4S006	T4	3142	0.30	13	1625.12	8.00	40790	26600
6.36 and 6.37.	C3T5S001	T5	3142	0.30	25	1325.12	18.87	20395	26600
	C3T5S002	T5	3142	0.30	25	1325.12	18.87	35250	26600
	C3T5S003	T5	3142	0.30	25	1325.12	18.87	40790	26600
	C3T5S004	T5	3142	0.30	13	1325.12	9.81	20395	26600
	C3T5S005	T5	3142	0.30	13	1325.12	9.81	35250	26600
	C3T5S006	T5	3142	0.30	13	1325.12	9.81	40790	26600
	C3T5S007	T5	30000	3.00	25	1325.12	18.87	20395	26600
	C3T5S008	T5	30000	3.00	25	1325.12	18.87	35250	26600
	C3T5S009	T5	30000	3.00	25	1325.12	18.87	40790	26600

Amount of Prestressed Reinforcement

Figure no.	Beam No.	Beam Type	A_s (mm^2)	A_s%	L (m)	d_{ps} (mm)	L/d_{ps}	F_e (kN)	A_{ps} (mm^2)
6.38	C4T1S001	T1	3142	0.15	45	1690.76	26.62	70500	53200
	C4T1S002	T1	3142	0.15	45	1690.76	26.62	70500	79800
6.39	C4T2S001	T2	3142	0.52	25	918.40	27.22	35250	26600
	C4T2S001	T2	3142	0.52	25	918.40	27.22	35250	53200
6.40	C4T3S001	T3	3142	0.52	25	1098.40	22.76	35250	26600
	C4T3S002	T3	3142	0.52	25	1098.40	22.76	35250	53200
6.41	C4T4S001	T4	3142	0.30	25	1625.12	15.38	35250	26600
	C4T4S002	T4	3142	0.30	25	1625.12	15.38	35250	53200
6.42	C4T5S001	T5	3142	0.30	25	1325.12	18.87	35250	26600
	C4T5S002	T5	3142	0.30	25	1325.12	18.87	35250	53200

Appendix D

Comparison on the number of nodes and tolerance used for analysis

Number of nodes used for analysis

Beam OA-1

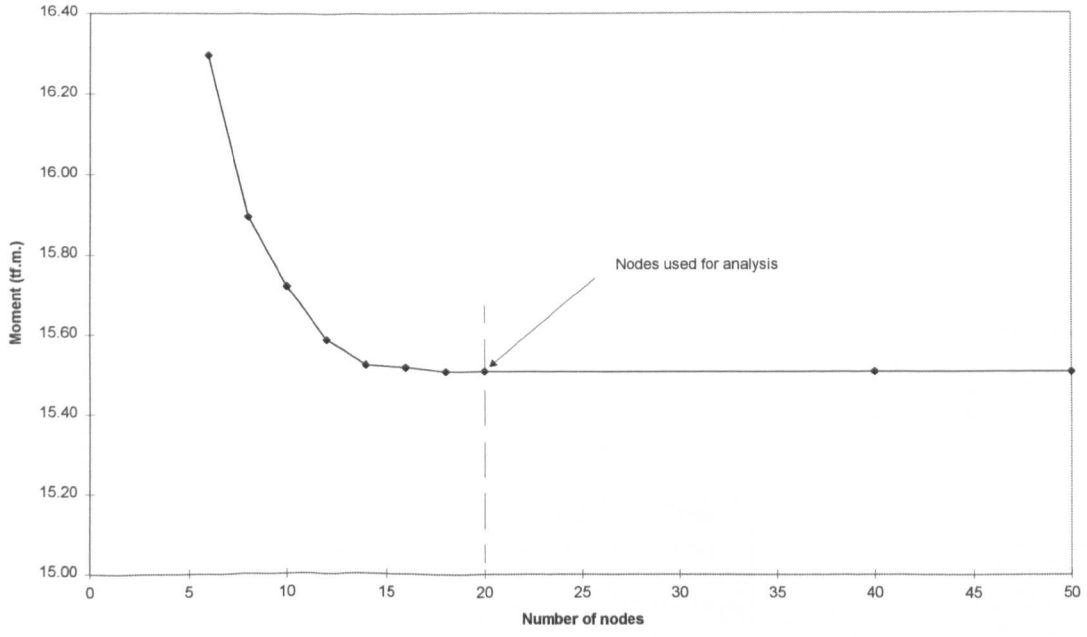

nodes	Moments (tf.m.)	Time (hrs)
6	16.2973	1.00
8	15.8944	1.20
10	15.7216	1.50
12	15.5868	1.50
14	15.5245	2.40
16	15.5173	3.00
18	15.5080	4.00
20	15.5080	4.50
40	15.5080	14.00
50	15.5080	21.00

Figure D.1: Ultimate moment derived from model vs. number of nodes curve for Beam OA-1

Beam OC88-1

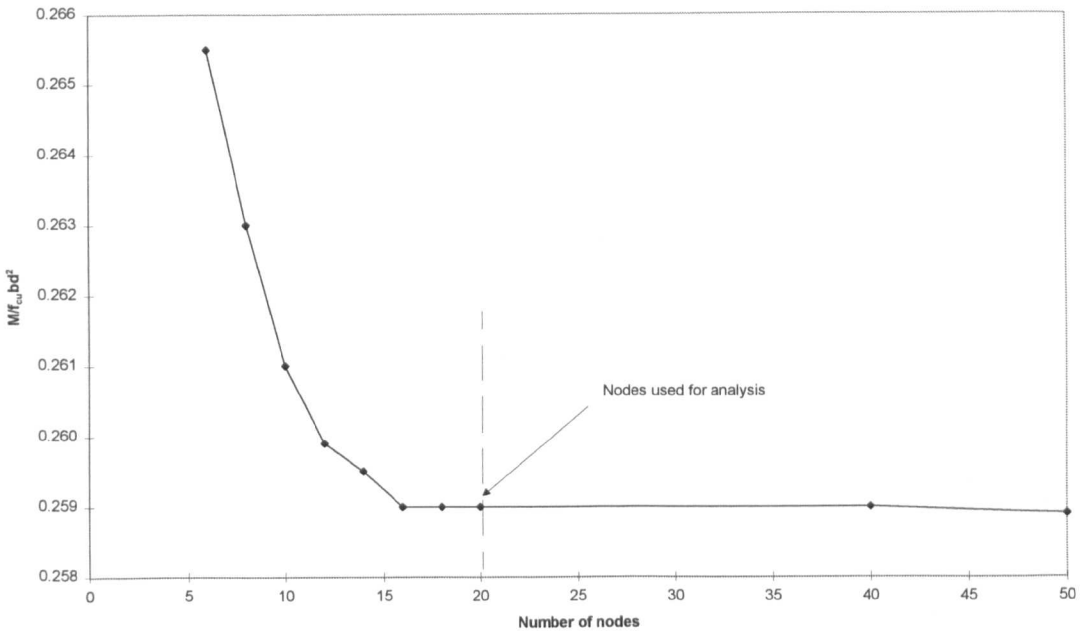

nodes	Moments ($M/f_{cu}bd^2$)	Time (hrs)
6	0.2655	1.50
8	0.2630	1.60
10	0.2610	2.00
12	0.2599	2.50
14	0.2595	2.70
16	0.2590	3.00
18	0.2590	4.50
20	0.2590	5.50
40	0.2590	16.50
50	0.2589	22.00

Figure D.2: Ultimate moment derived from model vs. number of nodes curve for Beam OC88-1

Tolerance used for analysis

Beam OA-1

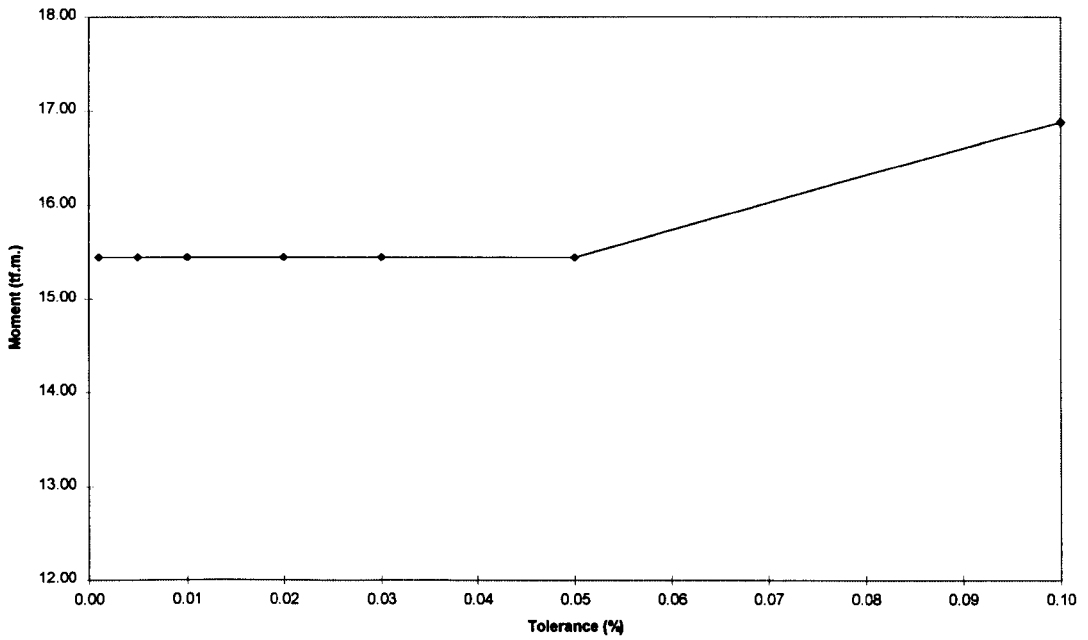

Tolerance (%)	Moments (tf.m.)	Time (hrs)
0.0001	*	1.2
0.0005	**	6
0.0010	15.4479	7
0.0050	15.4479	5
0.0100	15.4479	3
0.0200	15.4479	3
0.0300	15.4479	2.5
0.0500	15.4490	4
0.1000	16.8900	2.8

Note

* *premature termination at 10.5079 tf.m.*

** *premature termination at 15.3779 tf.m.*

Figure D.3: Ultimate moment derived from model vs. *% Tolerance* curve for Beam OA-1

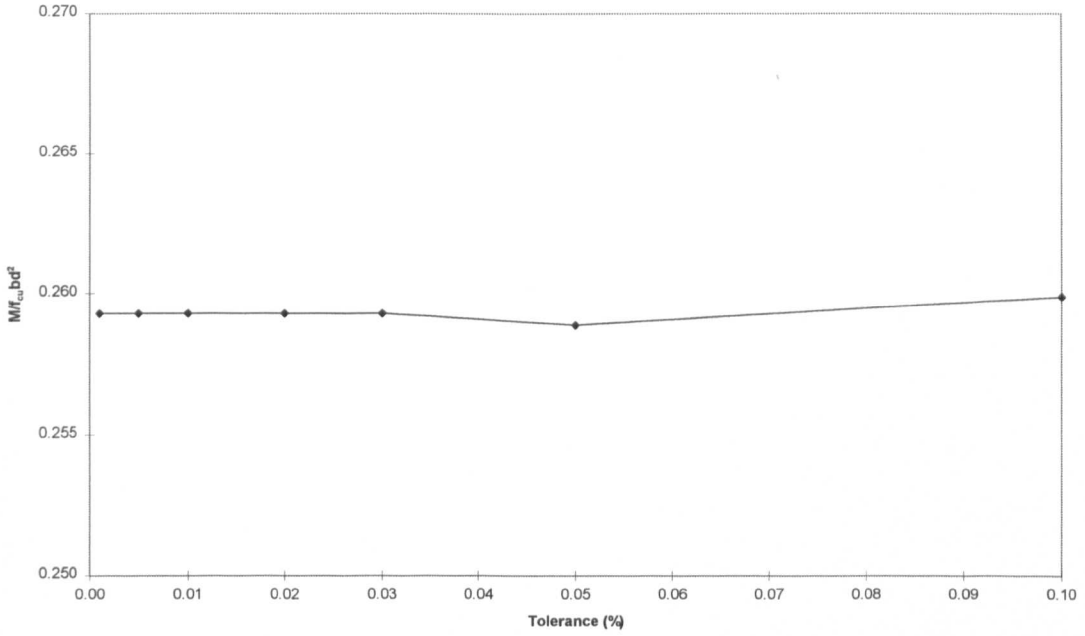

Tolerance (%)	Moments (kNm)	Time (hrs)
0.0001	*	5.5
0.0005	**	7
0.0010	0.2593	8
0.0050	0.2593	6
0.0100	0.2593	5
0.0200	0.2593	5.5
0.0300	0.2593	5.2
0.0500	0.2589	5
0.1000	0.2599	5

Note

* *premature termination at* $M/f_{cu}bd^2 = 0.05872$

** *premature termination at* $M/f_{cu}bd^2 = 0.25883$

Figure D.4: Ultimate moment derived from model vs. *% Tolerance* curve for Beam OC88-1